UNIVERSITÀ DI TRENTO
Department of Industrial Engineering

Doctoral School in Materials, Mechatronics and Systems Engineering

XXXV cycle

# Innovative composite enamel coatings with improved abrasion resistance and mechanical properties

**Francesca Russo**

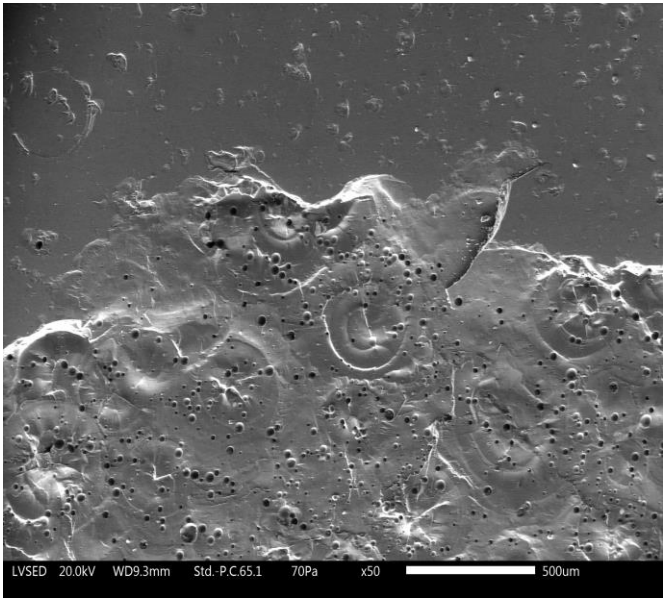


**July 2023**

# INNOVATIVE COMPOSITE ENAMEL COATINGS WITH IMPROVED ABRASION RESISTANCE AND MECHANICAL PROPERTIES

Francesca Russo
E-mail: francesca.russo-2@unitn.it

Approved by:

Prof. Stefano Rossi, Advisor
Department of Industrial Engineering
*University of Trento, Italy.*

Prof. Vigilio Fontanari,
Department of Industrial Engineering
*University of Trento, Italy.*

Ph.D. Commission:

Prof. Emiliano Rustighi,
Department of Industrial Engineering
*University of Trento, Italy.*

Prof. Tiziano Bellezze,
Dipartimento di Scienze e Ingegneria della Materia, dell'Ambiente e Urbanistica
*Università Politecnica delle Marche, Italy.*

Dr. Radek Mušálek, Ph.D.
Department of Materials Engineering
*Institute of Plasma Physics of the Czech Academy of Sciences, Czech Republic.*

University of Trento,
Department of Industrial Engineering

July 2023

**University of Trento - Department of Industrial Engineering**

**Doctoral Thesis**

**Francesca Russo - 2023**

*Dedicated to my old and new family*

# Abstract

The earliest method employed by ancient civilizations to decorate precious artifacts is vitreous enameling, which has its origins in antiquity. The use of vitreous enamels for technical purposes started in the nineteenth century with the First Industrial Revolution, as these coatings were able to combine aesthetically pleasing colors and surface finishing with superior technical properties, including durability, thermal resistance, and chemical resistance. Nowadays, vitreous enamels, which are silica-based inorganic coatings deposited by high temperature (580-890 ˚C) vitrification, are usually employed for the protection of metallic components that must show superior durability and resistance in corrosive and harsh environments, such as in chemical reaction vessels, heat exchangers, flue pipes, and gas turbines. Unlike organic coatings, enamel coatings are limitedly affected by UV weathering and corrosion phenomena, therefore their protective properties remain unchanged over time. Moreover, these coatings are resistant to acid and mild alkaline substances as well as organic solvents, and they have strong thermal shock and direct flame resistance. The strong adhesion between the enamel coating and the covered substrate is the reason why enameled materials show optimal resistance to corrosion. All these positive features make enamel coatings first-choice materials in many high-duty technological applications, but some issues still limit their application in some fields. Enamel coatings show non-optimal abrasion resistance and poor mechanical properties due to the brittle-prone behavior of the glassy matrix. Abrasion and tensile stresses are very common mechanical solicitations that these coatings are subjected to in everyday use. Degradation due to abrasive processes negatively affects the corrosion resistance of enameled artifacts, as the removal of material by brittle fracture and the opening of enamel's intrinsic porosity can put the covered metal in contact with the external aggressive environment. The same problem arises when enamel coatings are subjected to tensional stresses, as cracks nucleate and easily propagate through the whole coating thickness until reaching the metal substrate.

Therefore, it is imperative to improve the abrasion resistance and mechanical properties of enamel coatings to extend their durability and application areas. Many recent studies have focused their attention on the development of abrasion resistant enamels by the addition of mill additives, hard ceramic particles, such as WC and SiC, or graphene-based fillers. Nevertheless, there are still several issues to consider, for example, the study of composite $Al_2O_3$/enamel coatings, the study of graphene/enamel composite coatings with improved graphene dispersion, and the assessment of the effect of metallic powders on the mechanical properties of these coatings. The study of abrasion resistant enamel coatings is then a hot topic, but the assessment of enamel's mechanical properties still remains little investigated even though it is a critical aspect.

This work represents an attempt in the direction of exploring the effect of different types of fillers, with the aim to develop innovative enamel coatings with improved abrasion and cracking resistance. Moreover, this work also aims at investigating the behavior of composite enamel coatings by standardized testing methods coupled with in-situ techniques, to obtain novel insights into the failure mechanisms of these coatings and the effect of the different fillers. Thus, as this thesis covers a wide range of topics, the results of the research have been divided into independent Chapters, in the interest of a better presentation. Each of them has been provided with an abstract and an Introduction and divided into a Materials and Methods section, a Results and Discussion section, and finally Conclusions. Therefore, the main body of the thesis is organized into five chapters.

In the first Chapter, the background to the topics discussed in the subsequent chapters is provided and the relevant literature is reviewed, while in the fifth and last Chapter some conclusions are drawn, and future perspectives are discussed. The core of the work is contained in the three central chapters.

Chapter II presents the main aim of the thesis and describes the most important experimental techniques, that will be exploited to charcaterize the different types of composite enamel coatings.

In Chapter III, the effect of graphene-based filler on the abrasion resistance of composite enamel coatings is investigated. The main aim of this study is to develop an efficient way to deposit composite graphene/enamel coatings avoiding the agglomeration of the filler. The assessment of the abrasion resistance by Porcelain Enamel Institute (P.E.I.) test coupled with microscopic observations is the core of this chapter. The novelty of this study with respect to the present literature is represented by the deposition of homogenous coatings and the study of the abrasion behavior by means of a surface-limited abrasion method with a particular emphasis on the mechanisms underlying the abrasive damaging processes.

Chapter IV presents some investigations related to the development of abrasion resistant $Al_2O_3$/enamel composite coatings. This study is inserted in a wider project about the development of chemically resistant enamel coatings with improved abrasion resistance. Here, the effect of the size of the corundum particles on the abrasion resistance and chemical durability is investigated by means of traditional and accelerated tests. The novelty with respect to the present literature is represented by a complete investigation of the functional properties of enamel coatings mixed with corundum particles, which have found limited attention in this field up to now.

In Chapter V, the effect of 316L stainless steel flakes (SS-Fs) on the functional properties of enamel coatings is assessed by considering abrasion resistance, chemical resistance, and cracking resistance. The abrasion behavior of the coatings is investigated by the P.E.I. test coupled with microscopical observations to better explain and clarify the damaging mechanisms. The mechanical properties of the

composite coatings are assessed by means of different tests, namely scratch test, IF (Indentation Fracture) method, and bending tests. Quantitative data regarding the cracking resistance of the coatings are extrapolated thanks to in-situ Scanning Electron Microscopy (SEM) /Acoustic Emission (AE) measurements, which are helpful in better evaluating the cracking resistance of the coatings and the role of the filler in counteracting the negative effect of the external mechanical stresses. The novelty of this study with respect to the literature is represented by the development of enamel coatings with the addition of 316L SS-Fs, and the study of their properties by means of in-situ techniques.

# Table of contents

# Organization and structure of the thesis

Enamelling has its origin in ancient times and can be considered the oldest technique used by ancient civilizations to decorate precious objects. Only with the advent of the First Industrial Revolution, in the nineteenth century, this type of coating began to be used also for technical purposes. Enamel coatings combine aesthetically pleasing colors and glossy finishing with excellent technical properties, such as corrosion protection and durability: this was the main reason for vitreous enamel success in many fields, such as household and industry.

Independently on the covered substrate, enamel coatings possess very good engineering properties. These coatings are not significantly affected by UV exposure, so their aesthetical properties remain unchanged over time, differently with respect to organic coatings such as paints and polymers. They have good resistance to heat, direct flame, and thermal shock, and they can withstand chemical attack from acids and alkali maintaining gloss, color, and surface properties. Thanks to the strong adhesion between the enamel and the metallic substrate, enameled materials possess an intrinsic optimal corrosion resistance, and they can guarantee optimal protection of the covered metal substrates from weathering and corrosive environments. All these positive features make enamel coatings very attractive materials for application in heavy-duty components; in this sense, vitreous enamels are the first-choice materials in the lining of chemical vessels, flue pipes, heat exchangers, and gas turbines.

Despite all the positive aspects previously underlined, some issues limit the application of this type of coating in many industrial fields. Vitreous enamel coatings show nonexcellent abrasion resistance and poor mechanical properties due to the brittle-prone behaviour of the glassy matrix. Abrasion is a very common mechanism of degradation of enameled surfaces, as the loss of aesthetical properties, the disclosure of the intrinsic enamel porosity, and the loss of mass through brittle fracture events can negatively affect the aesthetical and functional properties of these coatings. Degradation due to abrasion processes negatively affects corrosion protection properties, as cracks may occur and propagate until reaching the metal substrate, thus allowing direct contact between the substrate and the external aggressive environment. The same problems arise when enamel coatings are subjected to tensional stresses, as cracks easily nucleate on the coating's surface and propagate until reaching the substrate. It is therefore necessary to improve the mechanical properties of vitreous enamel coatings by limiting the brittleness of the glassy matrix with the addition of suitable fillers.

Being a subject of great scientific and industrial interest, composite vitreous enamel coatings with different additives have recently been produced and investigated. However, little attention has been paid to study the effect of different fillers on the

abrasion resistance and mechanical properties of these coatings, exploiting standardized and in-situ methods. In this PhD thesis, it was therefore decided to combine the excellent properties of enamel coatings with the interesting characteristics of different types of fillers, namely graphene nanoplatelets (GNPs), corundum particles ($Al_2O_3$), and 316L stainless steel flakes (SS-Fs), and to investigate their effect on the abrasion resistance and cracking resistance of the produced composite coatings. Standardized and in-situ methods were exploited to obtain comparable results between different formulations and to acquire novel insights on the failure mechanisms of these functionalized coatings.

The realization of this thesis has seen the participation of numerous players, coming from both the academic and the industrial world. In this context, it had been necessary to establish a fruitful collaboration between all the stakeholders and create a way to positively value their different backgrounds. Some parts of this thesis were carried out in collaboration with Emaylum Italia (Chignolo d'Isola, BG, Italy), an industrial enamel producer we have collaborated with for the development of new enamel formulations, tailored frits, and industrial-scaled samples. From an academic point of view, some parts of this thesis were realized in collaboration with the Surface Engineering Group of the CIDETEC Research Center (Donostia, Spain) guided by Dr. Maria Lekka. Another important academic player, involved in this thesis work, is the Materials Engineering Group of the Institue of Plasma Physics of the Czech Academy of Science (Prague, Czech Republic) that hosted me for the realization of in-situ mechanical investigations.

Despite all possible commitments, the COVID-19 pandemic has forced us to temporarily stop the experimental activities and some collaborations (also in the supply of materials) were interrupted for many months due to government limitations. In this context, we decided to install an internal enamel production line to produce the samples internally at the University of Trento. This situation is the reason why some studies, that will be presented, are carried out on external-produced samples, whereas others are developed on internally produced samples.

This thesis work is part of a wide-ranging research that concerns the development of innovative composite enamel coatings with improved mechanical properties. It describes the materials and methods adopted, the experiments performed, and the results obtained, following the structured chapters:

- Chapter I: This chapter is designed to give the reader a basic knowledge of porcelain enamel coatings and explain the basic concepts related to enamels formulation and application. In addition to that, the main properties and application market segments of these coatings are presented to better highlight the versatility of this material.
- Chapter II: This chapter illustrates the aim of the thesis, providing a basic theoretical background and briefly explaining the ain experimental techniques that will be used in the following chapters.

- Chapter III: This chapter describes the results obtained in the study of composite enamel coatings with the addition of graphene nanoplatelets (GNPs). The main objective of this chapter is to outline the efforts taken to prevent the agglomeration of the graphene-based filler during the deposition of composite enamel coatings, and to study the abrasion behavior of these coatings by means of a standardized abrasion method, the P.E.I. test (UNI EN ISO 10545-7).
- Chapter IV: This chapter presents the results obtained in the study of composite enamel coatings with the addition of corundum particles. The objective of this study, which is part of a larger international project on chemically resistant enamel coatings for functional applications, is to investigate the influence of the size of the hard ceramic particle (HCP) – type filler on the abrasion and chemical resistance of the composite coatings. Standardized tests, coupled with chemical and electrochemical methods, are exploited to obtain reference data, that can be easily compared with other studies on similar systems.
- Chapter V: This chapter illustrates the results obtained in the study of composite enamel coatings with the addition of 316L SS-Fs. This study considers the influence of the chosen metallic filler on the abrasion resistance of the deposited coatings, considering their chemical resistance as well. The abrasion resistance is studied by means of standardized methods also in this case. The effect of the stainless-steel powder on the mechanical properties of the coatings is investigated by means of in-situ methods, that can provide realiable quantitative results and novel mechanicistic insights on the behaviour of these composite coatings under tensional-type external stresses.
- Chapter VI: This chapter is designed to resume all the important achievements of this thesis project, commenting on obtained results and presenting future developments in the field.

# 1 Theoretical background

This chapter will briefly introduce the main concepts related to the production of vitreous enamel coatings, and it will present the main functional properties of these coatings.

## *1.1 Terminology in the field of enamel coatings*

The material commonly known as *porcelain vitreous enamel* is a coating with a tradition dating back to the dawn of human civilization. Porcelain vitreous enamel has been used for many centuries, in ancient times, for purely decorative purposes, but, from the pre-industrial era onward, it became the first-choice material in many market sectors, such as in the household appliances and industrial vessels sectors[1, 2]. As the English term *vitreous* infers, porcelain vitreous enamel is a glass-ceramic coating, but its peculiar chemical composition makes it very different from both traditional glasses and traditional ceramics[3]. Porcelain enamels are suitable for protecting different substrates, such as metals and glass, as they guarantee optimal protection against corrosion and weathering[4, 5], while providing pleasing aesthetical features[6].

Porcelain vitreous enamel coatings are mainly made up of silica, and they are obtained by application of an enamel formulation on an appropriate substrate[7]. The starting material of all enamel formulations is the *frit,* a material obtained by smelting together a variety of non-organic raw materials and then by allowing them to solidify by rapid cooling[8, 9]. The obtained frit is then ground to an appropriate granulometry and mixed with other additives to obtain an applicable formulation[10]. The substrate materials are then covered with the enamel formulation and fired at high temperatures (580-890 ˚C dependently on the chosen metallic substrate) so that the enamel mixture undergoes vitrification. The high-temperature firing process allows the substrate material and the enamel layer to bond irreversibly, both from a chemical and a mechanical point of view. This new bond leads to the formation of a new composite material that brings out the best properties of the two starting components[5].

The *porcelain vitreous enamel* term can only be used to describe the large and differentiated family of non-organic coatings with a vitreous matrix, but, still today, many misunderstandings arise due to the misuse of this term. Indeed, it is not uncommon to find the *enamel* term used in the field of organic coatings, but great attention should be given not to confuse porcelain vitreous enamels with paints, as they greatly differ in chemical nature and functional properties[11-13].

As regards the standardized definition of *porcelain vitreous enamel*, it is possible to refer to the UNI 8762:2010 standard[14], which gives a precise definition of the *frit, porcelain vitreous enamel*, and *enamelling* terms. The frit is defined as "*the main*

*component of vitreous enamel, obtained by smelting of inorganic raw materials at temperatures ranging between 1000 ˚C and 1350 ˚C, and subsequent rapid cooling in water (granules) or between cooling cylinders (flakes)*". At the same time, the UNI 8762:2010 standard also describes *porcelain vitreous enamel* as a "*product for the vitreous coating of metal and glass surfaces, for protective, functional and/or decorative purposes. It is a solidified vitreous mass, obtained by the smelting and brusque cooling of non-organic components, primarily oxides. It is smelted onto the support at a temperature between 450 ˚C and 950 ˚C and has a cubic thermal expansion of between 150 and 450 · $10^{-7}$ °$K^{-1}$: these values vary specifically as a function of the type of support and the field of application*". Other important definitions are provided by the ASTM C286-99:2004 standard[15], which defines the *frit* as "*small friable particles produced by quenching of a molten glass material*" and the *porcelain enamel* as a "*substantially vitreous inorganic coating bonded to metal by fusion at a temperature above 800 ˚C*". This last definition of porcelain enamel is not perfectly correct, as enamel coatings can be also applied on aluminium alloy substrates and thus fired at temperatures of approximately 580 ˚C.
From a lexical point of view, it is common to find *porcelain vitreous enamel* both addressed as *vitreous enamel* and *porcelain enamel*: the terms are equivalent, but they are widespread in the UK and the US, respectively.

## *1.2 History of porcelain enamel and enamelled materials*

Vitreous enamel is one of the most ancient materials used to decorate the surface of objects. Many archaic civilizations were used to apply enamel to decorate and embellish religious objects and important artifacts[16]. With the advent of the First Industrial Revolution, in the 18$^{th}$ century, enamels started to be used as functional coatings, as they were able to guarantee optimal corrosion protection to the covered metal substrates. The low manufacturing cost associated with the production of enamel coatings allowed a wide diffusion of this material to all sorts of mass-consumption products made on at an industrial scale (such as saucepans, road signs, bath tubes, and household appliances). In the last decades of the 20$^{th}$ century, porcelain enamel coatings also started to be employed in high-technological applications, such as the lining of chemical reaction vessels and the protection of metals in harsh environments[17]. Nowadays, porcelain enamels are still appreciated for high-duty applications where good corrosion protection and chemical resistance are needed. In addition to that, enamel coatings can protect the covered substrates while retaining their aesthetical properties over time and under different operando condition[18].

### 1.2.1 From the ancient world to the 19th century

This section will briefly describe the main steps involved in the development of porcelain vitreous enamel from ancient times to the pre-industrial era.

**Proto enamel** The Egyptians were the first civilization to make extensive use of *faience*, which is considered the first precursor of porcelain enamel[19]. This society was able to create beautiful *faience* objects, having a glossy blue-green appearance[20]. These quartz-based objects were produced by cast molding: the quartz was mixed with alkali, calcite lime, and water; thus, the object was heat treated to form an inner siliceous body covered with a surface of soda-lime glass[19, 21, 22]. FIGURE 1-1 shows some fine examples of blue faience object found in Egypt on display at the Metropolitan Museum of Art in New York (NY, US).


**Figure 1-1: Examples of fine Egyptian faience objects, The Metropolitan Museum of Art, New York, NY, United States (a) Hippopotamus "William", ca. 1961-1878 BC, L 20 W 7.5 H 11.2 ; (b) Lotiform Chalice, ca. 945-664 BC, H 14.5.**

**The origins of enamel and its diffusion in the ancient world** The first known examples of enamelled metals date back to the 14th century B.C.E., and they were found in some tombs in Cyprus[23]. The most remarkable objects of these archaeological findings are represented by the famous Kouklia gold rings and the Kourion golden royal scepter, dating back to the Cyprus Golden Age period. Both these two treasures are the first recognized examples of the so-called *cloisonné* enamelling style[24].

The *cloisonné* technique was primarily developed by goldsmiths: the coloured cloisons were shaped by delimiting the decorated area with tiny gold strips soldered perpendicular to the metal surface: the areas were then filled with smelted pigmented sands, and the whole object was fired in a kiln until enamel was vitrified[25]. This technique rapidly spread all over the Middle East thanks to the Scythian, an Iranian warrior people who brought the art of enamelling to the Caucasian area and to Siberia as well[26]. As regards the diffusion of enamel in the Western world, other important cloisonné findings can be attributed to the Assyrian Empire, and they date back to the 7th century B.C.E., a period in which Assyria controlled territories, like Cyprus, where enamelling was already diffused[16]. The diffusion of the *cloisonné* style towards the western countries was favoured by the presence of the Phoenicians, who established close commercial relationships with colonies in Spain and Magna Grecia[27].
Another important area of development for vitreous enamel was among the Celts, where the use of enamel is dated to the 5th century B.C.E. Here enamels were mainly used to decorate small bronze objects, such as fibulae, by applying the *champlevé* technique. Differently with respect to the *cloisonné* method, the *champlevé* technique consists in carving the metal substrate, applying the enamel powder in the obtained carves, and then firing the whole object to obtain a glossy vitrified surface[28]. The Romans played an important role in the diffusion of this enamelling method throughout the area of southern Germany, Bohemia, Britain, and Ireland[29, 30], but the *champlevé* method only flourished at the end of the 11th century in Conques (France), where it was used for enamelling of copper[31].

**The diffusion of enamels during the Middle Ages** The diffusion of enamelling in Europe suffered a rapid decline with the success of the barbarian invasions, but it was reborn in Byzantium around the 7th century A.C. for the decoration of icons. Here, the *cloisonnè* technique reached its maximum splendour as enamel pieces were combined with precious stones and gold to obtain impressive religious objects[27]. Unfortunately, very few examples have survived to the present day due to the iconoclastic revolution of the 8th -9th century A.C., but the byzantine tradition rapidly spread all over Europe, giving rise to different artistic schools in Spain, Italy, France, and Germany[1, 32]. Some very fine examples of byzantine *cloisonnè* enamelling have survived to the present day only thanks to the dispersal of Byzantium's art treasures during the Fourth Crusade (13th century A.C.), as happened for the Pala d'Oro in the Basilica of San Marco in Venice[33].
In the same period, the existing enamelling techniques were further improved with the spread of the *champlevé* method, and many new artistic schools were born all over Europe, in particular in the Rhine region (with a focus in Cologne) and along the river Moselle (centred in Liège). The only school that survived over centuries was the one born in Limoges, which flourished around 1130 and took the champlevé technique to its maximum level[34]. Here, enamelled objects started to be produced

as luxurious decorations, and they lost the religious character that had been characterizing the enamelled production over centuries.

**From the Renaissance to the pre-industrial era** The Limoges's school, together with its artifacts, became famous throughout Europe and it gave birth to new artistic schools in Spain, Italy, and France. In this context, enameling was applied to the decoration of three-dimensional objects, such as lunettes and small statues[35, 36].
Between the 15th and 16th century, the art of enameling was attempted in high regard and the artists developed, in the different regions of Europe, new enameling and decoration techniques[16]. The Parisian goldsmiths mainly used the *baisse-taille* method (using translucent enamel): the pattern was created by working the metal surface, which was then covered with translucent enamel. This technique was imported in Paris from Avignon, where it had been brought during the period of the Papal exile by the goldsmiths of Siena. In the same period, the technique of *plique-a-jour* started making its own way. This technique involved the same procedure used for the realization of cloisonnè objects, but, in this case, the underlying substrate was then removed, and the enamel paste remained framed and visible from two sides[37]. The end of the 15th century brought the rise of *email des peintres*, also called *enamel-paint*. This technique allowed to realize objects with a pictorial-similar appearance: enamels were used as if were colors on a canvas and the pattern was drawn in black on a white enamel paste. In the 16th century, France saw the spread of the *grisaille* decoration method. In this case, enamellers only used black and white enamels, firstly preparing a black background, and then applying several layers of white enamels to create a chiaroscuro and a relief effect[38].
As regards Italy, the enamel production was mainly supported by the Medici family, and the advent of Benvenuto Cellini, the most renowned goldsmith to work with enamels, represented the finest example of craftsmanship of this era[39]. In the 18th century enamel was an extremely widespread material, and it was both used for decoration of religious objects and for the realization of domestic pieces. In the following decades, the production of enameled objects started to be relegated to small decorative objects, thus decreeing the definitive decay of artistic enameling[1].

### 1.2.2 From the First Industrial Revolution onward

With the advent of the First Industrial Revolution, enamels started to be applied to substrates such as iron and cast iron[40]. The development of industrial enameling was so closely linked to the advances in metallurgy and chemistry of the late 18th century, that the enameling industry was attracting the best chemists of that time[1]. Starting from the second half of the 18th century, some industries started to patent the first enameling processes on steel sheets, although the first manual on technical enamelling was published only many years later[41]. Around 1870, the almost total

enamelled production was limited to cast iron hollowware[40], but, in the following years, it was possible to produce high-quality cast iron pans, which were white enamelled both inside and outside[42].

In the second half of the 19th century, enamelling faced different technical problems, such as the lack of pure raw materials, and the development of new production methods for steel. Nevertheless, many advancements were achieved, such as the discovery of new production methods for pigments[41]. Probably, one of the most important discoveries in this field was represented by the use of clay to keep the powdered enamel in suspension in water: this way was possible to apply the enamel simply by painting, spraying, or by immersion[43]. Around the year 1900, John C. Reed introduced the machine molding of bath tubes, which boosted the sanitary enameling industry[44]. In the same years, the introduction of antimony compounds, used as opacifiers in dry coat enamels, is considered an important achievement[45].

The enamel industry boomed some years after World War I, in the USA, and vitreous enamel became the unchallenged star of the white-goods market[46]. The manufacturing of refrigerators, stoves, sanitary ware, and household objects grew very rapidly, but it suddenly stopped with the advent of World War II, when enameling plants were converted to the treatment of war materials. In 1942, the development of titanium-based white enamels gave a great boost to the rebirth of the enameling industry, and new products, such as chimney pipes, dishwashers, cooking hobs, and water heaters, started to be enameled[47]. In the following decades, the enamel industry continued to evolve, also thanks to the development of new deposition techniques, which made it possible to obtain better quality products in an increasingly efficient way. During the sixties, the industry started using direct enameling[48]: as the enamel's ability to adhere to metallic substrates had improved, it was no longer necessary to apply several enamel layers, but the benefits of a simpler deposition process were counterbalanced by the need to use decarburized steels[49]. In those years, one of the most important advances in enameling processing technologies was the introduction of the electrostatic powder application method, replacing the traditional wet methods[50, 51] and guaranteeing an important material savings. New *pickling free* steels were developed during the eighties, and the firing technologies were implemented to lower the firing temperatures, reduce costs, and save energy[52-54]. Another historical application of enamels is the production of publicity plaques and signs, that had their heyday between the twenties and the sixties of the 20th century. This application witnessed an unstoppable decline due to the spread of television and photographic advertisements: by the seventies, the production of enamelled advertising plaques has ceased all over the world at about the same time[55]. Nowadays, enamel is commonly applied to many everyday use objects, but it is also used in high-duty technological applications, where high functional properties are required.

## 1.3 Enamel formulations: raw materials and production technologies

The main peculiarities of enamel coatings depend on various elements, such as the application method and the firing parameters, but one of the most important aspects to be taken into consideration is certainly the composition and the production of the starting frit and starting enamel formulation. The frit is the basic component of all enamels, and it is obtained by smelting together different inorganic raw materials at temperatures ranging from 1000 to 1350 ˚C. The product of this process is then quenched rapidly in water or by using water-cooled rollers to obtain small glassy granules or chips, respectively. The frit can be admixed with different types of additives, opacifiers, and pigments to obtain the most suitable enamel formula in dependence of the chosen application technique[56]. FIGURE 1-2 summarizes the main steps involved in the production of wet and dry enamel formulations.

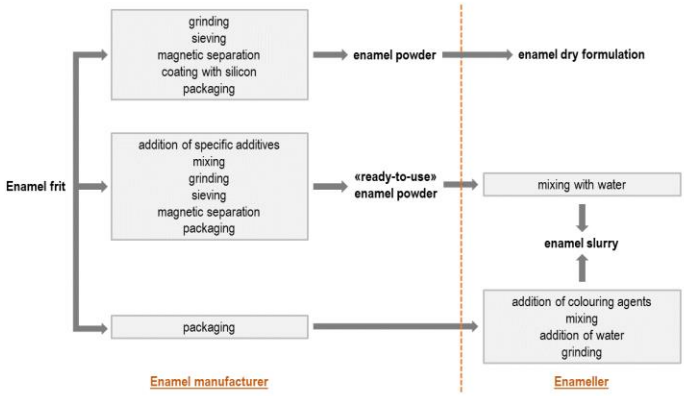


**Figure 1-2. Schematic representation of the steps involved in the production of dry and wet enamel formulations.**

The raw-materials selection is crucial for the development of good-quality enamels, as well as the use of high-purity materials has a great influence on the properties and durability of the final products. Thus, it is very important to consider the fineness, the grain shape, the manufacturing method, and the mineral composition of the chosen raw materials, as they all are important parameters to be kept under control when preparing enamel formulae[56, 57]. Raw materials can be both used as indispensable materials in the making of the frit or as mill additives in the preparation of dry and wet enamel formulae[58]. In the second case, the total additions rarely exceed fifteen per cent of the frit weight, but, also in this case, is still fundamental to use good-quality materials not to lower the quality of colour, resistance to

weathering, and adherence level[59]. In conclusion, it is possible to state that the quality of the final coatings directly depends on the grade of the starting raw materials.

### 1.3.1 The composition of enamels and raw materials

The raw materials used in the enamel industry can be mainly divided into six different groups, namely: refractories, fluxes, opacifiers, colours, floating agents, and electrolytes.

Refractories and fluxes represent the indispensable materials for the production of porcelain enamel coatings, as they constitute the enamel's vitreous matrix itself[7]. The refractories include acidic oxides, such as quartz and feldspar, that give body to the glass. The fluxes include raw materials such as borax, soda ash, and cryolite, that have a basic character and react with refractories to form the glass.

Opacifiers are used to give the enamels their usual opaque appearance[60] and they can be divided into two small groups: the classic opacifier agents (titanium oxide, zirconium silicate, tin oxide)[61, 62], which have a quite refractory behaviour, and the aiding opacifier agents (cryolite, fluorspar), which make the enamel more fusible and provide a certain degree of basic whiteness[63].

Colouring materials are mainly represented by mixed metal oxides, and they are commonly added in the preparation of the enamel formulae. These colours, or pigments, have a specific crystalline structure and are chemically inert and resistant to high temperatures[64]. Many of the most common pigments are spinels made of heavy metals, such as cobalt, lead, cadmium, and nickel[65]. As to give some examples, brown shades are often made by zinc iron chromite spinels, yellow shades can be achieved by using lead antimonates, cadmium sulfides, and nickel titanates, whereas blue shades are always created by using cobalt-based spinels[66-68]. Some of these pigments have always represented a reason of concern for public health (in particular cadmium-based pigments), though they can be classified as non-hazardous chemicals. Despite this fact, their use is strictly regulated as they can become a real threat to public health if they are released into streams, as chemical reactions could occur and release the toxic heavy metal from the inert non-toxic compound[69]. Colouring compounds, such as cobalt oxide, are also used to increase the degree of adherence between the enamel layer and the metallic substrate, as they are involved in some critical electrochemical reactions that lead to the formation of a strong bond between the glassy matrix and the metallic substrate[70].

The floating agents, also called suspension agents, are used in the preparation of wet enamel formulae, as they are able to keep the enamel particles suspended in liquid media, whereas electrolytes (such as sodium nitrite and sodium aluminate) help the enamel powder to be properly suspended in the liquid medium, avoiding

possible agglomeration phenomena of the clay used as a suspending agent[43, 71]. TABLE 1-1 reports and describes the main raw materials used in the frit-making process. For each one of them, the main functionalities are claimed.

**Table 1-1: Raw materials materials used in the production of enamel frits; adapted from [41].**

| Component | Mineral | Function |
|---|---|---|
| $SiO_2$ | quartz<br>feldspar | Refractory and hardening compound.Increases viscosity and chemical resistance. |
| $B_2O_3$ | borates | Flux agent. Reduces viscosity and increases surface hardness. |
| ZnO | zincite<br>wurtzite | Flux agent. Lowers the expansion coefficient. |
| $Na_2O$<br>$K_2O$<br>$Li_2O$ | albite<br>feldspar<br>spodumene | Alkaline oxides and flux agents. Lower the glass melting temperature and increase brilliance. |
| $Al_2O_3$ | feldspar<br>corundum | Amphoteric oxide.Increases chemical, mechanical resistance, and viscosity. |
| BaO<br>CaO<br>MgO | baryte<br>calcite dolomite | Alkaline-earth compounds. Lower the softening point of glasses and reduce their elasticity. |
| $ZrO_2$ | zirconia | Opacifier. Improves resistance to acids. |
| $TiO_2$ | rutile<br>anatase | Opacifier. Increases resistance to acids. |
| $Sb_2O_3$ | antimonite | Opacifier. Improves enamel's resistance to acids. |
| CuO | copper oxide | Adherence agent. Improves adherence. |
| CoO | cobaltite | Adherence agent. Guarantees a strong bond with the substrate. |
| NiO | niccolite | Adherence agent. Produces a structure with very few big bubbles. |
| $MnO_2$ | manganese dioxide | Colour. Oxides the impurities in the smelting phase. |
| $P_2O_5$ | apatite | Additive. Improves colour stability and reduces chemical resistance. |
| $F_2$ | fluorite | Opacifier. Softens glass and influences opacity. |

Silicon dioxide is the most important acidic oxide of the enamel composition as it is able to vitrify under the action of fluxes in a wide range of temperature. This component is introduced in the formulation in the form of quartz, quartz sand, feldspar, or feldspathic sands. Silica-rich coatings have great resistance to chemicals

and an increased hardness, but, on the other side, they show a very high firing temperature and a lower spreading ability[72]. In a second place, it is important to remark the important role of boron, which is introduced in the form of boric acid or sodium borax, and it works as a flux agent. Other important components of enamels are basic oxides, such as sodium, potassium, calcium and strontium oxides, which are able to lower the softening point of the frit formulation and to increase the impact resistance of the final coatings. Last but not least, adherence oxides are key elements to be added in the formulation of the frit, as they are responsible for the strong bond between the coatings and the metal surface[73, 74].

### 1.3.2 Classification of enamel compositions

**Enamel formulation for sheet iron and steel** Sheet iron or steel enamels can be classified into four different groups, namely: i) ground coat enamels, ii) white cover enamels, iii) coloured enamels, and iv) special application enamels. Sheet iron enamels are usually designed to fire at temperatures between 760 °C and 871 °C in a few minutes[41].

Ground-coat enamels represent the first layer which is deposited on the metal substrates; thus, they are formulated to develop a strong bond with the metal and prepare the surface for a subsequent enamel application. Ground-coat enamels usually contain adherence oxides, and their typical formula is made of feldspar, borax, quartz (82%), soda ash (7%), soda nitre (4%), fluorspar (5%), cobalt oxide (0.5%) and manganese dioxide (1.5%). The most important advancement in terms of new ground coats development is dated back to the 1970's, when clean-only ground coats were introduced into the market. These formulations, containing a high level of alkali oxides, were suitable for application on steels substrates that had not undergone to a pickling step but a cleaning step only[75]. As described before, ground coat enamels should guarantee good adhesion with the substrate layer, whereas cover coat enamels should give protection against external agents and provide the desired aesthetical features.

Cover-coats enamels can be mainly divided into white cover coats and coloured cover coats, but all of them should be processed at lower temperatures with respect to ground coats, in order to avoid possible blending. As regards white cover coat enamels, extensive changes have taken place in the past 20 years. The first great change was represented by the development of high antimony super opaque enamels, which greatly reduced the need for a high quantity of mill-added opacifiers (the opacifiers content was reduced from 10% to 2% in weight with respect to the enamel formulation)[45]. The most important advancement in this field was reached during World War II, when titanium-opacified white enamels were developed. This formulation, based on titanium, showed good covering power and superior acid resistance[71]. After World War II, enamellers put great efforts in developing high-

quality white enamels and they discovered the importance of titania crystallization form on the reflectance of white enamels coatings[76-79]. Coloured sheet-iron cover enamels are generally based on a transparent or semi-opaque frit, as the colours are added at the mill (for blue and black enamels the colouring agents are usually embedded in the frit making formulation). The glaze composition used as the basis for coloured enamels is very similar to the one used for the preparation of ground coat enamels, with adherence oxides left out, but it contains slightly less fluorspar and soda ash. An example of a typical coloured frit formulation is composed of 80% felspar, borax, and quartz, 5-10% soda ash, 3-8 % soda nitre, 3-7% fluorspar, 5-6% cryolite. The mill addition consists of 5 - 7% of colored clay[41].
As regards special application enamels, it is possible to make an important example over others: pyrolytic enamels[80]. Special enamels used in the production of pyrolytic ovens are very widespread and they are developed to guarantee a good food soil cleanability and great acid resistance. Their composition is mainly tailored by modifying the silica content and it should consider the necessity to guarantee good adherence with the substrate. One of the main issues related to the production of pyrolitic enamels is the development of enamels formulae suitable for application on pickle-free steel substrates, but, at the present moment, good alternatives are present on the market[80, 81].

**Enamel formulations for alumnium alloys** The introduction of aluminium enamels has opened an entirely new market for porcelain enamel coatings[82, 83]. These enamels can generally be classified under four groups: i) lead-bearing, ii) phosphate glass, iii) barium type and iv) vanadium pentoxide type[41]. The lead-bearing enamels are usually high in lead content (10 to 30%) and are lead borosilicate glasses containing small amounts of alkali, colours, and opacifiers. These enamels have been developed for decorative purposes mainly, but they show good acid resistance and satisfactory mechanical properties[84]. The phosphate enamels are not generally resistant to alkaline chemicals, but they melt at very low temperatures, and they show good chemical durability. The high barium glasses, on the other side, cannot be produced with low fusion temperatures. As regards vanadium pentoxide-based enamels, it is necessary to underline that this compound is necessary to improve the mechanical adherence of the enamel layer on the aluminium substrate, and for this reason is very widespread[85]. The major differences between enamels for steel and aluminium substrates are the enamel formulation itself, the firing temperatures at which the formulation is able to vitrify, and the formulation of the enamel slips. In steel enamels, clays are used to suspend the frit particles in the slip, whereas in the case of aluminium enamels clays cannot be used as they difficultly melt into the glass, but they are substituted by sodium and potassium silicates[86].

### 1.3.3 Frit production techologies

Nowadays, enamel frits are produced by efficient and automated processes: almost all production phases are handled mechanically and many control segments are installed to keep production deviations at a minimum level. The frit making process may be divided into three different phases: raw materials preparation, smelting, and frit handling. FIGURE 1-3 summarizes the main steps involved in the frit making process.

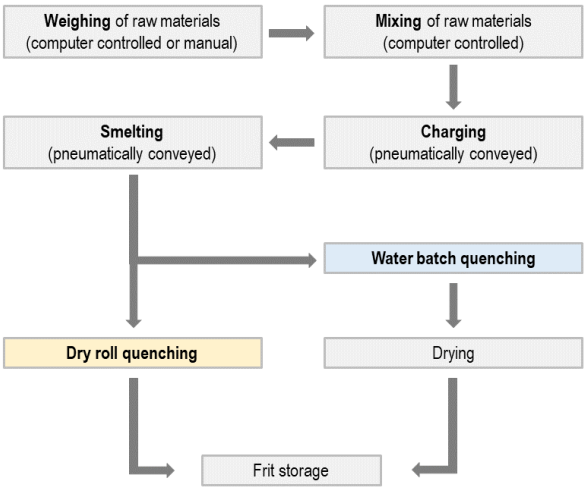


**Figure 1-3. Flow sheet for frit making.**

Raw materials are stored in silos and are weighted by computer-controlled equipment. The weighting step is then followed by the mixing phase, which greatly influences the quality and the homogenization level of the smelt: an incomplete mixing of raw materials requires a longer smelting time to obtain a homogenous vitreous mass, as fluxes and refractories would need longer times to react intimately. A good mixing phase is also beneficial in the development of uniform colour and opacity[1].

The second important phase of the frit production process is the smelting of the frit, which is exploited at temperatures up to 1350 ˚C[87]. During this phase, the more fusible materials melt first, giving the batch a wet appearance and hindering the loss of the more volatile compounds, which are slowly absorbed by the melt. This processing step is supported by many different chemical reactions, such as interaction of acids and bases, decomposition, fusion, compound formation,

dissolution, and crystallization. On heating a raw enamel batch, the first reaction that should be noticed is the decomposition of the borax (dehydration), which takes place between 60 ˚C and 260 ˚C[41]. The crystallization water of the borax is given up as steam and this process causes a considerable agitation in the batch. The molten borate readily dissolves metal oxides and it initiate chemical reactions among the other constituents; if alkali or alkaline earth carbonates are present, they decompose into carbon dioxide gas and oxides, which are strong bases. At temperatures higher than 851 ˚C, the soda ash (sodium carbonate) melts and becomes an active flux, attacking the more acid constituents. If fluorides are present in the batch, they are taken into solution with the evolution of volatile fluorides[88, 89]: thanks to these compounds the melt increases its attack power on feldspar and quartz. This phase of the smelting process is commonly known as the *glass-forming* period, mainly because many combinations reactions take place[90]. Two different types of kilns can be used for the smelting phase: the rotary kiln and the basin kiln. The rotary kiln is a cylindrical discontinuous smelter that turns slowly along its horizontal axis. On one side of the kiln, it is possible to find the hole where the burner is inserted and withdrawn to maintain the optimal smelting temperature over time, whereas, on the opposite side of the drum, another hole is present to allow exhaust gases to escape. Once the raw materials are smelted appropriately, the fused mass is unloaded and rapidly cooled to form the frit. On the other side, the rotative basin is a continuous smelter with a very high capacity. In this case, the raw materials are fed from one side of the kiln and are kept at the right temperature by electric elements or by methane/oxygen burners, then the smelt is discharged and cooled in the form of flakes by the use of four rotating cylinders.
After quenching, frits may be dried or may not be dried, depending upon the formulation of the enamel formulation. If the enamel will be applied by wet methods, the frit won't undergo a drying treatment, oppositely it will be dried and stored in appropriate conditions.

### 1.3.4 Enamel milling and mill additions

**Milling procedures and parameters** The milling of enamels is an operation requiring careful control since it affects the working property and the quality of the finished coatings[58]. In this phase, contaminations from heavy metals should be avoided, in particular when dealing with white and light-coloured enamels. The milling operations can be carried out in a dry environment on in wet conditions (in presence of water), dependently on the chosen application technique. The milling (or grinding) process is the first step to be carried out for the preparation of all enamel formulae, as it involves the reduction of the frit granulometry by grinding it against balls of a harder material at a controlled speed. The rotating speed of the mill is a primary parameter to be kept under control, as too slow speeds lead to an incorrect

milling and an overheating of the batch, whereas too high speeds reduce the charge-balls contact points as the balls are thrown to the walls of the mill itself and no milling power can be exploited[91]. The charge of the mill is another important parameter to keep under consideration: the balls should fill one half of the mill's volume and they should be covered by the material to be grinded in order to improve the efficiency of the process[92]. The quality of the grinded material is determined by the balls number and dimensions: too few balls allow the material to form some cushions that result in very little grinding effect, whereas too big balls greatly reduce the possible contact points between the materials and the balls themselves. The fineness of the enamel powder is another parameter to be strictly controlled, as it affects the colloidal behaviour of the slip in the subsequent application processes. The optimal fineness values are determined by the type of deposited layer (ground-coat or cover coat) and by the chosen substrate: too coarse enamels tend to produce a rough surface, whereas too fine enamels tend to overfire more readily[93]. In case of wet enamel formulations, specific gravity is another parameter of great importance, and it should be kept constant and controlled: if the slip is milled too fine, for example, the set-up is greater, and more water is required for the same thickness in application. TABLE 1-2 summarizes the typical milling specifications for different types of enamels and support materials. The fineness of grinding is tested by using the BAYER funnel, that can be equipped with different kind of sieves. The percentage of particles having dimensions bigger than the sieve mesh is calculated multiplying the read off units in the measuring column by a 1.7 factor.

**Table 1-2. Typical milling specifications for different types of enamels and metallic substrate materials; adapted from [41].**

| Type of enamel | Specific gravity ($g/cm^3$) | Fineness* (on 100 g) |
|---|---|---|
| **Sheet iron ground coat (dipping)** | 1.58 – 1.66 | 7-20% on 200 Mesh |
| **Sheet iron ground coat (spraying)** | 1.65 – 1.75 | 6-10% on 200 Mesh |
| **Sheet iron cover coat** | 1.70 – 1.78 | 2 % on 200 Mesh |
| **Aluminium enamel (leadless)** | 1.90 – 2.00 | 1 % on 325 Mesh |
| **Cast iron white cover coat (leadless)** | 1.80 – 1.90 | 2-6% on 200 Mesh |

*** 200 Mesh corresponds to 74 µm; 325 Mesh corresponds to 44 µm .**

**Mill additives** The milling process often requires adding the batch some additives that can be classified into four different groups: floating agents, opacifiers, colours,

and electrolytes[91]. TABLE 1-3 shows some examples of typical mill additives for sheet iron, steel, and cast iron, also describing their effect on the enamel layer.

**Table 1-3. Mill additions for wet process enamel frits for sheet iron, steel, and cast iron substrates; adapted from [41].**

| Mill additive | Amount added (%) | Effect |
|---|---|---|
| **Clay** | 2 – 8 | Suspend glass, hardens biscuit |
| **Bentonite** | 0 – 0.5 | Suspend glass, hardens biscuit |
| **Silica** | 0 – 15 | Increases refractoriness and resistance to heat and chemicals |
| **Magnesium carbonate** | 0 – 0.25 | Moderately softens biscuit |
| **Potassium carbonate** | 0 – 0.5 | Hardens biscuit |
| **Zinc oxide** | 0 – 2 | Fluxes enamel for lower firing temperatures |
| **Opacifiers** | 0 – 4 | Produces opacity in fired enamel |
| **Colouring agents** | 0 - 4 | Produces colour in fired enamel |

Floating agents are used to keep the frit particles into suspension. Clays, bentonite, colloidal silica, and gums are the most used materials in this regard[94]: clays and bentonites are often used together in order to make the slip more susceptible to the action of electrolytes[95], colloidal silica is usually implemented for thick one-coat enamels, whereas gums are useful in producing high acid-resistant enamels, as they do not alter this property as clays tend to do. As regards opacifiers, tin oxide and zirconium oxide are the most common additives, although zirconium oxide is much cheaper and just as effective. Mill-added opacifiers have never been used in dry process enamels as they tend to give a mottling effect[96]. Colours are the other important class of mill additives that should be discussed. In general, any colour is available for enamels, but dark blues and blacks are usually obtained using coloured frits, whereas opaque colours and pastel colours are realized by using a semi-transparent and a semi-opaque frit, respectively. The last class of mill additives that needs to be introduced is represented by electrolytes[97]. These compounds, such as sodium carbonate and magnesium sulphate, are soluble and they are usually added to the batch to control the properties of the slip[98, 99]. The necessity to add some additives during the milling process cannot be considered as a predetermined factor, but it usually relies on the operator's experience [41].

## *1.4 Enamelling support materials and pre-tretament processes*

Ancient civilizations were used to enamel precious metals, such as bronze, gold and silver, but the industrial enamelling makes use of steel, aluminium, cast iron, and glass[1]. Ferrous materials are the most traditional substrates as they are prone to degradation and for this reason they need to be protected against corrosion. In recent times, enamelling has also been applied to other supports, such as aluminium, copper, aluminized steel, and even stainless steel, as the vitreous layer gives these materials an extra plus in terms of protection and aesthetical features. The quality and the chemical composition of the base metals have an important influence on the quality of the produced enamelled material, as many chemical reactions should happen occur between the vitreous layer and the metal substrate. In addition to that, the quality of the pretreatment process directly influences the quality of the final coating.

### 1.4.1 Enamelling substrate materials

**Cast iron** Cast iron is a ferrous alloy with a carbon content higher than 2.14%. Its mechanical and physical properties mainly depend on its chemical composition and internal microstructure. The combined and uncombined carbon percentages play an important role in determining the suitability of this material for enamelling. White cast iron is high in combined carbon, whereas grey cast iron is high in uncombined graphitic carbon[100]. An increase in the combined carbon of cast iron, often present as cementite, results in an increase of the alloy hardness but is detrimental to the quality of the enamelling process. As defined by the UNI 8762 standard, only grey cast iron can be enamelled: thus, it is necessary that the iron has a pearlitic or pearlitic-ferritic matrix with a graphitic structure, and the presence of cementite must be avoided to counteract the presence of defects on the enamel surface.

**Sheet iron and steel** The choice of the right steels for porcelain enamelling is one of the most important factors to be taken under consideration. A good enamelling steel should be free from surface defects, and it should have a homogeneous composition. The chemical composition and the physical characteristics of suitable steels are listed in the EN 10209 standard[101], which divides them into three different categories: i) carbon-steels, ii) decarburized (or low-carbon) steels, and iii) interstitial-free steels. The maximum carbon percentage for these steels is 0.05%, 0.008%, and 0.02%, respectively[102]. Carbon steels are aluminium killed steels and they have been developed to replace enamelling iron; they perform well with both ground-coats and two coat/two fire applications. Decarburized steels perform in an

excellent way, and they are being used in all types of today's enamel systems, as the low carbon content eliminates primary boiling and consequent defects due to the evolution of carbon monoxide and dioxide during firing. Interstitial steels are products in which all the carbon and nitrogen are combined with an alloying element; they are used mainly for their superior drawing ability. Conventional enamelling is usually made on cold-rolled steels, which were developed in the 1960's by the Bethlehem Steel Corporation in 1956. Cold rolled steels should be used for non-critical appearance components, as they tend to cause boiling defects in the enamel layer. The most common cold rolled steels of enamelling grade are listed by the EN 10209 standard. DC01EK, DC04EK, DC06EK and DC07EK are all suitable for conventional enamelling (1coat/1fire, 2coats/2fire) and they differ from the level of drawing ability. DC03ED, DC04ED, and DC04ES are instead suitable for 2coats/1fire enamelling processes; DC04ES is principally intended for wet/powder or wet/wet applications after only degreasing, whereas the other two steel types are compatible for direct on white enamelling. Hot rolled steels have a high susceptibility to the formation of defects such as fish scales[103] (e.g., formation of blisters on the enamelled surface caused by oversaturation of hydrogen at the metal–enamel interface[104]); thus, their use is limited to special applications where a given strength is required, such as in the case of water heaters, and it is usually applied only on one side of the sheet to promote the removal of hydrogen from the unenameled side[105].

In addition to traditional steels, it is also important to underline that the enamelling process can be carried out on aluminised steel as well. Aluminized steel is made applying a layer of aluminium of about 15 μm on a sheet of interstitial free steel by electrolysis. The combination of steel and aluminium has several advantages over decarburized steel as the finished product is more corrosion proof and the enamelling process only requires one application and one firing steps at a significant lower temperature (560-580 ˚C for aluminium and 830-860 ˚C for steel). This material also presents some advantages over traditional aluminium substrates, as it shows higher mechanical properties.

**Aluminium and alunminium alloys** Aluminium shows some peculiar characteristics, such as lightweight, malleability, and corrosion resistance, which make it extremely interesting from a technological point of view[82, 83]. In fact, aluminium does not form rust, but it requires the use of low-melting enamels, and it shows lower mechanical properties with respect to the steel substrates[106]. Aluminium alloys can be mainly divided in two groups: the heat-treatable alloys and the non-heat-treatable alloys. The enamelling process converts the common alloys to the fully annealed temper and the heat-treatable alloys to the as-quenched temper. Another important classification of aluminium alloys is made on the alligant elements, as the chemical composition of the aluminium alloy greatly influences the enamelling process and the feasibility of the deposition itself. The most common

aluminium alloys for enamelling are the 3003 and 4006 series alloys, but, generally, a low content of magnesium is required to avoid adherence problems[107].

**Other support materials** Steel, cast iron and aluminium alloys are the most common substrates for the enamelling process, but other metallic substrates can be easily enamelled as well. Among the more than 60 possible alloys, it is possible to list Incoloy, Monel, Hastelloy, and Jetalloy[108, 109]. These alloys are usually treated by sand, grit or shot blasting before the enamel application to make the surface rougher and more active.

### 1.4.2 Pretreatment processes for metallic support materials

All metals should be properly prepared for enamelling to achieve a good bond with the enamel layer and obtain a defect-free surface. Metal pre-treatments are mainly exploited for two different reasons: cleaning the surface from rolling oils, rust and organic contaminants, and giving the metal a slightly rough finishing to promote adherence with the enamel layer[110]. Surface pre-treatments can be mainly divided in chemical processes and mechanical methods; chemical treatments are essential for the preparation of steel and aluminium panels, whereas mechanical methods, such as sanding, are used for the preparation of cast iron and steel substrates only. Precisely, mechanical sanding and blasting are also exploited for the treatment of heavy gauge steel elements, such as chemical vessels. Chemical treatments usually consist of many different steps such as immersion in alkaline baths, pickling in acid baths, rinsing, and drying. Enamellers put great efforts in reducing the economic and environmental impact of these treatments: the development of more efficient systems and new metal substrates has led to a reduction of the baths number, the operating bath temperature and the concentration of the used chemicals.

**Pretreatment process for cast iron substrates** The preparation of cast iron surfaces is exploited by mechanical action only[111]. Cast iron pieces, even with the best foundry practice, usually present many surface irregularities that should be eliminated[112]. For this reason, blasting is useful in cleaning the surface from production contaminants and open the residual subsurface porosity, which could cause important defects to the enamel layer[113]. The blasting process is sometimes followed by an annealing treatment at 800–850 ˚C, which is useful to improve the enamelability of high-cementite cast irons.

**Pretreatment process for sheet iron and steel substrates** The pre-treatment of steel substrates is much more complicated, as it consists of many different steps. The first step to be exploited is cleaning of the surface, also known as *degreasing*, which consists in cleaning the metal with aqueous solutions of alkaline detergents to

remove oils and greases. The cleaning procedure is commonly exploited at 40-70 ˚C for 5-10 minutes by immersing the metal piece into the cleaning bath[114]. A good degreasing solution should be alkaline (with a pH value between 10 and 13), and it should have a good saponifying and emulsifying action: typical components of commercial cleaners are sodium silicates, sodium carbonate, and metal hydroxides (which act as a source of alkalinity)[115]. Nowadays, traditional chemical cleaning is sometimes replaced by electrolytic cleaning, a rapid cleaning procedure exploited with the aim of a current flow[116]. Chemical cleaning is then followed by a *pickling* step, or immersion of the metal piece in an acid solution to eliminate superficial metal oxides[75, 117]. The most common pickling solution is made of sulfuric acid in 5 – 10 wt.% concentration and it is ordinarily used at 65–75 °C for 10 – 30 minutes[1]. The immersion time in the pickling solution greatly influences the final roughness of the metallic substrate and its adherence level with the enamel layer. The pickling step must be followed by a deep rinsing in water and by immersion in a neutralizing bath. The neutralizing bath, a hot aqueous solution of $Na_2O$, is added to completely remove all the traces of acid. As a last step, the cleaned metal substrate is appropriately dried and prepared for enamel deposition.

**Pretreatment process for aluminium alloy substrates** The successful application of enamel on aluminium is influenced both by the chosen aluminium alloy and by the quality of the pre-treatment process. As a first thing, aluminium substrates should be cleaned from dirt, greases, and oils by using an alkaline degreasing solution at 40-60 ˚C in concentrations of about 20-40 g/L for times up to 15 minutes[41]. If necessary, aluminium substrates can be leached in an alkaline bath (10 wt.% NaOH at 70 ˚C for up to 5 min) to remove the natural oxide film, de-smudged in acid water (25 wt.% nitric acid solution) to remove adherent hydroxides, rinsed several times, and in some case pre-fired at about 400 ˚C to reform a uniform oxide layer[106].

## *1.5 Application, drying, and firing of enamel coatings*

The proper application of enamels on the substrates to be covered is an extremely important operation, as the quality of the final coating strongly depends on it. The application of enamels can be exploited in the wet or in the dry form, thus with or without the aid of a liquid medium, respectively. In case of wet application, the enamelled material should undergo a drying step before firing to ensure a complete evaporation of the liquid medium and avoid possible reboiling of the vitreous layer.

### 1.5.1 Application methods

The available application techniques mainly differ from the starting state of the enamel formulation. Thus, dry milled enamel powders are used for dry-state application methods, whereas wet enamel slips are needed for wet-based application techniques[90].

#### *1.5.1.1 Wet application methods*

Among all the existing wet coating techniques, the most important methods are the following: dipping, flow coating, wet spray coating, wet electrostatic coating, and electro-coating.

**Dipping** The dipping or immersion application technique is commonly exploited to apply ground layer enamels on metallic elements with complex shapes, such as washing machines, boilers, and chimney pipes[118, 119]. This method involves the immersion of the metallic product in a tank containing the enamel slip and the subsequent removal of the covered piece with a controlled speed and angle to drain away the excess enamel slip. The dipping method guarantees an optimal coverage of the metal surface, but it could sometimes lead to enamel sagging (defect in which wavy lines of increased vitreous enamel thickness are evident due to flow or slippage of the coating)[120].

**Flow coating** The flow coating method takes advantage of a similar principle (with respect to the dipping method), but, in this case, the enamel slip is poured over the surface by means of pressurized systems or using gravity only. This method is commonly used to apply ground-coats enamels on very-large hollow tubular elements, such as stove pipes and boilers[121]. The industrial deposition system is very simple, and it consists of an application line with hooks that are designed to transport the piece and turning it during the enamelling process to avoid sagging.

**Spray coating** The spray coating technique is one of the most ancient application methods. In this case, the slip is atomized by air pressure guns and applied to the

piece to be covered. The principal function of the air pressure gun is to reduce the enamel slip into small drops while aiming them towards the piece to be covered with a jet of compressed air[122]. The air and the enamel slip can be mixed inside or outside the gun: in the first case it is possible to use less air and achieve a high output rate, whereas in the latter case a finer mist is produced, and an excellent surface finishing is achieved. A possible variant is the *pressure spray coating*: here the gun is fed with a pump to increase the productivity rate and/or better handle a very dense enamel slip.

**Wet electrostatic coating** The natural evolution of the spraying technique is represented by the wet electrostatic coating method. In this case, the slurry particles are electrically charged by passing through an intense electrical field and they are sprayed onto a metal having an opposite charge. Once the particles come in contact with the metal, they discharge immediately and insulate the part they have covered, so that the following enamel particles are attracted by uncovered areas: this way it is possible to obtain homogeneous coatings also on complex shaped objects and to avoid huge material losses (called *over sprayings*)[1, 41]. This application method is very efficient, but its output is greatly influenced by humidity, enamel specific weight, and enamel fineness. A low specific weight and a correct fineness allow the enamel slip to be atomized at a lower pressure and to obtain a high-quality coating. Summarizing, the wet electrostatic method is simple to handle, and it guarantees good results in terms of covering efficacy and aesthetical appearance.

**Electro-coating** The electro-coating process is one of the most recent industrial methods to apply enamel coatings on metallic pieces. The mechanism underneath this new technology is based on the migration of charged enamel particles in a water suspension towards a substrate having an opposite charge. Two electrodes are used to produce an electrical field, which convey they particles towards the metal to be covered[123]. This process is principally used for direct-on white enamelling, and it allows to obtain coatings with very uniform coatings in thickness. The main advantages of this method are: i) the possibility to obtain a good coverage of edges and holes, ii) the creation of very smooth surfaces, and iii) the possibility to apply enamel to hollow parts and complex-shaped objects[124]. Despite the listed pros, this application methods embodies important drawbacks as, for example, the need for constant monitoring of the electrical properties of the enamel slurry and the occurrence of electrolytic reactions[125]. The electro-coating method can be exploited in two different configurations: an in-line layout, where a conveyor serves different baths (e.g., subsequent process stages), and a carousel layout, where a central rotating device move the pieces; the first configuration is suitable for mass-production as it requires big investments in terms of costs and spaces, whereas the latter configuration is used for small series productions.

**Screen process** The screen process relies on forcing an enamel paste through a silk or metal lawn onto the ware, to deposit a suitable amount of formulation on the piece to be covered. The enamel must be first made into a thick slip with an oily or water based screen printing medium by milling at extreme fineness (particles should not be bigger than 70 μm). To apply the enamel. The lawn is laid over the piece to be enamelled, the slip is placed on the lawn, and by means of a rubber squeegee, it is forced through the lawn. The main advantages of this method are the possibility to apply different colours at one time and to finely control the thickness of the deposited layer by appropriately choosing the lawn and the viscosity of the enamel paste.

#### *1.5.1.2 Dry application methods*

Among the dry application methods, it is possible to underline the importance of the electrostatic powder technique and of the dredge coating (which is only used for cast iron enamelling).

**Electrostatic powder coating** The electrostatic powder coating method is one of the most widespread application techniques all over the world and it is based on the same operating principle as for the wet electrostatic method but transposed in dry conditions[126, 127]. In this case, enamel particles are coated with an organic envelope, which prevents hydration and ensures a correct deposition onto the metal substrate[128]. This process is highly effective for application on flat parts, and it is considered very useful in reducing material wastes when a proper suction system is integrated[129]. This method is generally used to produce steel-based ovens and kitchen stoves, oppositely it is not suitable for application on big components.

#### *1.5.1.3 Application cycles for steel, cast iron, and aluminium*

The application methodologies, described in the previous paragraph, were all developed for application on steel substrates, although some of them are also suitable for application on aluminium or cast iron. Regardless of the substrate, it is important to underline that the glazing process is almost never limited to the application of a single enamel layer, but often provides the application of a multi-layer coating[130, 131]. Multi-layered wet enamelling is the most common coating method, and it consists in the application of a ground-coat layer and a cover-coat layer. The need for a two-layer coating is particularly necessary when dealing with common cold-rolled steels, whereas direct-on applications show better results with decarburized steel substrates[132]. In the last years of the 1970's, multi-layer enamelling was experimented also in dry-based application systems: this way enamellers were able to eliminate drying treatments and exploit important coast savings[133]. Thanks to these experiments, multi-layer dry powder enamelling is now used also for application on pickling-free substrates[134]. TABLE 1-4 shows some examples of industrial enamelling cycles. As a rule, it is possible to classify three

different cycles: the 2A/1F (2 application – 1 firing) cycle, the 2A/2F (2 application - 2 firing) cycle, and the 3A/2F (3 application – 2 firing) procedure.

**Table 1-4. Main application procedures used in the enameller industry.**

| Procedure | Layer types | Enamel type |
|---|---|---|
| **1A/1F** | Direct-on wet-based | W / C / D / B |
| **1A/1F** | Direct-on dry-based | W / D / B |
| **2A/2F** | Ground + cover layers | W / C / D / B / SF |
| **2A/1F** | Special ground + cover layers | W / C |
| **3A/2F** | Ground + intermediate + cover layers | W / C |

***W: White, C: Coloured, D: Dark, B: Black, SF: Self-Cleaning**

### 1.5.2 Drying and firing of enamels

The application of enamel is followed by an appropriate heat treatment, called *firing*, which allows the enamel to completely vitrify. In case the enamel is applied in the liquid state, pieces need to be appropriately dried before firing. The drying treatment makes water evaporate slowly: a sudden evaporation of the watery part of the enamel formulation would lead to boiling, blistering, and formation of orange peel on the final coatings. In the following paragraph the main parameters and factors to be taken under consideration will be described.

#### *1.5.2.1 Drying of enamel coatings*

Drying of enamelled pieces is exploited into drying tunnels, which are heated by gas or by recycled hot air coming from the firing kilns[135]. The heat is transmitted by conduction, convection, radiation or a combination of the systems above. Forced convection guarantees a limited stay of the pieces into the drying tunnel as it is able to absorb large amounts of humidity coming from the piece surface very, but it could sometimes lead to the contamination of the enamel surface. On the other side, radiation systems are more reliable in terms of coatings quality and energy savings.

#### *1.5.2.2 Firing of enamel coatings*

*Firing* is the last step involved in the production of enamelled materials. This process is very important as it includes many physical and chemical reactions occurring between the enamel layer and the metal substrate. The development of adherence between these two materials is strictly correlated to the optimization of the firing treatment. Firing temperatures range as a function of the substrate: steel pieces are

usually fired at temperatures ranging between 760 and 870 ˚C, whereas aluminium substrates, due the low melting point of aluminium itself, are heat-treated between 420 and 570 ˚C. As regards sheet iron, ground coats are fired at higher temperatures (760-870 ˚C) with respect to the cover coat layers (730-840 ˚C) and the firing times are always between 1 and 4 minutes. Aluminium enamels are fired at lower temperatures, but the firing times are longer with respect to steel enamels (5-7 minutes). Within certain limits, the firing temperatures and times can be varied and modified in order to optimize the firing treatment for every product, but it is important not to exceed lower and upper firing temperatures limits, otherwise the enamel would not develop adherence with the metal, or it would over-fired, respectively. TABLE 1-5 shows typical firing temperatures and times for different type of enamels and support materials.

**Table 1-5. Typical firing temperatures and times for different types of enamels and substrate materials; adapted from [41].**

| Type enamel/support | Temperature (°C) | Time (min) |
|---|---|---|
| **Sheet iron ground coat** | 760 – 870 | 1 – 4 |
| **Sheet iron cover coat** | 730 – 845 | 1 - 3 |
| **Wet process cast iron** | 620 – 760 | 10 – 15 |
| **Dry process cast iron** | 815 – 930 | 1 – 5 |
| **Aluminium enamels** | 430 - 570 | 5 – 7 |

The firing step is usually exploited in kilns where the radiation effect, generated by combustion or by electricity, is used to transfer heat to the pieces to be fired[136]. Kilns are generally equipped with conveyors as the firing chambers are designed to make the most efficient use of the heat. The commonest kilns are the U-shaped ones: the enamelled materials exit in the direction opposite to that taken by the material entering, which is then pre-heated by recycling heat coming from finished products.

#### *1.5.2.3 Physical considerations and theory of adherence*

The firing of enamelled materials involves the melting of the enamel and also many different physical and chemical changes. The glass-metal reactions, occurring during firing, are the basis on which adherence is based occur. The adherence mechanisms are still quite unknown, but important contributions have been identified by enamellers. The importance of oxygen in the early stages of firing is widely recognized: oxygen ions are indeed necessary to induce the iron atoms to give up electrons and move away from the metal surface. As a result of this process, the

cathode area, negatively charged, attracts positively charged ions from any other element that is lower than iron in the electromotive series of element[137]. Good adherence requires the presence of the so-called *adherence oxides*, such as cobalt oxide, which is reducible by the base metal and have the tendency to share oxygen with iron ions forming an iron-rich area close to the glass-metal interface[138]. FIGURE 1-4 shows the main steps involved in the firing of enamelled objects.

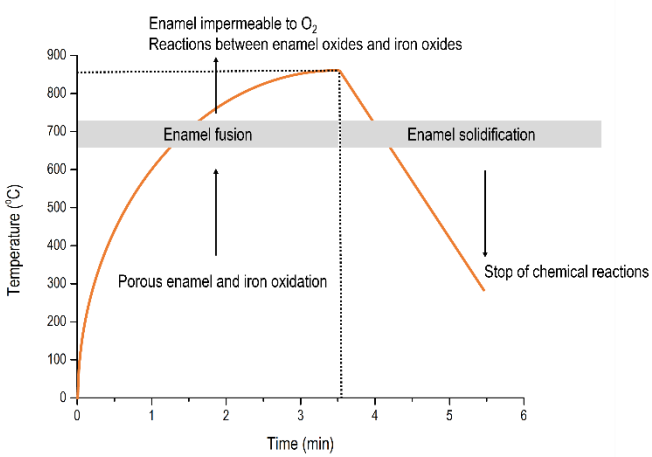


**Figure 1-4. Adherence mechanism - enamel firing curve for steel substrates.**

The adhesion of the enamel layer on steel substrates is achieved by means of chemical and electrochemical reactions that take place during the firing and cooling cycles. The first stage, ranging from room temperature up to 550 ˚C includes the oxidation of the support. The moisture and the oxygen in the furnace penetrate the porous enamel layer and oxidise the iron in the steel, creating a layer of iron oxide at the enamel/steel interface. The second stage, occurring between 550 and 830 ˚C includes the enamel fusion and the stabilization of the iron oxide layer. Here, the enamel softens until fusing and the gases exchange trough the coating is reduced to minimum. The third stage, occurring at temperatures around 800 ˚C includes the support corrosion and the formation of dendrites at the enamel/steel interface. In this step, chemical redox reactions take place between the metal oxides in the enamel and the iron oxide layer leading to the precipitation of Co-Fe alloys at the interface and the formation of dendrites. The fourth stage, occurring during the cooling phase, implies the solidification of enamel, and the stop of all reactions[41].

The firing treatment leads to the formation of an indissoluble bond between the enamel layer and the substrate, but it also represents the origin of the typical closed-porosity structure of all porcelain enamels. FIGURE 1-5 shows the typical internal

microstructure of a porcelain enamel coating made of three different layers, namely, the ground coat, the cover coat, and the top-coat. All the three different layers are enamels, but they mainly differ in chemical composition, chemical durability, surface aspect.

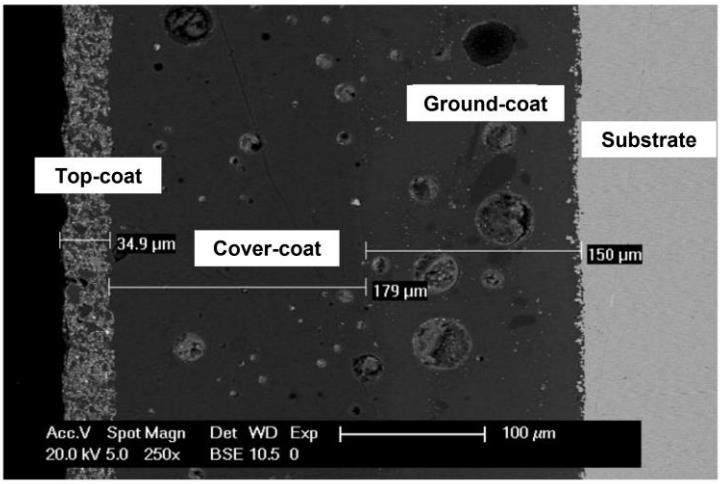


**Figure 1-5. Typical three-layers enamel cross-sectional micrograph, adapted from [139].**

The formation of the bubble structure can be mainly attributed to the combined action of the kiln atmosphere and evolution of gases emerging from the substrate, but it also depends on the frit fineness and firing times[140]. As an example, an increase in the enamel's grain size leads to the formation of bigger bubbles, the same effect being also caused by an increase in the firing times. The typical closed-porosity structure is a desirable feature as it gives the enamel a certain elasticity, but defects in the form of very big bubbles (caused by high furnace humidity or incomplete drying of the enamelled material) should be avoided[141]. Enamelling of sheet iron involves the evolution of hydrogen, water vapour, carbon monoxide, carbon dioxide and nitrogen at temperatures lower than 649 ˚C, whereas carbon monoxide, carbon dioxide and nitrogen are evolved at higher temperatures.

## *1.6 Functional and aesthetical properties of enamel coatings*

Porcelain enamel coatings show very peculiar functional and aesthetical properties. The glassy nature of the matrix and the strong chemical/mechanical bond, existing between the enamel layer and the substrate, are the main reasons for the excellent thermal and corrosion protection properties of all porcelain enamels.

### 1.6.1 Thermal, optical, and physical properties of enamel coatings

Porcelain enamel coatings are resistant to direct flames and prolonged exposure to high temperatures: their incombustibility and heat resistance directly originate from the glassy nature of the enamel matrix itself, which also resists thermal shocks of over 300 ˚C[142]. All these properties make enamel coatings suitable for application in kitchenware and stoves production. In addition to that, enamel coatings are fireproof, and they do not release toxic gases in case of fire, thus being the perfect candidates for application in wall cladding of cruise ships, metro stations, and high-way tunnels. The formulation of enamels is a key parameter to be controlled in order to tailor the thermal behaviour of these coatings: a very low thermal conductivity can have a negative influence on their thermal shock resistance, as rapid cooling/heating is accompanied by a slow release of heat from the internal layers of the coating. In addition to that, the enamel's formulation also has a great effect on the thermal expansion coefficient of the coating, which should display a CTE (coefficient of thermal expansion) as close as possible to that of the underlying substrate to avoid cracking and detachment of the coating from the metal. In general, the thermal expansion coefficient of the metal is greater than enamel's one and this difference leads due the development of compressive deformations states in the coating[108].
As for the electrical properties, enamel has insulating characteristics and its electrical resistance is mainly a function of its thickness and its content in alkaline oxides. The electrical resistivity of enamel coatings increases with the thickness, but it is decreased by the addition of high percentages of alkaline oxides. Enamel coatings represent an important solution to protect metals from corrosion, but the main reason why they are still very appreciated mainly originate from their glossy appearance and the stability of colours over time. Porcelain enamels can be coloured in a wide range of glossy and opaque colours, and the resulting surface is very smooth and free from open porosities. Thanks to these features, enamels are poorly affected by degradation caused by atmospheric agents, UV radiation, and corrosive media, thus finding a wide range of applications in many high-duty technological products[143].

### 1.6.2 Chemical properties of enamel coatings

The protective properties of vitreous enamel coatings against aggressive chemicals mainly depend on the frit's chemical composition. The frit can be considered a complex alumino-borosilicate glass and its structure can be visualized as a network of $SiO_4$ tetrahedra containing a high percentage of alkali metals and alkaline earth metals. These alkali-based components modify and breakdown the basic network of the matrix and lead to a decreased resistance against acid chemicals, differently with respect to traditional glasses[5]. Nowadays, vitreous enamel coatings possess good acid resistance, which can be improved by mill additions such as quartz, zirconium oxide, and bentonite. On the other hand, enamels suffer most when they come in contact with alkaline chemicals, particularly when concentrations and operating temperatures are high. The improvement of enamels chemical resistance can be achieved in two different ways: by increasing the chemical-resistant frit portion over the total enamel formulation or by adding different types of additives during the grinding operations[144]. Some of the most used additives are quartz and colloidal silicon dioxide, but their concentration should not overpass a certain threshold not to make the enamel formulation too viscous. Many recent studies[58, 145] have also considered the effect of other additives, such as spodumene or potassium feldspar, on the enamel's chemical resistance, pointing out the basic attack mechanisms. In acid media, a localized attack seems to occur near the grain boundaries, in particular when lithium, sodium, and potassium-rich additives are concentrated in these areas of the matrix, whereas the alkaline attack always occurs in a generalized way[146]. As regards enamels resistance to alkaline substances, it is important to take under consideration hindrance to commercial detergents. Resistance to detergents is an often overlooked property, but it has some important implications when enamel coatings are used for application in washing machine tubs, bathtubs, shower floors, and hobs[147]. An optimal detergent resistance does not directly imply good resistance to alkalis and vice versa, whereas acid-resistant titanium-based enamels generally show good resistance to detergents[148]. In conclusion, enamels commonly show a high resistance to chemical agents, but their degree of resistance largely depends on the application purpose for which they are formulated. In general, it is possible to state that enamels are resistant to most solvents, acid, and neutral solutions, while they are easily attacked by solutions containing fluorides and strong alkaline boiling solutions (pH > 12). Their resistance to solvents makes them suitable to be used in environments where cleaning with aggressive detergents is carried out frequently, such as in road signs and architectural panels in stations and subways.

### 1.6.3 Corrosion protection properties of enamel coatings

Vitreous enamel coatings are very appreciated for corrosion protection purposes, as they provide excellent protection against aggressive media[149-151]. It has been largely demonstrated, by accelerated tests and electrochemical studies, that these coatings strongly resist to exposure in aggressive and corrosive atmospheres, offering a good barrier towards aggressive ions[152]. Vitreous enamel coatings, being free from defects and having an insulating nature, are perfect candidates in applications where high protection of the metal substrate is required, and they offer a valid alternative to the use of the most common standard polymeric coatings[153]. The protective properties of enamels strongly depend on their degree of porosity and internal microstructure: if the porosity inside the coating results to be interconnected, the protective features may disappear almost completely. In addition to that, the level of adherence between the coating and the metal is a key feature that influences the protection properties of these coatings[154].

### 1.6.4 Mechanical properties of enamel coatings

Porcelain enamels have a very hard glass surface, with high resistance to shocks, scratches, abrasion, and wear. The hardness of enamels is comparable to that of glass, and it falls between grades 5 and 7 on the Mohs scale. Abrasion resistance is a particular property of enamels, although the fragile nature of the coatings can, in some cases, lead to the removal of small flakes and the opening of their intrinsic porosity, with a consequent decrease in their protective properties. For these reasons, many attempts have been made over the years to improve the abrasion resistance of these coatings[155]. The two most important ways to improve enamel's abrasion resistance are the modification of the frit's chemical composition and the use of mill additives, although the crystallization of enamels and the use of self-lubricating particles sometimes represent good actions to address this issue as well[106]. The most important factor to be considered when dealing with abrasive resistant enamels is the choice of the right additive, which should not have detrimental effects on other functional properties of these coatings. As regards the use of mill additives, many different compounds, such as feldspar, sodium silicate, and spodumene, have been taken into consideration, but only quartz showed a good compatibility with the matrix and no negative influence on other properties[145]. Another possible way to improve the abrasion resistance of enamel coatings is the addition of hard particles, such as tungsten carbide, corundum, and silicon carbide[156-159]. Several studies have pointed out that the shape of the fillers and their distribution inside the matrix are important to obtain a correct improvement of the abrasion resistance, but their concentration should be kept as low as possible to avoid a loss in the protection properties of the coating.

## 1.7 Enamel coatings in real world applications

Porcelain enamel is a very versatile material, and it is used on over 200 products. TABLE 1-6 summarizes the main market and applications of enamel coatings and reviews the main functional characteristics provided by these coatings[160].

**Table 1-6. Main application markets for enamel coatings and functional properties provided to the coated components.**

| Market | Manufactured component | High temperature stability | Thermal shock resistance | Corrosion resistance | Acid resistance | Alkali resistance | Resistance to cleaning | Abrasion resistance | Impact resistance | Fire resistance |
|---|---|---|---|---|---|---|---|---|---|---|
| Domestic appliances | Self-cleaning oven cavities | ● | ● | | ● | | ● | ● | | ● |
| | Washing machines | ● | ● | ● | ● | ● | ● | | | |
| | Cookware | ● | ● | ● | ● | | | | ● | ● |
| Industry | Water heaters | | ● | ● | | | | | ● | |
| | Heat exchangers | ● | ● | ● | | | | ● | | |
| | Chemical vessels | ● | | ● | ● | ● | | ● | | |
| Construction | Flues | ● | ● | ● | ● | | | | | |
| | Roof tiles | | ● | ● | | | | | | |
| Architecture and Infrastructure | Curtain walls | | | ● | | | ● | ● | ● | ● |
| | Exterior wall cladding | | | ● | | | ● | ● | ● | ● |
| | Signage | | ● | ● | | | ● | | | |
| Miscellaneous | Silos | | | ● | ● | ● | | | ● | |

Most people are familiar with porcelain enamel from their household appliances, as the production of enamelled stoves and kitchenware have always represented an important market segment for this material. Vitreous enamel coatings are the ideal partner for all methods of cooking that involve high temperatures, as they can withstand temperatures up to 650 °C without anything happening to their appearance or protection properties. As regards the production of stoves, the strong points, that enamel coatings can supply, are the resistance to heat and direct flame, the resistance to aggressive detergents and their ability not to absorb odors, flavors, and acidic foodstuff[161].

The first historical sector of application for porcelain enamels is the domestic microenvironment, where pyrolitic ovens, stoves, hobs, washing machines, dishwashers, and plumbing fixtures have benefited from the presence of enamel in terms of durability and resistance[162-164]. Porcelain enamels are in fact more durable than plastic and paints, but, in the case of laundry products, porcelain enamels have been almost completely replaced by high-quality and low-cost polymers[165].

Other important sectors where enamel has a long tradition of application are civil and industrial constructions, exterior and interior architecture, and street furniture: cladding of facades, balconies, support elements, road tunnels, toll booths, and claddings in stations and airports are just some examples of the enormous versatility of enamel in this market segment. In fact, enamelled materials are resistant to aggressive agents present in the atmosphere, resistant to abrasion, and invulnerable to vandalism (graffiti). In addition to these functional characteristics, enamelled coatings can be produced in a wide variety of colors, which makes them very attractive from a design point of view. In the architectural field, porcelain steel panels have been used for many years in the construction of ventilated facades, but despite the many offered advantages, such as excellent color maintenance, they present high production costs, which could be somehow limited using enameled aluminized sheets[166]. As regards cladding of indoor walls and structural elements, it is important to remark the great advantages that enamel coatings offer in terms of resistance to abrasion: for this reason, the enamel cladding of stairwells and lifts is suggested to achieve a great durability over time[167, 168]. The enamelled panels offer great advantages in terms of hygiene, non-toxicity, and resistance to chemical disinfection agents, for these reasons they are widely used in the healthcare environment for cladding of operating rooms, toilets, corridors, and laboratories.

Enamelled steel is a very interesting material for the creation of high-strength surfaces in outdoor and indoor urban areas, such as waiting areas for and of transport media, subways, railway stations, and airports. In the twentieth century, porcelain enamels found great application in the domestic appliances field, and still today they find multiple lines of application: some examples are boilers and water heaters[169-172]. Enamel coatings can be also used in the design of plant components such as chimney pipes, stove pipes, mantelpieces, and vehicle exhaust

pipes, as they guarantee resistance to aggressive molecules, thermal shock, and corrosion. For the same reasons, vitreous enamel is also extensively used in industrial plants, such as in industrial waste treatment plants, high-capacity chemical vessels, heat exchangers, and components for electronic circuits. Enamel-lined silos and vessels are very appreciated as they are chemically inert, thus reducing the risk of contamination of food and chemicals to a minimum level. The use of enamel in heat exchangers is very valued as these components usually work under extreme conditions of temperature and wear, being the enamel coating a perfect lining for guaranteeing a high degree of resistance[171].

## *1.8 Enamel coatings and their environmental impact*

The European Union recently passed a set of laws and actions plans to promote clean technologies as solutions to the problem of pollution. The expression "environmental and clean technologies" is referred to a set of changes, in production processes and in products, which aim to achieve the maximum functional result with the minimum use of raw materials, resources and work, producing a minimum residue and waste in the process. In this context, it is important to underline the contribution of two different elements in determining the environmental impact of a material: the product itself and the production process. As defined by the UNI EN ISO 9000:2015 standard[173], the product is the tangible output and object of a production process. In the specific case, the enamelled material is the tangible output of the enamelling process.

Enamelled materials and products, despite being based on a relatively ancient production technique, meet very modern criteria of environmental friendliness and they show some advantages over other coated products, such as galvanized and plastic-coated materials, in terms, for example, of toxic fumes emission. The low environmental impact of enamelled materials is mainly due to their high durability: the use of vitreous enamel increases the lifespan of metals (whose life is short because of their tendency to be corroded) and postpones the moment when the materials will be decommissioned. In addition to a high service life, enamelled materials show a full recyclability, as they can be treated as metal scraps, without the need to separate the coating form the metal substrate. Enamelled materials do not need special treatments prior to recycling as the enamel compounds become smelt waste that separates from the metal and does not alter the properties of the smelt itself. As regards coloured enamels, the presence of harmful metals is kept to a minimum and it is anyway regulated by the UNI EN 1388-2:1997 standard, which identifies the maximum acceptable levels of lead and cadmium that can be given off by enamelled products used for contact with aliments.

The environmental impact of enamelled materials is also conditioned by the ecology of the enamelling production process. Clean technologies are the basis on which the

circular economy exists, and they also represent the trigger which facilitates the shift from a linear production model to a closed-loop model. The closed-loop waste management refers to the process by which waste from one product is used to make another product, thus closed-loop production processes make provision to use the raw materials completely and be safe from an environmental standpoint. The analysis of the traditional enamelling process reveals several critical points about the production of noxious waste and effluents, and about the amount of energy consumed during the various production phases. TABLE 1-7 shows the main critical aspects determining the environmental impact of the enamelling process and the possible solutions to these issues.

**Table 1-7. Environmental impact of the enamelling process with possible solutions.**

| Action areas | Adopted solution |
|---|---|
| **Reduction of raw materials** | Reduction of chemical reagents for metal pre-treatment<br>Development of enamels with better substrate coverage<br>Reduction of enamel consumption during deposition |
| **Reduction of energy consumed** | Reduction of metal pre-treatment bath temperature<br>Elimination of drying steps and optimization of firing cycles<br>Development and use of more efficient tube kilns |
| **Reduction of wastes** | Reduction of chemical reagents for metal pre-treatment<br>Elimination of grinding<br>Recycling of effluents |
| **Reduction of production time** | Pre-treatment and coating line automation<br>Shorter processing times |

Considering the whole enamelling process, the metal pre-treatment represents one of the most impactful steps, as it involves the use of harmful chemicals in high concentrations and at high operating temperatures. Sheet metal pieces are normally pre-treated by subjecting them to cycles of degreasing, acid pickling, and several rinses: this procedure calls for a large amount of water and energy, involving the use of a large quantity of chemicals. In this context, many manufacturers have now taken steps to eliminate polluting substances such as nitrites, fluorides, and phosphates from the metal-pretreatment steps. In addition to that, enamel suppliers have already started to modify the chemical composition of their frits and products to make them more environmental friendly and less harmful[129]. Another aspect to be considered is the grinding of enamels: the traditional processes use wet milled enamels, but the development of new “ready to use” formulations allows to skip the milling step, thus avoiding the production of wastewater and mud coming from the mills. “Ready to use” enamels are also useful in reducing the stages of metal pre-treatment, leaving

just the degreasing of the metal piece as a necessary step to be carried out. As regards the firing process, many attempts have been made to reduce the firing temperatures and times, and a particular attention is now devoted to the elimination of nitrous oxides and fluorine compounds generated during the firing steps.

# 2 Introduction to the thesis project

## *2.1 Aim of the thesis*

Nowadays, both industry and academia conduct research and product development due to the growing need for high-performance materials. There are currently two ways to address this issue: either by developing new materials with specialized features or by carefully selecting existing materials with distinctive properties that can be modified to better suit specific high-duty applications.

Vitreous enamels are silica-based inorganic coatings that exhibit excellent durability over time [5] and outstanding functional properties. These coatings can be applied to a variety of substrates, including steel, cast iron, copper, aluminum alloys, and aluminum foams[82], and they are mostly employed for the production of high-duty technical components like gas turbines, flue pipes, and containers for chemical processes. One of the key factors contributing to the widespread use of enamelled materials is their ability to withstand corrosion and weathering[174, 175]. In addition to that, enamel coatings provide exceptional impermeability, washability, high temperature[176, 177], and fire resistance[83] thanks to the glassy nature of the matrix. In contrast to organic materials like paints and polymers, enamels are not affected by UV exposure, therefore their surface appearance does not change over time[6].

Abrasive wear is one the most frequent mechanical effects that porcelain enamel coatings encounter in real-world application areas. Even tough enamels are hard, they exhibit a less-than excellent level of abrasion resistance due to the high brittleness and low fracture toughness of the glassy matrix [179, 196]. Abrasion may interest the surface layer of the coatings (surface abrasion) or the material beneath it (sub-surface abrasion), with a consequent loss of functional and aesthetical properties. In the first case, the abrasion process usually leads to the formation of a rough surface and to the development of small cracks, thus mainly affecting the aesthetical properties and the ease of cleaning[178]. In the case of sub-surface abrasion, damage is more severe, and it usually involves an important loss of material[179]. The damages produced by sub-surface abrasion include material deformation, material removal, and formation of big cracks[180, 181]. These outcomes should be avoided because they lead both to the formation of through-thickness cracks and the opening of the enamel's intrinsic porosity, thus reducing chemical resistance and durability[5]. As a result, improving enamel's abrasion resistance and fracture toughness represents a key challenge that must be addressed to broaden the possible application fields of these coatings.

The enhancement of enamel's abrasion resistance and mechanical properties could be achieved following four different approaches: i) the modification of the frit

composition by the addition of mill additives, such as quartz[58, 145, 182], potassium feldspar ($KAlSi_3O_8$)[58, 183], zirconium silicate ($ZrSiO_4$)[58, 183], or spodumene ($LiAl[Si_2O_6]$)[58, 145]; ii) the addition of self-lubricating agents, such as graphite and graphene flakes[106, 145], iii) the use of hard ceramic particles (HCPs), such as silicon carbide (SiC)[146], tungsten carbide (WC)[146, 158], titanium diboride ($TiB_2$)[159], or alumina ($Al_2O_3$)[156, 157, 184]; iv) the addition of ductile metallic fillers, such as Ni[185-187], Al[188], and Mo[189, 190] particles.

The choice of the right approach to be followed depends on many different factors, but in every case, it is important to improve the abrasion resistance of the coatings without producing negative effects on other functional properties. It is always necessary to consider some important factors, such as the thermal resistance and the shape of the additives, the affinity between the enamel matrix and the added particles[159], and possible agglomeration phenomena[158]. Since glass-ceramic coating's (GCCs) abrasion mechanism is driven by brittle fracture phenomena, degradation and irreversible damage of the coatings usually starts from stress concentration points: angular-shaped and/or incompatible particles create weak points at the matrix/particle interface that can serve as preferential sites for nucleation and propagation of cracks[183, 191]. The agglomeration of particles is another factor to be considered, in particular when dealing with nano-sized particles or lamellar powders (e.g., graphene), as big agglomerates could promote the chipping off of the coating[106]. Furthermore, the internal microstructure of the coatings should also be examined, as voids and pores demonstrate low resistance against mechanical effects since they have a high-stress amount[192, 193]. Thus, the presence of uniform pores, both in size and dimension, increases the energy barrier for crack propagation and damaging of the coating[191].

Several recent studies have examined enamel's abrasion resistance only searching for the optimal additive concentration that could increase abrasion resistance. The majority of these studies are focused on the positive effects of mill additives on abrasion resistance of enamels. On the other side, it would be more useful to follow a comprehensive approach, which aims at improving the coating's abrasion resistance and cracking resistance, with a particular attention to chemical resistance[194]. This thesis will consider three different types of fillers: graphene nanoplatelets (GNPs), $Al_2O_3$ particles, and 316L SS-Fs, as representative of self-lubricant, HCPs, and metallic fillers, respectively.

In the literature few papers study the effect of graphene-based fillers on the tribological properties of enamel coatings. Graphene is considered an innovative material of remarkable scientific and academic interest, as it shows impressive electrical, optical, and mechanical properties. In the present context, graphene is considered for its self-lubricant properties, as it was demonstrated that is is able to reduce the wear and mechanical failure of sliding surfaces, providing a general toughening effect[195, 196]. Regarding the possibility to use auto lubricant particles, it is necessary to both consider the compatibility of the fillers with the high firing

temperatures and the possible agglomeration phenomena which could occur. Now, this thesis aims at assessing the influence of GNPs on abrasion resistance of enamels when subjected to uniform surface abrasion and when appropriate efforts are made to avoid agglomeration phenomena.
The second approach consists in the use of HCPs, that are widely employed in the fabrication of resistant polymeric, metallic, and ceramic matrix composites[197-200].
The use of HCPs, in particular SiC, in the development of innovative composite enamel coatings is very common, but few studies on $Al_2O_3$ composite enamels are present in the literature. In this context, this thesis aims at investigating if and how the size of corundum particles influences the abrasion and chemical resistance of enamel coatings.
The last opportunity to improve the mechanical properties of enamels is represented by the addition of metallic particles, that are able to counteract evolution of damages due to abrasion and delay the propagation of existing cracks by several mechanisms that absorb energy during crack propagation[201]. The addition of 316L SS-Fs could be then useful to improve the abrasion and cracking resistance of enamel coatings by the creation of the so called "ductile particle glass-ceramic matrix composite"[201].
Throughout this thesis emphasis has been put into the evaluation of enamel's mechanical properties and abrasion resistance by testing the effectiveness of diverse fillers and monitoring the evolution of coating's functional properties in the round. Typical surface-sensitive techniques have been exploited and coupled with other methods aimed at assessing the chemical and mechanical properties of the coatings. In addition to that, in-situ mechanical testing has been carried out to investigate the failure mechanisms and obtain further insights on the mechanical behaviour of these coatings.

## *2.2 Experimental methods – an overview*

The study of porcelain enamels is a field in which diverse properties must be considered and monitored. In particular, the typical coating characterization techniques can be exploited to characterize the surface properties and microstructure of the deposited enamels. Some examples of the properties to be considered are thickness, surface roughness, and microstructure. In this regard, optical and electron microscopy observations are crucial to assess the quality of the deposition process, check the uniformity of porosity and filler distribution, monitor the evolution of mechanical damage.
Vitreous enamel coatings are widely appreciated as they show superior chemical resistance and inertia with respect to organic coatings: the addition of reinforcing fillers inside the matrix should not lead to a decreased chemical resistance and it is really important to check this aspect when dealing with composite enamel coatings.

The chemical resistance of enamels can be checked by means of immersion in aggressive acid or alkaline solution interspersed with Electrochemical Impedance Spectroscopy (EIS) measurements, that are useful to assess the protective properties of the coatings.
The addition of reinforcing fillers inside the enamel matrix is exploited to improve the abrasion resistance and mechanical properties of the coatings. Abrasion resistance can be assessed by means of different techniques, but the P.E.I. abrasion technique is the most realiable method as it imparts a uniform abrasion damage to the sample's surface. The evolution of damage during the abrasion process can be monitored by means of surface-sensitive techniques, microscopy observations, and EIS analyses.
Another important aspect to be considered when dealing with composite enamel coatings is the improvement of mechanical properties, with a special attention to cracking resistance. Enamel coatings tend to fail when subjected to tensile stresses or compressive localized stresses, thus scratch test, identation, and bending tests are first-choice methods to study the mechanical behaviour of these coatings. In addition to that, in-situ bending tests coupled with AE analyses can provide further details on the damaging mechanisms and the role of the fillers in improving the toughness of the coatings under study.
In this section the reader will find a general description of the main experimental techniques used in the thesis, whereas specific details about in-situ mechanical techniques will be provided in the most appropriate Chapters.

**Substrate pretreatment** The quality of the enamelling process greatly depends on the cleanliness and reactivity of the substrate. Prior to deposition, the surface of the substrate must be cleaned, by removal of traces of grease and surface oxides, which could influence the deposition process by reducing adhesion with the enamel layer. A controlled increase of the surface roughness has indeed a positive effect on the creation of a strong bond between the metal and the enamel layer. The cleaning of the substrate must be carried out before any deposition process: a highly reactive surface is thus obtained, ready to interact with the coating to be deposited. Surface pretreatment consists of three distinct phases: i) *degreasing*, for removing traces of oils and greases; ii) *alkaline etching* to activate the surface; iii) acid *desmutting*, for removing surface oxides. Alkaline etching and acid desmutting are common pretreatment processes for removing surface oxides, subsurface defects, and inclusions[202]. Following the pretreatment process, the substrate surface is very reactive, so the samples must be coated in a short time, to avoid the possible spontaneous formation of further traces of corrosion products and oxides. In the present case, all the samples were coated within 3 hours from the pretreatment process.

**Thickness, surface roughness, and gloss** The assessment of the coating's thickness is the first analysis that is carried out on enamel coatings, and it is useful to check the quality and reproducibility of the deposition methods. The mean coating thickness was measured using a Phynix Surfix FN thickness gauge. This is the simplest and most immediate method for measuring the dimensions of coatings thickness.

After that, surface properties of the enamel coatings were characterized by means of roughness and gloss measurements. The roughness of the samples was measured using a MAHR Marsurf PS1 roughness tester. A sampling length (lr) of 0.8 mm and an evaluation length (ln) of 5.6 mm were used in accordance with the UNI EN ISO 4288 (2000) standard[203] to measure the Ra parameter, defined as the arithmetic average of the roughness profile, and Rz, defined as the average value of the absolute values of the highest peaks and deepest valleys. Gloss measurements were carried out with a Glossmeter Erichsen NL34 and the results were reported for an angle of 20°, as suggested by the ASTM D523-14 standard, as the gloss measured at 60° was higher than 70 GU.

The assessment of the surface properties of enamel coatings is usually put besides by optical and scanning electron microscope (SEM) observations. In the present thesis optical observations are carried out with Nikon SMZ25 stereo-optical microscope, whereas most of the SEM images are acquired using the JEOL IT300 microscope.

**Electrochemical Impedance Spectroscopy** Electrochemical techniques are one of the most employed methods in the characterization of coatings. Among these, EIS stands out for its relevance, being very useful for veryfing the protective properties characteristics of coatings[204]. EIS measurements allow obtaining different information such as the presence of defects, water barrier properties, and evolution of protective properties[205]. FIGURE 2-1 shows the schematic representation of the EIS setup and testing methodology. The electrochemical cell (plastic tube) was glued to the sample to avoid leakage of the testing solution.The setup was composed of three electrodes: a platinum wire used as counter electrode, an Ag/AgCl (+207 mV vs Standard Hydrogen Electrode) electrode used as reference, and the sample to be analyzed as working electrode. The testing solution was a 0.3 wt.% $Na_2SO_4$ aqueous solution, as it is a suitable electrolyte to perform EIS measurements but is does not induce further damages, differently respect to the corrosive action of NaCl based solutions. The evaluation of the impedance modulus at low frequencies allows to assess the evolution of the protective properties of the coatings at increasing abrasion cycles.

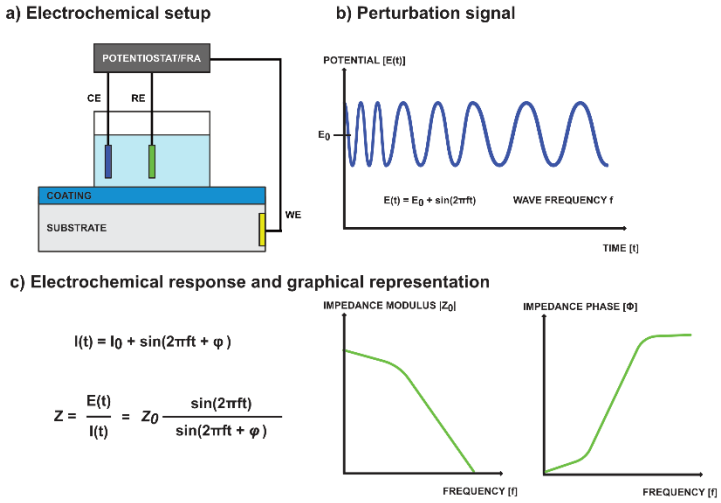


**Figure 2-1: Schematic representation of the Electrochemical Impedance Spectroscopy setup and testing methodology.**

**P.E.I. abrasion test** The assessment of abrasion resistance of glass-ceramic coatings is usually exploited by means of Taber test or P.E.I. test. The Taber test is the first-choice technique in many studies[145, 156], on the other side many others compare the abrasion damages obtained both by Taber and P.E.I. tests[126, 146]. In the present case it was chosen to exploit only P.E.I. testing because it produces a more uniform and surface-limited damage in comparison with the Taber test, thus avoiding the production of localized defects and cracks, that could quickly reduce the protection properties of the coating[206]. In addition to that, P.E.I. testing is the widespread and standardized test used by industries to check abrasion resistance of enamelled substrates. FIGURE 2-2 shows a schematic representation of the P.E.I. abrasion system and testing method. The abrasive process exploited by the P.E.I. apparatus can be classified as a three-body abrasive process[207] and it leads to a superficial uniform abrasion action on the sample's surface[208]. The abrasion resistance of the coatings was evaluated using a P.E.I. abrader (Ceramic Instruments, Sassuolo, MO, Italy), according to the UNI EN ISO 10545-7(2000) standard[209]. The testing apparatus imparts to the samples a circular horizontal motion at 300 rpm while the abrasive action is achieved by using a composite abrasive medium. The complete P.E.I. abrasion system consisted of 3 g of F80 alumina powder dragged by steel spheres of different diameters (5 mm, 3 mm, 2 mm, 1 mm diameter balls in a quantity of 70 g, 52.5 g, 43.75 g, and 8.75 g respectively) and by 20 ml of deionized water, used as a lubricating agent. The

evolution of damage can be monitored by means of mass loss, surface roughness, residual gloss measurements, SEM observations, and EIS analyses.

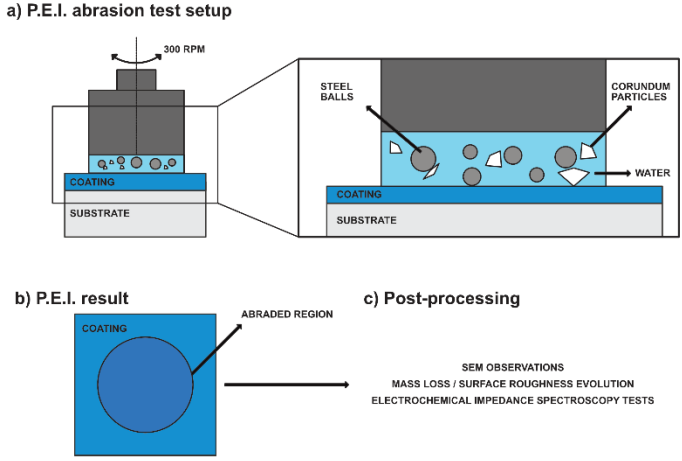


**Figure 2-2: Schematic representation of the P.E.I. abrasion system and testing methodology.**

**Scratch test** Scratch test is generally accepted as one of the simplest methods to assess adhesion strength of a film or a coating on its substrate[210, 211], but it can be also used to assess the mechanical properties of surfaces[212]. In particular, the scratch test can be exploited to study the mechanisms that take place during a two-body abrasion process of brittle materials, such as ceramics surfaces[213]. In the scratch test process, a diamond tip is drawn across the coated surface under a progressive load at a constant velocity. Sensors are able to measure the AE, the tangential force, the penetration depth, and the residual depth. FIGURE 2-3 shows a schematic representation of the scratch system and testing methodology.

Considering hard brittle coatings, it is possible to identify loads corresponding to sudden events during scratching: these loads are called “critical loads (Lc)” and they can be quantitatively assessed for the characterization of the scratch resistance of the coating under study. Lc1 is the minimum load at which the first crack occurs, Lc2 is the load at which catastrophic cohesive failure begins, and Lc3 is the load at which adhesive failure begins (e.g., peeling off of the coating and uncovering of the substrate). This classification we will use in this study is made according to the ISO 20502 standard, but many different nomenclatures can be find in the literature: generally, Lc1 is addressed as the lower critical load at which cracking begins, and Lc2 is addressed as the higher critical load at which the delamination of the coating occurs[214]. The values of the Lc loads, together with a detailed analysis of other

testing outputs, such as penetration depth, coefficient of friction, and wear track morphology, are analyzed to determine the fracture behaviour of the material

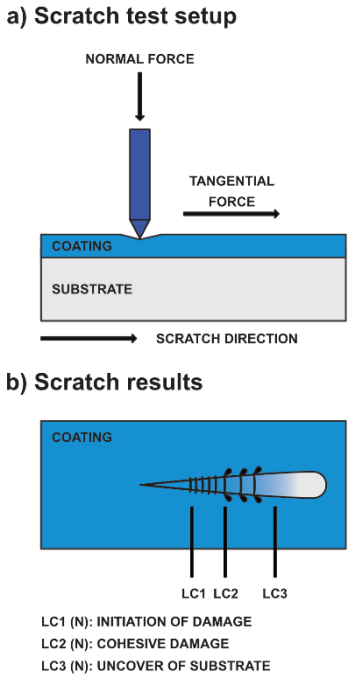


**Figure 2-3: Schematic representation of the scratch test system and testing methodology.**

**Bending tests** The mechanical properties of brittle hard coatings can be studied using a variety of different experimental techniques, such as indentation, scratch test, and bending test[214]. Bending tests are usually exploited by creating a precrack on freestanding thick films, applying stress to induce crack propagation, and then measuring the critical stress needed to inflict failure[215]. Unfortunately, the creation of a precise precrack in the coating is usually very difficult; therefore, bending without pre-cracking can be exploited and the “cracking resistance” (i.e., the threshold strain over which the density of cracks sharply increases[216]) of the coating can be measured. This threshold can be easily individuated by directly measuring the crack density as a function of strain or displacement during bending tests. Bending tests are very easy to be performed and they can be used to explore the fracture behaviour of hard coatings on more ductile substrates and to compare the cracking resistance among different coatings[217]. For this reason, the

assessment of the enamels mechanical properties will mainly follow this approach. FIGURE 2-4 shows a schematical representation of the bending setups used in this thesis and the testing methodology. In particular, 3-point and 4-point bending tests will be exploited to obtain the stress-strain curves and assess the evolution of crack density. In some particular cases, the bending tests will be coupled with AE tests to in-situ monitor the evolution of mechanical damage.

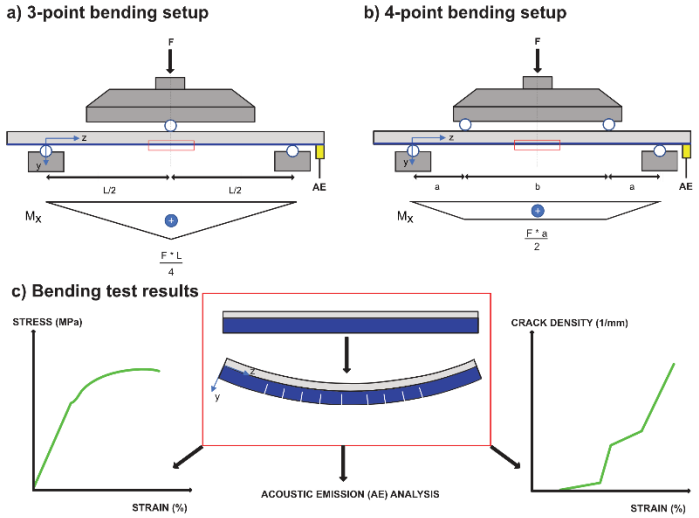


**Figure 2-4: Schematical representation of the bending setups and testing methodology.**

# 3 The influence of graphene-based filler on the abrasion resistance and surface properties of composite vitreous enamel coatings

***Part of this chapter has been published in:***

S. Rossi, F. Russo, N. Gasparre, V. Fontanari, **"Influence of graphene addition on the mechanical and surface properties of vitreous enamel coatings",** *Surface and Coatings Technology,* 398 (2020) 126071.

*Conceptualization*: S. Rossi; *Methodology*: S. Rossi, V. Fontanari; *Investigation*: F. Russo, N. Gasparre; *Formal analysis*: F. Russo; *Validation*: F. Russo; *Supervision*: S. Rossi, V. Fontanari; *Writing*: F Russo.

## *3.1 Introduction*

Aluminum alloys are now attracting increasing attention in technical fields where component weight plays a key role, such as in cookware, building construction, outdoor furniture, transportation, and marine industry. Because of their strength and light weight, aluminum alloys are therefore being used more frequently. However, they can suffer from corrosion in aggressive environments, at low and high pH values, as in these conditions aluminum cannot produce a stable and protective passivity layer[218-220]. Enamel coatings could be a valid solution to overcome these issues, as they show optimal corrosion protection and chemical resistance, but great efforts must be devoted to improve their abrasion resistance by the addition of suitable fillers.

Graphene shows a combination of physical and mechanical properties that make it suitable for use in fields of full technological development, such as electronic engineering, and aerospace. Graphene is defined as a 2D carbon allotrope, whose atoms represent the sp2 vertex of a monoatomic hexagonal lattice, forming a honeycomb structure of monoatomic thickness[221]. This material shows impressive optical properties, as it has excellent transparency towards visible light[222], good electronic properties, as it shows a high electron mobility at room temperature[223], high thermal conductivity[224], remarkable mechanical properties[225], as for example a tensile strength of 1 TPa[226], and self-lubricating action[227, 228]. For these reasons, graphene can be exploited to produce transparent conductive membranes, thermal sensors, drug delivery components, photocatalytic compounds, and composite materials[229]. The combination micrometric structure and excellent properties make graphene suitable as a filler in composite materials. Graphene has been extensively used as a filler in several types of coatings, ranging from polymeric coatings[230] to organic and ceramic composites[231]. Graphene can be added in polymeric matrices in the form of functionalized nanosheets, simple fillers, or as

intercalated films, thus increasing the electrical, thermal, and mechanical properties of the polymeric matrix. The majority of these polymeric-based materials are often made by using graphene in its various forms[232] (such as graphene oxide GO, reduced graphene oxide, rGO, and functionalized graphene oxide, fGO, as reinforcing fillers for several types of polymer, such as epoxy resins, polystyrene, PVC, PET[233-236]). Although the polymeric matrix composite materials are the most widespread in the industrial field, the use of graphene as a reinforcement in metallic or ceramic materials is also important. In fact, several works have been carried out to investigate the improving effects of graphene addiction on the mechanical properties of copper-based materials, in particular the effect of the filler quantity and the affinity between copper and carbon[237] were studied. In a similar way, some studies have tried to achieve anisotropic electrical, thermal, and mechanical properties of ceramic matrices exploiting graphene flakes addition[238]. The research on ceramic/graphene composites has mostly been focused on the enhancement of the fracture toughness of the ceramic matrix.The $Al_2O_3$ and $Si_3N_4$ are the most studied systems[239-242], although many studies can be found also regarding SiC, $ZrO_2$, $ZrB_2$, TiC, or hydroxyapatite (HA)[243-247]. A general outcome from the available literature is the attested toughening effect induced by the presence of the graphene nanostructures, that can both bridge and deflect the crack paths during mechanical failure[248].

Graphene can be also considered a promising candidate for wear and scratch resistant coatings because it represents the thinnest, lightest, and strongest known material[221]. Graphene based composite coatings can reduce the wear/mechanical failure of sliding surfaces: for example, rGO has studied as an antifriction and anti-wear filler, while graphene has proved to increase the tensile strength of PTFE coatings[249], as well as to improve the wear resistance of polyamide composites[250]. Finally, graphene and GO have been reported to be effective as solid lubricants, decreasing the friction coefficient in several environments[251]. As regards examples of wear-resistant ceramic composites, many studies in the literature are focused on the addition of graphene-based fillers in $Si_3N_4$, $Al_2O_3$, $SiO_2$, and $ZrO_2$ bulk composites[252-255]. Generally, the addition of graphene nanoplatelets (GNP) or graphene oxide (GO) sheets leads to at least a 50% improvement over the matrix wear resistance and it is maximal for very low amounts (0.5–1.0%) of filler in the case of $Al_2O_3$/graphene composites[256] and for high amounts (4-5%) of filler in the case of $Si_3N_4$/graphene composites[257]. The most widely claimed mechanism for explaining the enhanced tribological performance of ceramic/graphene composites is the formation of an adhered carbon-based tribofilm on the worn surface that produces a lubricating effect and protects against wear[257].

In the literature it is possible to find only one example of a study focused on the abrasion resistance of enamel coatings with the addition of graphene-based fillers[145]. This study considers composite enamel coatings with the addition of 1

vol.% and 2.5 vol.% of graphite and assess their abrasion resistance by means of the Taber test. The study points out that, in the mentioned conditions, the presence of graphite particles leads to a decreased abrasion resistance due to flakes production. Considering that many papers in the literature highlight the positive action of graphene towards abrasion resistance, it would be interesting to assess the influence of graphene-based fillers on the abrasion resistance of composite enamels produced by the addition of different quantities of filler (lower than 1 wt%) following a new dispersion method that should decrease the agglomeration tendency of graphene. Thus, the main goal of this chapter is to investigate the influence of graphene nanoplatelets (GNPs) addition on enamel coatings abrasion resistance using the P.E.I. test, thus subjecting the samples to uniform abrasion processes.

## *3.2 Materials and methods*

### 3.2.1 Materials

**Graphene powder** The graphene powder was provided by COMETOX (Milan, Italy). The sheets have an average thickness of 6 nm and a typical surface area ranging from 120 to 150 $m^2/g$. The average particle diameter is equal to 25 µm. An additional characterization of this graphene powder can be found in other studies by our research group[258].

**Metal substrate** AA4006 aluminium alloy panels, having dimensions of 10 cm x 10 cm x 0.25 cm, were used as metallic substrates. The AA4006 aluminium alloy is an Al-Si alloy with the following composition: 0.80 wt.% Si, 0.50 wt.% Fe, Al balancing. This aluminium alloy is a typical substrate to produce enamelled cookware, since it is easily enamelled.

**Enamel frit** The enamel coatings were deposited starting from a ready-to-use transparent frit free from vanadium oxide, lead, and nickel. The frit was produced by Emaylum Italia (Chignolo d'Isola, BG, Italy). The composition of the frit is the following: 35 wt.% $Na_2O$ + $K_2O$ + $Li_2O$, 20 wt.% $TiO_2$ + $Al_2O_3$, 5 wt.% $B_2O_3$, 5 wt.% SrO + $Sb_2O_3$ + $Zn_2O$ + $P_2O_5$, $SiO_2$ balancing. The high content of alkali metal oxides is necessary to lower the firing temperature of the enamel formulation, as aluminium substrates cannot withstand firing temperatures higher than 570-580 °C. In addition to that, the absence of $V_2O_5$ is of great importance as, since 2007, products containing vanadium pentoxide in concentrations higher than 1 wt.% are considered dangerous for the environment and human health[85]. FIGURE 3-1 shows the dimensional characterization of the ready-to-use frit, providing an electron microscope micrograph and the dimensional analysis exploited using the ImageJ software.

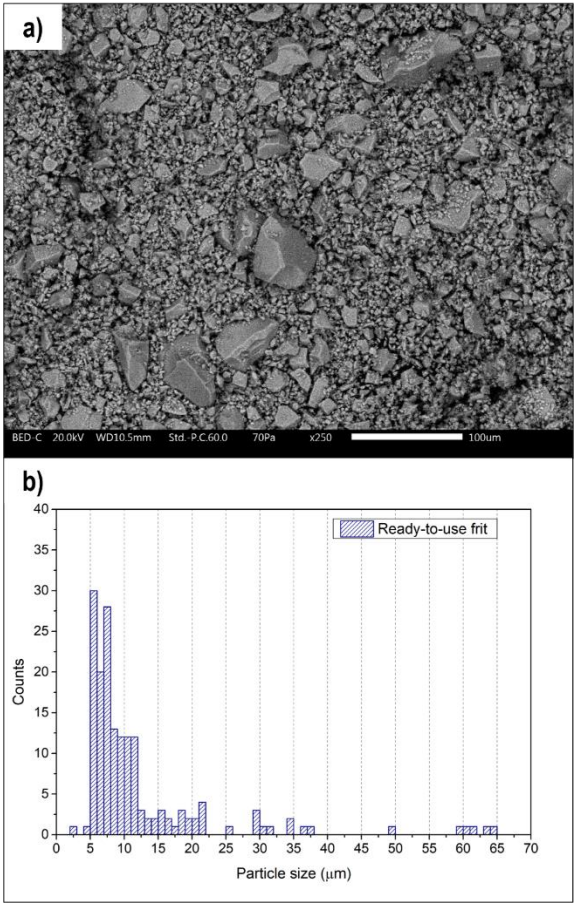


**Figure 3-1: Ready-to-use frit characterization (a) SEM image (250x magnification, 100 μm marker, BSE), (b) dimensional analysis.**

The dimensional analysis carried out with the ImageJ software gives us the opportunity to evaluate the D90 and D50 parameters, that are equal to 22 μm and 9 μm, respectively. These values are perfectly in line with the required frit dimension suggested by technical manuals[41].

### 3.2.2 Methods

#### *3.2.2.1 Samples preparation*

The first step is necessarly the choice of the substrate that will be coated. Then, the enamel deposition process parameters must be optimized to obtain coatings which can guarantee the best performances.

**Substrate pretreatment** AA4006 aluminium alloy panels were chosen to be used as substrates for the production of composite enamel coatings. The substrates were degreased by immersion in acetone for 2 minutes with ultrasound bath stirring, and then they were carefully washed in distilled water. The desmutting step was exploited by immersion of the substrates in 20 wt.% HCl acqueous solution for 10 minutes. After that, the treated substrates were cleaned by water rinse and airflow dried. All the samples were coated within 3 hours from the pretreatment process.

**Deposition process parameters** As a first thing, the ready-to-use frit was mixed with an appropriate quantity of GNPs powder to obtain four different batches with a known and fixed amount of graphene filer. The graphene/frit powder was then smelted at 1400 °C and water cooled to obtain glassy granules. This step was performed to improve the dispersion of the graphene powder inside the glassy matrix. Thereafter the powders were ball milled for 10 minutes to achieve a granuometry not exceeding 80 µm, and an amount of 50 wt.% water was added to obtain applicable slips. The wet formulations were then mechanically stirred for 5 minutes and then the samples were deposited by means of the manual wet spray method. The samples were dried at 200 °C for 10 minutes and fired at 570 °C for 10 minutes in a box-furnace to obtain vitrified coatings.

**Sample typologies** This study focuses on four types of enamel coatings deposited starting from the same ready-to-use frit. TABLE 3-1 summarizes the sample typologies taken into consideration.

**Table 3-1: Samples labelling, with relative graphene filler concentration.**

| Starting frit | Graphene concentration (wt. %) | Sample labelling |
|---|---|---|
| Ready-to-use transparent frit | 0.00 | G0 |
| | 0.25 | G025 |
| | 0.50 | G05 |
| | 1.00 | G1 |

The first sample type, called *G0*, was deposited with the simple ready-to-use frit, without the addition of graphene, and it acts as a reference condition.The other three samples, namely *G025*, *G05*, and *G1*, were deposited using the composite graphene/frit powder: the concentrations were chosen to systematically explore the concentration range from 0.00 to 1.00 wt.%, as an higher graphene filler quantity has been described in literature to have a strong agglomeration tendency and negative influence on the abrasion resistance of some coatings[256]. FIGURE 3-2 shows the appearance of the as-made enamel samples.

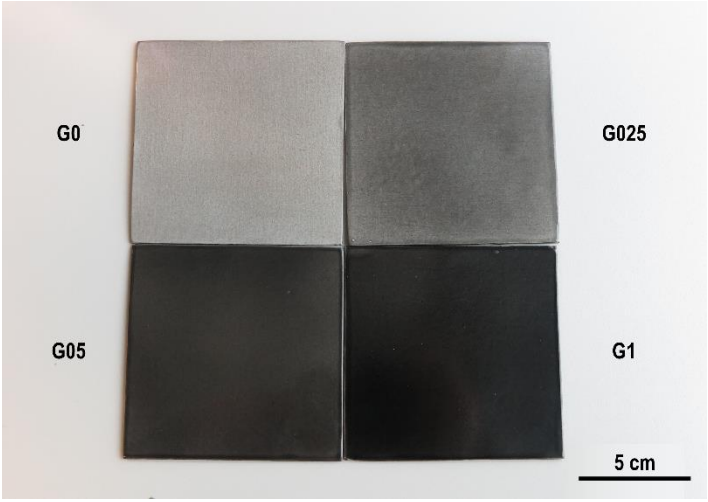


**Figure 3-2. Photograph of the as-made enamel samples.**

### *3.2.2.2 Coatings characterization*

This section introduces the characterization techniques used for the investigation of the coatings and their performances. First of all, a complete surface and microstructural characterization of the different coatings was carried out. The abrasion resistance of the coatings was assessed by means of standardized wet abrasion test, and the effect of the filler was evaluated by microscopy observations and EIS measurements.

**Surface and microstructural analysis** The thickness was measured as described in SECTION 2.2. For each coating type 10 measurements on 3 samples were made, for a total of 30 measurements. The mean coating thickness was 70 ± 13 µm. The great dispersion of data is due to the variability of the manual-base deposition method, whose reproducibility greatly depends on the operator's experience. Despite

this, the thickness dispersion does not influence the abrasion resistance test results, as the abrasive process affects only the most superficial layers of the coating.
The roughness measurements were carried out according to SECTION 2.2. 3 specimens were considered for each sample type, 5 measures were made on each sample, thus obtaining 15 measurements from which the mean Ra value and the standard deviation were calculated. Gloss measurements were performed on 2 specimens for each sample-type, 5 measures were performed on both of them, for a total of 10 measures each. Optical (Nikon SMZ25) and low-vacuum scanning electron microscopes (SEM) (JEOL IT300) were used to observe the sample surfaces and cross-sections.

**Abrasion resistance test** The abrasion resistance of the coatings was evaluated by exploiting 750 P.E.I. cycles, according to the procedure described in SECTION 2.2. Mass loss, surface roughness, and gloss measurements were collected out after 100, 250, 500, and 750 abrasion cycles. The measurements were repeated on two samples. The evolution of damage and protective properties were assessed by EIS measurements and by optical and electronic microscope observations.

**Electrochemical Impedance Spectroscopy measurements** EIS measurements were carried out using the potentiostat Princeton PARSTAT 2273 and software PowerSuit ZSimpWin, using the three-electrode configuration described in SECTION 2.2. A 20 mV (peak-to-peak) amplitude and a $10^{6}$ – $10^{-2}$ Hz frequency range were used. The test area was 28.27 $cm^{2}$. The sampling rate was equal to 5 points per decade.

## *3.3 Results and discussion*

### 3.3.1 Surface and microstructural analysis

TABLE 3-2 shows the results of the thickness, roughness, and gloss evaluations.

**Table 3-2. Thickness and surface properties of enamel coatings under investigation.**

| Sample | Sample thickness gauge (μm) | Sample roughness Ra (μm) | Sample roughness Rz (μm) | Sample Gloss 20° (GU) |
|---|---|---|---|---|
| **G0** | 84 ± 11 | 0.34 ± 0.07 | 1.61 ± 0.67 | 74 ± 6 |
| **G025** | 53 ± 14 | 0.33 ± 0.13 | 1.61 ± 0.77 | 71 ± 6 |
| **G05** | 82 ± 20 | 0.34 ± 0.10 | 1.64 ± 0.62 | 71 ± 6 |
| **G1** | 60 ± 12 | 0.40 ± 0.11 | 1.92 ± 0.62 | 52 ± 7 |

The thickness of the samples shows a high variability, as the coatings were deposited by a manual-based deposition method. As regards roughness and gloss assessment, it is important to remark that these two surface properties depend on a certain extent to each other: on a smooth mirror like surface, parallel beams of light are reflected in the same direction, whereas on an irregular surface beams of light are diffusely scattered, and the surface appears to be opaque. Considering the error bars, all the samples show low and comparable values of Ra and Rz, altought a small increase in the order of 18% can be noticed for the sample *G1*. The samples under study show a very low roughness values with respect to similar systems having an Ra value of about 1.50 μm[145]. Thus, it is possible to state that the production of a composite graphene/frit powder and the choice of the process parameters described in SECTION 3.2.2 have allowed to obtain coatings of good quality. If significant filler agglomeration phenomena had occurred, they would have led to higher roughness values. On the other hand, the increase in the surface roughness values and the decrease in the gloss value of sample *G1* are probably due to the beginning of an agglomeration phenomenon and highlight how the 1 wt.% concentration can be considered as a threshold value not to be exceeded to obtain smooth coatings.

FIGURE 3-3 shows optical in-plane images of the enamelled samples. Thanks to the transparency of the formulation, it is possible to investigate the dispersion of the graphene-based filler inside the enamel matrix. All the composite samples show the presence of uniformely dispersed graphene flakes and the absence of important agglomeration phenomena, although in the *G1* sample it is possible to observe the presence of some agglomerated flakes. Most of the graphene flakes seem to have a

lower in-plane dimension with respect to the dimension stated by the supplier (see SECTION 3.2.1) probably due to the ball milling process that the composite graphene/frit composite powder has undergone before the production of the torbida. Thus, it is possible to state that the microstructural optical investigations are in accordance with the roughness measurements, highlighting the good dispersion of graphene into the enamel matrix.

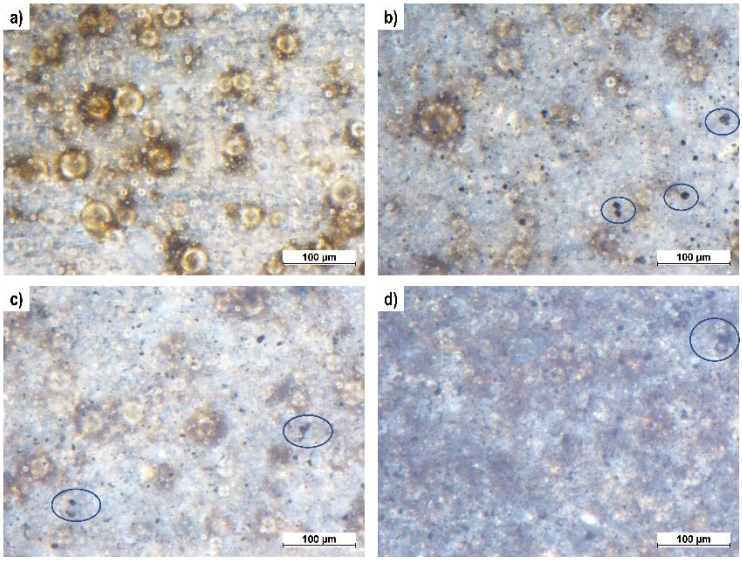


**Figure 3-3. Stereo-optical images of the enamelled samples (a) G0, (b) G025, (c) G05, (d) G1.**

The optimization of the deposition process must be checked by controlling the internal microstructure of the coatings. FIGURE 3-4 shows scanning electron micrographs of the samples cross-sections. The different sample types show an average thickness of about 69 µm, 45 µm, 59 µm, and 50 µm for the *G0*, *G025*, *G05*, and *G1* samples, respectively. These results are in line with the values obtained by thickness-gauge measurements. The presence of a closed porosity structure is a typical feature of enamel coatings, as bubbles are formed by gas evolution (hydrogen, carbon dioxide, carbon monoxide, nitrogen, and water vapour) during the firing treatment[41]. The presence of a closed porosity structure does not alter the corrosion protection properties of the enamel coatings unless the pores are connected to each other forming a direct pathway between the external environment and the metallic substrate. As it possible to observe from FIGURE 3-4, pores are present through the whole enamel coating thickness and they have dimensions up to 30 µm, perfectly in line with the typical bubble dimension of composite enamels[146].

Therefore, it is interesting to observe that the increased graphene content does not seem to change neither the size neither the pore density with respect to the reference sample. In addition to that, it is possible to observe that all the samples show good adhesion with the metallic substrate: no crack or defects can be detected at the enamel-metal interface.

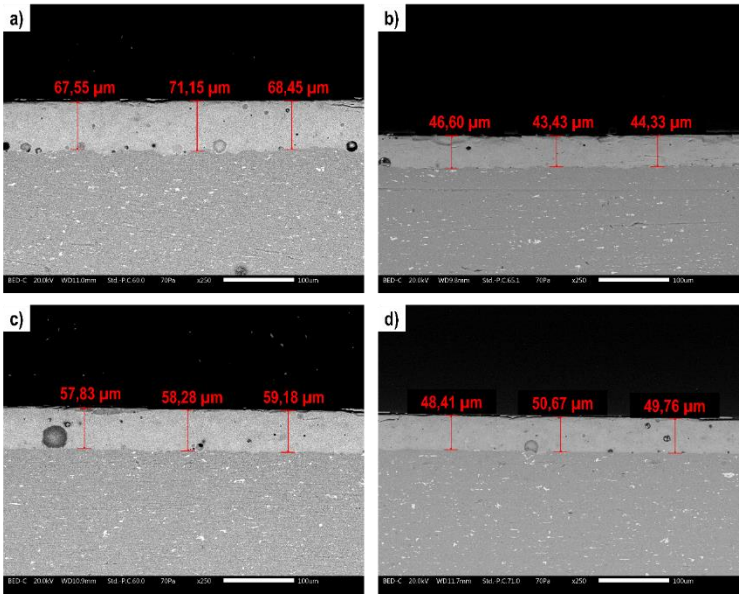


**Figure 3-4. SEM cross-sectional micrographs (250x magnification, 100 µm marker, BSE) of the enamelled samples (a) G0, (b) G025, (c) G05, (d) G1.**

### 3.3.2 Abrasion resistance

FIGURE 3-5 shows the mass loss trends of the different samples during the P.E.I. abrasion test. The evolution of mass loss with the increase of abrasion cycles does not follow a uniform trend for all the samples. The *G0*, *G025*, and *G05* samples undergo a uniform mass loss process over time, whereas the G1 sample shows a discontinuity after 500 abrasion cycles, the moment after which the rate of mass loss dramatically increases. This behaviour is probably due to the formation of big enamel chips that are detached during the abrasive process. It is necessary to point out that mass loss data must be coupled with other data, such as gloss change, roughness evaluation and microscopic observations, in order to better evaluate the damage mechanisms: some artefacts can arise due to the opening of enamel porosity and subsequent incorporation of the debris.

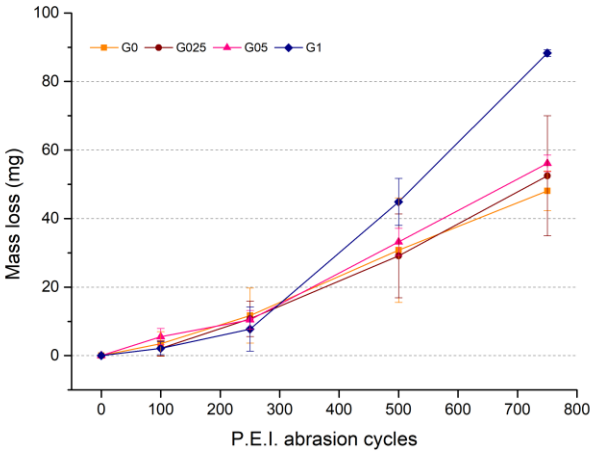


**Figure 3-5. Mass loss evolution during P.E.I. abrasion test.**

TABLE 3-3 shows a comparison of mass loss data present in the literature. The presented data are both acquired by means of Taber and P.E.I. test.

**Table 3-3. Comparison of mass loss data of different enamel systems.**

| Samples | Abrasive test/cycles | Mass loss reduction (%) |
|---|---|---|
| **10 wt.% spodumene[145]** | Taber / 500 | 29 % |
| **10 wt. % quartz[145]** | Taber / 500 | 50 % |
| **1 wt.% WC[145]** | Taber / 1000 | - 525 % |
| **1 wt.% WC sonicated[145]** | Taber / 1000 | 50 % |
| **5 wt.% SiC[145]** | Taber / 1000 | 65 % |
| **5 wt.% SiC[146]** | P.E.I. / 1000 | 86 % |
| **10 wt.% $Al_2O_3$[156]** | Taber / 1000 | 15 % |
| **1 wt.% graphite[145]** | Taber / 1000 | -150 % |

As it is possible to observe from literature data, SiC particles are able to provide a greater mass loss reduction with respect to the reference samples, in particular when the abrasive action is uniform on the sample's surface. The addition of graphene was

demonstrated to provide a decreased abrasion resistance, probably due to the combined effect of an aggressive abrasion action (exploited by the Taber test) coupled with the tendency of the flakes to agglomerate thus facilitating the formation of enamel chips. In the present study the mass loss variation of the samples after 750 P.E.I. cycles was assessed to be -84%, -16%, and -9% for the *G1*, *G05*, and *G025* samples, respectively. Thus, the addition of a high concentration of flakes is confirmed to have detrimental effects on the abrasion resistance of these enamel coatings, whereas the addition of 0.25 wt.% of graphene-based filler seems to have a neutral effect on this property.

FIGURE 3-6 shows the evolution of surface roughness and gloss along with the exploited P.E.I. abrasion cycles.

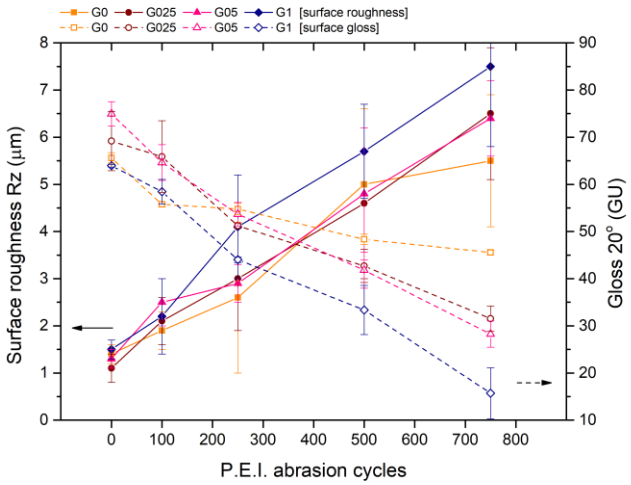


**Figure 3-6. Evolution of surface roughness and gloss during P.E.I. abrasion test.**

The *G0* sample is the only specimen that keeps a satisfactory gloss level (> 50 GU or close) also after 750 abrasion cycles, whereas the other samples show gloss values lower than 35 GU. The evolution of the gloss is different between the reference sample and the composite enamels: the first shows a discontinuity in the gloss loss trend after 100 abrasion cycles, whereas all the other samples follow a linear decreasing trend along all the tested interval. Considering the error bars and the differences between the starting surface roughness values, it is possible to state that the higher is the graphene-based filler concentration, the greater is the measured gloss loss, as the *G025*, *G05*, and *G1* samples have a residual gloss (at 750 abrasion cycles) of 46%, 38%, and 24%, respectively.

The evolution of the surface roughness follows an opposite trend with respect to the gloss, as it increases along with the applied abrasion cycles. The intermediate samples (*G025* and *G05* samples) follow a similar trend, whereas the extreme samples (reference sample and *G1* sample) show some discontinuities in the surface roughness evolution. In particular, the *G1* sample undergoes an important surface roughness increase after 100 abrasion cycles, whereas the reference sample undergoes a stabilization of the surface roughness after 500 abrasion cycles. Despite these differences, it is important to consider the large error bars related to the surface roughness vaues of the *G1* and reference samples and try to investigate the damaging mechanisms by SEM observations and to evaluate the whole status of the abraded samples. FIGURE 3-7 reports a photograph of the samples at the end of the P.E.I. test.

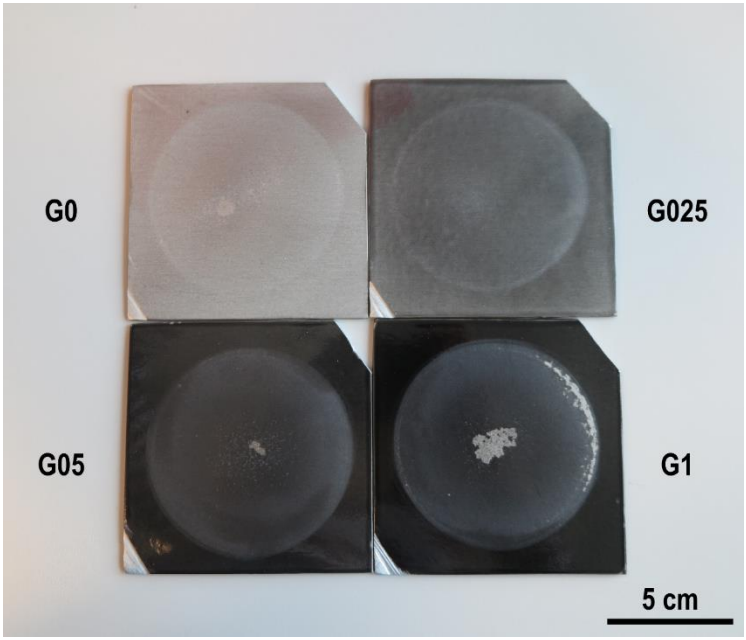


**Figure 3-7. Photograph of the enamelled samples after 750 P.E.I. abrasion cycles.**

At the end of the P.E.I. abrasion test, the enamelled samples appear to be differently damaged. The *G0* shows a small and superficial enamel detachment, *G025* sample appears to be very uniformly damaged, whereas the *G05* and *G1* sample undergo a quite significant enamel detachment in the central area. In order to better understand the damage mechanisms, it was necessary to investigate the surface damaging

status by means of SEM analyses. FIGURE 3-8 shows the in-plane SEM micrographs of the tested samples after 750 abrasion cycles.

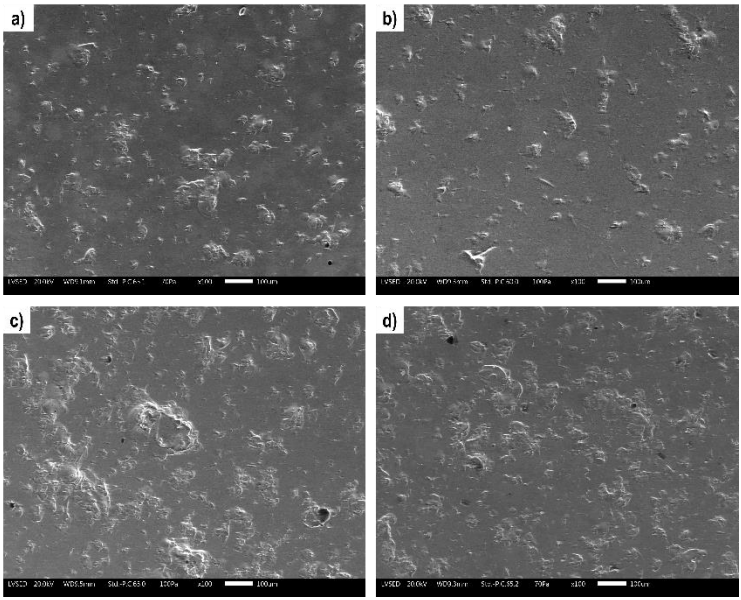


**Figure 3-8. SEM images (100x magnification, 100 µm marker, SE) of the enamelled samples after 750 P.E.I. abrasion cycles, (a) G0, (b) G025, (c) G05, (d) G1.**

The micrographs reported in FIGURE 3-8 show the abraded surfaces in an area of the sample where no detachment phenomena have occurred, and no defects are visible by naked eye. The *G0* sample surface is not uniformly damaged, as it is possible to highlight the presence of some large defects and the disclosure of some small pores. The *G05* and *G1* samples show a very high damaged surface, whereas the *G025* sample's surface appears to be uniformly damaged, with a lower density of defects that are limited to the more superficial layer of the coating. As seen in FIGURE 3-7, all the samples, except from the *G025* sample, undergo enamel detachment after 750 abrasion cycles. Then, the damaging morphology at the microscopic level is in perfect accordance with the macroscopic status of the samples, evidencing the good performance of the *G025* samples with respect to the other formulations.
It is then interesting to better examine the areas of the samples where detachment phenomena have occurred. FIGURE 3-9 shows SEM images of the interface between the central detachment areas and the surrounding sample surface.

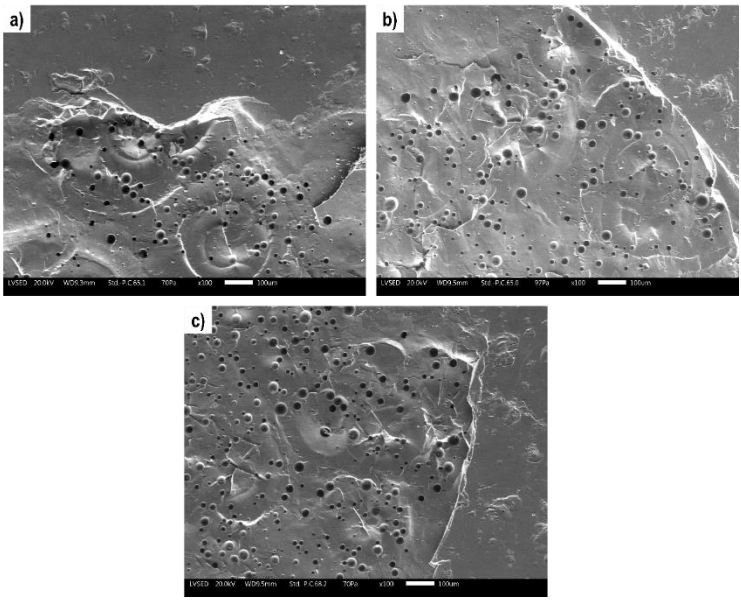


**Figure 3-9. SEM images (100x magnification, 100 µm marker, SE) of the enamelled samples after 750 P.E.I. abrasion cycles at the interface between the detached area and the uniform abraded surface area, (a) G0, (b) G05, (c) G1.**

All the samples show the opening of porosity in the area where enamel detachment has occurred. It is important to underline that the opening of porosity can deeply influence the mass loss results, due to the insertion of material debris inside the pores. In addition to that, it is also possible to highlight the presence of sharp fracture lines, that can be considered as preferential sites from which chipping of enamel coating happens. Thus, the addition of a small quantity of graphene filler seems to improve the resistance of the coatings to the abrasive action of the composite tribosystem, whereas the presence of a higher concentration of graphene flakes eases the formation of enamel chips during the abrasive process. The abrasive process leads to the natural exfoliation of the graphene-based filler[257], and the presence of agglomerated flakes can induce the detachment of big enamel portions.
In order to have further details of damage mechanisms it was decided to exploit 20 abrasion cycles and carry out SEM investigations subsequently. FIGURE 3-10 shows the morphology of *G0* sample surface after 20 and 750 P.E.I. abrasion cycles.

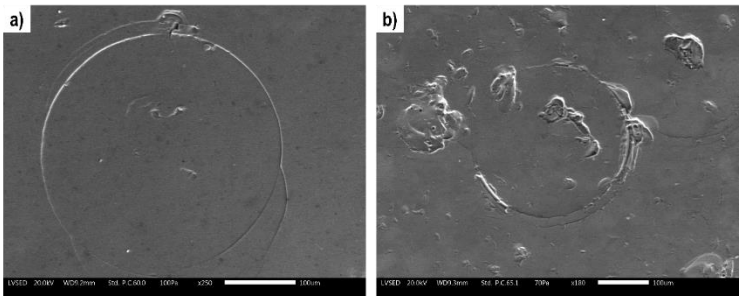


**Figure 3-10. SEM images (100 µm marker, SE) of the G0 enamel sample after (a) 20 and (b) 750 P.E.I. abrasion cycles.**

FIGURE 3-10(A) shows the presence circular cracks on enamel surface just after 20 abrasion cycles. The shape of these cracks is attributable to the impact caused by the stainless-steel spheres of the abrasion charge used for P.E.I. testing. By observing the morphology of the surface after 750 abrasion cycles it is possible to notice that circular cracks seem to be the starting point and activators for the propagation of the damage. The damage morphologies observed in FIGURE 3-9 and in FIGURE 3-10 are typical of ceramic and vitreous material. As already studied and highlighted by Rossi et al.[145] the abrasion mechanism probably starts from the porosity where the crack nucleates and then it propagates from one pore to another.
Abrasion could lead to the opening of enamel's porosity, thus the possible contact points between the metallic substrate and the external environment could destroy the protective action of the enamel layer. Useful information about the coating resistance properties and produced wear damage can be obtained performing impedance spectroscopy measurements, thus, monitoring the impedance modulus |Z| at low frequency values, which is correlated to the protection of layer. A decrease in the low frequency modulus value is the signal of presence of defects throughout the whole enamel, such as cracks. FIGURE 3-11 shows the trend of the impedance modulus at low frequency values ($10^{-2}$ Hz) in function of P.E.I. cycles number. It is possible to see how, by increasing the amount of graphene inside the matrix, the obtained coating does not offer the same protection as the graphene-free sample, although they can all be considered as good protective deposits, since their |Z| is higher than $10^6$ $\Omega$*cm$^2$. During P.E.I. testing, the impedance modulus continues to decrease, indicating that the coating is more and more defective and less protective. Both considering the trend in time and the value of |Z| after 750 abrasion cycles it is possible to observe that an increase in the graphene flakes inside the enamel matrix leads to lower protective properties, probably due to the higher defectiveness inside the coating created by the onset of cracks and enamel chips by brittle fracture.

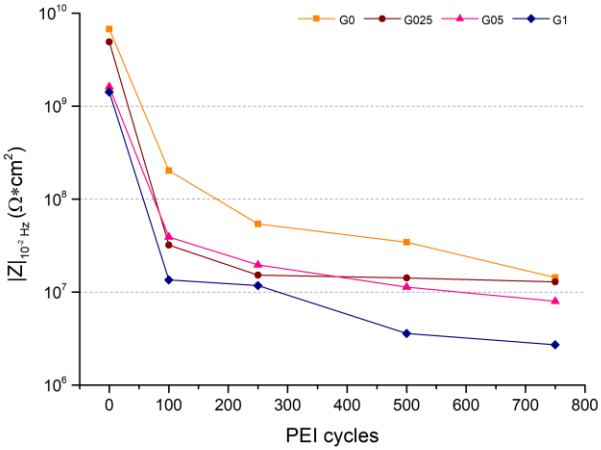


**Figure 3-11. Evolution of impedance modulus along with the P.E.I. abrasion cycles.**

## *3.4 Conclusions and future perspectives*

In order to assess the abrasion resistance of different enamelled samples it is necessary to consider all the listed aspects, starting from gloss and roughness changes to microscopic observations:

- Gloss and roughness measurements underline the good behaviour of the *G0* sample and the bad performances of the *G1* sample, probably caused by the high surface roughness and the tendency of lamellar GNPs to produce flakes during the mechanical damaging process.
- SEM analyses show that the *G025* sample is the only sample that does not undergo enamel detachment. In addition to that, its surface appears to be homogeneously and limitately damaged. It seems that the presence of small GNPs amounts could reduce the nucleation of cracks and improve the abrasion resistance, thus limiting the damage to small and superficial defects.
- The effect of graphene is then clearly explained: a small amount of GNPs (0.25 wt.%) inside the enamel matrix allows a uniform damage of the surface with respect to the sample without GNPs. A further increase in graphene concentration leads to a worsening of both the aesthetical and the functional properties of the coating. On the contrary, the *G0* sample has an overall good behaviour but it undergoes a small enamel

detachment. Thus, it is possible to state that a small amount of graphene inside the matrix could help to improve the mechanical properties of the coating without carrying negative side effects.

## *3.5 Acknowldegments*

The authors gratefully acknowledge Emaylum Italia (Chignolo d'Isola (BG), Italy), in particular Attilio Compagnoni, for the samples produced and for useful discussion.

# 4 The influence of micro and macro sized $Al_2O_3$ hard particles on the abrasion and chemical resistance of composite vitreous enamel coatings

***Part of this chapter has been published in:***

S. Rossi, F. Russo, M. Calovi, M. del Rincòn, D. Velez, **"The influence of the size of corundum particles on the properties of chemically resistant porcelain enamels"** *Ceramics International,* 47 (2021) 11618-11627.

*Conceptualization*: S. Rossi, D. Velez; *Methodology*: S. Rossi; *Investigation*: F. Russo, M. Calovi, M. del Rincòn; *Formal analysis*: F. Russo; *Validation*: F. Russo; *Supervision*: S. Rossi, D. Velez; *Writing*: F. Russo, M. Calovi.

## *4.1 Introduction*

The main weakness of enamel coatings is represented by the glassy and brittle nature of the matrix: therefore, it is necessary to find some solutions to address this issue effectively and improve their resistance to abrasion. A possible way to improve the resistance of enamel coatings could be the use of hard ceramic particles (HCPs), such as silicon carbide (SiC), tungsten carbide (WC), titanium boride ($TiB_2$) and alumina ($Al_2O_3$). These HCPs are widely employed in the fabrication of resistant polymeric, metallic, and ceramic matrix composites[197-200]. Important consideration to be done when choosing the filler are the following: temperature resistance, agglomeration behavior, shape of the filler, and affinity with the matrix. Many possibilities can be exploited to achieve an improved abrasion resistance, but the choice should be calibrated in dependence of the chosen application and the resistance to other elements (chemicals, weathering, corrosion). Nevertheless, it is important to consider the compatibility and the solubility of the particles into the vitreous matrix, as it is necessary to avoid the formation of residual stresses or the complete solubilization of the particles during the firing treatment, which could reduce or even cancel the desired positive effects.

SiC and WC were the most common HCPs used in these studies: it was demonstrated that the positive effects of these particles are only exploited at high concentrations, from 5 wt.% to 10 wt.%[146], but great attention should be devoted to avoid particle agglomeration, in particular when dealing with WC particles[145]. The distribution of the filler inside the matrix is a crucial point to be considered as it could influence the abrasion resistance of the coatings and it acquires great importance when dealing with nano-dimensional particle, mainly because the agglomeration phenomena are increased. As a rule, it is possible to state that if

nanoparticles are considered, the threshold amount of particles not to be exceeded to avoid negative effects is very much lower with respect to the addition of micro-sized particles. As in the case of SiC and WC particles, the shape of the filler also play an important role in determining the abrasion resistance of the coatings. When the samples are subjected to Taber test, encouraging results have been obtained only with the addition of tungsten carbide, because the sharp shape of SiC particles could be a point of initiation of cracks and fractures[146]. An opposite behavior was observed in the samples subjected to PEI test, as the main factor influencing the abrasion behavior is the distribution of the particles in the enamel matrix and tungsten carbide always show some aggregation phenomena, despite the sonication process underwent.

In the literature, there are many other papers about the effect of hard particles addition on the properties of enamel coatings. A recent work evidenced that the addition of $Cr_2O_3$ particles in an enamel coating can retard the precipitation of $BaSi_2O_5$, promoting the formation of nanoscale crystallites of $BaCrO_4$ and/or $BaCr_2O_4$ which involve the formation of a lubricating glaze layer[259]. Consequently, the glazed layer exhibits a decrease of the friction coefficient and wear rate. Moreover, zirconia powders are usually employed to improve the glass-ceramics resistance to acids and alkali, as well as their mechanical properties due to stress-induced phase transformation of tetragonal-$ZrO_2$ particles[260-262].

Other possibilities are represented by the addition of $TiB_2$[159, 263] or alumina particles[264, 265]. A recent study evidence the possibility to use a small amount of micrometric-sized $TiB_2$ particles to reduce the wear rate of enamel coatings[159]. Finally, alumina particles represent one of the most reliable reinforcing fillers for enamel coatings[156, 157]. Strengthening effects are dependent on both the volume fraction and the size of the included alumina particles[266]. The use of alumina particles was demonstrated to have a positive effect on the abrasion resistance of enamel coatings, as these particles are very hard, and even if some of them are exposed on the surface of the coating, they provide optimal resistance to abrasion[156].

The study presented in this chapter is part of bigger project, about abrasion resistant enamel coatings with the addition of corundum particles, that this research group has started some years ago in collaboration with the Surface Engineering Group of CIDETEC, San Sebastian, Spain. To better explain the significance of my study in relation to this project it is necessary to summarize the main results obtained by previous works carried out on these systems[156, 157].

The previous works on this topic investigated the effect of the size and concentration of corundum particles on the surface properties and abrasion resistance of chemically resistant enamel coatings. The microstructural modifications caused by the addition of the corundum particles were studied, then the abrasion resistance of these coatings was assessed by means of Taber test, and the functional properties

of the enamels were monitored by EIS measurements and exposure in an aggressive environment by means of the Kesternich chamber test.
The corundum particles have been added into the enamel formulations to obtain 6 different formulas with different corundum content. Details about the studied formulations are shown in TABLE 4-1.

**Table 4-1: Nomenclature of the samples with component formulations, adapted from[156].**

| Component | Sample name | | | | | | |
|---|---|---|---|---|---|---|---|
| | **S0** | **A5** | **A10** | **A20** | **B5** | **B10** | **B20** |
| **Macro α- $Al_2O_3$** | 0 | 5 | 10 | 20 | - | - | - |
| **Micro α- $Al_2O_3$** | 0 | - | - | - | 5 | 10 | 20 |

Thus, three different concentrations of the filler were taken under consideration for each of the two particle's sizes (micro-size and macro-size. FIGURE 4-1 shows the particle size distribution of the corundum particles used in these studies.
The particle size has been analyzed by Mastersizer3000 MAZ6140 (MALVERN Instruments Ltd.), and by SEM microscopy. The macro alumina particles are characterized by an irregular shape with sharp edges. On the contrary, the micrometric particles are aggregated and present a rounded surface.
The samples were deposited by wet-spray deposition method starting from wet slips, once deposited the samples were dried at 80 ˚C for 20 minutes and fired at 830 ˚C for 6 minutes.
First, the presence of corundum particles modified the surface roughness of the obtained samples, with a relevant increase with respect to standard values (0.15 μm) , in particular for the A20 and B20 formulations, that had an Ra value of about 0.60 μm and 2.25 μm, respectively. Although this aspect could be negative for corrosion resistance, it can be useful for anti-wear properties of enamel, as the hard corundum particle emerging on the surface could increase the resistance of the coatings. The high surface roughness value obtained for the "B" sample serie are probably due to the incomplete firing treatment occurred in these cases. This theory is also confirmed by the lower adherence resistance (tested by impact test) of the B serie samples with respect to the A serie. In addition to that, the presence of corundum particles has a marked effect on the internal microstructure of the coatings, that appears to be formed by non interconnected pores in all cases.

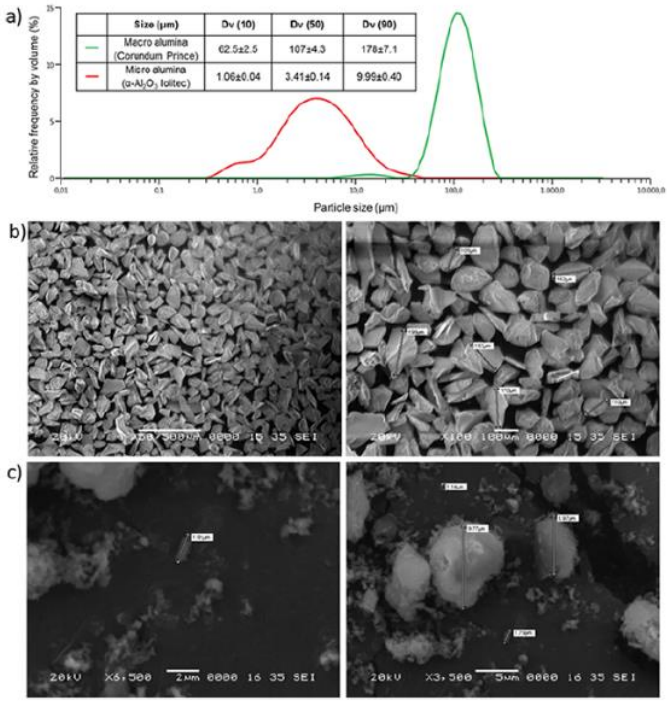


**Figure 4-1: (a) Alumina particles size (Macro H-924 Prince, micro α-$Al_2O_3$ Iolitec), (b) SEM micrographs of macro sized corundum and (c) SEM micrograph of micro sized corundum particles, adapted from [156].**

FIGURE 4-2 shows the microstructural investigations of the layer cross section of the samples under consideration. The addition of an increasing corundum particle concentration leads to the size and amount reduction of bubbles. This effect is more marked for micro-sized alumina particles, as they can be almost completely solubilized in the enamel matrix reducing the production of gases during firing. Thus, the integration of corundum particles in the enamel matrix depends on the particles size: macro alumina particles are partially solubilized and are heterogeneously distributed in the enamel matrix, whereas micrometric alumina particles are homogeneously distributed in the coatings thickness.

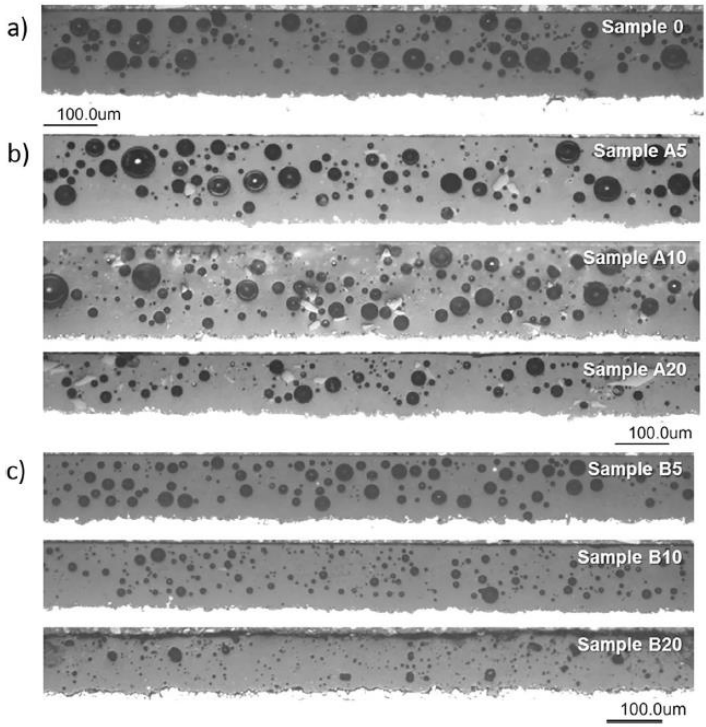


**Figure 4-2. Optical micrograph of cross section of (a) 0 sample (reference), (b) A samples and (c) B samples, adapted from [157].**

The abrasion resistance of the coatings was tested by means of Taber tests expoited by using two H22 abrasive wheels and applying 250 g of weight to each of them. A total of 1500 Taber abrasion cycles were carried out, and the protective properties of the coatings were assessed by means of EIS measurements in 0.3 wt.% $Na_2SO_4$ solution. All the samples showed a linear mass loss trend with the increasing Taber abrasion cycles. At the end of the test, all the samples, except A5 and B5, showed a decreased mass loss with respect to the reference sample, probably due to the presence of big pores. EIS measurements performed before abrasion, showed that a greater quantity of corundum particles generates more defects in the coatings, leading to a decreased EIS modulus value[156]. This effect was more marked in the presence of smaller corundum particles, probably due to the underfiring state of the coatings. Once subjected to the abrasion test, the samples show a different trend: the impedance modulus decreases with the abrasion cycles as all the composite coatings become more and more defective, but with a lower speed compared to the

reference sample. This effect is probably due to the improved microstructure (less and smaller pores) and by the effectiveness of the particles in counteracting the abrasive damaging process. The increase in particles concentration has positive effects on abrasion resistance but it also represents a negative aspect, as the presence of small particles creates preferential sites for chemical attack in aggressive environments. FIGURE 4-3 shows the surface state of the enamelled composite samples after 10 cycles of exposure in the Kesternich chamber.

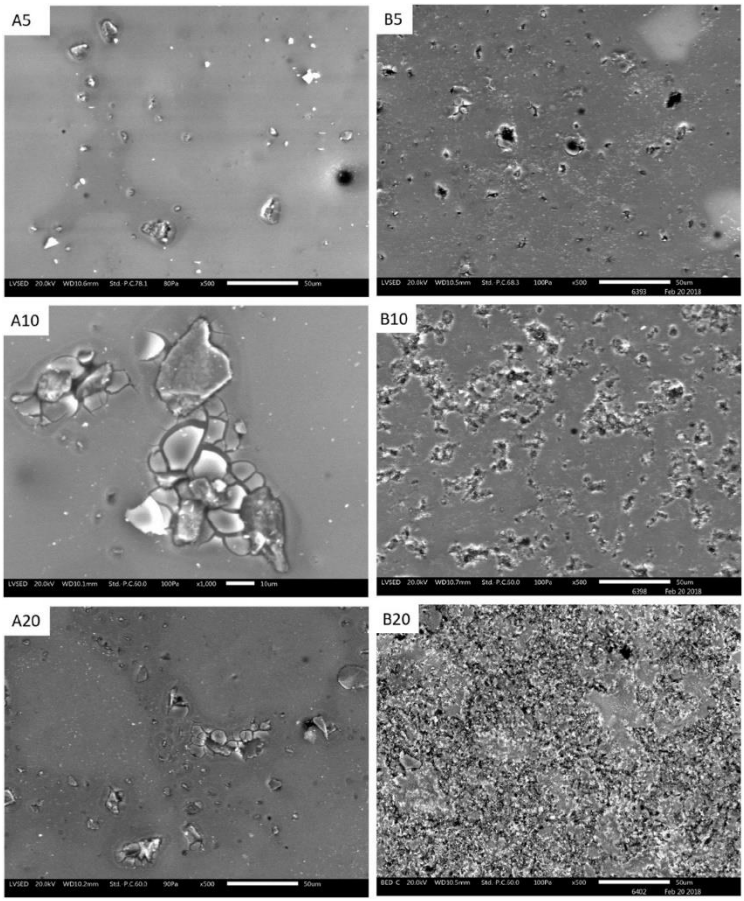


**Figure 4-3. SEM micrographs (SE) of the degradation of the A serie and B serie enamel samples after 10 cycles exposure in the Kesternich chamber, adapted from [156].**

The corrosive attack is more evident increasing the amount of particles. In sample B5 it is evident how the corrosive attack occurs below the surface layer, in the

correspondence of porosity, with consequent detachment of glassy layer. This attack is more and more intense in the presence of greater quantities of particles, up to leaving only a few areas of the surface intact, as can be seen in the sample B20[156]. Otherwise, the addition of macro-sized particles leads to an improved abrasion resistance with no detrimental effects on the resistance to harsh chemical environments. These studies were exploited by keeping the firing treatment constant, but it resulted evident that a non-optimized firing step can modify the microstructure of the coatings and their functional properties as well.

Thus, the main aim of this work is to study the abrasion and functional behaviour of composite enamel coatings deposited on a low carbon steel substrates with the addition of micro and macro sized $Al_2O_3$ particles, after the optimization of the firing treatment. The alumina particles concentration was chosen to be 20 wt.% in all cases, but the firing treatment was optimized for each of the investigated sample. After the optimization of the deposition parameters, this study focused on the influence of the alumina particles size on the abrasion and chemical resistance of the coatings. First, a microstructural characterization of the obtained composite coatings was carried out. The abrasion behaviour of the composite enamel coatings was studied by means of the P.E.I. test. The produced damage was evaluated by mass loss measurements, EIS measurements, and microscopy analyses. Considering a possible technical application, the chemical resistance of the modified enamels was evaluated by Kesternich test, simulating an acidic industrial environment. This chapter is therefore focused on the effect of the alumina particles size on the properties and performances of enamel coatings in harsh environments.

## *4.2 Materials and methods*

### 4.2.1 Materials

**Enamel frit** The samples were produced starting from the commercial frit VP15/1546 (Prince Minerals). This frit, based on $SiO_2$, $Na_2O$, $TiO_2$ is used to protect chemical reactors and heat exchangers, where good chemical and corrosion resistance are required. The frit composition, analyzed by Energy Dispersive X-Ray Spectroscopy (EDXS) is the following and the results are expressed as normalized % mass with 2σ errors: O 46.5 ± 0.5, Si 34.5 ± 0.4, Na 14.4 ± 0.5, Ti 1.4 ± 0.1, Co 0.9 ± 0.3, Al 0.7 ± 0.2, Ca 0.6 ± 0.1, K 0.5 ± 0.1, Cu 0.5 ± 0.1.

**Metal substrate and pretreatment process** The enamel samples were deposited on carbon steel (DC04EK) panels, having dimensions of 100 mm x 100 mm x 1.5 mm.

**Corundum particles** In this study, corundum particles of two different size (micro and macro) have been used to produce the composite enamel coating. The macro-sized α- $Al_2O_3$ alumina powder is the Corundum H-924 (Prince Minerals) having a D90 of 178 μm., whereas the micro-sized α- $Al_2O_3$ alumina powder (Iolitec) has a D90 of 9.99 μm. The complete characterization of the corundum particles have been shown in SECTION 4.1.

### 4.2.2 Methods

#### *4.2.2.1 Samples preparation*

The first step consists in the choice of the substrate that will be coated. Then, the enamel deposition process parameters must be optimized to obtain coatings which can guarantee the best performances.

**Substrate pretreatment** The steel substrates were cleaned in acetone for 2 minutes to remove traces of grease and oils, and then they were sandblasted to improve adherence between the substrate and the enamel layer. After the sandblasting step, the samples were cleaned again in acetone for 2 minutes using an ultrasound bath. The final surface roughness ($R_a$) of the pretreated steel substrates was ranging between 1.30 – 1.40 μm.

**Deposition process parameters and sample types** The enamel samples studied in this work have been deposited by manual wet deposition methods starting from different enamel slips. The commercial frit was mixed with $Al_2O_3$ particles, additives and water to obtain three different enamel formulations, including the reference formulation free from corundum particles. Details of the prepared formulations, together with the chosen sample labelling, are shown in TABLE 4-2.

The designation of samples is in accordance with the labelling and convention used in previous studies, where “A” stands for macro-size corundum, and “B” stands for micro-sized corundum particles. Clay was used to keep the frit particles suspended in the slip, borax was added to improve the setting effect and inhibit rusting of the substrate, cobalt oxide was added as an adherence oxide, and sodium nitrite was used as a set-up salt with excellent rust inhibiting properties. The enamel formulations were prepared by wet-milling process until obtaining an enamel fineness of 0.5 in 3600 mesh/cm$^2$, according to the BAYER enamel test sieve. The specific gravity of the slips, measured by Pemco densitometer, was adjusted to be in the 1.70 - 1.74 g/cm$^3$ range. The enamel slips were applied onto the DC04EK substrates by wet spray deposition and the applied mass was 5 g/cm$^{-2}$.

**Table 4-2. Enamel samples formulation (g) and sample labelling.**

| | Sample name | | |
|---|---|---|---|
| **Component** | **S0** | **A20** | **B20** |
| **Frit VP15/1546** | 100 | 100 | 100 |
| **Macro α-$Al_2O_3$** | - | 20 | - |
| **Micro α-$Al_2O_3$** | - | - | 20 |
| **Clay** | 5 | 5 | 5 |
| **Sodium nitrite** | 0.10 | 0.10 | 0.10 |
| **Borax** | 0.30 | 0.30 | 0.30 |
| **Cobalt oxide** | 0.50 | 0.50 | 0.50 |
| **Water** | 55 | 55 | 55 |

The samples were dried at 80 ˚C for 20 minutes to let water evaporate, and then they were fired at appropriate temperatures. The firing temperatures were optimized for each enamel formulation, evaluating their sintering behaviour by heating microscope. TABLE 4-3 shows the results obtained by heating microscope analyses. The effect of the $Al_2O_3$ particle size on the thermal properties of the composite formulation is very clear: all the characteristic temperatures are moved to upper ranges when alumina is included in the formulation, and the presence of micro-alumina makes this effect stronger as it partially dissolve faster respect to coarse-grained alumina, thus increasing enamel formulation viscosity.

**Table 4-3. Characteristic temperatures of the enamel formulations, assessed by heating microscope analysis.**

| | Temperature (ºC) | | | | |
|---|---|---|---|---|---|
| | **Sintering** | **Softening** | **Sphere** | **Half sphere** | **Melting** |
| |  |  |  |  |  |
| **S0** | 648 | 700 | 750 | 789 | 818 |
| **A20** | 628 | 680 | 764 | 806 | 857 |
| **B20** | 681 | 688 | 903 | 925 | 959 |

Considering the results obtained, the S0, A20 and B20 samples were fired in hot air at 789 °C for 10 min, 806 °C for 10 min and 925 °C for 10 min, respectively.

#### *4.2.2.2 Coatings characterization*

This section introduces the characterization techniques used for the investigation of the coatings and their performances, including a complete surface and microstructural characterization, the assessment of their abrasion resistance and chemical resistance.

**Surface and microstructural analysis** The surface aspect of the samples was investigated by SEM in order to see if and how the addition of alumina particles of different dimensions modify the surface topography. The coatings thickness was measured according to SECTION 2.2, performing 9 measurements on three different samples (3 measurements on each sample). The coatings surface roughness was characterized according to SECTION 2.2, repeating 3 measurements on 5 samples replicates. In order to have further information on the surface properties, it was also decided to perform contact angle measurements by the optical tensiometer Theta 200-Basic Biolin Scientific, by means of 3 measurements for each sample typology. Micro-hardness tests were also exploitedon sample's cross-section with a Micro Hardness testing HM 2000 (Fischer), following the ASTM C 1327-03 standard. After these measurements, a detailed study of the enamels microstructure was performed by means of SEM (Jeol JSM-5500LV), also used in the coatings thickness determination. The adherence between the enamel layer and the substrate was evaluated by impact test, according to the UNI EN 10209 (2013) Annex 3 standard.

**Abrasion resistance test** The abrasion resistance of these composite enaels was evaluated by means of P.E.I. test for a total of 5000 abrasion cycles. Mass loss and surface roughness ($R_a$) were monitored at intermediate abrasion cycles. The reported roughness values are the average of 5 measurements. At the end of the test, the damage morphologies were observed by optical and SEM microscope and the damage evolution was assessed by EIS measurements.

**Electrochemical Impedance Spectroscopy measurements** EIS measurements have been carried out using the potentiostat Parstat 2273 with the software PowerSuit ZSimpWin in the three-electrode configuration described in SECTION 2.2 . A signal of 15 mV (peak-to-peak) amplitude in the $10^5$–$10^{-1}$ Hz frequency range has been applied. The tested area was equal to 28.27 $cm^2$. The sampling rate was equal to 5 points per dcade.

**Kesternich test** Moist air containing sulfur dioxide quickly produces easily visible corrosion on many metals in a form resembling that occurring in industrial

environments. It is therefore a test medium well suited to detect pores or other sources of weakness in protective coatings and deficiencies in corrosion resistance associated with unsuitable alloy composition or treatments. In order to assess the behaviour of the coatings in aggressive environments simulating the harsh conditions of chemical reactors and industrial vessels, the samples were subjected to 10 cycles of Kesternich test, following the ASTM G87 standard ant the UNI EN ISO 3231. The samples to be tested are placed in a 300 liters chamber that is kept at 40 ± 3 °C. The chamber is filled with a $SO_2$ atmosphere for 8 hours, and then the aggressive atmosphere is removed but keeping the samples conditioned at the same temperature for 16 hours. A complete Kesternich cycle then lasts 24 hours. The damaged surface was observed after 1,3,6, and 10 cycles by optical microscope and, at the end of the test, the samples were subjected to SEM investigations.

## *4.3 Results and discussion*

### 4.3.1 Surface and microstructural analysis

The thermal treatment was optimized for each sample type, thus a detailed characterization of the samples including roughness, surface aspect, bubble structure, dispersion of the alumina particles, and adherence is needed. FIGURE 4-4 shows the photograph of the produced samples.

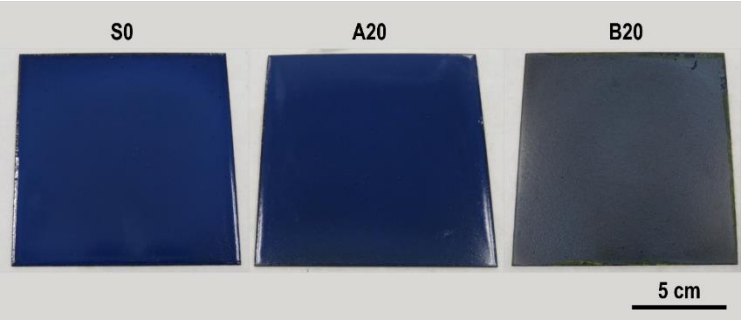


**Figure 4-4. Photograph of the enamel samples under study.**

The addition of macro-sized alumina particles do not lead to great changes in the colour and surface roughness of the samples, whereas the addition of micro-sized alumina leads to an important change in colour, surface aspect (as the surface becomes matt), and surface roughness. TABLE 4-4 summarizes the evaluation of the samples surface characteristics and thickness.

**Table 4-4. Surface roughness and surface gloss of the enamel samples under investigation.**

| | Sample name | | |
|---|---|---|---|
| **Surface property** | **S0** | **A20** | **B20** |
| **Thickness (µm)** | 185 ± 12 | 174 ± 14 | 214 ± 26 |
| **Ra (µm)** | 0.18 ± 0.03 | 0.52 ± 0.10 | 1.40 ± 0.17 |
| **Rz (µm)** | 1.36 ± 0.35 | 2.81 ± 0.61 | 9.21 ± 0.62 |
| **Gloss 20° (GU)** | 47 ±.3 1.1 | 20.0 ± 0.4 | 1.7 ± 0.1 |
| **Gloss 60° (GU)** | 79.5 ± 0.4 | 58.0 ± 0.3 | 10.8 ± 0.5 |
| **Gloss 80° (GU)** | 91.8 ± 0.6 | 71.1 ± 0.3 | 16.8 ± 0.9 |

Considering the chosen deposition method, the samples have a similar thickness. The surface roughness increases with the addition of corundum particles, and this effect is more evident in presence of micro-sized particles. This result is probably due to the difficulty of creating a well-fired enamel in presence of a high amount of micro alumina particles, that being easily dissolved into the matrix, increase the refractoriness of the formulation. The measured roughness values are coherent with the results achieved in previous studies on similar samples[156, 157]. The A20 and B20 samples show an increase in the Ra value of about 190% and 680%. The optimization of the firing treatment had a marked effect on the surface properties of the B20 sample as its roughness was improved from about 2.00 µm to 1.40 µm.
TABLE 4-5 shows the results of the contact angle (CA) measurements.

**Table 4-5. Contact angle measurement on the enamel samples under study.**

| | S0 | A20 | B20 |
|---|---|---|---|
| **CA mean [°]** | 33.2 ± 3.0 | 45.4 ± 8.9 | 50.7 ± 4.2 |
| |  |  |  |

All the samples show a contact angle value lower than 90°, the threshold over which the surfaces are considered hydrophobic. Thus, all the enamels, show a good wettability and hydrophilicity, although the presence of macro-sized and micro-sized alumina particles increase the CA values towards more hydrophobic values.The main reason behind these results can be attributable to the possibility of micro-sized

alumina particles to easily dissolve in water, increasing the equilibrium surface tension of the water drop[267].

FIGURE 4-5 shows the microstructure of the enamel samples under study. The enamel microstructure is made of a glassy layer containing the typical closed porosity. This porosity develops during the firing treatment, and it is caused by the evolution of gases such as $N_2$, $CO_2$, CO, $H_2O$ and $CH_4$. The bubble size and distribution strongly depend on many process parameters, such as the firing treatment, the viscosity and surface tension of the enamel formulation. The bubble structure also determines the mechanical properties of the enamel coating, as the presence of many small cavities leads to a low adherence between the coating and the substrate, whereas the presence of big bubbles makes the enamel layer very brittle also under low impact or stress.

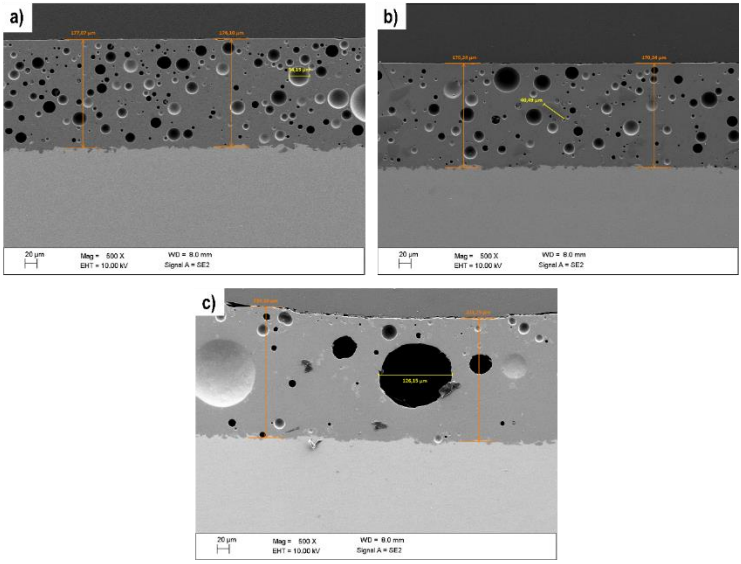


**Figure 4-5. SEM micrographs (500x magnification, 20 µm marker, BSE) of samples cross-sections (a) S0 sample, (b) A20 sample, (c) B20 sample.**

The important microstructural parameters are summarized in TABLE 4-6. The reference sample S0 possesses a homogeneous structure with bubbles having a maximum diameter of 33 µm. The sample containing macro-sized alumina (A20) exhibits a decrease in the bubble amount of about 14% and a maximum diameter for the pores of 38 µm. Thus, the main microstructural difference among the S0 and A20 samples is the total amount of pores. The embedded $Al_2O_3$ particles in the A20 sample have an average dimension of 33 µm, which is consistently lower than the

original particles diameter. These alumina particles show a micro-hardness of 2461 ± 114 HV versus 793 ± 33 HV of the enamel matrix. Thus, the microstructural observations confirm the partial dissolution of the particles inside the enamel matrix. As regards the B20 sample, the addition of micro sized alumina does not influence the homogeneity of the enamel layer, which is free of particle agglomerates, but the coating shows a lower density of bubbles with dimensions about half of the whole coating thickness and representing non-negligible defectiveness. Considering the microstructural features of these enamel coatings it is possible to state that in all cases the porosity is not interconnected, and it is distributed along the whole layer thickness, thus guaranteeing optimal protection properties of the covered substrate.

**Table 4-6. Summary of the microstructural properties of the enamel coatings investigated by SEM.**

| | Sample name | | |
|---|---|---|---|
| **Microstructural property** | **S0** | **A20** | **B20** |
| **Thickness (μm)** | 175 ± 3 | 161 ± 3 | 208 ± 6 |
| **Porosity (%)** | 17.4 ± 3.7 | 14.9 ± 2.2 | 23.3 ± 1.0 |
| **Max. pore diameter (μm)** | 33.0 ± 2.0 | 37.7 ± 1.2 | 123.7 ± 1.2 |
| **Average pore diameter (μm)** | 7.9 ± 2.2 | 6.7 ± 1.4 | 14.6 ± 4.4 |
| **Average circularity** | 0.94 ± 0.12 | 0.91 ± 0.03 | 0.87 ± 0.01 |

A detailed SEM/EDX characterization enables to identify the distribution of different elements and the alumina particles into the enamel coating layer, as shown in FIGURE 4-6. The EDXS maps highlight the presence of an interface area between the substrate and the coating that is rich in iron, because of the chemical reactions occurring at the interface during the firing treatment, leading to the formation of a strong bond between the metal and the enamel. The distribution of aluminium is greatly affected by the size of the added alumina particles. The coating obtained by the addition of macro-sized alumina (sample A20) shows a heterogeneous distribution of this element, because of the partial solubility of the big alumina particles embedded in the matrix. In the case of the B20 sample, aluminum seems to be homogeneously distributed in the coating thickness and no big agglomerates can be detected. Thus, the deposition process enables a good distribution of the fillers, also in presence of micro-sized particles, avoiding undesired agglomeration phenomena.

Further insights on the distribution of the corundum particles inside the coating can be obtained by in-plane SEM/EDXS analyses. FIGURE 4-7 shows the in-plane SEM micrographs of the enamel samples and the distribution of aluminium and silicon. As

regards the A20 sample, it is possible to notice the presence of the corundum particles and two different regions with different compositions: the darker areas surrounding alumina particles, and ligher regions. The first reveal a higher presence of Al, equal to 7.72 ± 0.59 % (normalized % mass), whereas the latter show a decreased Al content, equal to 2.58 ± 0.23 % (normalized % mass). Thus, the lighter areas in the backscattered SEM micrographs are portions of the coating that were not affected by the partial solubilization of the corundum particles. As regards the B20 sample, it is possible to notice a quite homogenous distribution of the micro-corundum particles that is accompanied by the presence of coating's portions free from particles.

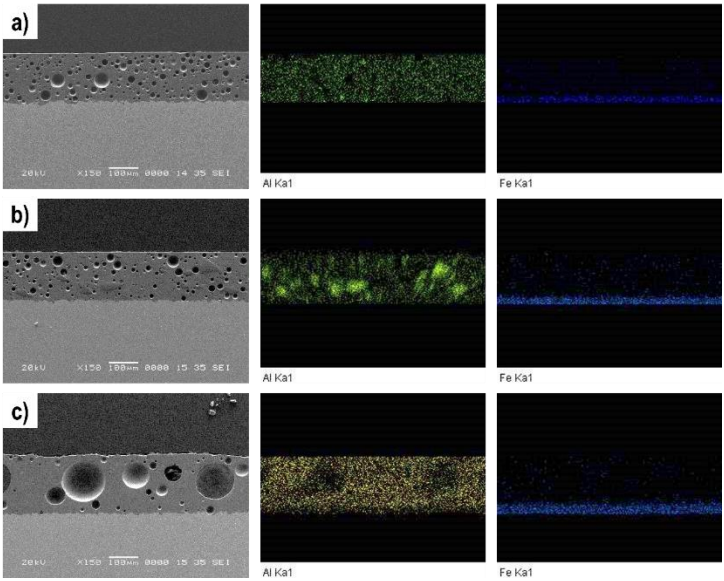


**Figure 4-6. Cross-sectional SEM micrographs (150x magnification, 100 µm marker, BSE) and EDXS maps (Al, green - Fe, blue) of the enamel samples under investigation (a) S0, (b) A20, (c) B20.**

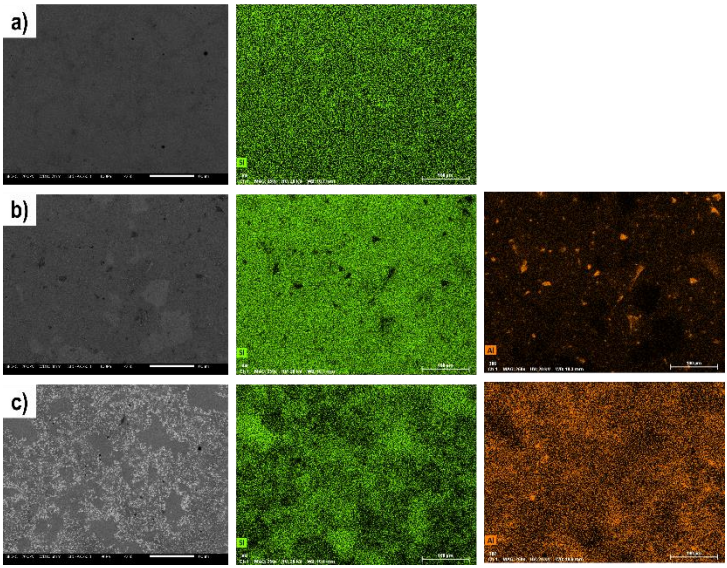


**Figure 4-7. In-plane SEM micrographs (200x magnification, 100 µm marker, BSE) and elemental maps (Si, green - Al, orange) of the enamel under study (a) S0, (b) A20, (c) B20.**

The determination of the adherence level between enamel coatings and the substrates is usually done evaluating the resistance of the enamel piece to deformation caused by impact. According to the UNI-EN 10209 (2013) Annex 3, if the enamel detaches and exposes the steel substrate, the adherence is considered as poor (class 5); on the other side, if enamel cracks but still covers the substrate, the adherence is considered as excellent (class 1). FIGURE 4-8 shows the results obtained by impact tests on the different samples under investigation. The addition of macro-sized alumina (sample A20) does not significantly affect the results of the adhesion test, whereas the presence of micro-sized alumina decreases the adhesion of the enamel coating. Thus, the size of the added alumina particles influences the adhesion behaviour of enamel coatings, as the samples S0 and A20 can be classified as “class 2” enamels, whereas the sample B20 is classified as “class 3” enamel, as a portion of clean substrate (light grey in the picture) is shown up. Recent studies in literature [31] suggest that the incorporation of $Al_2O_3$ in the enamel matrix leads to the formation of a denser glass network and to a consequent diffusion barrier capability of oxygen to the enamel-substrate interface[109]. The presence of micro-sized alumina particle, compared to macro-sized particles, could lead to an increase in the oxygen diffusion path and to a reduction of the efficiency of the oxidation reactions occurring at the enamel metal interface, explaining the decreased

adherence of the coating on the substrate. Thus, despite the optimization of the firing parameters, the sample B20 does not show an optimal adherence level.

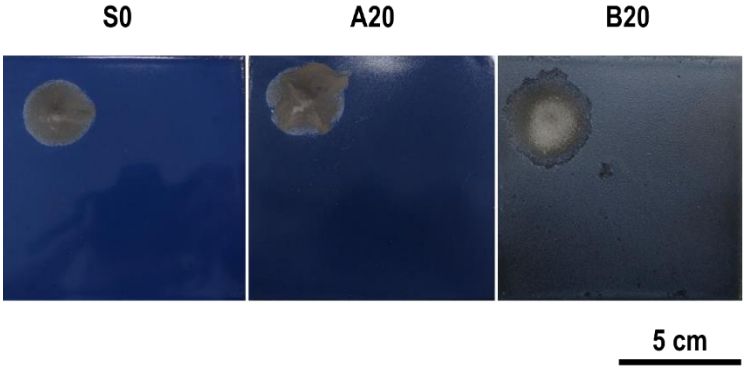


**Figure 4-8. Photograph of the enamel samples after impact test.**

### 4.3.2 Abrasion resistance

FIGURE 4-9 shows the results of mass loss and surface roughness measurements exploited at intermediate P.E.I. abrasion cycles. The mass loss appears constant in all the tested range for all the three samples. Therefore, it is not possible to detect a clear evolution of the enamel layer structure at increasing abrasion cycles, but the abrasion mechanism causes a constant loss of material over time, as already observed by previous studies[156]. It is possible to observe that the behaviour of the samples is quite similar until 1000 abrasion cycles, after which there is a differentiation between the samples with and without alumina particles. The abrasion resistance of corundum-admixed samples seems to be higher as it presents lower mass loss. In addition to that, it is important to consider the different density of silica (2.65 g/cm$^3$) and alumina (3.95 g/cm$^3$), as the two composite enamels have a higher density, then the loss volume material is much lower compared to the reference sample. Considering previous studies on composites enamels containing alumina particles[156], it is not possible to fully compare the mass loss values at the same abrasion cycles, as Taber and P.E.I. tests cause different abrasion damages and the mass loss values are influenced by the abrasion mechanism being limited to the surface or being sub-superficial. All these data translate into an improvement of the abrasion resistance given by the corundum particles, which increase the surface hardness of the enamelled layer. In addition to that, it is also important to consider the effect of the internal microstructure on the abrasion resistance of these coatings. As already pointed out by recent studies[145], the presence of big pores reduces the

abrasion resistance of the enamel coating, as they act as critical defects that favour the nucleation and propagation of cracks. The optimization of the firing process had a positive effect in determining the best microstructure for the composite enamels, thus increasing their abrasion resistance respect to the reference sample much more than it was registered in previous studies. The addition of macro-sized and micro-sized alumina particles have different effects on the abrasion resistance of the coatings, but the final result in terms of mass loss is the same. Macro-sized particles are only able to counteract locally the abrasive damaging process, but their addition in the matrix improves the microstructure of the coating, reducing its brittleness. On the other side, micro-sized particles can increase the hardness of the coating in a more homogenous way, but at the same time they detrimentally modify the enamel's internal microstructure.

The surface roughness of the coatings was measured in the central area subjected to a uniform mechanical damage at the same cycles steps with respect to the mass loss measurements. The roughness values remain almost stable until 1000 abrasion cycles, when an increase becomes detectable indicating an increase of the damage rate. Both composite enamel coatings experience a constant increase of the roughness value, and same variation between the final and initial roughness value. On the other side, sample S0 shows a rapid increase in the roughness value after 1000 abrasion cycles. These roughness values agree with the mass loss data, highlighting the good behaviour of composite enamels respect to the S0 sample, which experience a more intense abrasion process. Both mass loss and roughness measurements show that no relevant differences can be noticed among all the samples until 1000 abrasion cycles, after which the abrasion damaging process seems to affect the reference sample more seriously than the other samples, which show a similar behaviour.

FIGURE 4-10 shows SEM images of the samples after 5000 P.E.I. abrasion cycles. All the images were taken in the central part of the samples, thus avoiding border effects. As regards the S0 sample, it possible to observe the clear disclosure of enamel intrinsic porosity. The A20 sample shows the presence of a very low number of open pores, and the surface seems to be homogeneously abraded. As it regards the sample B20, it is possible to observe the disclosure of some big pores, whose dimensions are comparable to the dimension observed in the microstructural SEM investigation.

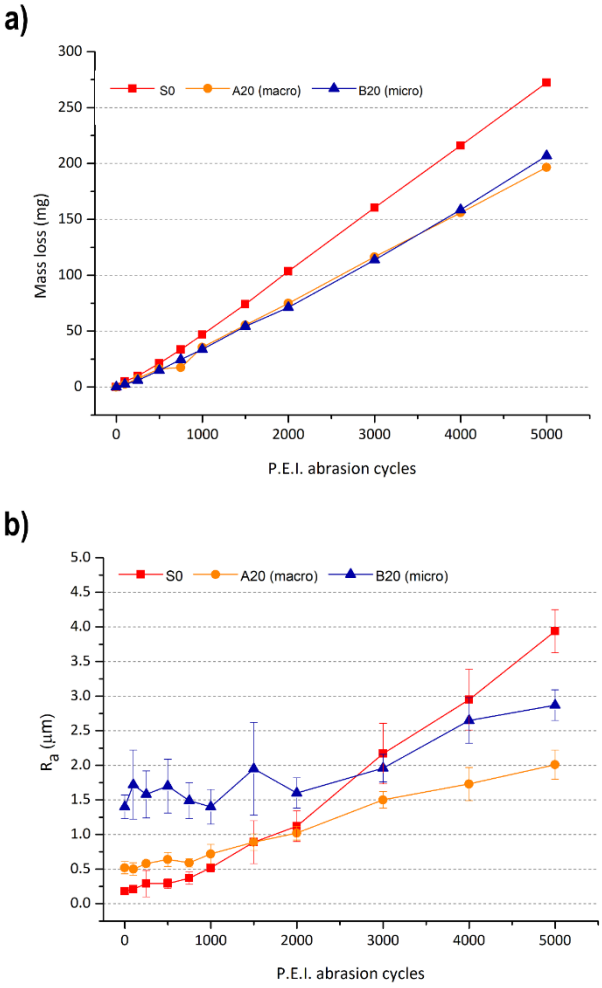


**Figure 4-9. Evolution of (a) mass loss and (b) surface roughness during the P.E.I. abrasion test.**

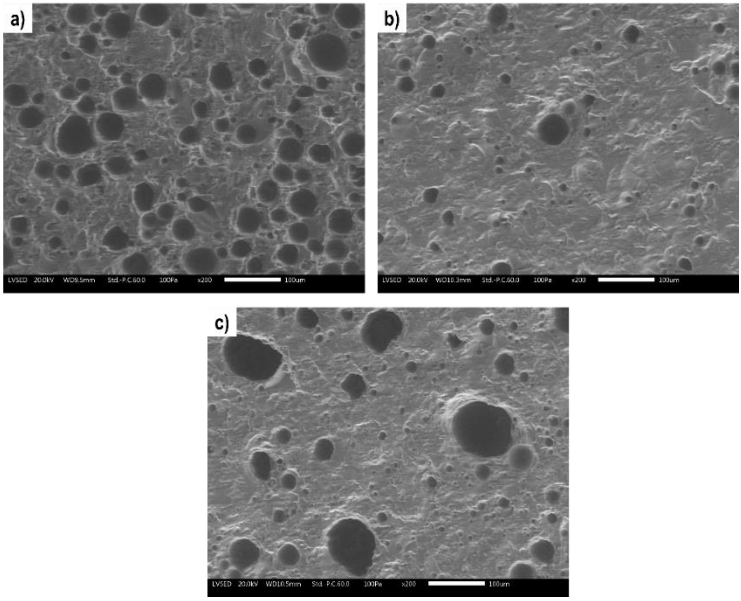


**Figure 4-10. SEM micrographs (200x magnification, 100 µm, SE) of the enamel samples after 5000 P.E.I. abrasion cycles, (a) S0, (b) A20, (c) B20.**

Before subjecting the samples to the P.E.I. test, the protective properties of the coatings were assessed by electrochemical impedance measurements. In addition to that, the same measurements were repeated at the end of the abrasion test. The results are showed in FIGURE 4-11.

The impedance modules |Z| at low frequencies ($10^{-1}$ Hz) of the different samples before the abrasion test highlight the absence of defects and cracks, also in the case of the B20 sample. As regards the samples protection properties after 5000 abrasion cycles, it possible to see a different behaviour among the samples. The |Z| values of samples S0 and A20 show no relevant differences before and after the abrasion test, whereas the |Z| value of the sample B20 undergoes a drastic drop to $10^9$ $\Omega*cm^2$. Despite the big drop in the |Z| impedance modulus, the B20 sample can be still considered as protective, and the obtained results are mainly due to the presence of big pores, that reduces the capacitance behaviour of the coatings.

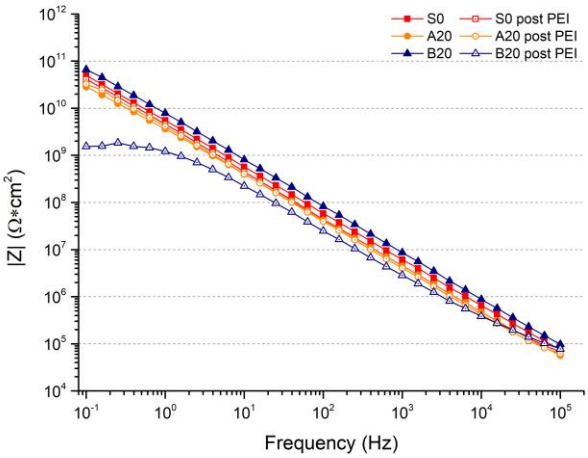


**Figure 4-11. Bode modulus diagram for the enamel samples before and after 5000 P.E.I. abrasion cycles.**

### 4.3.3 Chemical resistance by Kesternich test

The enamel samples were tested in the Kesternich chamber for 1,3,6, and 10 cycles. The S0 and A20 samples showed no macroscopical changes until 10 cycles, whereas the B20 sample showed an important whitening just after 1 exposure cycle. In order to get more informations on the degradation mechnaisms, the samples were observed by scanning electron microscope after 10 exposure cycles. FIGURE 4-12 shows the SEM micrographs taken before (for each picture on the left) and after 10 Kesternich cycles (for each picture on the right). The images highlight the high chemical resistance of the enamel coating, as sample S0 does not exhibit any defects or degradation phenomena. Similarly, sample A20 reveals an almost negligible level of degradation, with limited extent of defectiveness. On the other side, sample B20, containing microscopic fillers, suffers the chemical attack of the aggressive $SO_2$ atmosphere. The surface undergoes a homogeneous and intense degradation, exposing the large internal porosity.

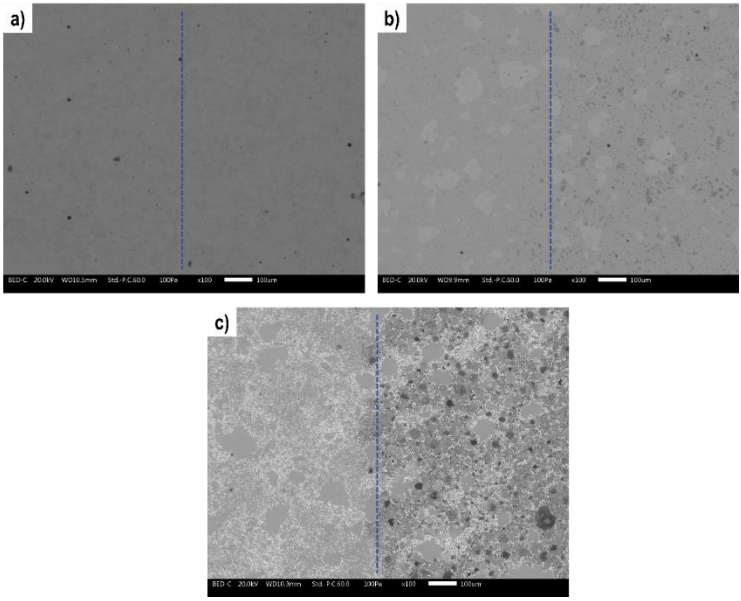


**Figure 4-12. SEM micrographs (100x magnification, 100 µm, BSE) of the enamel samples after 10 exposure cycles in the Kesternich chamber at the interface between non exposed area (left side) and exposed area (right side), (a) S0, (b) A20, (c) B20.**

FIGURE 4-13 shows the micrographs, both in secondary electrons and backscattered electrons mode, of the surface of the enamel samples after 10 cycles of exposure in the Kesternich chamber. FIGURE 4-14 shows high-magnification micrographs of the phenomena occurring at the matrix/particle interfaces in both the composite samples. The samples S0 and A20 are limitedly affected by the exposure to the aggressive atmosphere, although in the case of the A20 sample, the alumina particles seem to be more exposed on the surface and some aggressive phenomena can be observed at the matrix/particle interface. In the case of the B20 sample, many pores are disclosed, and the sample is homogenously attacked in correspondence of the particles.

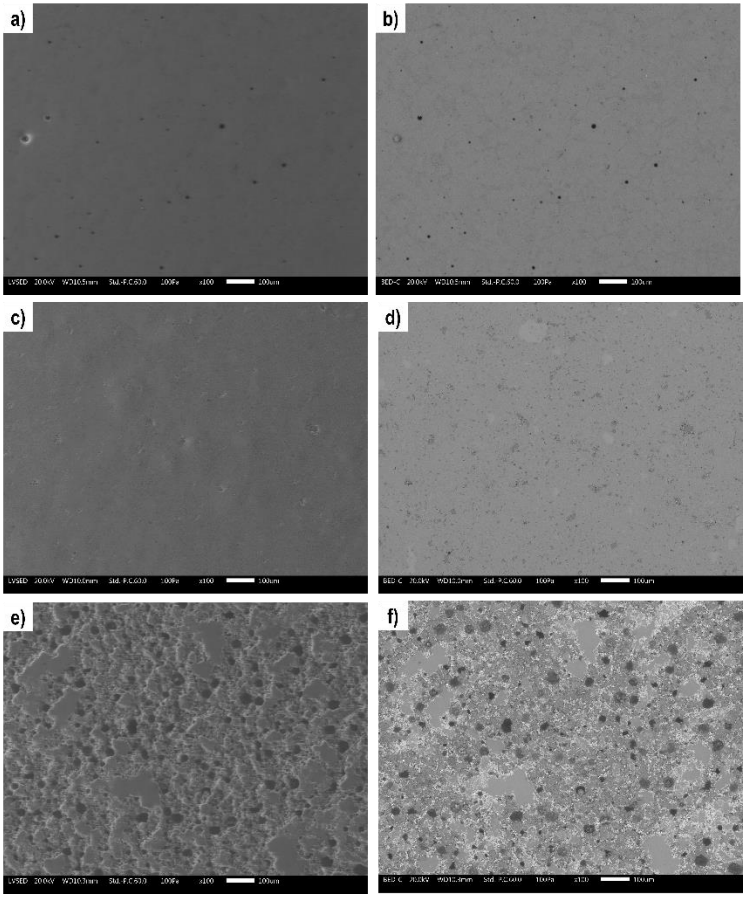


**Figure 4-13. SEM micrographs (SE left and BSE right, 100x magnification, 100 µm marker) of the enamel samples after 10 exposure cycles in the Kesternich chamber, (a-b) S0, (c-d) A20, (e-f) B20.**

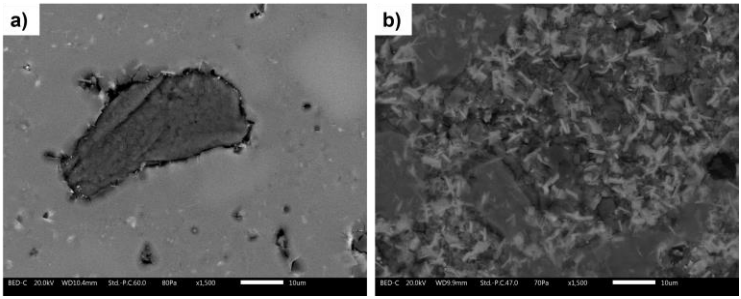


**Figure 4-14: SEM micrographs (BSE, 1500x magnification, 10 µm marker) of the enamel samples after 10 exposure cycles in the Kesternich chamber, (a) A20, (b) B20**

## *4.4 Conclusions*

This study analyses the effect of corundum particles on the abrasion resistance of chemically resistant enamels. In particular, an effective optimization of the firing process was carried out before the sample's deposition and a fixed concentration of alumina particles (20 wt.%) was chosen to be admixed in the composite coatings. It was initially observed that the addition of micro particles reduces the levelling ability of the enamel layer during the last firing phase, thus producing a rough surface, whereas both the reference sample and the sample with macro alumina particles show a smooth surface with low roughness values. The microstructural analyses highlighted the good dispersion of the fillers in the enamel matrix, but the sample with micro alumina particles is characterized by the presence of big pores, which constitute a non-negligible defectiveness. The abrasion resistance behaviour of the two composite coatings is similar between each other and improved with respect to the reference sample, but the sample with micro alumina show the disclosure of big pores, which has detrimental effects on the protection properties of the coating. Regarding the resistance of the coatings to very aggressive atmospheres, the presence of micro alumina particles constitutes a preferential site for chemical attack, whereas the presence of macro particles does not influence the resistance of the coating towards aggressive environments. In conclusion, the addition of macro-sized alumina particles could represent a valid solution to improve the abrasion resistance of enamel coatings without modifying the chemical protection properties of the frit itself and guaranteeing a limited cost for the production of the composite coatings as well.

## *4.5 Future perspectives*

As it was shown in this chapter, the addition of alumina particles inside the enamel matrix can guarantee optimal resistance to abrasive wear. The size of the added

particles greatly influences the chemical resistance of the enamel coatings, that is negatively affected in presence of micro-sized particles. Thus, the addition of macro-sized alumina particles is able to improve the abrasion resistance of the coatings without having detrimental effects on their chemical resistance.
Glasses and glass-ceramics, as enamel coatings, have good prospects to be used as coatings materials for high-temperature corrosion protection, but their essential brittleness would always lead to unstable cracks nucleated and propagated during thermal shock. The ceramic incorporated glass matrix composites are very studied, and alumina is a well known reinforcing filler[268-271], and it was demonstrated to have a positive effect on fracture strength, indentation toughness, and thermal shock resistance in concentration up to 30 wt.%[264]. $Al_2O_3$ platelets represent probably the most widely reported reinforcement in pressureless sintered glass and glass–ceramic matrix composites. This is due both to the specific reinforcing mechanism provided[272, 273], i.e. crack deflection (the propagation of cracks in the glass matrix is altered by a system of residual stresses, caused by the thermo-elastic mismatch between the matrix and the reinforcement and enhanced by the particular aspect ratio of platelets), and to the low commercial cost (alumina platelets are commonly employed as abrasives, so that they are produced in very large amounts), consistent with the overall cheap processing of the composites. Some examples of recent studies regarding the production of $Al_2O_3$ reinforced composites demonstrated that is possible to obtain glass ceramics composites with enhanced fracture strength and fracture toughness[274-276]. Thus, it would be very interesting to better explore the possibility to produce composite enamel coatings with the addition of alumina particles, focusing the attention on the study of their mechanical properties and chemical resistance properties in different operando resembling conditions. It is then important to consider that the addition of every type of reinforcing filler should guarantee improved mechanical properties, leaving unaltered the other functional properties of the coating.

## *4.6 Acknowledgements*

The authors gratefully acknowledge CIDETEC (Spain), in particular Dr. Velez for the samples produced and for useful discussion.

# 5 The influence of 316L stainless steel lamellar powder on the abrasion resistance and mechanical properties of composite vitreous enamel coatings

***Part of this chapter has been published in:***

F. Russo, V. Fontanari, S. Rossi, "**Abrasion behavior and functional properties of composite vitreous enamel coatings fabricated with the addition of 316L stainless steel flakes",** *Ceramics International* 48 (2022) 23666-23677.

*Conceptualization*: F. Russo, S. Rossi; *Methodology*: F. Russo; *Investigation*: F. Russo; *Formal analysis*: F. Russo; *Validation*: F. Russo; *Supervision*: S. Rossi, V. Fontanari; *Writing*: F. Russo.

F. Russo, V. Fontanari, E. Rustighi, M. Lekka, L. Hernandez, S. Rossi **"Composite vitreous enamel coatings with the addition of 316L stainless steel flakes: Novel insights on their behaviour under mechanical stresses"**, *Surface and Coatings Technology* 459 (2023) 129393.

*Conceptualization*: F. Russo, S. Rossi, V. Fontanari; *Methodology*: F. Russo, V. Fontanari; *Investigation*: F. Russo, L. Hernandez; *Formal analysis*: F. Russo; *Validation*: F. Russo; *Supervision*: S. Rossi, V. Fontanari, E. Rustighi, M. Lekka; *Writing*: F. Russo.

## *5.1 Introduction*

Glass-ceramics and glass-based coatings, like enamels, are the metarials of choice in many demanding applications such as tribological applications, automobiles engines, and power generators, mainly because they show chemical and thermochemical inertia, and optimal resistance to corrosive environments[277-279]. These unique attributes are offset by an important Achilles heel: low toughness. Toughness is a key property for application involving load bearing, mechanical impact, thermal shock, or combinations thereof[280]. Since the major goal is to reduce the susceptibility of these materials to brittle fracture when they face external mechanical solicitations, there is a growing interest in optimizing their mechanical behavior[281].

Toughening of ceramic/glass-based material can be exploited by many different methods[282]: microstructure engineering, minimization of grain size, creation of compressive surface stresses[283], ceramic fibers reinforcement, minimization of internal porosity, and addition of metallic particles. The incorporation of ceramic particles (spheres, rods, whiskers) is the most common reinforcing method used in the field of ceramic-matrix composites[284, 285], as it is also suitable in high-temperature applications[36, 37], but the addition of metal reinforcements

guarantees satisfactory results as well[38-40]. Within the class of composites reinforced with metallic fillers, cermets are the most renowed, as they show extreme strength and toughness, despite being far from matching the performances of fiber-reinforced ceramics, as the presence of fibers guarantees the development of crack bridging mechanisms and makes the difference between one order of magnitude in enhancing the fracture energy of the material[286]. On the other side, ceramic fibers are not ductile, and ductility reinforcement cannot be exploited. Thus, a possible solution to combine the effect of fibers (ability to bridge an advancing crack) with ductility (ability to absorb mechanical energy without failure) is to create metal-reinforced ceramics[201], where several toughening mechanisms may operate together[287-289].

The presence of metallic particles, thus the creation of a particulate-reinforced glass-ceramic matrix composite[290], favours the activation of a toughening mechanism addressed as "*toughening by ductile particles*"[281], which involves the combination of crack deflection, crack bridging, and reinforcement by increased ductility[291]. In considering metal-reinforced ceramics, metallic fillers play an important role regarding their ductility (i.e., the ability to absorb mechanical energy without failure). The presence of a metallic filler then allows increasing the stress needed to initiate the cracks (composite's strength) and to delay the propagation of existing cracks (composite's fracture toughness) by several mechanisms that absorb energy during crack propagation[201].

Metallic particles toughening has proven to be effective both with ceramics, glasses, and GCCs: the first composites were reinforced with Ni[185-187] and W particles, but other metals such as Al[188], Mo[189, 190], V[292], Cu[293], NiCrAlY[193], iron[294], and 316L stainless steel[295] have been reported to be same way effective.

The successful toughening of GCCs by the addition of a second ductile phase mainly relies on the hypothesis of optimum interfacial adherence and low thermal expansion mismatch between the matrix and the second metallic phase[185]. The coefficient of thermal expansion (CTE) of the particles should be higher than that of the matrix so that compressive residual stresses are created around the particles upon cooling: the presence of these stresses reduces the tensile stress at a crack tip and increases fracture toughness by favouring the crack tilting mechanism[296]. The combination of matrix/filler with much different CTE can lead to the creation of microcracks in the matrix, and for this reason, this situation should be avoided[297]. All these assumptions are valid only if the particle/matrix bonding is sufficiently strong[284]. the stronger the bond the more favourable is the ductile deformation of the filler, whereas the weaker the bond, the greater the probability to have fiber pull-out[280]. As a general consideration, many studies pointed out that the pull-out mechanism has an insignificant relevance in the reinforcement of ceramic matrix composites, as the matrix/filler interface is usually strong, and the fibers usually have a high aspect ratio[298]. On the other hand, crack deflection mechanisms and crack

branching are the main processes through which the cracking resistance of the CMCs is increased.

The use of ductile particles within ceramic matrix composites is able to provide important improvements in terms of toughness, but it is also expected to produce changes to other properties, like wear resistance and thermal conductivity[201], as reported by some studies making use of metallic powders or stainless-steel fibers[299, 300]. Metallic particles usually undergo plastic deformation (cutting, plowing) when subjected to abrasive processes, and therefore, they can be useful for reducing the abrasion rate of brittle materials, as material removal via fragile fracture is much greater[300] with respect to material removal due to plastic deformation.

In this context, it would be interesting to investigate if and how it is possible to exploit this toughening approach to improve the mechanical properties and abrasion resistance of vitreous enamel coatings. The addition of metallic particles inside the enamel matrix was proven to have a positive effect on thermal shock resistance, self-healing properties of enamel coatings[185, 301], and it could be a valid solution to improve their mechanical properties as well. The presented study will focus its attention on the improvement of enamel's mechanical properties and abrasion resistance by the addition of 316L stainless steel micrometric lamellar powders. Many examples regarding the use of steel fillers as a second phase in ceramic and glass based composites can be easily found in the literature[295, 299].

An important task in coating development is the adequate and targeted characterization of the coating's mechanical properties. In particular, the evaluation of the crack resistance is very challenging in practice due to the interaction with the substrate and the presence of residual stresses[302]**.** The toughness of brittle materials is really dependent on the testing techniques, which are widely classified into long crack and short crack methods; the first class includes the single edge notched beam (SENB), single edge v-notched beam (SEVNB) technique, and the chevron notched beam (CNB) method, whereas short crack techniques involve measurement of the crack length around hardness indentation[280] The indentation fracture method is an easy way to have a qualitative idea about the toughness of materials, but it includes strong limitations when thin, porous coatings are taken into consideration. At the same time, classical fracture toughness testing by long crack methods is difficult to apply on brittle coatings due to difficulties in preparing sharp cracks. The study of the mechanical behaviour of composite vitreous enamel coatings by in-situ 3 point flexural tests and 4-point flexural tests, without pre-notch on the samples, could be a valid solutions to have realiable results. Flexural tests are useful to understand the mechanical behaviour of vitreous enamel coatings and the efficacy of the metallic filler in delaying the occurrence of cracks and their propagation, as they can be performed inside a scanning electron microscope chamber and in-situ observations on the sample's cross sections can highlight the damaging mechanisms and the filler-crack interaction phenomena. This combined approach is useful to correlate the obtained stress-strain curves together with failure

mechanisms and obtain quantitative data, despite this is a very time-demanding and expensive method, as the sample's preparation should be carefully carried out.

In this regard, it is possible to take advantage of the AE technique in order to real-time monitor the evolution of damage in the coatings in a cheap and quick way[303, 304]. The use of AE for monitoring mechanical failure and structural integrity in different materials is well-established in the NDT&E (non-destructive testing and evaluation) field[305]**.** AE is a very efficient and reliable technology for the monitoring of damage evolution in composite polymeric[306-309], ceramic-matrix[310-312], and metallic materials[313-315], as it is able ability to detect low stress damages that are not visible in the stress strain curves during tensile tests and it can give real time information on initiation and evolution of damage. When a failure mechanism is activated, a burst of energy is released as transient elastic sound waves in the range of ultrasound, that propagate through the medium and are recorded by sensors placed on the sample's surface. The analysis of the AE can include an activity analysis (i.e., analysis of number of events, always referred as "hits") and a parametric analysis (amplitude and absolute energy of the events), that together can provide valuable information about wide range structural failures[316]. The interpretation of the signals, and hence establishing of a relationship between a specific failure mode and its acoustic signature is the major problem in the interpretation of AE signals[305]. Thus, a complete analysis by means of SEM in-situ mechanical analysis and AE technique could provide valuable information on the properties of composite enamel coatings.

This study aims to assess the mechanical properties and abrasion behaviour of composite vitreous enamel coatings deposited on AA5005 aluminium alloy substrates and fabricated with the addition of 316L SS-Fs in a 1 wt.% and 5 wt.% concentration. As a first thing, this study is focused on the characterization of the samples surface properties and microstructure. The influence of the addition of the 316 stainless steel filler on the chemical resistance of the coatings was assessed by means of chemical assays coupled with Electrochemical Impedance Spectroscopy (EIS) measurements and microscopy evaluations. The abrasion behavior of these composite coatings was evaluated by P.E.I. test, following the ISO 10545-7 (1996) standard[209]. The produced damage was evaluated by mass loss measurements, electrochemical measurements, and SEM observations. The role of the stainless-steel filler was further investigated, and the damage mechanisms were described. The evaluation of the crack resistance is very challenging in practice due to the interaction with the substrate and the presence of residual stresses. Unlike bulk materials, there is neither standard procedure to follow, but many different approaches can be followed, such as bending tests, scratch tests, and indentation. Thus, the samples were mechanically characterized by different tests (ex-situ 4 point bending test, scratch test, and indentation fracture (IF) method). The results of these tests will be presented, and the efficacy of these tests will be described. The

role of the SS-Fs filler will be deeply investigated, and the damage mechanisms will be described. All these testing methods have some significant limitations, but they can be complementary in the assessment of the coating's mechanical behavior. When using such methods, it is important to refrain from speaking of fracture toughness: the term crack resistance can be used as a generic term to describe these properties, which is essentially based on phenomenological and comparative observations of the crack behavior. Then, the mechanical properties of the composite enamel coatings will be investigated by means of in-situ techniques (SEM and AE) exploited during 3 point and 4 point flexural tests. The role of the SS-Fs filler will be deeply investigated, and the damage mechanisms will be described. After that, the results of in-situ AE test during 3 point and 4 point flexural tests will be discussed. The main positive and negative features of this tests will be highlighted, giving new perspectives on the mechanical analysis of brittle coatings. As a final thing, experimental assessment of residual stresses in the coatings will be exploited to investigate if residual stresses after the firing process have an impact on the mechanical performances of these coatings.

## *5.2 Materials and methods*

### 5.2.1 Materials

**Enamel frit and pigment** The samples were deposited starting by a vanadium-based RTU (ready-to-use) frit developed by Emaylum Italia (Chignolo d'Isola, BG, Italy). The compositional analysis of the frit was investigated by EDXS analysis (JEOL IT300 equipped with Bruker Quantax EDXS) and the results are expressed as normalized % mass with 2σ errors: O 35.8 ± 8.0, K 16.8 ± 1.0, Ti 14.6 ± 0.8, Si 13.5 ± 1.1, Na 12.5 ± 1.6, V 5.9 ± 0.4, P 0.6 ± 0.1, Al 0.3 ± 0.1. The frit contains a high content of alkali metals, almost equal to 29%, that is necessary to make the enamel more fusible, thus being able to exploit the firing process at temperatures lower than 580 °C (as aluminium cannot withstand higher temperatures[41]). The density of the RTU frit was measured by a He-pycnometer (Accupyc 1330, Micromeritics) at 23 °C and it resulted equal to 2.57 ± 0.02 g/cm$^3$. The density of the frit is perfectly compatible with the typical density values of porcelain enamels. A cobalt aluminate blue spinel ($CoAl_2O_4$) commercial pigment was used to obtain opaque blue enamel coatings and improve the adherence with the substrate. FIGURE 5-1 shows the electron miscroscope micrographs of the frit and the pigment used in this study.

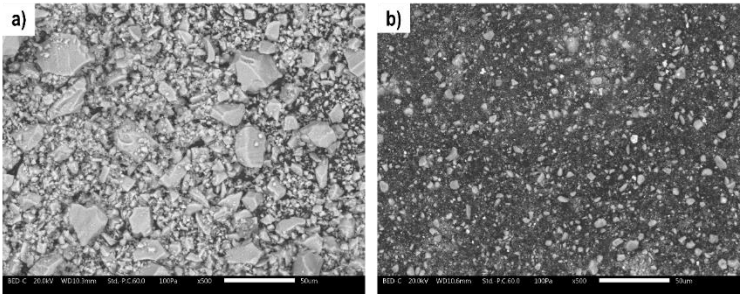


**Figure 5-1: SEM micrographs (500X magnification, 50 µm marker, BSE) of the (a) RTU frit, (b) cobalt-blue pigment used in this study.**

As it is possible to observe from the micrographs, the RTU frit dimension seems not to exceed 60 µm, whereas the pigment is made of smaller particles, whose average dimension is around 8 µm. A detailed particle analysis of the RTU frit was exploited using a Mastersizer3000 MAZ6140 (Malvern Instruments Ltd.) particle analyzer: five different tests were made to obtain a standard deviation.The results of the particle size analysis are shown in FIGURE 5-2.

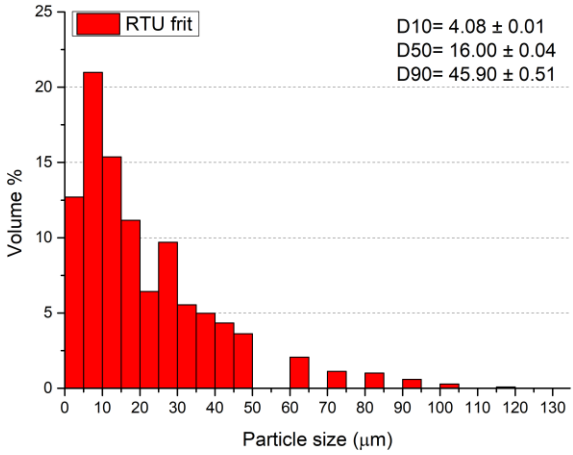


**Figure 5-2. Particle size analysis of the RTU frit.**

The D90, D50, and D10 parameters are characteristic outputs of the particle size analysis. These parameters represent the maximum particle diameter below which 90%, 50%, and 10% of the sample volume exists, respectively. The D90 value of the

RTU frit is perfectly in line with the technical specification requested for aluminium enamels on technical manuals[41].
The thermal behaviour of the frit was assessed by means of heating microscope analyses carried out at Emyalum Italia using a lab-built instrument. TABLE 5-1 shows the characteristic temperatures and the parameters obtained thanks to the heating microscope analysis.

**Table 5-1: Thermal behaviour of the RTU frit assessed between 20 °C and 700 °C with a heating microscope.**

| | Sintering | Softening | Sphere | Half-sphere | Melting |
|---|---|---|---|---|---|
| |  |  |  |  |  |
| **RTU frit** | 463 ˚C | 531 ˚C | 561 ˚C | 601 ˚C | 617 ˚C |
| **Height (%)** | 95 | 80 | 67 | 43 | 34 |
| **Angle (°)** | 90 | 85 | 70 | 101 | 123 |

**Metal substrate and pretreatment process** The enamel samples were deposited on AA5005 aluminium alloy panels having a thickness of 1.5 mm. The composition of the alloy is reported in TABLE 5-2.

**Table 5-2. Elemental composition of the raw materials used in this study (expressed as weight %).**

| Element | 5005 aluminium alloy | RTU frit | 316L SS-F |
|---|---|---|---|
| **C** | - | - | 0.03 |
| **O** | - | 35.80 | - |
| **Na** | - | 12.50 | - |
| **Mg** | 0.50 – 1.10 | - | - |
| **Al** | balancing | 0.30 | - |
| **Si** | 0.30 | 13.50 | 0.75 |
| **P** | - | 0.60 | 0.04 |
| **S** | - | - | 0.03 |
| **K** | - | 16.80 | - |
| **Element** | **5005 aluminium alloy** | **RTU frit** | **316L SS-F** |

| | | | |
|---|---|---|---|
| **Ti** | - | 14.60 | - |
| **V** | - | 5.90 | - |
| **Cr** | 0.10 | - | 16.00 – 18.00 |
| **Mn** | 0.20 | - | 2.00 |
| **Fe** | 0.70 | - | balancing |
| **Ni** | - | - | 10.00 – 14.00 |
| **Cu** | 0.20 | - | - |
| **Zn** | 0.25 | - | - |
| **Mo** | - | - | 2.00 – 3.00 |

**316L stainless steel lamellar powder** The 316L stainless-steel flakes (SS-F) used in this study can be found as commercial non-leafing pigment (STAY/STEEL 316L K, Eckart Italia, Rivanazzano, Pavia, Italy). The given composition of this powder is shown in TABLE 5-2. The SS-F density was measured with the same equipment described before and it resulted equal to 7.31 ± 0.03 g/cm$^3$. The D50 and D90 declared by the supplier are 35 ± 4 µm and 66 µm ± 5 µm, respectively. A particle size analysis carried out with the ImageJ software, evidenced a D50 of 28 µm ± 1 µm, and a D90 of 78 µm ± 1 µm. FIGURE 5-3 shows the scanning electron micrographs of the stainless-steel flakes: their average in-plane dimension is around 50-70 µm and their thickness is about 0.25 µm. Their dimensions are perfectly suitable for the production of enamel coatings with a thickness of about 120 – 150 µm.

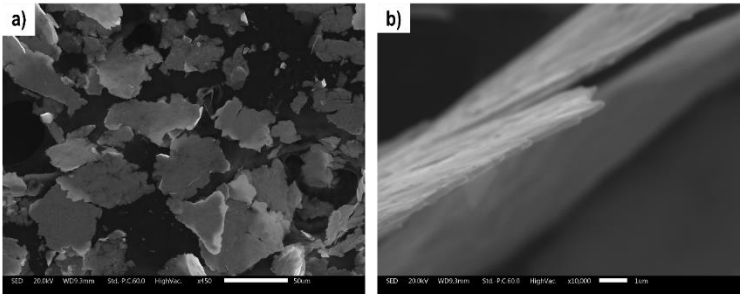


**Figure 5-3. SEM micrographs of the 316L stainless steel lamellar powder, (a) in-plane (450x magnification, 50 µm marker, SE), (b) section (10000X magnification, 1 µm marker, SE).**

## 5.2.2 Methods

### *5.2.2.1 Samples preparation*

The first step is necessarly the choice of the substrate that will be coated. Then, the enamel deposition process parameters must be optimized to obtain coatings which can guarantee the best performances.

**Substrate pretreatment** The aluminium alloy panels were chemically pre-treated following the steps described in SECTION 2.2. The pretreatment process was exploited as follows: immersion in acetone for 2 minutes in an ultrasound bath, rinsing with distilled water, immersion in a 10 wt.% NaOH aqueous solution for 5 minutes at room temperature, rinsing with distilled water, immersion in a 25 wt.% $HNO_3$ aqueous solution for 20 seconds at room temperature, rinsing with distilled water, and drying with compressed air. The Ra value for the aluminum substrate before and after 5 minutes of immersion was equal to 0.18 ± 0.08 µm and 0.56 ± 0.12 µm, respectively. No further changes in the substrate's surface roughness were detected by increasing the immersion times up to 10 minutes. The surface roughness values obtained are comparable with data reported in the literature[317] and the relative increase is in the order of 300%. In the present case, the concentration of the alkaline bath was slightly increased with respect to common literature values (5 w/v %)[317] but the operating temperature was kept around 25 °C to make the process simpler.

**Deposition process parameters and sample typologies** The three different components (frit, pigment, and SS-Fs) were mixed to obtain one reference formulation (without SS-F) and two composite formulations, according to the ratios reported in TABLE 5-3.

**Table 5-3. Composition of the enamel formulations and labelling.**

| Component | Reference | 1 % SS-F | 5 % SS-F |
|---|---|---|---|
| **RTU frit** | 85 g | 84.15 g | 80.75 g |
| **$CoAl_2O_4$ pigment** | 15 g | 14.85 g | 14.25 g |
| **316L SS-F** | - | 1 g | 5 g |
| **Total powder** | 100 g | 100 g | 100 g |
| **Screen printing medium** | 45 g | 45 g | 45 g |

The quantity of the 316 SS-Fs filler represents the 1 wt.% and 5 wt.% of the total powder content of the 1 % SS-F and 5 % SS-F formulations, respectively. The ratio between the RTU frit and the blue pigment was kept constant to 5.66 for all the formulations. The ratio between the frit and the pigment was optimized by preliminary studies, aimed at finding the optimal concentration of pigment that can guarantee a uniform colour to the matrix without leading to an important change in its thermal behaviour. The mixed powders were then suspended in a water-borne screen-printing medium to obtain an applicable formulation, then the screen-printing paste was passed through a three-cylinder refiner to obtain a uniform dispersion of the SS-F filler into the application medium. In all cases, the powder to medium ratio was kept constant to 100:45, which is a typical formulation for enamel screen-printing pastes preparation. The samples were deposited using an 18-wire screen-printing mask and exploiting a 2A/1F (2 applications/1 firing) cycle. A schematic representation of the application cycle is represented in FIGURE 5-4.

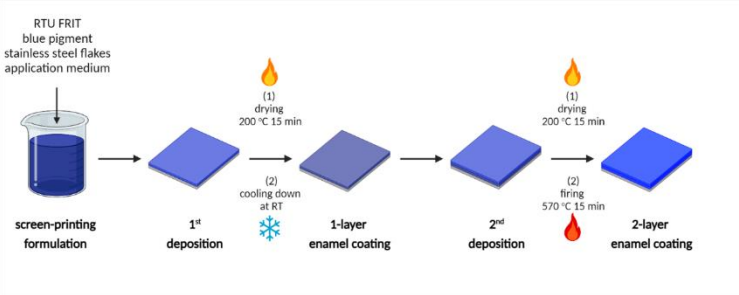


**Figure 5-4. Schematic representation of the 2A/1F application cycle used for the production of the enamel samples.**

The deposition of the first enamel layer was followed by a drying treatment, carried out at 200 °C for 15 minutes. The drying step led to the creation of the so-called

"biscuit" (e.g., dried enamel), which is suitable for the application of a second enamel layer. The samples were let naturally cool down to room temperature before applying the second enamel layer. The application of the second layer was followed by a drying treatment (same conditions as before) and a firing treatment exploited at 570 ˚C for 15 minutes in a static muffle furnace.

#### *5.2.2.2 Coatings characterization*

This section introduces the characterization techniques used for the investigation of the coatings and their performances. First of all, a surface and microstructural characterization has been performed for all the samples. The abrasion resistance of the coatings was assessed by means of P.E.I. test, and the effect of the filler was evaluated by microscopy observations and EIS. The mechanical properties have been investigated by scratch test, Indentation Fracture (IF) method, and in-situ SEM/AE bending tests.

**Surface and microstructural analysis** The thickness of the coatings was measured according to SECTION 2.2, performing 30 measurements on 3 different samples. The reported surface roughness evaluations, performed according to SECTION 2.2 are the average of 15 measurements carried out on three different samples (5 measures each). Optical and low-vacuum SEM were used to observe the sample surfaces and cross-sections. Thanks to these microscopical investigations, it was possible to assess the distribution of the stainless-steel flakes inside the enamel matrix and evaluate the internal microstructure of the coatings, with a particular focus on pores dimension and distribution.The evaluation of porosity was exploited by means of the ImageJ software and the reported values are the average of three measurements on different samples.

**Chemical resistance and protective properties by EIS** The chemical resistance behaviour of the composite enamel coatings was assessed by two different tests. The first test was exploited to assess the resistance of these coatings to strong acids. A confined area of the sample was exposed to a 20 wt. % HCl aqueous solution for 48 hours at room temperature and the surface was then observed by scanning electron microscope to highlight the damage morphology. The concentration of the acid and the exposure time was chosen to create an aggressive environment towards the 316L SS-F filler, as stainless steel suffers when in contact with strong acids[318].

The chemical resistance of the samples was also tested in an aggressive alkaline solution and the loss of protective properties was monitored along with the immersion time. The chosen testing solution was a tetra potassium pyrophosphate aqueous solution having a concentration of 65.41 g/L (0.198 M) and maintained at a temperature of 96 °C. The testing conditions were adapted from the ASTM C614-20 standard. The samples were immersed in this solution for 6 hours and their

protective properties were assessed at intermediate immersion times (1h, 3h, and 6h) to study the evolution of the coating protection properties. The EIS measurements were conducted on a Gamry 600+ potentiostat using a three-electrode configuration, as explained in SECTION 2.2. The signal amplitude was set at 15 mV in the $10^5$ - $10^{-2}$ Hz frequency range and the test area was 6.15 $cm^2$. The sampling rate wad equal to 5 points per decade. SEM analyses have been exploited at the end of chemical resistance test to evaluate the coating surface morphology.

#### *5.2.2.3 Abrasion resistance assessment*

**Abrasion resistance test** The abrasion behaviour of these coatings was evaluated using a P.E.I. abrader. All the samples were tested for a total of 5000 P.E.I. cycles. The behaviour of the samples was evaluated by mass loss and surface roughness measurements at 100, 250, 500, 1000, 2000, 3000, 4000, and 5000 abrasion cycles. The test was repeated on two replicates to obtain a standard deviation and verify the reproducibility of the procedure. The damage morphology was investigated by SEM observations at different abrasion cycles. In addition to that, the protection properties of the samples were evaluated after 5000 abrasion cycles by EIS measurements and following the procedure previously described. The abrasion mechanisms and the role of the different components of the tribosystem were further investigated exploiting SEM observations on samples after 1000 abrasion cycles. It was chosen to exploit these observations at 1000 abrasion cycles as this value represents a threshold over which the samples are usually heavily damaged, and no differences can be appreciated.

#### *5.2.2.4 Coatings preliminary mechanical characterization*

**Indentation fracture (IF) method** The assessment of fracture toughness on brittle materials can be difficult to be estimated by conventional methods: the indentation fracture (IF) technique is the most widely used tool reported in the literature to do so[214]. This test is relatively simple, and it only requires a micro hardness tester, although the sample should have a homogenous microstructure, a fine porosity, and a good surface finishing free of pores and cracks. The indentation fracture (IF) method relies on the experimental procedure commonly followed in hardness tests, and it consists in relating the lengths of the cracks growing in the corners of the Vickers indentation when a load is applied, with the fracture toughness of the material[319]. The length of the radial cracks can be quantitively related to the fracture toughness of the material using some empirical and experimental equations, such as the ones proposed by Evans et al.[320], or Nihara et al.[321]. However, several requirements should be respected at the same time for a well-determined evaluation of fracture toughness, and sometimes it is very difficult to comply with these specifications [322, 323]. Many scientists have sharply criticized the reliability of this method in determining fracture toughness; however, it still represents an

effective possibility to perform exploratory tests for probing the fracture susceptibility of brittle materials[324]. In particular, the use of micro indentation tests can be useful in the evaluation of the sample's crack resistance, simply calculating the "probability of crack initiation" (PCI), as suggested by many studies in the literature[325-328]. The PCI (%) is calculated by dividing the number of corners of the indentations presenting radial cracks by the total number of the corners of indentations. This procedure is repeated at increasing loads in order to identify the "crack resistance" (CR), defined as the load at which the PCI value is equal to 50 %[325]. This method, coupled with other experiments could give some interesting insights into the mechanical behavior of composite enamel coatings.
PCI and CR were measured by Vickers micro-indentation tests. A FUTURE-TECH FM-310 microhardness tester equipped with a Vickers diamond indenter was used in this study. The PCI was evaluated at loads ranging between 25 gf and 1000 gf, with a load dwell time of 10 s, and by performing 10 indentations for each load. The cracks were counted 2 min after indentation. In order to estimate the error at important load values (100 gf, 200 gf, and 300 gf), the experiment was repeated on three different samples (10 indentations x 3 samples, for a total of 30 indentations). All the indentations considered for the calculation of PCI were free from chipping and spalling at the indentation edges. The coating is thick enough not to display the substrate effect during the indentation measurements.

**Evaluation of cracking resistance by four-point bending tests** A small four-point bend jig was designed and built in the laboratory, taking inspiration from the work of Ramsey et al.[329]. The bending-setup was built to fit the SEM (JEOL IT300) specimen stage. FIGURE 5-5 shows an image and some details of the laboratory-built setup. The system is designed to apply an increasing load to the sample rotating the screw in the bottom part of the jig, the resulting displacement is measured using an analog comparator with a resolution of 0.01 mm, the sample's surface is inspected by optical or/and scanning electron microscope. As it is possible to observe from FIGURE 5-5 the jig is anchored to two support bars connected to a base steel plate. The jig can be easily removed from the support system by unscrewing the bolt on the left to be placed in the SEM for further observations. The third support bar is necessary to place the analog comparator, which measures the resulting displacement.
The aluminium alloy substrates (20 mm wide and 120 mm long samples) were coated following the procedure described in SECTION 5.2.2.1. In the four-point bending configuration, the sample is loaded at two points (by means of two load rollers) each at an equal distance from the adjacent support point: the ¼- ½ - ¼ configuration implies that the distance between the load rollers (loading span) is one half of the support span. The support span (upper span), and the loading span (lower span) are equal to 64 and 32 mm, respectively. The diameter of the loading and support rollers is 4 mm. A support span-to-depth ratio of 40:1 was chosen in this

case to ensure that failure occurs in the outer fibers of the specimens due only to the bending moment, as suggested by the ASTM D6272-17 standard.
Scanning electron images were acquired using a JEOL IT300 microscope. The number of cracks on the surface is counted at different displacements, in the sample's area between the load rollers, as in the four-point bending setup the maximum axial fiber stress is uniformly distributed within the load span. The bending moment is maintained during observations: this is an essential point since after unloading the fractures are virtually undetectable because of compressive residual stresses present in the coating[330]. The tests were carried out on three samples for each filler concentration, including the reference sample.

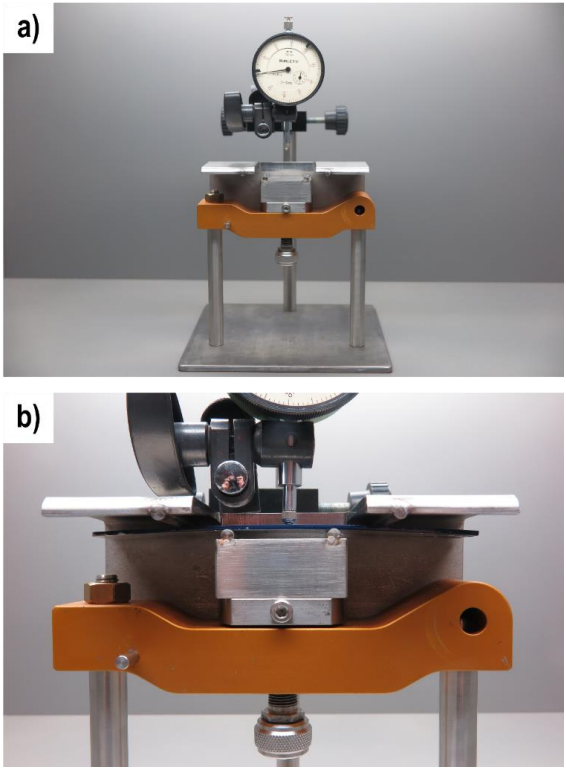


**Figure 5-5. Four point bending home-built setup, (a) complete overview of the system, (b) detail of the loading and support parts including the sample and the analog comparator.**

**Scratch test** In the present study, the scratch tests were carried out using a Revetest RST scratch tester (CSM Instruments) equipped with a Rockwell 200 μm diamond indenter. The tests were performed in a progressive load (PL) mode, increasing the load by 11.44 N/min in the range 0.5 N- 100 N, with a sliding speed of 0.92 mm/min on a sliding distance of 8 mm. A preload of 0.5 N was applied in all cases. The tests were carried out on unpolished samples, as to avoid the creation of flaws and topographical alterations due to polishing. Six scratch tests were performed for each sample type. The scratch tracks were observed by confocal microscope Leica DCM3D (Leica Microsystems) and scanning electron microscope JSM 5500LV (JEOL) to have further insights on the fracture mechanisms involved.

#### *5.2.2.5 Assessment of residual stresses by thermal methods*

Vitreous enamelled materials are composite systems made of two different layers with different physio-chemical properties. The coupling of two materials (e.g., the enamel layer and the aluminium substrate) with different thermal behaviors leads to the onset of residual stresses in the final system[331]. Thus, on the hypothesis of homogeneous and isotropic materials, it is possible to evaluate the residual stresses in the composite system by combination of optical dilatometric and optical flexure analyses**.** This testing methodology is a well-known procedure in the ceramic tiles industrial field, but it is not so common in other fields, so the theoretical basis of this method, shown in FIGURE 5-6, are brielfy described.

FIGURE 5-6A shows typical expansion curves for enamel and aluminium. The dilatometric curve for the metallic substrate follows a linear trend with the increase in temperature, whereas the expansion curve of the enamel shows the presence of important deviations from the linear trend, which are always caused by physical changes occurring in the material. The expansion curve of the enamel shows a first linear zone that ends in correspondence of the glass transition temperature (Tg), where it undergoes to a slope variation, caused by the increased mobility of the molecular groups of enamel, that starts behaving like a plastic liquid. By further increasing the temperature, the enamel continues to expand until the softening temperature (Ts), which correspond to the maximum of the curve. Above this temperature, the slope of the curve reverses , as the surface tension takes control of the shape and causes the edges of the sample to round off. The glass transition temperature (Tg) and the softening temperature (Ts) are also identified as the lower and upper transition temperatures, respectively, and they are taken as the limits of the so-called “transition zone”[332]. The transition zone refers to the temperature region in which the slope of the thermal-expansion curve of the enamel is greater than the slope of the thermal-expansion curve of the metal[333, 334].

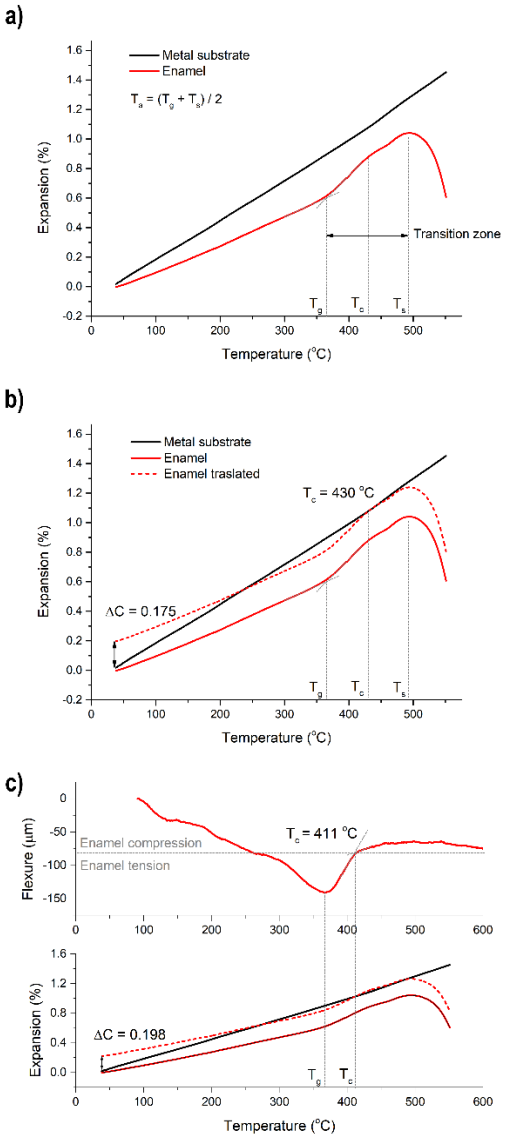


**Figure 5-6: Experimental assessment of residual stresses by thermal analysis (a) dilatometric curves, (b) flexural curves, (c) experimental assessment of residual stress with coupling temperature Tc calculated by optical fleximeter measurements.**

Another characteristic point of the enamel-metal system is the coupling temperature (Tc), at which the enamel starts to soften and release stresses in heating or starts solidifying and accumulate stresses in cooling. Thus, $T_c$ can be regarded as the temperature at which the enamel adheres to the substrate and a new combined material is created. The coupling temperature (Tc) is always located between Tg and Ts: some literature studies state that it can be mathematically calculated from the dilatometric curve with the following formula Tc= (Tg + Ts)/2, but experimental tests put into light the rough approximation of this statement. The first approach to assess the residual stresses in the enamel-metal system includes the determination of the Tc by the analysis of the dilatometric curve of the enamel and the metal substrate, the overlay of the two dilatometric curves in correspondence of Tc and the assessment of the percentage difference in contraction at room temperature between the two materials (FIGURE 5-6). This difference constitutes a direct measurement of the stress level in the composite system. Despite this method is rapid, it does not assure a correct determination of the coupling temperature, which can be correctly evaluated by optical flexural analyses[335]. After the enamel deposition, the coating is dried (creation of enamel "biscuit") and does not develop perceptible stresses. During firing and with gradual heating, the enamel is put in compression as it expands faster than metal, but further heating produce stress relieving as a consequence of the enamel's viscous behaviour[336]. On cooling the development of tension is gradual as enamel becomes more and more viscous, and from Tg downward the contraction of enamel is lower than the metal, thus putting the coating in compression. It is possible to test enamelled samples at the end of the cycle in the optical fleximeter, to experimentally assess the coupling temperature. FIGURE 5-6C shows a typical curve obtained after optical flexural test: the curve shows a collapse up to the temperature of Tg, where it is possible to find a negative peak, caused by the largest difference in the expansion between the two materials. As the temperature increases, the difference between the dilatation curves of the enamel and metal decreases, and the sample shows an upwards flexure. The coupling temperature is identified as the temperature at which a rapid variation on the curve slope is presented. Subsequent heating does not change the curve anymore, as the enamel is in the liquid state and stresses are completely relieved. To obtain a quantitative evaluation of the stress state of the system, it is necessary to translate the expansion curve of the enamel so that it coincides with that of the metal at Tc. The two superimposed curves no longer coincide at room temperature, and the difference (expressed in expansion percentage) between the points of origin of the two curves is proportional to the level of compression established between the glaze and the support, as shown in FIGURE 5-6C. So then, the main difference between the two methods relies in the assessment of the coupling temperature, that is determined mathematically or experimentally in the first and second case, respectively. In the present case, the experimental approach was followed[334].

To exploit the dilatometric analyses, suitable prismatic samples (reference, 1% SS-F, and 5% SS-F) having dimensions of 50 mm x 5 mm x 5 mm were produced. The amount of 5 g of dry formulation (frit, pigment, and SSF filler only) was mixed with 0.5 g of water and the mixture was compacted in a die; the compacted samples were dried at 90 °C for 30 minutes to ensure complete evaporation of water. The samples were fired in a furnace following a thermal cycle as close as the one exploited to produce the original samples: increase of temperature from 25 ˚C to 570 ˚C at a rate of 80 °C/min, firing at 570 °C for 15 minutes and cooling until room temperature.
Dilatometric analyses were carried out using the ELS-MDF horizontal optical dilatometer (Expert Lab Service) with a heating rate of 5 °C/min and a maximum temperature of 570 °C. In addition to the three enamel samples, an additional analysis was exploited on an aluminium A5005 plate having dimensions of 50 mm x 5 mm x 1.5 mm.
No-load bending analyses were carried out using the ELS-MDF optical fleximeter (Expert Lab Service ) with a heating rate of 5 °C/min and a maximum temperature of 570 °C. The samples for the flexural analyses were saw cut to obtain samples with dimensions of 85 mm x 10 mm x 1.6 mm.

#### *5.2.2.6 Coatings mechanical characterization by in-situ techniques*

**In-situ three-point and four-point bending tests with Microdeben tensile tester**
The Young's modulus, and the yield stress of the metal were assessed by tensile tests. The metallic samples were heat treated following the same thermal cycle adopted for the firing of the enamel coatings (heating at 200 °C 15 minutes, cooling at RT, heating at 200 °C 15 minutes and heating at 570 °C for 15 minutes) in order to test the metallic substrate in a condition similar to the one that can be found after the production of the coatings. Three tests were carried out on a UTM Instron 8516 in position control with a cross-head speed set at 0.5 mm/min. The elastic modulus resulted 71.7 ± 3.7 GPa and the tensile yield stress (calculated with the 0.2% method) resulted 49.5 ± 8.5 MPa. Thanks to these measurements it is easily possible to identify the elastic/plastic limit of the stress-strain curves obtained during 3-point and 4-point bending tests.
Starting from the coated flat specimens, sample bars were prepared by two parallel cuts perpendicular to the coating surface in order to have a sample's width of 2.5 mm and a length of 30 mm. In the following step, the cross-sections were polished using a standard metallographic procedure up to 1 µm diamond suspension.
Samples were loaded in an instrumented in-situ stage Microtest 200 N tensile tester (Deben, UK) mounted on Zeiss EVO MA15 (Zeiss, Germany) scanning electron microscope. Observation was carried out in low-vacuum mode (30 Pa) to prevent specimens from charging, and in back-scattered electron mode as to put into evidence the presence of multiple phases, namely the enamel matrix and the SS-Fs.

The tests were performed in both three-point and four-point bending setup, as to provide details on the behaviour of these composite coatings when the maximum loading is applied in a well-defined spot or when the load is homogenously distributed on a wider area. The diameter of the supports was 3.94 mm and a displacement rate of 0.2 mm/min was used. In the case of three-point bending tests, the span between the outer supports (support span) was equal to 23 mm. In the case of four-point bending setup the support span was equal to 23 mm, and the distance between the loading supports (loading span) was equal to 6 mm. The middle loading supports of the jig were in contact with the substrate side of the coating so that crack initiation on the coating free-surface side was ensured and the coating is tested in tension. FIGURE 5-7 shows a picture of the adopted setups. A preload of 0.5 N was applied to all samples prior to testing. Load was applied by controlled displacement of the loading support/supports and it was stopped after regular displacement steps to acquire high-resolution images of the loaded specimens at different magnifications. Applied displacement and force were recorded during the tests. The whole procedure, which is then carried out in "stepwise" mode, consisted of several subsequent steps up to a displacement equal to 1 mm is reached. Areas above the middle support (three-point bending setup) or in the central region between the loading supports (four-point bending setup) were documented by a series of micrographs. At the end of the tests, the samples (still loaded) were tilted to acquire micrographs of the samples free surface.

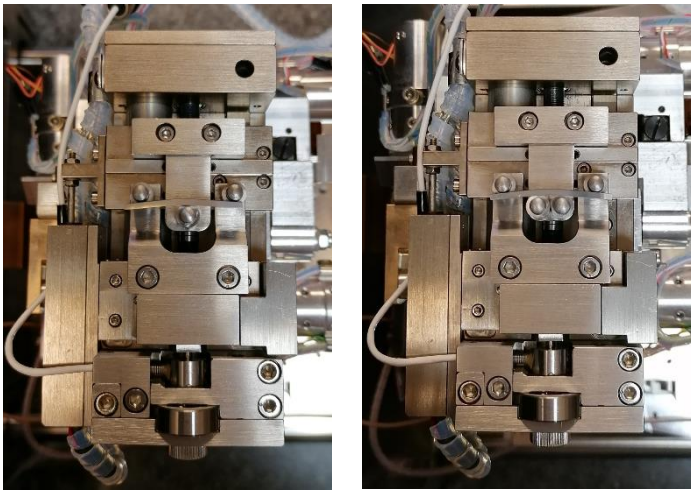

**Figure 5-7: Photograph of the three-point (left) and four point (right) bending setups for in-situ testing inside a scanning electron miscroscope chamber at the end of the test.**

The force/displacement data were converted into stress/strain data using the following formulae for three-point bending tests:

$$\sigma = \frac{3FL}{2bd^2} \; ; \varepsilon = \frac{6d\delta_c}{L^2}$$

where σ is the stress (MPa), F is the load at a given point on the load-deflection curve (N), L is the support span (mm), b is the sample width (mm), d is the sample thickness (mm), ε (mm/mm) is the maximum strain in the outer fibers, $\delta_c$ (mm) is the deflection at the center of the beam[337].
As regards the four-point bending tests, the stress/strain data were calculated using the following formulae:

$$\sigma = \frac{3F(L-L_i)}{2bd^2} \; ; \varepsilon = \frac{3d\delta_a}{(3aL-4a^2)}$$

where σ is the stress (MPa), F is the load at a given point of the load-displacement curve (N), L is the support span (mm), $L_i$ is the loading span (mm), b is the sample width (mm), d is the sample thickness (mm), ε (mm/mm) is the maximum strain in the outer fibers, δa (mm) is the deflection in correspondence of the supports (equal to the displacement of the cross-head)[337]. Both formulae are valid in the elastic regime up to incipient yielding, which is the most interesting part of the specimen behaviour.

**In-situ AE tests in three-point and four-point bending setup (UTM)** For the AE measurements, the samples were saw cut to obtain bar of dimensions equal to 20 mm x 60 mm. The samples were tested in three-point and four-point bending setup using a Tinius Olsen H10KT universal testing machine (Tinius Olsen, UK) equipped with a 5kN loadcell and operating at a 0.2 mm/min cross-head displacement rate. The tests were stopped after 2 mm displacement, The coatings were loaded in tension. The diameter of the supports was equal to 4 mm. In the three-point bending setup the support span was equal to 24 mm, in the four-point bending setup the support span was equal to 30 mm and the loading span was equal to 10 mm (1/3-1/3-1/3 configuration). Applied displacement and force were recorded during measurements.
A Mistras 1283 AE USB node AE equipment (Mistras Group, France) was used to record the AE. AE signals were detected by a trasducer (model PICO 80) placed on the coating, outside the support span area. The threshold value in AE measurement was set at 40 dB and the frequency range used for acquisition was set between 20 kHz and 1 MHz. A total of three samples were tested for each flakes concentration. The bare substrate was also tested in order to obtain a reference measurement.ts

## 5.3 Results and discussion

### 5.3.1 Surface and microstructural analysis

FIGURE 5-8 shows the photograph of the as-made enamel samples. As it easily observable, the addition of the stainless steel filler modifies the aesthetical appearance of the coatings, in particular at higher concentrations.

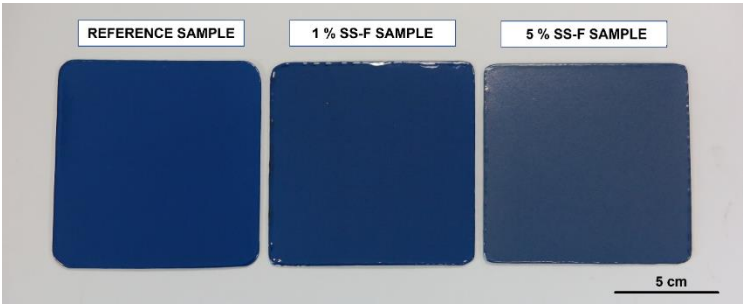


**Figure 5-8. Photograph of the samples under investigation.**

The thickness of the samples is very homogenous, but it was varied from one batch to another as to slightly adjust the fluidity of the screen printing paste, that tends to become more viscous over the weeks. All the samples produced for the analyses that will follow have a thickness that is between 110 µm and 160 µm.
TABLE 5-4 shows the results of the surface roughness investigations.

**Table 5-4. Surface roughness of the enamel samples under investigation.**

| | Sample name | | |
|---|---|---|---|
| **Surface property** | **Reference** | **1 % SS-F** | **5 % SS-F** |
| **Ra (µm)** | 0.17 ± 0.03 | 0.20 ± 0.03 | 1.06 ± 0.15 |
| **Rz (µm)** | 0.87 ± 0.03 | 1.30 ± 0.18 | 5.99 ± 0.75 |

The values obtained for the reference and the 1 % SS-F sample are comparable with the typical surface roughness value of enamel samples. On the other side, the 5 % SS-F sample shows an important increase in roughness, probably due to the very high concentration of SS-Fs, which hinder the creation of a smooth surface. The high surface roughness value of the 5 % SS-F sample is clearly the reason why this sample appears opaquer with respect to the other samples typologies.

Thus, the addition of a limited quantity of stainless-steel filler does not modify the surface topography of the sample, whereas the addition of a higher concentration of SS-Fs leads to an increase of the roughness parameters in the order of 600%.
FIGURE 5-9 displays the optical and the electron miscroscope images of the sample's surfaces.

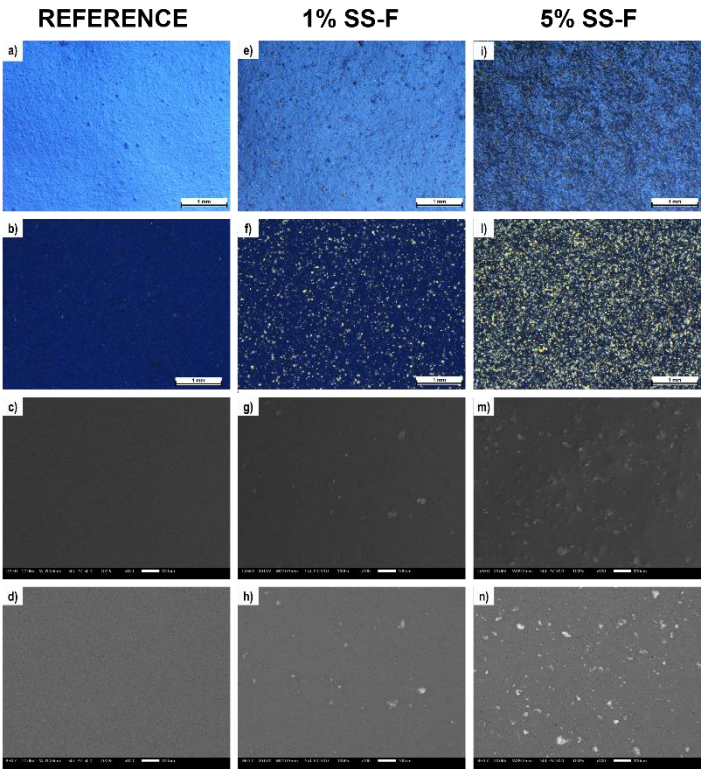


**Figure 5-9: In-plane optical (1 mm marker) and SEM images (100X magnification, 100 µm, SE third line, BSE fourth line) of the samples under study, (a-d) reference, (e-h) 1 % SS-F, (i-n) 5 % SS-F.**

As it is possible to observe from the optical micrographs, the addition of 5 wt.% of SS-F filler leads to the creation of a rougher surface, made up of rounded peaks and valleys, probably due to the inability of the enamel formulation to form a smooth layer at the chosen firing temperatures. The distribution of the stainless-steel powder inside the whole matrix appears to be homogeneous at a millimetric scale and no agglomeration phenomena can be detected from the optical micrographs. On the

other side, SEM images show that the surface distribution of the filler in the 1 % SS-F sample cannot be considered as uniform at a micrometric scale, mainly due to the low probability that some flakes are present in the most superficial layers of the coating. These topographical features of the samples will be important when considering surface-concentrated mechanical stresses, such as in the case of abrasive phenomena or scratching processes. It is in fact crucial to consider the effect of the surface distribution of the filler when mechanical stresses are concentrated on the more superficial layers of the samples. The response of the material greatly depends on the size and distribution of second phase regions (filler particles) with respect to the scale of deformation caused by the stressing system. If the scale of deformation is greater than the size of the second phase regions and it involves a wide area of the sample, the composite material will behave homogenously. If the second phase regions are larger than the scale of deformation or they are not homogenously distributed, the material will show an heterogeneous response[207]. In the case of P.E.I. abrasion tests, the involved surface is very large with respect to the dimension of the filler, and it is possible to observe the average properties of the coating, without negative effects arising from the non-homogenous distribution of the filler at a micrometric scale. In the case of single particle-like abrasive tests (e.g. scratch test), the distribution of the filler on the surface will play an important role, as the area of interaction between the sample and the stressing system will be very limited.

The scanning electron micrographs make possible to observe the close bonding existing between the glassy matrix and the stainless-steel lamellar powder: no interface debonding phenomena can be observed and good compatibility exists between the two components, as no microcracking occurs around the embedded flakes.

The good bonding between the metallic filler and the enamel matrix is confirmed by FIGURE 5-10. These SEM micrographs are attained after subjecting the 5 % SS-F sample to fragile fracture in liquid $N_2$. The images highlight the good compatibility between the two components, as the flakes are partically covered and inserted in the enamel matrix also after an aggressive preparation procedure as the abrupt fragile fracture in liquid nitrogen.

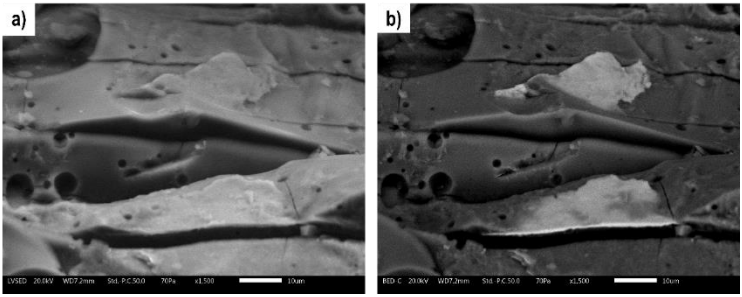


**Figure 5-10. SEM micrographs (1500X magnification, 10 µm marker) of the 5 % SS-F sample after fragile fracture in liquid nitrogen: a) SE mode, b) BSE mode.**

FIGURE 5-11 shows the cross-sectional micrographs of the samples under study, highlighting their internal microstructure, and porous structure.

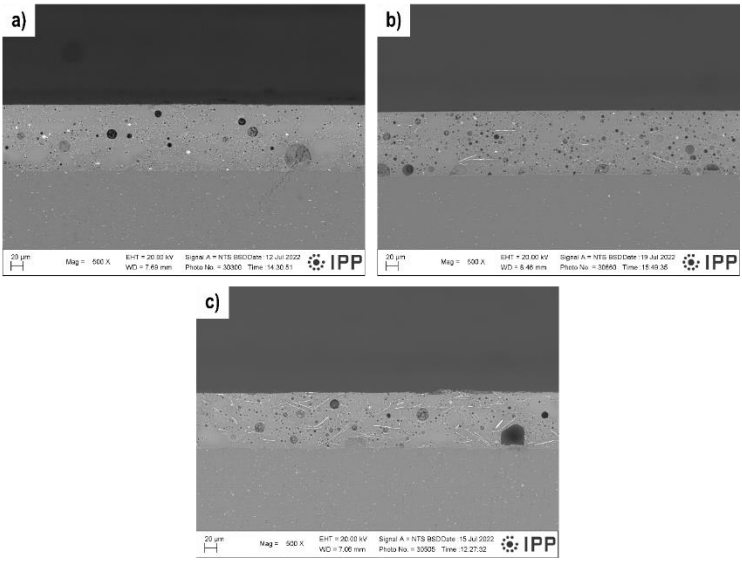


**Figure 5-11. Cross-section SEM micrographs (500X magnification, 20 µm marker, BSE) of the enamel samples under study (a) reference, (b) 1 % SS-F, (c) 5 % SS-F.**

All the samples show the presence of a closed-porosity structure, which is a typical feature of all enamel coatings, as the bubbles are formed by gas evolution during firing. As revealed by FIGURE 5-11 the pores are homogenously distributed through the whole coating thickness and they are not interconnected, assuring good protective properties to the covered substrates.

TABLE 5-5 shows the assessment of porosity level for the samples under investigation. The porosity percentage, the maximum diameter of the pores, and the circularity of the pores are reported. Considering the error bars, no relevant differences can be noticed as regards the maximum diameter of the pores and their circularity, on the other side, a great difference can be highlighted regarding the total internal porosity of the different samples, that increases with a higher concentration of metallic filler.

**Table 5-5. Porosity evaluation for the enamel samples under study.**

| | Porosity (%) | Maximum diameter (μm) | Circularity |
|---|---|---|---|
| **Reference** | 4.5 ± 2.1 | 33 ± 10 | 0.94 ± 0.03 |
| **1 % SS-F** | 8.3 ± 0.7 | 23 ± 5 | 0.97 ± 0.01 |
| **5 % SS-F** | 10.3 ± 2.0 | 31 ± 14 | 0.98 ± 0.00 |

This effect is probably caused by three simultaneous factors: i) an incomplete densification and firing of the frit particles during the firing treatment, ii) an increase in the viscosity of the formulation caused by the addition of the metal-based filler, iii) a most favourable nucleation of bubbles in correspondence of the stainless-steel flakes[338]. All these three aspects could play a role in the case under study, although the first reason can be considered as the prevalent one. As an additional highlight, it is possible to point out that the increase in the internal's porosity is matched by an increase in surface roughness: thus, the addition of the metallic filler seems to cause an incomplete densification of the frit particles leading to a rougher and more porous coating.

As regards the distribution of the SS-Fs inside the matrix, it is possible to observe that the flakes are randomly oriented inside the enamel layer, and they do not assume preferential orientations. The dispersion behaviour of the filler can be clearly explained by its "non-leafing" nature, as the 316L SS-Fs are produced as "non-leafing" metallic effect pigments[339]. Non-leafing pigments show good wettability into the medium they are dispersed in; hence they are uniformely dispersed within the coating.The cross-sectional micrographs also show the homogenous distribution of the cobalt-based blue pigment particles, which can be easily identified as lighter areas in the enamel layer.

### 5.3.2 Chemical resistance and protective properties by means of EIS

The behaviour of the samples in a concentrated acid solution was assessed by means of immersion tests and scanning electron observations. FIGURE 5-12 shows the morphology of the samples after 48 h of immersion in the 20 wt.% HCl solution.

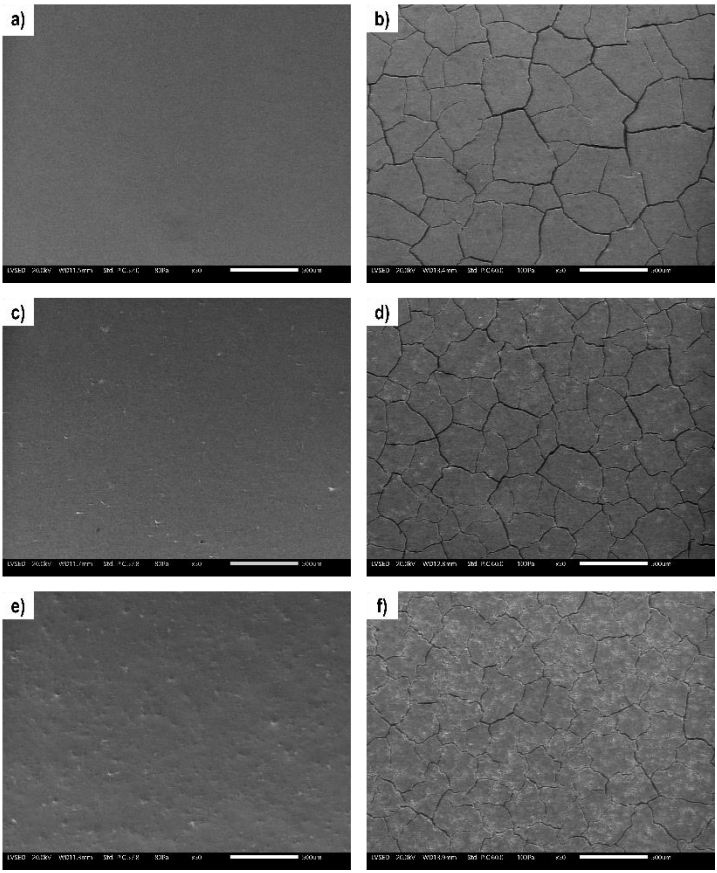


**Figure 5-12. In-plane SEM images (50X magnification, 500 µm marker, SE) of the samples surfaces before (left column) after immersion in HCl 20 wt.% at RT for 48 h (right column): (a-b) reference, (c-d) 1 % SS-F, (e-f) 5 % SS-F.**

The enamel matrix does not seem to be affected by the exposure to the strong acid solution, whereas the stainless-steel flakes are almost destroyed by its action. The lighter areas, present on the samples surfaces, can be attributed to the local

damaging of the matrix in correspondence with the pristine steel flakes.The density of these areas are directly correlated to the creation of more attack nucleation points in the 5 % SS-F sample and the creation of a more segmented attack pattern. An EDXS analysis, carried out on the attacked surfaces, highlighted that an ion exchange occurs between alkali ions from the coating and hydrogen ions from the testing solution, leaving a silica-rich layer on the surface[340].

The chemical attack in concentrated acids evolves by the ion exchange, hydrolysis reactions and formation of a gel layer on the surface of the enamel coating. In the case of alkali-rich enamels, the gel layer is very thick, brittle, and permeable, thus allowing the leaching of different types of elements[340, 341]. In addition to that, the maximum leachability takes place in presence of 20 – 30 wt% concentrated acids. All these mechanisms clearly explains the complete leaching of K, Na, and Ti, shown in FIGURE 5-13. The results of the EDXS analysis are shown as normalized % mass with 2σ errors.

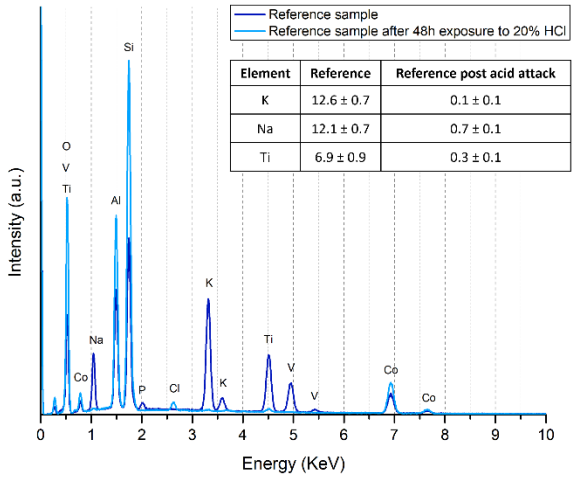


**Figure 5-13: EDXS spectra of the reference sample before and after 48 h exposure to 20% HCl solution.**

Concentrated acid solutions can cause an aggressive chemical attack towards the enamel, but in the present case, the samples were tested towards the hydrochloric acid solution as to assess the resistance of the stainlees steel filler, as they are susceptible in concentrated acidic solutions. On the other side, the enamel matrix is highly susceptible to alkaline hot solutions[5], thus it is important to test the

resistance of the composite coatings in these conditions and see if and how the addition of a metallic filler modifies the overall behaviour of the samples.

The chemical resistance of the samples was assessed by immersion in a 65.41 g/L $K_2P_4O_7$ solution at 96 °C followed by EIS measurements. The EIS tests were carried out at increasing immersion times in the hot alkaline agent solution. FIGURE 5-14 shows the Bode modulus and Bode phase diagrams of the three different samples under study at increasing immersion times in the hot alkaline solution.

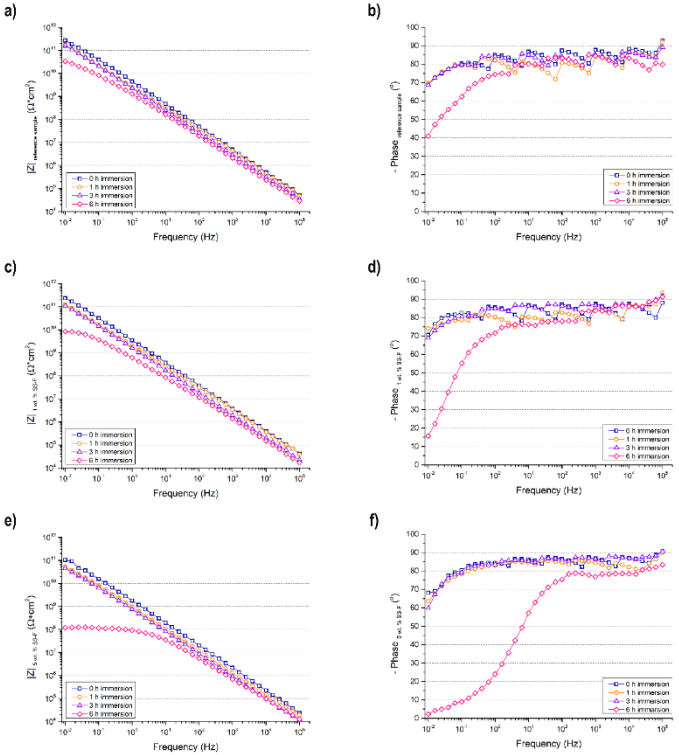


**Figure 5-14. Bode diagrams registered in the $10^{-5}$-$10^{-2}$ Hz range for the samples after different immersion times in the hot $K_2P_4O_7$ solution at 96 °C: (a-b) reference, (c-d) 1 % SS-F, (e-f) 5 % SS-F. The testing solution is a 0.3 wt.% $Na_2SO_4$ acqueous solution.**

As it is possible to observe from the graphs, all the samples keep their protective properties unaltered during the first 3 h of immersion. A great decrease of the impedance modulus |Z| can be detected after 6 h of immersion, ad its reduction is more marked increasing the concentration of the SS-F filler. Nevertheless, all the

samples can be still considered protective towards the substrate, as their impedance values suggest a predominance of the coatings capacitance[150].
TABLE 5-6 and FIGURE 5-15 shows the impedance modulus values |Z| registered at $10^{-2}$ Hz. The reported values are the average of two measurements carried out on different samples.

**Table 5-6. Impedance modulus |Z| at $10^{-2}$ Hz before and at increasing immersion time in the $K_2P_4O_7$ solution at 96 °C.**

| | Impedance modulus \|Z\| at $10^{-2}$ Hz (Ω*cm$^2$) | | | |
|---|---|---|---|---|
| **Sample type \ Time** | **0 h** | **1 h** | **3 h** | **6 h** |
| **Reference** | 2.43 x $10^{11}$ | 1.58 x $10^{11}$ | 1.05 x $10^{11}$ | 2.12 x $10^{10}$ |
| **1 % SS-F** | 2.07 x $10^{11}$ | 1.22 x $10^{11}$ | 7.53 x $10^{10}$ | 5.52 x $10^{9}$ |
| **5 % SS-F** | 1.07 x $10^{11}$ | 5.27 x $10^{10}$ | 2.38 x $10^{10}$ | 2.34 x $10^{8}$ |

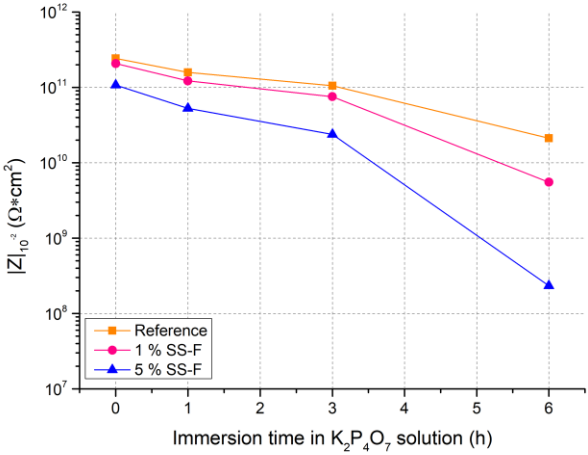


**Figure 5-15: Evolution of impedance modulus |Z| at $10^{-2}$ Hz before and at increasing immersion time in the $K_2P_4O_7$ solution at 96 °C.**

The protective property of all samples decreases with an increasing immersion time in the aggressive alkaline solution, but this decrease is more evident and quicker in the case of composite coatings with a greater concentration of metallic filler. The electrochemical behaviour of the samples can be correlated with their damage morphologies by SEM observations.

FIGURE 5-16 shows the electron microscope images of the samples after 6 h of immersion in the aggressive alkaline solution.

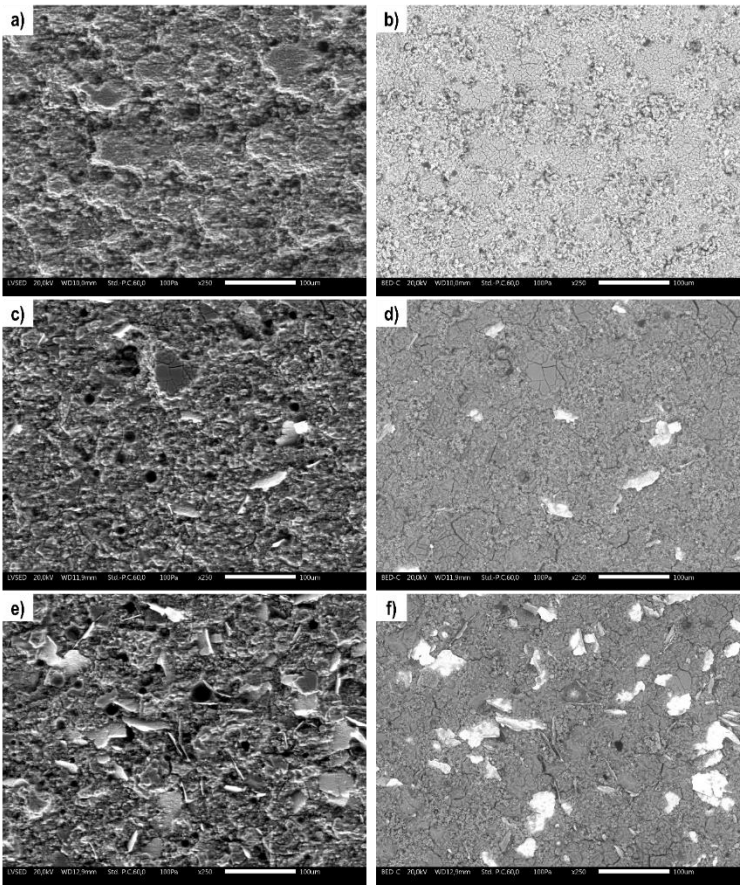


**Figure 5-16. In-plane SEM micrographs (250X magnification, 100 µm, SE left and BSE right) of the samples surfaces after 6 h immersion in the $K_2P_4O_7$ solution at 96 °C: (a-b) reference, (c-d) 1 % SS-F, (e-f) 5 % SS-F.**

FIGURE 5-17 shows higher magnification micrographs and the related elemental maps. All the samples show a generalized attack carried out by the hot alkaline solution, but some important differences can be noticed.

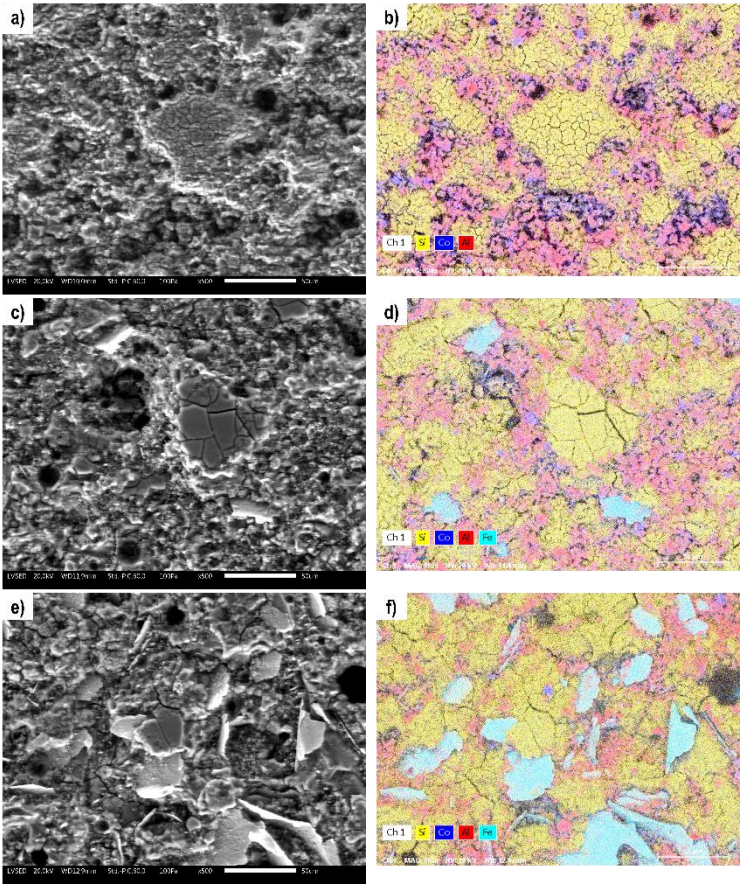


**Figure 5-17: In-plane SEM micrographs (500X magnification, 50 µm marker, SE) and elemental maps (500X magnification, 50 µm) of the surfaces after 6 h immersion in the $K_2P_4O_7$ solution at 96 °C: (a-b) reference, (c-d) 1 % SS-F, (e-f) 5 % SS-F.**

The reference sample shows the presence of some Si-rich (enamel frit) islands: the presence of the pigment particles probably constituted a preferential site from which the chemical attack started[6], but no important damages can be observed. In the case of the 1% SS-F sample some Si-rich areas can still be detected, but the chemical attack seems to be more pronounced as some internal pores are disclosed. In the case of the 5% SS-F sample, many open pores are present on the enamel surface and a uniform reduction of thickness can be observed. The presence of big pores is surely an important cause for the significant drop in the impedance modulus values experienced by this sample type. The stainless-steel filler is not damaged by

the action of the alkaline hot solution, as easily predictable from its Pourbaix diagram[342]. Thus, the presence of the stainless-steel flakes, then the presence of many interfaces, speeds up the chemical attack, that becomes more homogeneous and less localized with respect to what happens to the reference sample.
Considering the chemical resistance tests described in this section, it is possible to state that the presence of the stainless-steel flakes has a negative influence on enamel's resistance to alkaline chemicals, probably because the presence of many interfaces creates more attack points and the chemical attack can proceed more rapidly, degrading all the surface in a homogenous way. The protective properties of the samples decrease with the increase immersion time, and the greater decrease in protection is observable in correspondence of the higher metallic filler concentration. Despite these considerations, all the samples can be considered protective also after 6 hours immersion in the $K_2P_4O_7$ hot solution.

### 5.3.3 Abrasion resistance

The abrasion resistance properties of these coatings were evaluated by P.E.I. test. FIGURE 5-18 shows the mass loss values at different abrasion cycles and the evolution of the surface roughness during the abrasion test. FIGURE 5-18A displays the mass loss variation at different abrasion cycles: all the samples follow a similar trend at low abrasion cycles, but a net differentiation can be detected from 1000 cycles onward. The positive effect of the SS-F filler presence is more and more visible at increasing abrasion cycles. The evolution of the surface roughness (FIGURE 5-18B) follows a sigmoidal trend. At low abrasion cycles all the samples show a limited variation in surface roughness, whose value rapidly increases between 1000 and 2000 abrasion cycles, until reaching a plateau value. It is then possible to assume that the abrasive process starts to have an important effect on the samples morphology only after 1000 abrasion cycles.
The effect of the metallic filler is only visible from 2000 abrasion cycles onward, when the samples surface can be considered as almost homogenously damaged, and the filler can exploit its action without other interferences. The behaviour of the samples, both as regards the mass loss trend and the evolution of the surface roughness, is similar to the one presented in other studies[146]. 1000 abrasion cycles can be considered as a threshold value from which the produced damage assumes a generalized characteristic and the surface roughness rapidly increases up to 2.0 µm. As regards the mass loss data reported in the literature for other systems, it is possible to briefly compare the results with the present study, considering that different frit compositions and firing treatments could influence the abrasion resistance of enamel coatings.

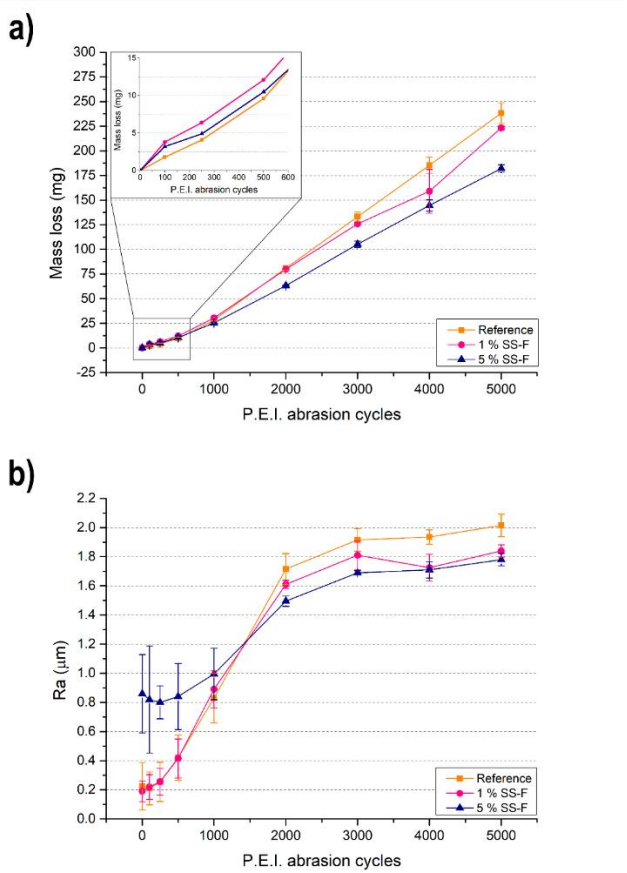


**Figure 5-18. Evaluation of the samples behaviour during P.E.I. abrasion test: (a) evolution of mass loss, (b) evolution of surface roughness.**

TABLE 5-7 shows a brief comparison of the results obtained in this study with literature data. The mass loss values related to reference samples are in almost perfect accordance with each other, indicating a definite reproducibility of the P.E.I. test and suggesting a limited influence of the enamel production parameters and enamel composition on the abrasion results.

**Table 5-7. Comparison of the mass loss data of different enamel systems tested by P.E.I. test with the results obtained in this study.**

| Literature study no. | Sample type | 1000 cycles | 2000 cycles | 5000 cycles |
|---|---|---|---|---|
| **Present study** | Reference | 28 mg | 81 mg | 238 mg |
| | 5 wt% SS-F | 25 mg | 63 mg | 182 mg |
| | *% reduction* | *11 %* | *22 %* | *24 %* |
| **Study no.1[184]** | Reference | 47 mg | 104 mg | 273 mg |
| | $Al_2O_3$ 20 wt.% | 34 mg | 72 mg | 197 mg |
| | *% reduction* | *40 %* | *35 %* | *27 %* |
| **Study no.2[146]** | Reference | 32 mg | 80 mg | 214 mg |
| | SiC 10 wt.% | 5 mg | 15 mg | 65 mg |
| | *% reduction* | *83 %* | *84 %* | *74 %* |

The stainless-steel flakes guarantee better performances with respect to other fillers, such as corundum particles[184], but their effect is far from being competitive with SiC particles[146]. In the present case, the addition of 1 % SS-F reduces the mass loss of about 2% and 6% at 2000 and 5000 abrasion cycles, respectively. The addition of 5 % of SS-F leads to an important decrease of the mass loss, which, in both cases, is about 22–24%. These differences are relatively underestimated, as it is also necessary to consider the real density of the coatings as they are composed by two different elements, having different densities. The density of the 5 % SS-F sample should be 3.5% higher than the reference sample and 3% higher than the 1% SS-F sample, thus the volume loss differences between the samples will be slightly greater than the differences measured considering the mass loss.

The change in protective properties of the coatings after the P.E.I. test were assessed by means of EIS analysis. The EIS analyses were carried out only at the end of the P.E.I. test, as it was not possible to perform the analysis without damaging the sample irreversibly. FIGURE 5-19 shows the value of the |Z| impedance modulus before the tests,after abrasion test, and after the chemical resistance test in the alkaline hot solution.

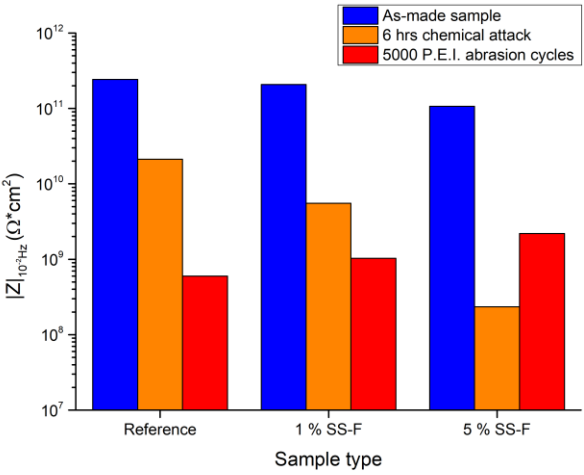


**Figure 5-19. Evolution of impedance modulus |Z| at low frequency of the as-made samples, after 6 hours chemical attack in the $K_2P_4O_7$ solution at 96 °C, and after 5000 P.E.I. abrasion cycles.**

The abrasive action has a negative effect on the protective properties of the coatings, due to the development of small cracks and the opening of porosity. The protective properties of the coatings after abrasion are greatly reduced with respect to the values reported after chemical tests, because the chemical tests, despite being aggressive, are limited to most superficial layers of the enamel matrix, whereas the abrasive process can cause the formation of cracks and defects also in the deepest layers of the coating. The opposite effect is observable in the case of the 5 % SS-F sample, as the samples show better protection after the abrasive process with respect to after chemical tests. The presence of the SS-Fs limit the creation of defects during the abrasive process, whereas represent weak interfaces during chemical tests.

FIGURE 5-20 presents the electron micrographs of the abraded samples after 1000 and 5000 P.E.I. cycles. After 1000 abrasion cycles, all the samples show a damaged surface, characterized by localized material removal and fragile fracture phenomena. In presence of 5 wt.% SS-F filler, the abrasive damage seems to be more generalized, although the fragile fracture behaviour is still predominant. The morphology of the samples surfaces clearly explains the increase in roughness detected at about 1000 abrasion cycles: the presence of some crater-like damages increases the average surface roughness that it is measured on all the samples. As long as abrasion cycles increase, the topography of the sample becomes more homogeneous, as it is possible to observe from FIGURE 5-20(B-D-F).

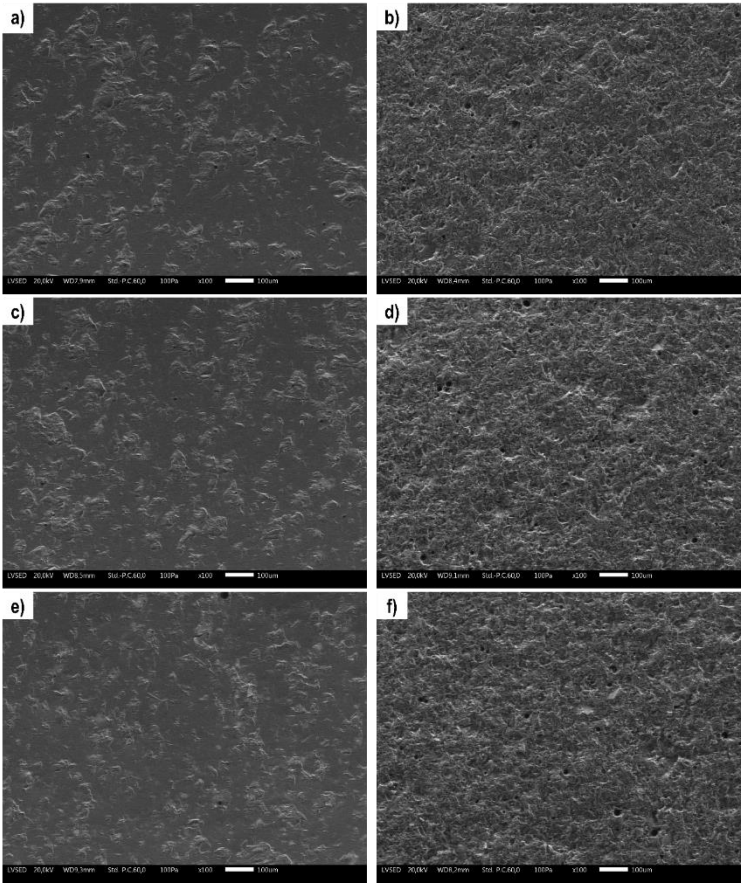


**Figure 5-20. SEM micrographs (100X magnification, 100 µm marker, SE) of the samples after 1000 P.E.I. cycles (left) and after 5000 P.E.I. (right) of the samples under study, (a-b) reference, (c-d) 1 % SS-F, (e-f) 5 % SS-F.**

The role of the stainless-steel flakes and the effect of the different tribosystem components in the abrasive wear process of these composite enamel coatings were investigated by means of some P.E.I. modified tests. As a first step, three reference samples were subjected to the P.E.I. test until 1000 cycles using three different abrasive systems: stainless steel spheres and water, F80 alumina particles and water, and the complete P.E.I. abrasive system (spheres, alumina particles and water). This way, the effect of the different components of the tribosystem was

investigated separately. FIGURE 5-21 reports the electron micrographs carried out on the reference samples after these tests.

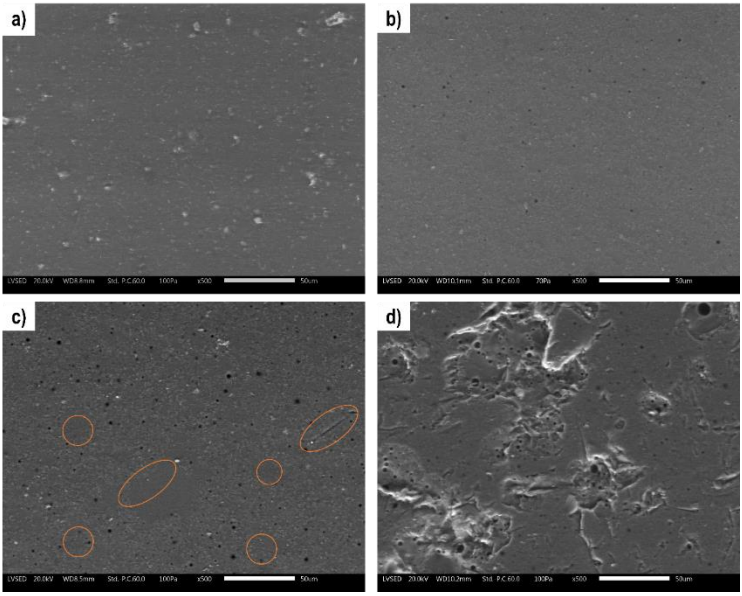


**Figure 5-21. SEM micrographs (500X magnification, 50 µm, SE) of the abraded reference sample after 1000 P.E.I. cycles, (a) non-abraded sample, (b) alumina and water abrasive medium, (c) stainless steel spheres and water abrasive medium, (d) complete P.E.I. system.**

As it is possible to observe from FIGURE 5-21A, the action of the alumina particles has a negligible effect on the modification of the sample's topography, thus being possible to exclude possible erosive phenomena. Differently, the occurrence of some small cracks can be observed when the abrasive system is made of steel balls and water (FIGURE 5-21B). A very distinct situation occurs in the simultaneous presence of stainless-steel spheres and alumina particles: the sample's surface undergoes a deep damaging which includes the removal of material by brittle fracture, opening of enamel's internal porosity and propagation of cracks. Thus, the damaging of the surface is mainly due to the combined action of the spheres and the alumina particles together, which exploit a three-body abrasive process on the sample's surface.

The effect of the composite abrasive medium was then investigated on the 5 % SS-F sample, by carrying out 1000 abrasion cycles and focusing the observations on the behaviour of the metallic flakes only. FIGURE 5-22 reports some high-magnification micrographs on the abraded stainless-steel flakes.

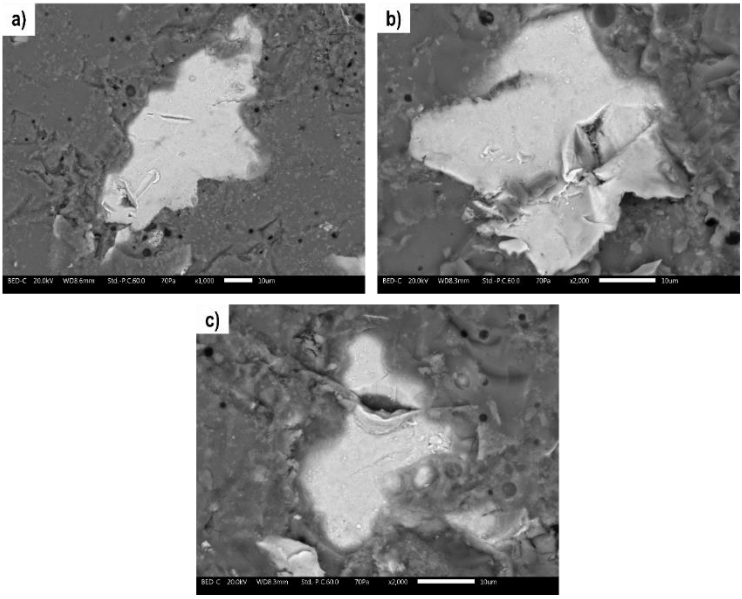


**Figure 5-22. SEM micrographs (10 µm marker, BSE) of the 5 % SS-F sample after 5000 P.E.I. abrasion cycles (a-c) details of the abraded stainless steel flakes.**

FIGURE 5-22A show the presence of some plastic grooves with a dimension compatible with the shape of the alumina abrasing particles. The abrasive action did not lead to a complete asportation of the material, which is accumulated at the groove's borders. FIGURE 5-22B shows a quite different situation: some plastic grooves are still detectable, but an important breakage phenomenon can be observed. This phenomenon was probably caused by the intersection of some subsequent deep grooves, which leaded to the partial detachment of a flake's portion. In the case of FIGURE 5-22C the stainless-steel flake was almost broken by a single penetrating groove.

Considering the results of the P.E.I. abrasion tests, it is possible to state that the presence of the SS-Fs decreases the abrasive rate of vitreous enamel coatings. An increase in the concentration of the metallic filler leads to a decrease of the sample's mass loss. The abrasive process mainly occurs in three different steps: i) inizialization (0 – 1000 cycles), ii) localized abrasive process (1000 – 2500 cycles), iii) generalized abrasive process (from 3000 cycles onward). The three steps involve the formation of small cracks, brittle fracture events with material removal and roughness increase, and generalized damaging, respectively. The stainless-steel flakes exploit their abrasive-resistant action from 2500 cycles onward. The metallic

flakes experience plastic deformation due to the complex tribosystem, and they are able to absorb part of the energy involved in the process, avoiding the brittle damaging of the matrix.

### 5.3.4 Cracking resistance estimated by Indentation fracture (IF) method

The indentation fracture method (IF) is a widely used tool to quickly estimate the fracture toughness of brittle materials and coatings. The relationship between the applied load and the percentage of crack initiation for the samples under investigation is shown in FIGURE 5-23.

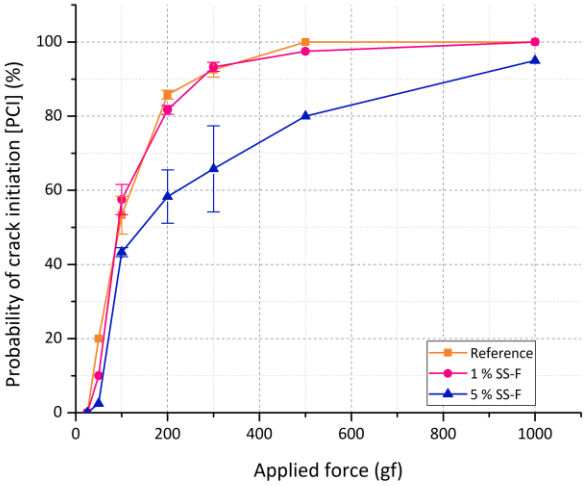


**Figure 5-23. Evolution of probability of crack initiation (PCI) for the samples under investigation tested by the indentation fracture method.**

A rapid increase in PCI can be observed at loads between 50 gf and 100 gf for all the samples, and a real difference in the onset of crack formation cannot be clearly distinguished. However, the 5 % SS-F sample shows lower PCI values with respect to the other two samples in all the tested loads. As regards the CR threshold value, it is possible to notice an increase from $\simeq$ 95 gf for the reference sample, and $\simeq$ 92 gf for the 1 % SS-F sample, to $\simeq$ 145 gf for the 5 % SS-F sample. Then, the addition of a higher concentration of SS-Fs causes a significant improvement of the resistance

to flaw formation as evidenced by the crack formation probability analysis, whereas the sample with 1 wt.% of SS-Fs does not show relevant differences with respect to the reference sample.
The IF method is a cheap and quick testing method to assess the material's toughness by the measurement of the length of cracks that emanate radially outward and downward from the indentation. This method exploits conventional hardness equipment and does not require precracking of the specimen, but its correct application requires very flat specimens with uniform microstructure. In the present case, it was not possible to realiably assess the coating's toughness as the specimens were not flat and their internal microstructure was characterized by a high degree of porosity. Nevertheless, it was feasible to estimate the probability of crack initiation (PCI) and the cracking resistance (i.e., the load correspondent to a PCI of 50%).The samples with 1 wt.% and 5 wt.% filler showed a varied cracking resistance of 4% and 52%, respectively, with respect to the reference sample. Thus, the IF analysis highlighted that the 1 wt.% of SS-Fs is not enough to guarantee an increased cracking resistance, as big differences can be only noticed for the sample cointaining a higher concentration of filler.

### 5.3.5 Cracking resistance estimated by four-point bending tests

FIGURE 5-24 shows the evolution of the number of cracks on the surface of the sample at increasing displacements. In particular, the crack density, defined as the number of observed mode I cracks per unit sample length, is plotted versus deflection in the centerline of the specimen. The tested specimen have a thickness of about 131 ± 5 µm, with the reference samples having an average thickness of 124 ± 1 µm, the 1 % SS-F samples having an average thickness of 132 ± 2 µm, the 5 % SS-F samples having a thickness of 135 ± 2 µm.
The three different samples show similar evolutions, but some differences can be highlighted. The onset of the damage is delayed by increasing the concentration of the SS-F filler into the enamel matrix: considering the error bars it is possible to state that the 1st crack on the samples surfaces can be detected at 1.4 mm, 1.5 mm, and 1.6 mm for the reference, 1 % SS-F and 5 % SS-F samples, respectively. The displacement at which the first crack is observed will be named as "1° crack displacement". After the onset of the damage, the crack density linearly increases until 2.0 mm deflection value. This first stage can be considered as the early crack multiplication stage[343]. At later stages the density of the cracks still increases but with a different rate, and in the case of the composite samples it seems to tend to reach a stabilization stage, where the crack rate tends to a stationary state and then to an almost constant value. Another important point to consider analyzing the data

is the value of the error bars: in this case, the error values are very small, and the trends of the different samples can be really considered as different and separated.

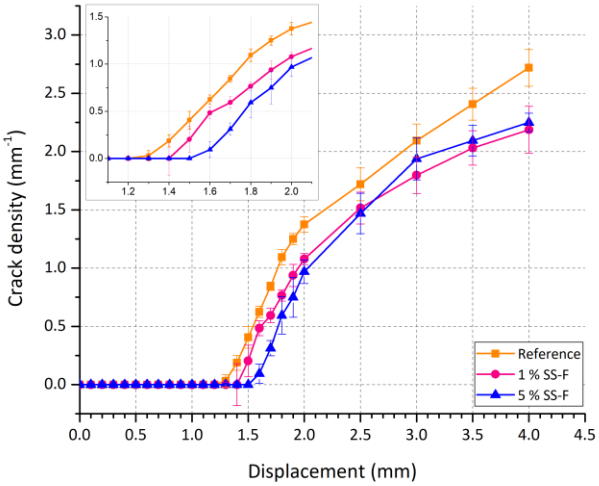


**Figure 5-24. Evolution of the transversal crack density on the sample's surface at increasing displacements during four point bending test.**

FIGURE 5-25 shows optical images of the surface of the samples after 4.00 mm deflection: to highlight surface cracks, the samples were colored with a black spray varnish.

The cracks are perpendicular to length of the beam and their spacing is almost constant; in the case of the 5 % SS-F sample the density of the cracks is notably decreased with respect to the reference sample. In monolayer coatings the cracks are usually almost straight, and they terminate at the substrate, as the stress concentration at the crack tip is reduced and the crack stops propagating[344].

FIGURE 5-26 shows some detailed SEM images of the 5 % SS-F sample's surface after 4.0 mm displacement: a clear interaction between the cracks and the second ductile phase can be noticed. When a crack encounters an interface, it experiences a change in elastic properties and perhaps in coating morphology. This increases the possibility for the crack to deflect, loose energy by plastic deformation of the filler, or branch into several cracks[344]. All these processes may reduce the stress intensity at the crack tip, leading to a more "cracking resistant" coating[217].

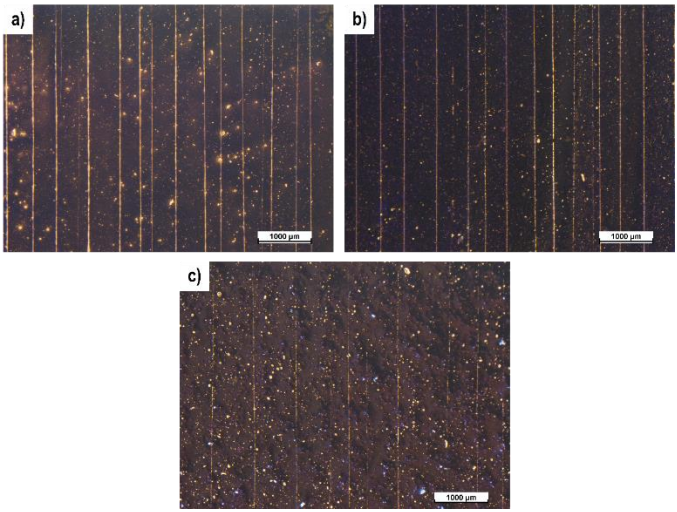


**Figure 5-25. Optical images of the enamel surface after 4.00 mm displacement during four-point bending tests: (a) reference, (b) 1 % SS-F, (c) 5 % SS-F.**

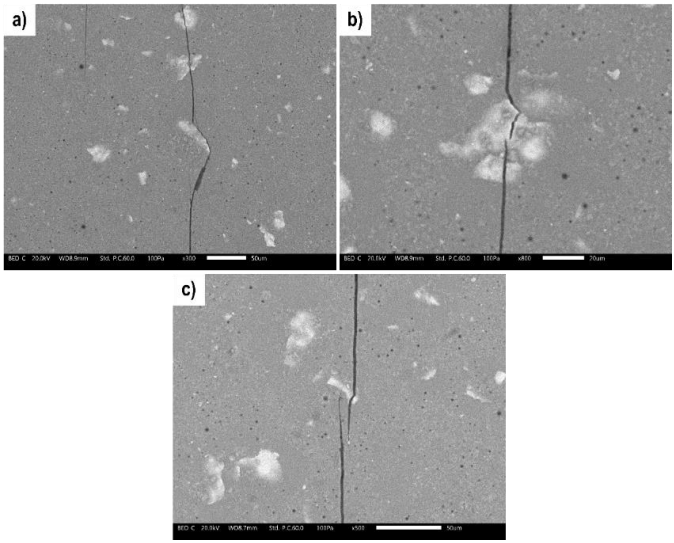


**Figure 5-26. In-plane SEM micrographs (BSE) of the 5 % SS-F sample after 4.00 mm displacement during four point bending tests: (a) crack deflection (300X magnification, 50 µm), (b) crack deflection and plastic deformation (800X magnification, 20 µm), (c) crack branching (500X magnification, 50 µm).**

Enamel coatings exhibit cracking in the transverse direction of the tensile load[345]. The presence of the 5 % SS-F filler seems to create many interaction points with the propagating cracks. Although many flakes are broken during the propagation of the cracks, phenomena of crack deflection and plastic deformation of the filler can be clearly noticed.
In conclusion, the bending tests were useful to evaluate the crack density of the different samples at increasing displacements. All the samples showed an abrupt increase of the crack density with the applied displacement, which is a typical behaviour of hard brittle coatings addressed as “crack multiplication stage”. However, only the composite coatings seemed to reach a phase (known as “crack stabilization stage”) in which the rate of crack density increase is considerably lower than in the previous step. Some important differences also raised in terms of displacement needed for observing the first crack on the sample’s surface: an increased filler concentration inside the matrix seemed to be beneficial in delaying the initiation of cracks. This testing method is really demanding in terms of time required and sample preparation procedures, but it gives the possibility to understand the damaging mechanisms and the role of the metallic filler in counteracting the propagation of cracks. In the present case, it was possible to identify the crack deflection and the ductile rupture of the filler as the main crack/ filler interaction mechanisms. These toughening mechanisms are responsible for the better cracking resistance of the composite sample with 1 wt.% and 5 wt.% of stainless-steel flakes, as the metallic filler is responsible for increasing the tortuosity of the crack’s propagation path and can absorb part of the propagation energy by ductile deformation. In this regard, a higher concentration of filler guarantees many more interactions between the propagating cracks and the filler itself, leading to an increased cracking resistance.

### 5.3.6 Tribological and mechanical behaviour by means of scratch test

The scratch test is a powerful technique to understand the fracture behaviour of brittle materials under a two-body abrasive action. Many parameters can be taken under consideration, both by a quantitative point of view and by a qualitative point of view. In particular, it is possible to consider the values of the critical loads, the trend of the coefficient of friction, the penetration depth, and the morphology of the wear track.
TABLE 5-8 shows the results of the Lc value analysis. The assessment of Lc values was exploited by considering the friction coefficient (COF) trend, optical observations of the damaged areas, and the AE signal.

**Table 5-8. Critical loads Lc1, Lc2, and Lc3 for the vitreous enamel samples under investigation. Average values of 6 different tests.**

| Sample | Lc1 (N) | Lc2 (N) | Lc3 (N) |
|---|---|---|---|
| **Reference** | 6.4 ± 1.4 | 15.9 ± 3.2 | 55.9 ± 4.6 |
| **1 % SS-F** | 8.0 ± 1.4 | 17.5 ± 2.2 | 63.7 ± 3.1 |
| **5 % SS-F** | 3.6 ± 0.7 | 14.6 ± 2.0 | 61.8 ± 4.2 |

The Lc1 values of the reference and 1 % SS-F samples are very similar to each other, whereas the 5 % SS-F sample shows a very low Lc1 value. The Lc1 values (apart from the 5 % SS-F sample) are comparable to data found in the literature, although their value is quite low as these coatings are expected to show a low degree of crystallization[346, 347]. The Lc1 value of the 5 % SS-F sample is very low, but this difference can be easily explained by the topography of the sample's surface, which shows a very high surface roughness with respect to the other samples. As extensively described in the literature, the surface roughness of a sample has a great influence on the results of scratch tests, as in case of high surface roughness small cracks immediately form at the first contact between the surface asperities and the indenter tip, and as a consequence, the Lc1 value is shifted to lower loads[346]. As regards the Lc2 values, all the samples show similar values around 15 N, which are also in good agreement with literature data on similar enamel systems[348]. Considering the Lc3 values, it is possible to observe that the Lc3 of the reference sample is 10% lower with respect to the other samples. Thus, it seems that the addition of only 1 % SS-F is able to improve the scratching resistance of the coating and no further improvements can be noticed by increasing the filler concentration. This last statement should not be considered totally reliable without the confirmation of other observations, as the error connected with this type of measurements is very high, in the order of 5 - 10%[349]. Summarizing, the quantitative analysis of Lc values on composite enamel coatings cannot provide definite and reliable results discriminating between the coatings with different filler concentrations, whereas the sample's surface roughness has an evident influence on these results. In addition to that, it is important to remark that the addition of the flakes does not seem to have an important influence on the scratch resistance of the coatings, but the results are mainly dependent on the matrix itself. The critical load values coming as outputs of the scratch analysis can be useful to calculate the "scratch propagation resistance" as suggested by Zhang et al.[214], but in this case the Lc1 value of the 5 % SS-F is not reliable to perform this analysis.

The study of the wear track topography (penetration depth, residual depth, and width) could provide important information about the failure mechanism of the coatings and the influence of the SS-F during this wear process. In the case of brittle

coatings, the analysis of the residual depth after the removal of the load cannot be performed as the error associated with these measurements is large due to the generation of cracks, material removal, and formation on debris. FIGURE 5-27 shows the representative graphs of the average penetration depth and average friction coefficient (defined as the ratio between the tangential force and the normal applied force) of the investigated samples.

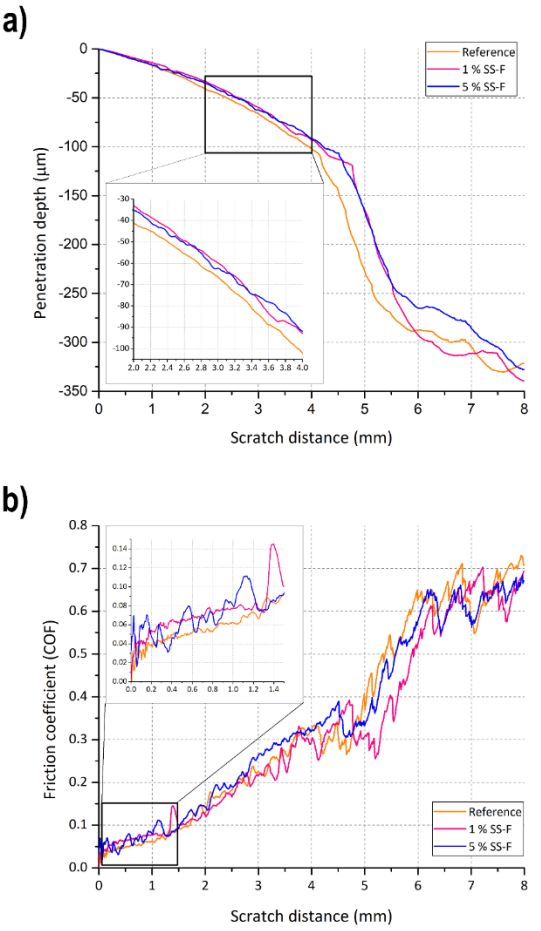


**Figure 5-27. Evolution of (a) penetration depth, and (b) coefficient of friction for the enamel samples under study during scratch tests performed at 11.44 N/mm in the 0.5 - 100 N range.**

As shown by FIGURE 5-27A the penetration depth of the composite enamel coatings seems to be lower with respect to the reference sample (in the order of 10%): this difference is particularly relevant after a scratch distance of 1.5 mm (equal to an applied normal force of 18.6 N), which corresponds to the onset of cohesive failure of the coating, but no relevant differences can be noticed between the composite samples. As expected, the most important area to make comparisons between the samples is the cohesive damaged area, where the effect of the flakes plays a relevant role, as the whole matrix is involved in the abrasive process and the flakes can act together in counteracting the penetration of the indenter and the propagation of damage driven by brittle fracture. FIGURE 5-27B show the evolution of the friction coefficient (COF) for the reference and the composite samples. The COF values are similar between the three sample types, and they are comparable with literature data[346]. The COF evolution can be divided in two regions having different slopes: the first region corresponds to the region where no cohesive damages can be detected, whereas the second region having a higher slope corresponds to the area between Lc2 and Lc3. As clearly observable from FIGURE 5-27B the COF evolution in the first region until Lc1 shows great oscillations, which could be due to both the high surface roughness of the samples and/or the presence of many SS-Fs on the surface of the sample.

The next part of this section will be devoted to the in depth analysis of three representative samples, in order to obtain topographical informations, related to the penetration depth, COF, track depth, and track width.

TABLE 5-9 shows the width and the depth of the scratch tracks at the critical loads values Lc1, Lc2, and Lc3.

**Table 5-9. Scratch wear track width and depth at critical load values (Lc1, Lc2, and Lc3) for the enamels under study.**

| Sample | Lc1 (N) | Width (µm) | Depth (µm) | Lc2 (N) | Width (µm) | Depth (µm) | Lc3 (N) | Width (µm) | Depth (µm) |
|---|---|---|---|---|---|---|---|---|---|
| **Reference** | 4.8 | 85 | 18 | 16.8 | 761 | 40 | 58.6 | 1029 | 185 |
| **1 % SS-F** | 7.8 | 204 | 27 | 19.1 | 343 | 42 | 63.6 | 1409 | 211 |
| **5 % SS-F** | 3.6 | 153 | 7 | 13.3 | 345 | 27 | 62.4 | 2386 | 178 |

These results are the output of confocal microscope acquisitions, and they highlight important differences between the samples. The results at Lc1 and Lc3 are greatly dependent respectively on the surface roughness of the samples (at Lc1), and on the catastrophic cohesive/adhesive damaging (at Lc3) and they cannot be considered as much reliable, however, the results at Lc2 represent a clear indication of the damage evolution in the coating when cohesive damaging starts to occur. In particular, a reduction of 50% in the track width can be observed between the reference and the

composite samples, and an important decrease in the depth of the track can be observed with 5 wt.% of stainless steel filler. Thus, it is possible to state that the addition of a 5 % SS-F has a great positive effect in reducing both the lateral and transversal extension of the damage caused by the scratching indenter.

FIGURE 5-28 shows the confocal images of the three scratches made on the three different sample, and the regions of interest where line scans were performed to assess the penetration depth and the width of the scratch track. FIGURE 5-29 shows the evolution of their penetration depth and COF profile.

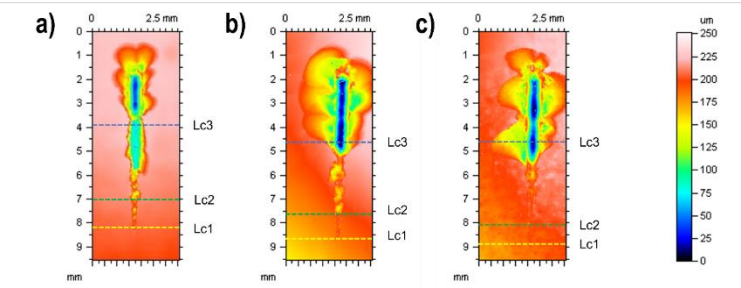


**Figure 5-28. Confocal images of the scratch wear track of the samples (a) reference, (b) 1 % SS-F, (c) 5 % SS-F.**

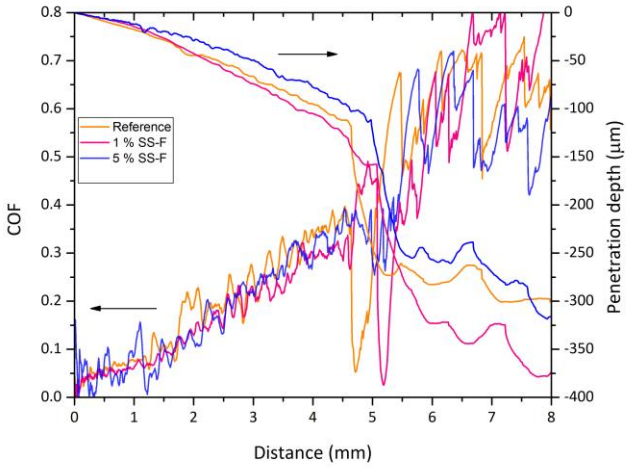


**Figure 5-29. Penetration depth and COF evolution for the samples whose confocal images are shown in Figure 5-28.**

FIGURE 5-30 shows the SEM micrographs of the samples consididered for the morphological analysis.

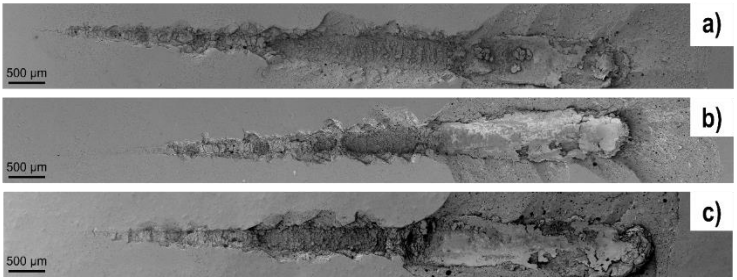


**Figure 5-30. SEM micrographs (500 µm marker, SE) of the scratch wear track of the enamel samples (a) reference, (b) 1 % SS-F, (c) 5 % SS-F.**

The damaging mechanism does not differ from one sample to another, as the matrix is the same and the flakes do not have the ability to modify the damaging mechanisms, but only to limit the extent of the damage. In the region between Lc1 and Lc2 it is possible to observe tensile type hertzian cracks. The formation of tensile type cracks is a typical feature of brittle coatings deposited on more ductile substrates[350] and they are well described by other studies on glazed materials[351]. In the area after Lc2 cohesive spallation at the track borders starts to be observed, although greater cohesive spallation is only visible in regions close to the Lc3 values.

In conclusion, the scratch technique is an established method for the characterization of adhesion and failure of coatings. This technique can provide useful information about the scratch crack resistance of the studied materials by considering both the load at which the first crack is initiated and the load at which catastrophic failure occurs. This evaluation did not give realiable results on enamel composite coatings, as the high surface roughness of the 5 % SS-F sample negatively influenced the values of the crack initiation load. All the samples showed a similar behaviour, mainly characterized by cohesive damaging and absence of chipping. This technique therefore confirmed the excellent adhesion of the enamel on the metallic substrate. Despite the difficulty in obtaining quantitative results about cracking resistance, a confocal microscope analysis of the scratch track highlighted a great difference in the width and depth of the wear track for the different samples, as shown in TABLE 5-9. The 5 % SS-F sample was the only one showing a great reduction in both width and depth of the scratch track, with reduction values of about 55% and 33%, respectively. Thus, the presence of high concentration of metallic filler was able to limit the extent of the cohesive damage occurring in the coating due to the mechanical action of the scratch indenter.

FIGURE 5-31 summarizes the results obtained in this study by the mechanical characterization of the composite enamel coatings exploiting bending tests, IF method, and scratch test analyses.

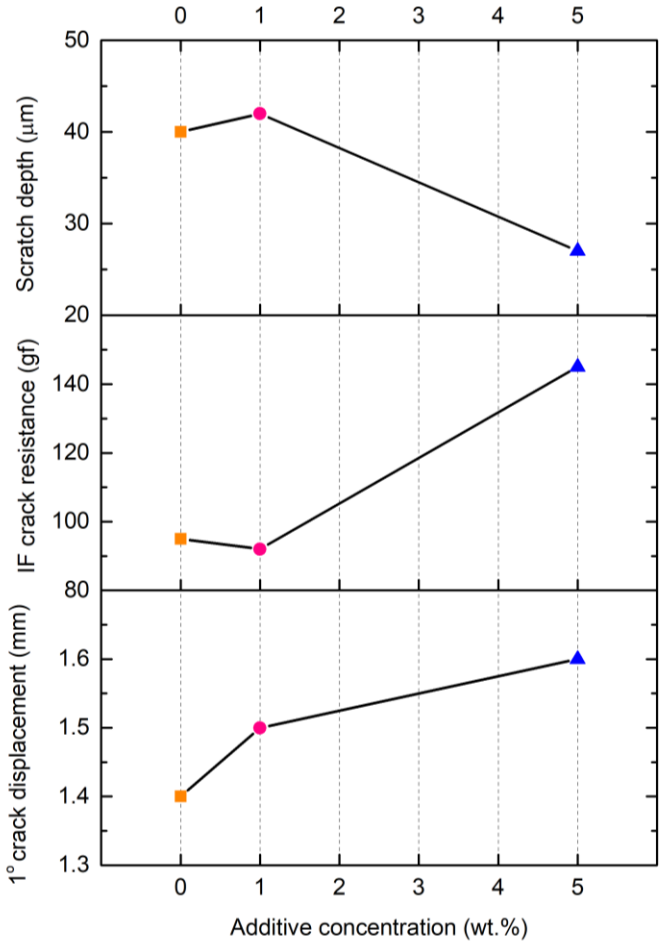


**Figure 5-31. Summary of the results of the mechanical investigations carried out by four point bending tests, IF method, and scratch test analyses.**

The bending test results highlight that by increasing the concentration of filler beneficial effects in delaying the initiation of cracks are attained, although the filler concentration is not linearly related to an increase in the strain needed to initiate the

first crack. On the other side, the benefit guaranteed by the presence of a high concentration of stainless-steel flakes (5 wt.%) is clearly highlighted by the results of the IF tests and scratch analyses. These two techniques provide complementary results as an increase in the IF cracking resistance corresponds to a decrease in the depth of scratch wear track. The addition of 1 wt.% filler seems not to provide considerable differences with respect to the reference sample, whereas the addition of 5 wt.% SS-Fs seems to be beneficial in limiting the extent of the damage at high stresses. It is important to point out that the IF method and the scratch test involve the use of an indenter and the sample's volume is at is tested is really limited with respect to the bending tests: in this case the distribution of the filler and the interaction volume are critical as the stress is localized and the response of the material could be not homogeneous, as for the 1 % SS-F sample. Thus, the results of these two techniques can be considered reliable only at higher applied loads, when the interaction volume is quite large with respect to the dimension of the filler and the response of the material is approximately homogeneous. Thus, all the three techniques were useful for the characterization of the coatings, as together they were able to provide both quantitative data and damaging mechanisms insights.

### 5.3.7 Residual stress assessment by thermal analysis

FIGURE 5-32A shows the dilatometric curves of the metallic substrate and the different enamel formulations. The metallic substrate has a linear thermal expansion in the studied range, whereas the enamel formulations show some important deviations from the linear trend. The reference and 1 % SS-F formulations have a fine linear trend until the glass transition temperature of about 360 °C, subsequently the curves increase in slope until reaching a maximum (494 °C and 512 °C for the reference and 1 % SS-F formulations, respectively) followed by an apparent shrinkage of the material. This is where the enamel begins to soften, and the edges of the samples become rounded. Enamel with 5 % stainless steel follows a linear trend up to 350 °C temperature range within which the glass transition is observed. The curve then increases with a steeper slope until it reaches a maximum (430 °C) followed by an apparent shrinkage which, in turn, follows an expansion. These last two phenomena can be associated with the fact that the ends of the specimen are detached from the supporting substrate and make the equipment records an apparent expansion and shrinkage of the material. These dilatometric analyses highlight that the aluminum support undergoes thermal expansion significantly higher than that of enamels, with a CTE of about $27 \times 10^{-6}$ $K^{-1}$ in the 100-300 °C range.

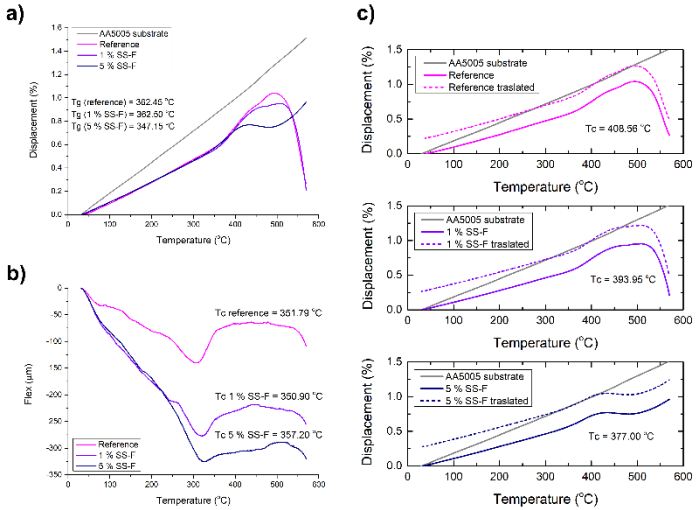


**Figure 5-32: Experimental assessment of residual stresses by thermal analysis (a) dilatometric curves, (b) flexural curves, (c) experimental assessment of residual stress with coupling temperature Tc calculated by optical fleximeter measurements.**

The enamel formulations do not present differences in net expansions (showing a similar linear CTE) each other to justify the differences in behavior shown by the specimens subjected to fleximeter analyses. The only difference among the enamel formulation is the absence of a clear softening maximum (Ts) for the 5 % SS-formulation, whose Ts seems to be shifted at temperatures higher than 569 °C.

FIGURE 5-32B shows the results of the optical fleximeter analyses. All the samples show a downward flexure until reaching a minimum, which corresponds to the glass transition temperature Tg. This bending is caused by the greater thermal expansion of the substrate than that of the enamel. Such a downturn is gradually more accentuated by the presence of stainless steel which causes variations in the elastic modulus of the enamel. Subsequently, the curves tend to return towards zero as the enamel now expands more rapidly than metal substrate. Around 500 °C there is a new decrease of the curve since the aluminium undergoes a pyroplastic deformation. As reported in TABLE 5-10, it should be noted that the glass transition is recorded by the fleximeter at temperatures lower than the ones registered during the dilatometric tests. This difference can be connected to the different shape of the samples used in the two tests and their different positioning with respect to the thermocouple. The absolute difference between the Tg registered during dilatometric and flexural tests decreases with the increase in the metallic filler concentration probably due to the different thermal diffusivity of the different formulations. The coupling temperature was extrapolated by the inflection of the fleximeter curves, and it was corrected by

the ΔT assessed by comparing the differences in Tg of the dilatometric curves and flexural curves. At this point, the dilatometric curves of the enamel formulations and the metallic substrates were made to coincide at the extrapolated coupling temperatures and the level of compression at 50 °C was established (FIGURE 5-32). As shown in TABLE 5-10, the level of compression of the glaze with respect to the metal support increases with the concentration of metallic filler, although the greatest variation (26%) is recorded with the addition of only 1 % SS-F, whereas an increase up to 5 % filler increases the compression level of only 4% with respect to the previous filler concentration.

**Table 5-10: Characteristic temperatures and parameters assessed by thermal analysis.**

| | Sample type | | | |
|---|---|---|---|---|
| | **AA5005** | **Reference** | **1 % SS-F** | **5 % SS-F** |
| | 27 | 19 | 18 | 18 |
| **Tg dilatometry (°C)** | - | 362.45 | 362.50 | 347.15 |
| **Ts dilatometry (°C)** | - | 494.14 | 511.91 | > 569 |
| **Tg flexural (°C)** | - | 305.68 | 319.45 | 327.35 |
| **Tc flexural (°C)** | - | 408.56 | 393.95 | 377.00 |
| $\Delta C_{40}$ | - | 0.201 | 0.253 | 0.262 |

## 5.3.8 Coatings mechanical characterization by in-situ SEM analyses

### *5.3.8.1 In-situ three-point flexural tests*

In-situ mechanical tests inside the SEM chamber give the opportunity to study the failure mechanisms of the different samples and to quantitatively assess their resistance to cracking. In this context it is possible to calculate the stress-strain curves, to follow the evolution of the crack density together with the applied strain, and to assess of the failure strain (i.e. strain level at which is possible to observe the onset of damage/evolution of the first crack). The crack density is calculated by counting the transversal cracks visible in the sample's cross-section at 100x magnification. In the same way, it is possible to assess the strain level at which the first crack is visible in the sample's cross-section. TABLE 5-11 shows the failure strain values for the different samples taken under consideration.

**Table 5-11: Failure strain (%) for the samples tested in three-point bending configuration.**

| | Sample type | | |
|---|---|---|---|
| | **Reference** | **1 % SS-F** | **5 % SS-F** |
| **Sample no.1** | 0.33 | 0.35 | 0.35 |
| **Sample no.2** | 0.33 | 0.35 | 0.40 |
| **Sample no.3** | 0.32 | 0.40 | 0.42 |
| **Average** | 0.33 ± 0.00 | 0.37 ± 0.02 | 0.39 ±0.03 |

Considering the yield stress calculated by the tensile tests, as explained in SECTION 5.2.2.6 it was possible to get the elastic-plastic limit of the stress-strain curves of the samples tested in three-point bending setup. The end of the elastic regime of the metallic substrate corresponds to a strain value of 0.18 ± 0.5 %. Thus, it is easy to state that the failure of the coating starts when the substrate is considerably in the plastic regime.

FIGURE 5-33A shows the average stress-strain curves for the samples tested in three-point bending mode and FIGURE 5-33B shows the evolution of crack density with the increased applied strain. The crack density evolution follows the same trend for all the studied formulations until 0.7 % strain, the point at which a discontinuity in the crack increase rate can be noticed for all the samples. The crack density value is greatly reduced in the case of the 5 % SS-F sample, which shows a first increase of the crack density, a small retardation area between 0.7 % and 1.1 % strain, and again a crack density increase.

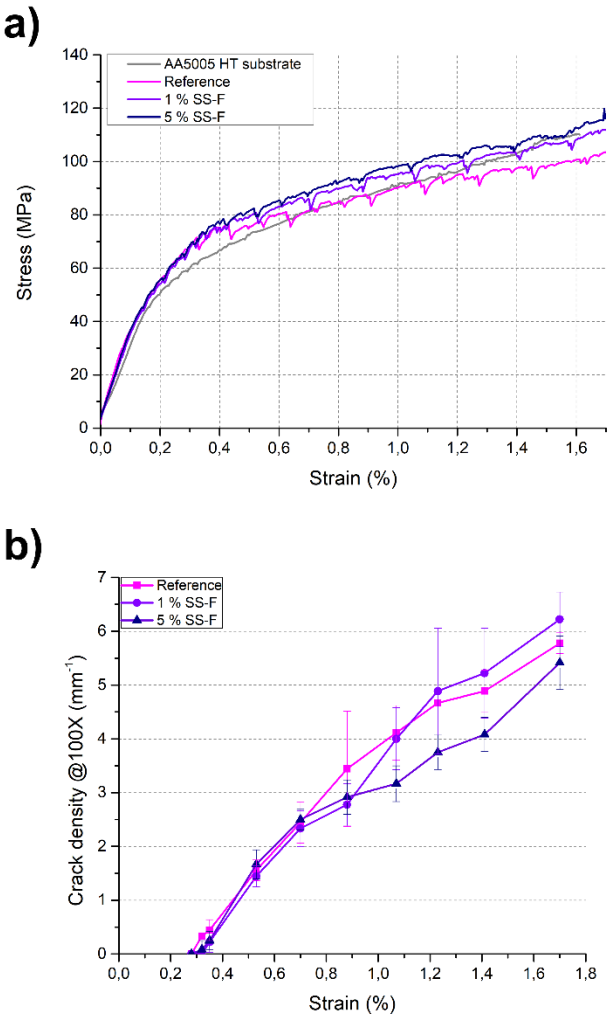


**Figure 5-33: Output results from three-point bending tests with Microtest 200 N Deben tensile tester: (a) stress-strain curves, (b) crack density evolution with increasing strain.**

Exploiting in-situ measurements is also useful to better understand the evolution of damage and the role of the metallic filler in counteracting the propagation of cracks. FIGURE 5-34 shows panoramic micrographs of the samples tested in 3-point bending configuration after 1.00 mm displacement. As it is easily observable, all the samples show the presence of transversal cracks, that propagate through the coating's

thickness and are then stopped at the enamel/metal interface. As the metallic filler concentration increases, the cracks on the free surface seem to follow a more tortuous path, as many of them experience deviation and/or branching phenomena. The density of cracks in the cross-section is very similar between all the tested samples.

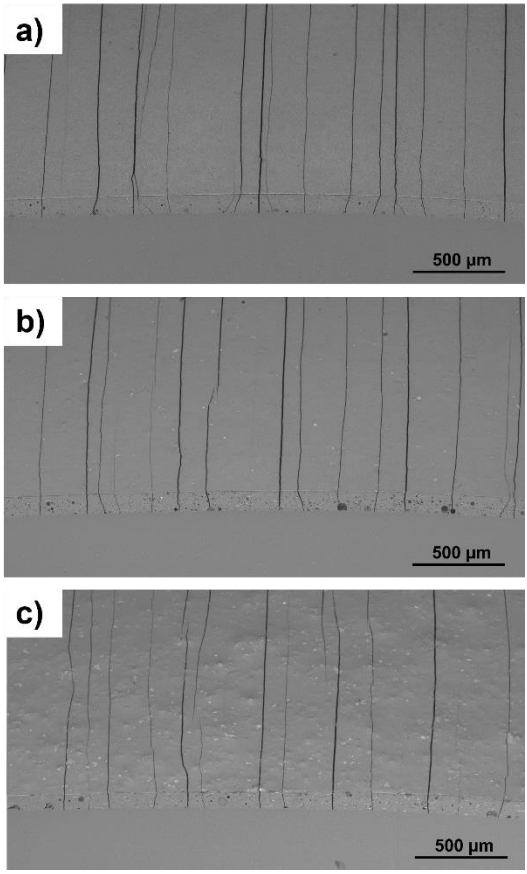


**Figure 5-34: SEM panoramic reconstructed images (500 µm marker, BSE) of the investigated samples tested in 3-point bending configuration after 1.00 mm extension (a) reference, (b) 1% SS-F, (c) 5% SS-F.**

A detailed view of the cross-sections after the 3-point bending test is shown in FIGURE 5-35**.** This figure better shows the propagation path of the transversal cracks and their interaction with the stainless-steel flakes and the present pores. In all the

three cases the cracks seem to preferentially propagate in correspondence of internal pores, often deviating their position along the x axis to reach some interfacial pores. This effect is less evident as the concentration of the metallic filler increases, probably because the interaction between the 316L flakes and the cracks is the dominant factor. Another important effect to be highlighted is the branching of the cracks. This effect is really evident in the reference sample, and still occurring in the 1% SS-F samples, but almost absent in the 5% SS-F sample. The presence of the 316L flakes is in both composite samples accompanied by important crack/flakes interaction phenomena that lead to the deviation of cracks and to an increase of the crack propagation path. No delamination phenomena can be noticed at the interface.

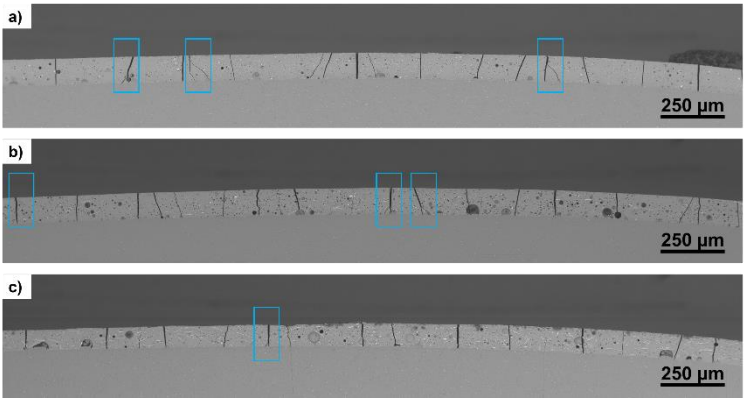


**Figure 5-35: Cross-sectional SEM images (250 µm marker, BSE) of the investigated samples tested in 3-point bending configuration after 1.00 mm extension: (a) reference, (b) 1% SS-F, (c) 5% SS-F.**

FIGURE 5-36 shows some detailed SEM images of crack/flakes interaction phenomena after testing at 1.00 mm displacement. These details were acquired on the same samples that are shown in FIGURE 5-35. FIGURE 5-36(A-C) represents some details of the 1% S-F sample, whereas FIGURE 5-36(D-F) shows some details of the 5% SS-F sample. Three main interaction mechanisms can be noticed: crack bridging (FIGURE 5-36A,E), crack deflection (FIGURE 5-36C), and filler plastic deformation/rupture (FIGURE 5-36B,D,F), that is often combined with crack deflection.

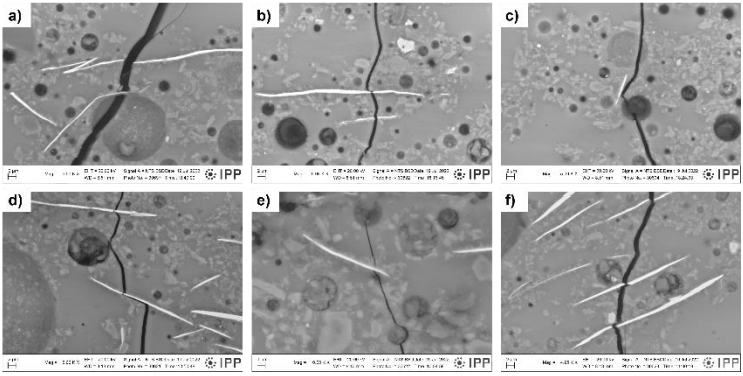


**Figure 5-36: Detailed cross-sectional SEM images (BSE) of the investigated samples tested in 3-point bending configuration after 1.00 mm extension: (a-c) 1% SS-F sample, (d-f) 5% SS-F sample.**

### *5.3.8.2 In-situ four-point flexural tests*

As previously described, it was possible to calculate the stress strain curves, and assess the evolution of the crack density together with the applied strain and assess the failure strain. TABLE 5-12 shows the failure strain values for the different samples taken under consideration.

**Table 5-12: Failure strain (%) for the samples tested in four-point bending configuration.**

| | Sample type | | |
|---|---|---|---|
| | **Reference** | **1 % SS-F** | **5 % SS-F** |
| **Sample no.1** | 0.31 | 0.45 | 0.45 |
| **Sample no.2** | 0.40 | - | 0.47 |
| **Sample no.3** | 0.41 | - | 0.51 |
| **Average** | 0.37 ± 0.04 | 0.45 ± 0.00 | 0.48 ±0.02 |

As described before, it is possible to easily identify the limit of the elastic deformation region of the metallic substrate in the stress-strain curves of the samples tested in four-point bending setup. In this case the end of the elastic regime corresponds to a strain value of 0.21 ± 0.6 %. Also in this case, the failure of the coatings starts in the plastic regime of the substrate and the failure strains are shifted to higher values with respect to the three-point bending configuration. FIGURE 5-37A shows the average

stress-strain curves for the samples tested in four-point bending configuration, and FIGURE 5-37B shows the evolution of crack density with the increased applied strain.

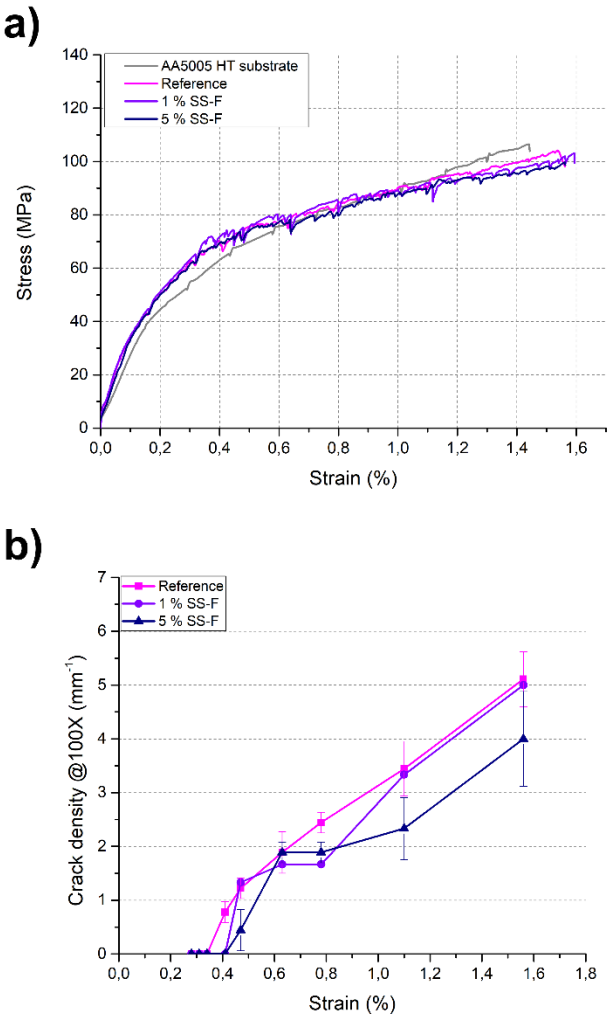


**Figure 5-37: Output results from four-point bending tests with Microtest 200 N Deben tensile tester: (a) stress-strain curves, (b) crack density evolution with increasing strain.**

The crack density evolution follows different trends for the three sample types. All the samples show an initial crack increase stage, that is delayed to higher strain values by the increase of filler concentration. After this initial stage, the reference and the composite samples behave differently: the reference formulation undergoes a linear increase of crack density, whereas the other samples show an intermediate plateau area, where no important variations in crack density are observed. This plateau area is observable in the range 0.5%- 0.8% strain and in the range 0.6%-1.0% for the 1 % SS-F and 5% SS-F samples, respectively. After this intermediate stage, the crack density starts to increase linearly again, but the 5% SS-F sample always shows a lower value of crack density.
A detailed view of the cross-sections after the 4-point bending test is shown in FIGURE 5-38**.** This figure better shows the propagation path of the transversal cracks and their interaction with the stainless-steel flakes and the pores. In the present testing configuration, the different crack density among the samples is more evident with respect to the three-point bending configuration.

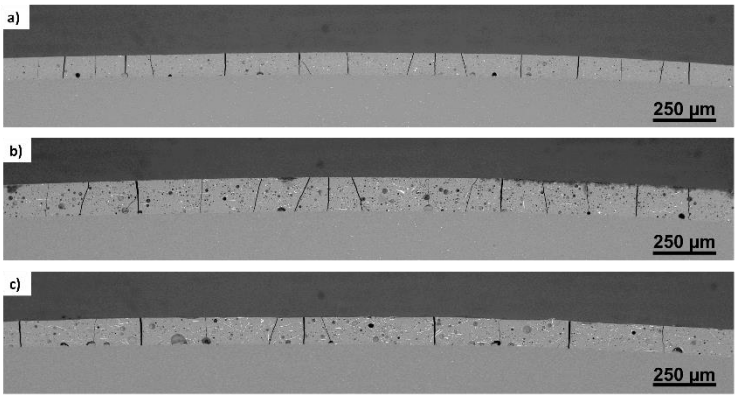


**Figure 5-38: Cross-sectional SEM images (250 µm marker, BSE) of the investigated samples tested in 4-point bending configuration after 1.00 mm extension: (a) reference, (( c) 5% SS-F**

### 5.3.9 Coatings mechanical characterization by in-situ AE analyses

The mechanical damaging of enamel coatings was monitored by AE during both three-point and four-point bending tests. This section will show the activity and the paramtric analysis for the samples taken under consideration.

#### *5.3.9.1 In-situ AE analyses in three-point and four-point bending*

TABLE 5-13 reports the activity and the parametric analysis for the samples taken under consideration.

**Table 5-13: Activity and parametric analysis for in-situ 3-point bending AE tests.**

| AE parameters | Samples | | | |
|---|---|---|---|---|
| **Sample** | **Metal HT** | **Reference** | **1% SS-F** | **5% SS-F** |
| 3PB Hits | 442 ± 310 | 2278 ± 327 | 4366 ± 227 | 5295 ± 952 |
| 4PB HIts | 36 ± 3 | 1157 ± 206 | 2584 ± 856 | 1796 ± 378 |
| 3PB Amplitude max. (dB) | 59 ± 6 | 99 ± 1 | 100 ± 0 | 100 ± 0 |
| 4PB Amplitude max. (dB) | 49 ± 1 | 92 ± 2 | 92 ± 1 | 87 ± 3 |
| 3PB Amplitude average (dB) | 41 ±1 | 48 ± 1 | 48 ± 1 | 48 ± 1 |
| 4PB Amplitude average (dB) | 42 ± 0 | 48 ± 1 | 48 ± 0 | 50 ± 1 |
| 3PB Energy max. (aJ) | $4.8 \times 10^3 \pm 5.1 \times 10^3$ | $6.1 \times 10^7 \pm 4.0 \times 10^7$ | $10.0 \times 10^7 \pm 7.2 \times 10^7$ | $6.1 \times 10^7 \pm 0.6 \times 10^7$ |
| 4PB Energy max. (aJ) | 196 ± 76 | $7.5 \times 10^6 \pm 2.0 \times 10^6$ | $6.8 \times 10^6 \pm 1.8 \times 10^6$ | $2.1 \times 10^6 \pm 1.3 \times 10^6$ |
| 3PB Energy average (aJ) | 37 ± 23 | $1.8 \times 10^5 \pm 0.8 \times 10^5$ | $1.3 \times 10^5 \pm 0.4 \times 10^5$ | $0.8 \times 10^5 \pm 0.4 \times 10^5$ |
| 4PB Energy average (aJ) | 29 ± 12 | $4.7 \times 10^4 \pm 1.8 \times 10^4$ | $3.0 \times 10^4 \pm 9.7 \times 10^4$ | $1.1 \times 10^4 \pm 1.3 \times 10^4$ |

The results are the average values of three tests on different samples. In all the two configurations it is evident that the substrate gives rise to a limited number of events with respect to the enameled samples, and the metal-related events have amplitude and energy really different with respect to the enamel samples. Considering the average amplitude of the substrate-related events it is possible to state that the events with amplitudes lower than 40 dB cannot be clearly linked to the enamel coating, as they are possibly due to the elastic-plastic deformation of the substrate and to friction events between the anvils and the metallic substrate.

The enamel samples produce an increase in the AE activity, and the values of the events amplitude and energy are really different with respect to the metal substrate. The presence of the stainless-steel flakes produces an increase in the AE activity of the sample, probably due to the many interaction phenomena between the flakes and the cracks that generate many distinct mechanical events.

As regards the maximum amplitude, two different behaviours can be noticed between the samples tested in three-point and four-point configurations. In the first case, all the samples experience transversal cracking, that gives origin to high amplitude/high energy events, and no relevant differences can be noticed among the different sample types. In the second case, a slight decrease in the maximum amplitude can be noticed for the 5% SS-F sample.
As regards the average amplitude, no differences can be noticed between the samples because this parameter is not sensitive to small changes as the large number of events easily level the average amplitude.
The energy maximum for the samples is quite similar for the same reasons explained before with the maximum amplitude, but interesting results can be observed as regards the energy average values. In this case, the presence of the stainless-steel flakes seems to reduce the average energy of the events, probably because the flakes are able to absorb part of the energy by plastic deformation and reduce the magnitude of the acoustic events. The difference among the samples is more evident in the case of the four-point bending configuration, as the flakes are able to absorb part of the energy in a more efficient way with respect to three-point bending test, where the load was concentrated in a small volume of the sample.

#### *5.3.9.2 In-situ AE analyses – representative examples*

This section will show some examples of the AE patterns of some representative samples for both the three-point and four-point bending configuration.

**Representative examples of samples tested in three-point bending**

FIGURE 5-39 shows the evolution of AE events during the three-point tests for four representative samples of the typologies taken under consideration.
The graphs report the number of cumulative events, the amplitude of the registered events together with stress-time curve. As it is possible to evidence from the amplitude scatter, there are some differences to be highlighted: the addition of 1% stainless-steel flakes leads to an apparent increase of the number of the events in the 55-65 dB region, and in the case of the 5 % SS-F sample to a concentration of the events in the 65-85 dB region as well. This concentration is particularly evident in the first 150 seconds of the test, that correspond to the area where plastic deformation of the substrate takes place as the first cracks develop in the coatings.

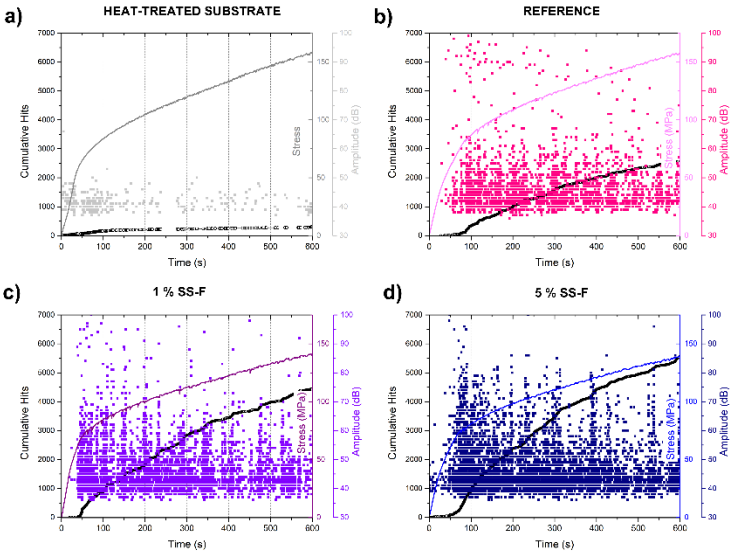


**Figure 5-39: AE activity/parametric overview of the samples tested in 3-point bending, (a) metal substrate, (b) reference, (c) 1% SS-F. (d) 5% SS-F.**

FIGURE 5-40 shows the evolution of the number of hits and energy average of the samples taken under consideration to better visualize the differences.

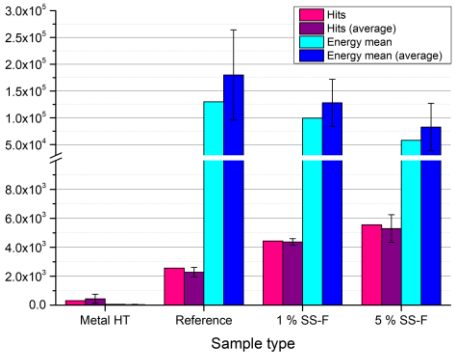


**Figure 5-40:Overview graph of the activity/parametric analysis of samples tested in 3-point bending setup. The average values are reported in Table 5-13, the other values are relative to the samples investigated in** Errore. L'origine riferimento non è stata trovata..

The reduction of the average energy of the AE events is not linear with the concentration of the stainless-steel flakes, as in the case of the 1 % SS-F and 5 % SS-F samples it is possible to notice a reduction of 24% and 55% of the involved average energy, respectively. The increase of the number of events is not linear as the increase for the 1% SS-F and 5% SS-F samples with respect to the reference sample are in the order of 73% and 116% respectively.
To have more insights it is possible to plot histograms of the amplitude of the events towards the number of events registered.

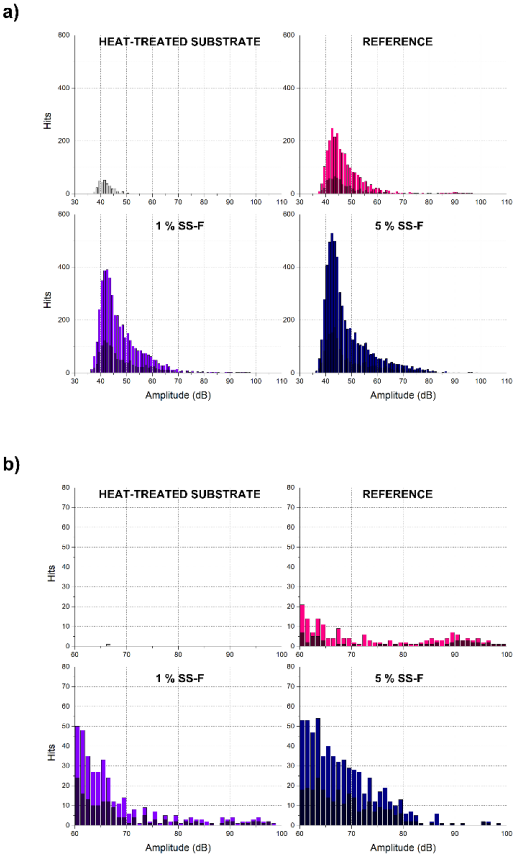


**Figure 5-41: Amplitude histogram of the AE test performed in 3-point bending configuration, (a) complete amplitude range, (b) 60-100 dB amplitude range. In gray are reported the events registered in the first 150 s of test.**

FIGURE 5-41A reports the amplitude histogram in all the tested interval (600s) and the histograms of the events registered in the first 150s of test (in grey superimposed). It is evident the number of the events increase with the concentration of flakes. FIGURE 5-41B shows the same graphs but in a more restricted amplitude range. It is possible to observe that the events in the 55-65 dB range increase with the stainless-steel flakes, but in the case of the 5% SS-F more events in the range 70-85 dB and less events in the 85-100 dB are observable.

**Representative examples of samples tested in four-point bending**

FIGURE 5-42 shows the evolution of AE events during the tests for four representative samples of the typologies taken under consideration.

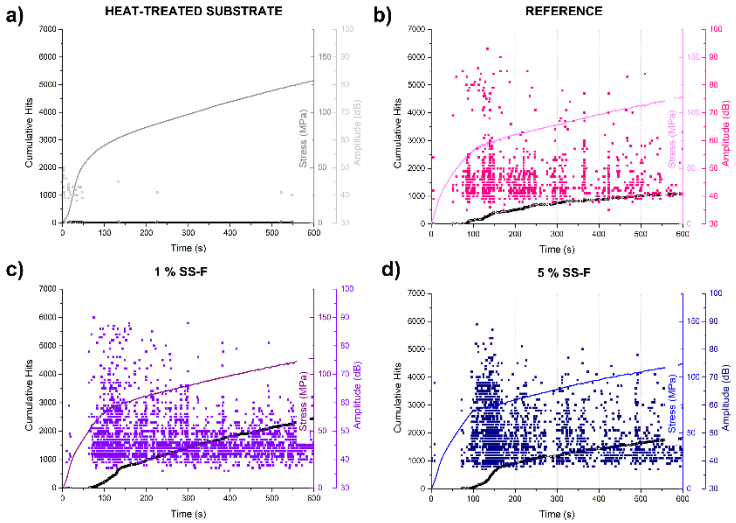


**Figure 5-42: AE activity/parametric overview of the samples tested in 4-point bending, (a) metal substrate, (b) reference, (c) 1% SS-F. d) 5% SS-F.**

The graphs report the number of cumulative events, the amplitude of the registered events together with stress-time curve. As it is possible to evidence from the amplitude scatter, there are some differences to be highlighted: the addition of 1% stainless-steel flakes leads to an apparent increase of the number of the events in the 55-65 dB region, and in the case of the 5 % SS-F sample to a concentration of the events in the 55-65 dB region and a reduction of events in the 70-100 dB region as well. All these differences are particularly evident in the first 170 seconds of the test, that correspond to the area where plastic deformation of the substrate takes place as the first cracks develop in the coatings.

FIGURE 5-43 shows the evolution of the number of hits and energy average of the samples taken under consideration to better visualize the differences.

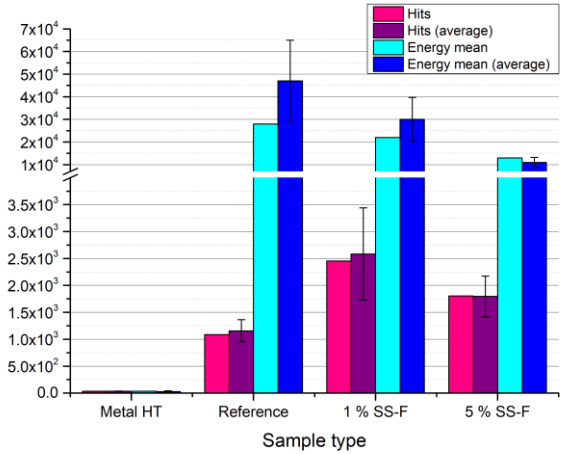


**Figure 5-43: Overview graph of the activity/parametric analysis of samples tested in 4-point bending setup. The average values are reported in** Errore. L'origine riferimento non è s tata trovata.**, the other values are relative to the samples investigated in** Errore. L'origine riferimento non è stata trovata..

The reduction of the average energy of the AE events is not linear with the concentration of the stainless-steel flakes, as in the case of the 1 % SS-F and 5 % SS-F samples it is possible to notice a reduction of 22% and 54% of the involved average energy, respectively. These values are comparable to the reduction values obtained during three-point tests. The trend for the number of events is not definite, but it is necessary to consider to high error bar of the 1% SS-F sample. Despite this fact, it is possible to state that in presence of 316L SS-Fs, the number of events is increased with respect of the reference sample.
To have more insights it is possible to plot histograms of the amplitude of the events towards the number of events registered.

a)

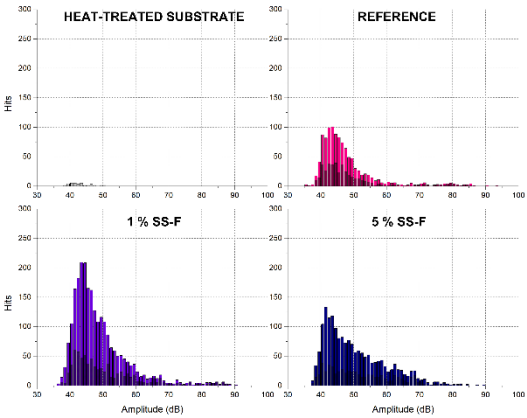


b)

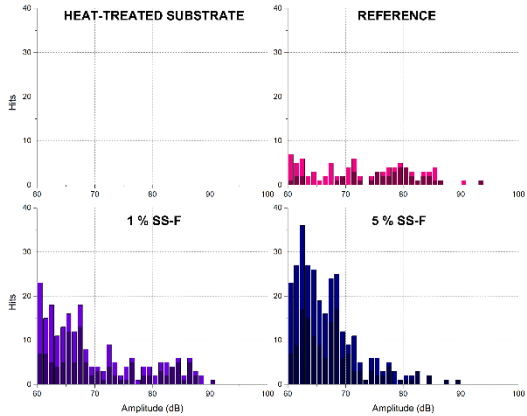


**Figure 5-44: Amplitude histogram of the AE test performed in 4-point bending configuration, (a) complete amplitude range, (b) 60-100 dB amplitude range. In gray the events registered in the first 170s of test.**

FIGURE 5-44A reports the amplitude histogram in all the tested interval (600s) and the histograms of the events registered in the first 170s of test (in grey superimposed). FIGURE 5-44B shows the same graphs but in a narrower amplitude range.

It is possible to observe that the events in the 55-65 dB range increase with the stainless-steel flakes, but in the case of the 5% SS-F few events are observable in the 80-100 dB range.

#### *5.3.9.3 In-situ AE analyses – cumulative energy analysis*

The cumulative number of AE represents the number of mechanical events that are generated during the test, but it does not give information about the magnitudes of these events, that are well represented by the AE energy involved. Thus, to quickly monitor the evolution of the damage in the enamel coatings is possible to consider the evolution of the cumulative energy with the testing time. Considering the trend of the cumulative energy it also possible to identify the time at which the registered events start to have a damaging effect on the coating, as relay on the amplitude only can let us make some errors as also small cracks or border effect can be noticed.

TABLE 5-14 reports the cumulative energy registered in all the tests, the cumulative energy after 150 s (thus just after the elastic-plastic limit of the substrate), and time moment in which the slope of the cumulative energy graph changes[352-354].

**Table 5-14: Cumulative energy analysis for the samples tested in three-point bending configuration.**

| | Samples | | | |
|---|---|---|---|---|
| **AE parameters** | **Metal HT** | **Reference** | **1% SS-F** | **5% SS-F** |
| **Cumulative energy (aJ) at 600 s** | $1.1 \times 10^4 \pm 5.6 \times 10^3$ | $4.9 \times 10^8 \pm 2.0 \times 10^8$ | $5.7 \times 10^8 \pm 2.2 \times 10^8$ | $4.0 \times 10^8 \pm 1.4 \times 10^8$ |
| **Cumulative energy (aJ) at 150s** | $0.9 \times 10^4 \pm 0.6 \times 10^4$ | $2.4 \times 10^8 \pm 0.8 \times 10^8$ | $2.9 \times 10^8 \pm 1.0 \times 10^8$ | $2.2 \times 10^8 \pm 0.6 \times 10^8$ |
| **Time for cumulative energy increase (s)** | - | 37 ± 7 | 33 ± 15 | 52 ± 3 |
| **Onset strain (%)** | - | 0.21 ± 0.04 | 0.19 ± 0.09 | 0.28 ± 0.01 |

The cumulative energy at the end and after 150 s of the test is similar for all the tested samples, but great differences can be noticed for the time threshold at which a great increase in the cumulative energy can be noticed. In particular, the sample with 5% flakes shows a delayed increase of the cumulative energy in time of about 40% with respect to the other samples.

TABLE 5-15 reports the cumulative energy registered in all the tests, the cumulative energy after 170 s (thus just after the elastic-plastic limit of the substrate), and time moment in which the cumulative energy starts to dramatically increase.

**Table 5-15: Cumulative energy analysis for the samples tested in four-point bending configuration.**

| | Samples | | | |
|---|---|---|---|---|
| **AE parameters** | **Metal HT** | **Reference** | **1% SS-F** | **5% SS-F** |
| **Cumulative energy (aJ) at 600 s** | $9.9 \times 10^2 \pm 3.0 \times 10^2$ | $5.7 \times 10^7 \pm 3.1 \times 10^7$ | $7.3 \times 10^7 \pm 1.6 \times 10^7$ | $1.8 \times 10^7 \pm 4.2 \times 10^6$ |
| **Cumulative energy (aJ) at 170s** | $8.4 \times 10^2 \pm 4.4 \times 10^2$ | $4.1 \times 10^7 \pm 2.1 \times 10^7$ | $5.1 \times 10^7 \pm 0.6 \times 10^7$ | $1.4 \times 10^7 \pm 0.5 \times 10^7$ |
| **Time for cumulative energy increase (s)** | - | 68 ± 8 | 80 ± 4 | 121 ± 11 |
| **Onset strain (%)** | - | 0.22 ± 0.03 | 0.25 ± 0.02 | 0.38 ± 0.04 |

Differently with respect to the three-point bending tests, the cumulative energy at the end and after 170 s of the test is decreased for the 5% SS-F sample (-69% and -66% after 170 s and 600 s, respectively), and the same difference can be noticed for the time threshold at which a great increase in the cumulative energy can be noticed. In particular, the sample with 5% flakes shows a delayed increase of the cumulative energy in time of about 78% with respect to the other samples.

#### *5.3.9.4 In-situ AE analyses – final considerations*

FIGURE 5-45 shows a brief overview of the main results obtained by this study.

As a first thing it is important to highlight the correlation between the onset strain during three-point and four-point bending tests together with the compressive residual stresses in the coatings. The onset strain levels are reported for both in-situ SEM analyses and AE tests.

As regards the failure strain (SEM) in 3-point bending tests, an increase of 12 % and 18 % with respect to the reference formulation is observed for the 1 % SS-F and 5 % SS-F formulations, respectively. Thus, it is possible to state that an increase of the metallic filler from 1 % to 5 % does not lead to a significant increase in the failure strain (+ 6%) with respect to the difference in filler concentration. The same trend can be observed in the case of 4-point bending tests with an increase of 22 % and 30 % with respect to the reference formulation for the 1 % SS-F and 5 % SS-F formulations, respectively

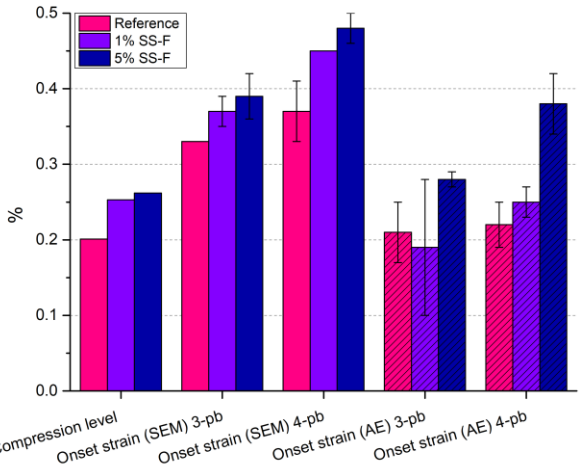


**Figure 5-45: Comparison graph between the compression level and the onset strain of the different samples under study.**

The effect of the metallic filler on the failure strain is more evident is the case of four-point bending tests. The non-linearity between the failure strain and the concentration of the metallic filler can be clearly correlated with the residual stress state of the coatings prior to testing. The compression state of the composite samples is 26% and 30% higher with respect to the reference for the 1% SS-F and 5% SS-F formulations, respectively. In particular, when the samples are tested in four-point bending configuration the difference in the strain at the first crack onset with respect to the reference is stricly related to the different level of compression stresses that is present in the sample, as the stress is distributed over a wider volume. The addition of stainless-steel flakes is then able to modify the thermal properties of the formulation, leading to the creation of different compressive states, that are the direct cause of the delayed strain at which the first damaging event (propagating crack can be noticed). The experimental assessment of the residual stresses is then useful to understand the cause of the different behaviour of the samples in terms of initialization of damage.

Thanks to in-situ scanning electron microscope observations, it is then possible to assess the strain value at which the damage of the coatings starts to occur, but it is also possible to evaluate the evolution of the crack density during the bending tests. The evolution of the crack density during three-point bending is similar for all the samples under investigation. The number of cracks increase in the same manner for all the samples until 0.7 % strain, where a differentiation among the three

formulations can be noticed. The reference and the 1 % SS-F formulations follow a similar trend and the crack density values are comparable; on the other side the crack density evolution of the 5 % SS-F is quite different and can be divided into three different regions: the region until 0.7 % strain where the behaviour is dominated by the crack multiplication stage, the region between 0.7 % and 1.1 % strain where a small plateau area can be noticed, and the region higher than 1.1 % strain where crack density starts increasing again. This behaviour is probably due to the effect of the stainless-steel flakes, that at relatively small strains are able to bridge the cracks and absorb part of the energy thus delaying the formation of new transversal cracks, but then the filler is no longer able to withstand the applied stress and the crack density starts to increase again. In the case of the four-point bending test it is possible to highlight further details with respect to the other testing configuration. The reference sample show a crack density increase in all the explored region with a decreased rate from 0.6 % strain, whereas the 1 % SS-F and 5 % SS-F samples shows three different regions: a first crack density increase, a plateau area where the crack density does not show a visible variation, and a third region where the crack density increases again. Thus, both the two samples containing the metallic filler are able to counteract the formation of cracks at intermediate strains (0.5 – 1.1 %) but a higher concentration of filler leads to a wider plateau region, which corresponds to a greater ability to counteract the propagation of cracks. In addition to that, after the plateau region, the 1 % SS-F sample returns to follow the trend of the reference sample, whereas the 5 % SS-F sample is still able to provide some limitations to the formation of new cracks. The four-point bending setup, where the bending moment is uniform in all the investigated volume, give us the possibility to better compare the behavior of the different samples. The main interaction mechanisms between the advancing cracks and the metallic fillers are crack deflection, crack bridging, and plastic deformation of the filler.

The exploitation of in-situ scanning electron microscope analyses is very time-demanding, whereas the use of the AE technique can provide valuable information on the studied systems by simple and quick measurements. In particular, it is possible to have insights into the onset strain, the energy of the events and the different type of mechanical events that are taking place during the testing of the coatings.

As a first thing, it was possible to notice an increased number of AE events with the higher concentration of metallic filler, probably due to the many interaction phenomena occurring between the flakes and the advancing cracks. As regards the amplitude of the AE events, it is possible to highlight that events with amplitudes lower than 50 dB are due to the deformation of the metallic substrates, as already reported by literature studies[355]. Events with high amplitudes (85-100 dB) can be linked to the formation of through-thickness cracks[355], and they decrease in number with the presence of the metallic filler, in a very pronounced way during 4-point bending tests. The assignation of events with intermediate amplitude values

can be made as follows: AE events with 55-65 dB amplitude can be attributed to the formation of discontinuous cracks, as they can be detected for all the tested formulations[316], whereas events with 70-85 dB amplitude can be attributed to the interaction phenomena between the flakes and the cracks, as their number increase with the concentration of the metallic filler.

As regards the energy of the events, the substrate-related events have a maximum energy of about $10^4$ aJ, as reported in literature studies, whereas coatings-related events have energy up to $10^8$ aJ and $10^6$ aJ for three-point and four-point bending configurations.

The energy-related parameters are more reliable to assess the evolution of damage, as they consider the magnitude of the events. In this context, it was possible to notice a reduction of the average and maximum AE energy with the increase in the filler concentration. In addition to that, it is possible to consider the evolution of cumulative energy and assess the onset strain, as a rapid increase in the cumulative energy indicates the formation of transversal cracks[354, 356]. In the present case, the onset strain of the 5% SS-F sample is 33% and 78% higher with respect to the reference sample for the three-point and four point bending configurations. Thus, the addition of the 5% SS flakes seems to be beneficial in delaying the initiation of catastrophic damaging (confirming data from the failure strain obtained by SEM in-situ analyses) and in reducing the energy involved in the damaging process. Thus, the presence of 5% SS-F seems to have a beneficial role in counteracting the nucleation and evolution of damage in particular when the stress is distributed over a wider volume of the sample.

By a quantitative point of view, both the in-situ SEM and AE analyses confirm that the damaging of the enamel coatings starts after the initialization of the plastic deformation of the substrate. On the other side, the AE technique is shown to have a higher sensibility, as the onset strains are shifted to lower values with respect to the ones obtained by SEM in-situ analyses, and the differences between the samples are greatly appreciable.

## *5.4 Conclusions and future perspectives*

The main aim of this study was to characterize the abrasion resistance and mechanical properties of composite enamel coatings admixed with 316L SS-Fs. The main conclusions of this study are the following:

- The metallic flakes are homogeneously distributed through the coating thickness, and they are tightly bonded to the enamel matrix. No microcracking or detachment at the enamel/flakes interface can be noticed. Despite this, a high concentration of filler leads to the formation of a rougher surface and to the development of bigger pores inside the coatings.

- The presence of the stainless-steel flakes has a negative influence on enamel's resistance to alkaline chemicals, although all the samples retain their protective properties towards the substrate also after 6 h of exposure to a hot (96 °C) $K_2P_4O_7$ solution.
- The presence of the stainless-steel flakes decreases the abrasive rate of vitreous enamel coatings. An increase in the concentration of the metal filler leads to a decrease of the sample's mass loss. The abrasive process mainly occurs in three different steps: i) initialization (0–1000 cycles), ii) localized abrasive process (1000–2500 cycles), iii) generalized abrasive process (from 3000 cycles). The three steps involve the formation of small cracks, brittle fracture events with material removal and roughness increase, and generalized damaging, respectively. The stainless-steel flakes exploit their abrasive-resistant action form 2500 cycles upwards. The metallic flakes experience plastic deformation due to the abrasive phenomena.
- It is possible to assess the mechanical properties of composite enamel coatings by means of different techniques. The IF method is useful for a quick quantitative assessment of the cracking resistance of enamel coatings, but the reliability of the results should be carefully considered. The bending test method is useful in discriminating the behaviour of the different samples at low strain values, and it gives valuable information on the damaging mechanisms. The scratch test method is particularly useful in assessing the behaviour of the composite coatings at high stress levels thanks to the observation of the scratch track morphological parameters.
- The presence of the stainless-steel flakes is able to limit the extent of cohesive damaging during scratch abrasion tests. The failure mechanisms do not change with respect to the different concentration of filler, and it resembles the typical failure process of brittle coatings deposited on more ductile substrates.
- The addition of 316L SS-Fs is useful to counteract the propagation of cracks in vitreous enamel coatings, in particular at intermediate strain levels (0.6-1.0%).
- The addition of different concentration of 316L flakes inside the enamel matrix modifies the thermal properties of the coatings and affects the residual compressive stresses at the end of the production process.
- In-situ SEM analyses are effective in highlighting the damaging mechanism and the interaction phenomena between the advancing cracks and the metallic filler. The main interaction phenomena are crack deflection, crack bridging, and filler plastic deformation and/or rupture.
- In-situ AE analyses are able to provide valuable information about type of damaging events, onset strain, and energy evolution. Thus, in-situ AE analyses can be considered as election technique to explore the

mechanical properties of composite enamel coatings thanks to their high sensitivity and ease of process.

Considering the positive results obtained in this study, it would be interesting to better investigate the effect of the metallic filler concentration on the mechanical properties of these composite enamel coatings. The development of multi-layer coatings, with a mechanical-resistant ground coat admixed with 316L SS-Fs and a chemical resistant cover coat could be an interesting product to be studied and developed, also at an industrial level.

# 6 Overall conclusive remarks and future perspectives

This work is an investigation into the abrasion resistance and mechanical properties of composite vitreous enamel coatings. The improvement of the abrasion resistance and cracking resistance of these brittle coatings is necessary to broaden the possible applications of enamelled components and find a possible solution to the main Achille's heel of these materials. Many recent studies have focused their attention on the development of abrasion resistant enamels by the addition of mill additives, hard ceramic particles, such as WC and SiC, or graphene-based filler s. Nevertheless, there are still several issues to consider, for example, the study of composite $Al_2O_3$/enamel coatings, the study of graphene/enamel composite coatings with improved graphene dispersion, and the assessment of the effect of metallic powders on the mechanical properties of these coatings. This work represents an attempt in the direction of exploring the effect of different types of fillers, with the aim to develop innovative enamel coatings with improved abrasion and cracking resistance. Moreover, this work also aims at investigating the behavior of composite enamel coatings by standardized testing methods coupled with in-situ techniques, to obtain novel insights into the failure mechanisms of these materials. In the first part, the effect of graphene-based fillers on the abrasion behavior of enamel coatings have been assessed by means of P.E.I. test. In the second part of the work, the effect of $Al_2O_3$ particles on the abrasion and chemical behaviour of composite enamel coatings was investigated, highlighting the effect of the particle's size on the functional properties of the coatings. In the third part of the thesis, the deposition, and the complete mechanical characterization of 316L SS-Fs/enamel composite coatings are investigated. The aim was to assess the role of the metallic filler on the abrasion and cracking behaviour of the enamel coatings, by exploiting both traditional and in-situ assessment methods.

## *6.1 Concluding remarks*

This thesis work has taken under consideration different composite enamel systems. In particular, three types of fillers were considered: graphene-based filler, as a lubricating agent, corundum particles, as HCPs, and 316L SS-Fs, as metallic filler.
The addition of graphene-based fillers inside the enamel matrix is quite complex, and great care should be devoted to ensuring the correct dispersion of graphene inside the matrix and avoid agglomeration phenomena. Despite this thesis shows the possibility to deposit graphene/enamel systems avoiding huge agglomeration phenomena, the effect of graphene on the abrasion resistance of enamel coatings is not so huge to make this filler interesting by an industrial point of view. Considering

the many drawbacks of graphene/enamel systems it is not worth it to make further investigations on this system.

The addition of HCPs inside the enamel matrix is a renowned possibility to improve the mechanical properties of these coatings. In the present case, the addition of corundum particles was proven to be effective in improving the abrasion resistance of the coatings, but the particle size has a great effect on the chemical resistance of these coatings. In particular the particle size do not alter the abrasion resistance of the coatings, but the smaller the particles, the lower is the resistance to aggressive atmospheres.

The addition of metallic fillers is a well-exploited system to improve the fracture toughness of brittle coatings. Thus, the effect of the SS-Fs on the functional properties and cracking resistance of the coatings was assessed. The steel flakes were able to improve the abrasion resistance of the coatings, but they caused a lower resistance to chemicals. The steel flakes resulted useful in improving the mechanical properties of the coatings as they were able to interact with the advancing cracks, increasing their propagation path or absorbing part of the energy by ductile deformation and rupture.

Considering the results obtained in this thesis, it is now clear that the combination of traditional and in-situ techniques can provide valuable information on the functional and mechanical properties of enamel coatings, giving the possibility to compare the efficacy of different type of fillers.

## *6.2 Future perspectives*

Conidering the results obtained, several directions of continuation of the research are open. Among the many options, the following themes are natural prosecution of the work carried out until now:

- The addition of corundum particles inside enamels is an effective way to improve the abrasion resistance of these coatings. A complete mechanical characterization of $Al_2O_3$/enamel systems should be made by means of traditional and in-situ techniques.
- A comparison study about the effect of different type of hard particles, including $Al_2O_3$, can be exploited to provide complete and comprehensive data about different composite enamel systems.
- The addition of 316L SS-Fs was demonstrated to have a positive effect on enamel's abrasion behaviour and mechanical properties. The optimization of the filler concentration should be investigated, and the optimization of the firing treatment/enamel composition are key problems to be addressed.

# 7 Appendix A – Scientific production

S. Rossi, F. Russo, N. Gasparre, V. Fontanari, "**Influence of graphene addition on the mechanical and surface properties of vitreous enamel coatings**", *Surface and Coatings Technology* 398 (2020) 126071.

S. Rossi, F. Russo, B. R. Lotfi, **"Study of the durability and aesthetical properties of powder coatings admixed with pearlescent pigments"**, *Coatings* 10 (2020) 229-243.

S. Rossi, F. Russo, A. M. Lemmi, M. Benedetti, V. Fontanari, **"Fatigue corrosion behavior of friction welded dissimilar joints in different testing conditions"**, *Metals* 10 (2020) 1-14.

S. Rossi, F. Russo, M. Calovi, "**Durability of vitreous enamel coatings and their resistance to abrasion, chemicals and corrosion: a review**", *Journal of Coatings Technology and Research (2021)* 39-51.

M. Calovi, F. Russo, S. Rossi, **"Synergic behavior of graphene-based filler and thermochromic pigments in cataphoretic coatings"**, *Progress in Organic Coatings* 150 (2021) 105978-105978.

M. Calovi, F. Russo, S. Rossi, **"Aesthetic performance of thermochormic pigments in cataphoretic and sprayed coatings for outdoor applications"**, *Journal of Applied Polymer Science* 138 (2021) 50622.1-50622.15.

S. Rossi, F. Russo, M. Calovi, M. del Rincon, D. Velez, **"The influence of the size of corundum particles on the properties of chemically resistant enamels",** *Ceramics International* 47 (2021) 11618-11627.

F. Russo, B. Furlan, M. Calovi, O. Massidda, S. Rossi, **" Silver-based vitreous enamel coatings: Assessment of their antimicrobial activity towards Escherichia coli and Staphylococcus aureus before and after surface degradation",** *Surface and Coatings Technology* 445 (2022) 12870201-12870211.

F. Russo, V. Fontanari, S. Rossi, "**Abrasion behavior and functional properties of composite vitreous enamel coatings fabricated with the addition of 316L stainless steel flakes",** *Ceramics International* 48 (2022) 23666-23677.

H. Rehman, F. Russo, M. Calovi, O. Massidda, S. Rossi **"Antimicrobial performance of innovative functionalized surfaces based on enamel coatings: the effect of silver-based additives on the antibacterial and antifungal activity"**, *Journal of Molecular Sciences* 24 (2023) 236401-236417.

F. Russo, V. Fontanari, E. Rustighi, M. Lekka, L. Hernandez, S. Rossi **"Composite vitreous enamel coatings with the addition of 316L stainless steel flakes: Novel insights on their behaviour under mechanical stresses"**, *Surface and Coatings Technology* 459 (2023) 129393.

M. Benedetti, M. Orempuller, F. Russo, V. Fontanari, S. Rossi **"Fatigue corrosion behavior of friction-welded stainless and carbon steel dissimilar joint"**, *Fatigue and Fracture of Engineering Materials & Structures* 46 (2023) 555-573.

# 8 Appendix B – Participation to congresses and schools

F. Russo, M. Calovi, S. Rossi, "**Comportamento sinergico di pigmenti termocromici e filler a base grafene in rivestimenti cataforetici'',** XIV Giornate Nazionali Corrosione e Protezione 2021; 29 June – 2 July 2021, Torino (IT)

F. Russo, V. Fontanari, S. Rossi, **"The influence of stainless-steel flakes on the protection and cracking resistance of vitreous enamel coatings",** ECASIA Congress 2022; 29 May – 3 June 2022, Limerick (IR)

F. Russo, E. Rustighi, V. Fontanari, S. Rossi, "**In-situ monitoring of the damage evolution of composite vitreous enamel coatings using the acoustic emission technique**", 51esimo Convegno AIAS; 7-9 September 2022, Padova (IT)

# 9 List of abbreviations

AE……Acoustic Emission
BED……Back-scattered Electrons Detector
CA……...Contact Angle
CMC……..Ceramic Matrix Material
CNB……..Chevron Notched Beam
CTE……...Coefficient of Thermal Expansion
EIS……Electrochemical Impedance Spectroscopy
GCC……Glass-Ceramic Coating
GNP……Graphene NanoPlatelets
GO……..Graphene Oxide
GU……Gloss Units
HCP……..Hard Ceramic Particle
HT……Heat Treated
IF……..Indentation Fracture
LVSED……Low Vacuum Secondary Electron Detector
NDT&E……..Non-Destructive Testing and Evaluation
P.E.I……...Porcelain Enamel Institute
PCI……Probability of Crack Initation
RTU……Ready-To-Use
SEM……...Scanning Electron Microscope
SENB……..Single Edge Notched Beam
SEVNB……...Single Edge V-Notched Beam
SS-F……Stainless Steel Flake

# 10 List of Figures

# 11 List of Tables

# 12 References


[1] F. Russo, S. Rossi, A.M. Compagnoni, *Porcelain enamel coatings*, Encyclopedia, 1 (**2021**) 388-400.

[2] G. Shippy, *Reclamation of scarp frit*, in: W.D. Smothers (Ed.) *Proceedings of the 41st Porcelain Enamel Technical Forum: Ceramic Engineering and Science Proceedings*, John Wiley & Sons**1980**.

[3] D. Tulyaganov, F. Baino, *Silicate glasses and glass–ceramics: types, role of composition and processing methods*, in: F. Baino, M. Tomalino, D. Tulyaganov (Eds.) *Ceramics, Glass and Glass-Ceramics: From Early Manufacturing Steps Towards Modern Frontiers*, Springer International Publishing, Cham, Switerzland, **2021**, pp. 119-152.

[4] D.R. Goetchius, *Porcelain enamel as a protective coating for hot-water tanks*, Journal of the American Ceramic Society, 25 (**1942**) 164-168.

[5] S. Rossi, F. Russo, M. Calovi, *Durability of vitreous enamel coatings and their resistance to abrasion, chemicals, and corrosion: a review*, Journal of Coatings Technology and Research, 18 (**2021**) 39-52.

[6] E. Scrinzi, S. Rossi, *The aesthetic and functional properties of enamel coatings on steel*, Materials & Design, 31 (**2010**) 4138-4146.

[7] W.M. Carty, U. Senapati, *Porcelain— raw materials, processing, phase evolution, and mechanical behavior*, Journal of the American Ceramic Society, 81 (**1998**) 3-20.

[8] H.H. Clark, *A new type of gas-fired vitreous enameling furnace*, Journal of the American Ceramic Society, 5 (**1922**) 478-487.

[9] C. Schwier, *An electric furnace for vitreous enameling*, Journal of the American Ceramic Society, 6 (**1923**) 1030-1039.

[10] E.P. Poste, *The fineness distribution of vitreous enamel as affected by variations in grinding*, Journal of the American Ceramic Society, 18 (**1935**) 303-305.

[11] C.S. Clark, K.G. Rampal, V. Thuppil, S.M. Roda, P. Succop, W. Menrath, C.K. Chen, E.O. Adebamowo, O.A. Agbede, M.K.C. Sridhar, C.A. Adebamowo, Y. Zakaria, A. El-Safty, R.M. Shinde, J. Yu, *Lead levels in new enamel household paints from Asia, Africa and South America*, Environmental Research, 109 (**2009**) 930-936.

[12] M. Kokkori, F. Casadio, K. Sutherland, M. Vermeulen, *Charting the development of oil-based enamel paints through the correlation of historical paint technology manuals with scientific analysis*, in: K.J. Van den Berg, A. Burnstock, M. De Keijzer, J. Krueger, T. Learner, d.A. Tagle, G. Heydenreich (Eds.) *Issues in Contemporary Oil Paint*, Springer International Publishing, Cham, Switerzland, **2014**, pp. 117-125.

[13] H.H. Al-Kayiem, A.A. Ismaeel, A.T. Baheta, M.A. Aurybi, *Performance enhancement of solar vortex power generator by $Al_2O_3$-in-black paint coating*, Journal of Cleaner Production, 316 (**2021**) 128303.

[14] *UNI 8762 "Smalti porcellanati – definzione e classificazione"*, Ente Nazionale Italiano di Certificazione, Milano, Italy, **2010**.

[15] *ASTM C286-99 "Standard terminology relating to porcelain enamel and ceramic-metal systems"*, ASTM International, West Conshohocken, PA, US, **2004**.

[16] W.H. Rogers, *On the history of enamelling*, Journal of the British Archaeological Association, 3 (**1848**) 280-296.
[17] R.L. Cook, A.I. Andrews, *Chemical durability of porcelain enamels*, Journal of the American Ceramic Society, 28 (**1945**) 229-256.
[18] W.J. Baldwin, *Color stability in enamels*, Journal of the American Ceramic Society, 18 (**1935**) 321-322.
[19] C.F. Binns, M. Klem, H. Mott, *An experiment in Egyptian blue glaze*, Journal of the American Ceramic Society, 15 (**1932**) 271-271.
[20] K.C. Kiefer, A. Allibert, *Pharaonic blue ceramics: the process of self-glazing*, Archaeology, 24 (**1971**) 107-117.
[21] M.S. Tite, M. Bimson, *An investigation of the microstructures associated with the different methods of glazing*, Archaeometry, 28 (**1986**) 69-78.
[22] M.S. Tite, I.C. Freestone, *Egyptian faience: an investigation of the methods of production*, Archaeometry, 25 (**1983**) 17-27.
[23] M.U. Tomalino, D. Tulyaganov, *The historical development of porcelain and glass*, in: F. Baino, M. Tomalino, D. Tulyaganov (Eds.) *Ceramics, Glass and Glass-Ceramics: From Early Manufacturing Steps Towards Modern Frontiers*, Springer International Publishing, Cham, Switerzland, **2021**, pp. 1-46.
[24] H. Tait, *Enamelwork - history*, Encyclopedia Britannica, **2016**.
[25] *The history of the enamelling technique*, Design, 58 (**1957**) 158-162.
[26] J.E. Curtis, M. Kruszynski, *Ancient caucasian and related material in the British Museum*, British Museum Occasional Paper, The British Museum, London, UK, **2002**.
[27] J.D. Von Bothmer, C.A. Picòn, J.R. Mertens, E.J. Milleker, A. Hermann, *Recent acquisitions: a selection 1994-1995*, Bulletin of the Metropolitan Museum of Art, The Metropolitan Museum of Art, New York, US, **1995**.
[28] J.D. Bateson, R.E.M. Hedges, *The scientific analysis of a group of Roman Age enamelled brooches*, Archaeometry, 17 (**1975**) 177-190.
[29] M.J. Hughes, *A technical study of opaque red glass of the Iron Age in Britain*, Proceedings of the Prehistoric Society, 38 (**1972**) 98-107.
[30] F. McIntosh, *A study into Romano-British enamelling - with a particular focus on brooches*, The School of Historical Studies Postgraduate Forum E-Journal Edition, 7 (**2009**) 1-18.
[31] J. Romero-Pastor, J.V. Navarro, M. Del Egido, M. Ortega-Huertas, *A nondestructive methodology for the study of colored enamels: insights into manufacturing and weathering processes*, Journal of the American Ceramic Society, 96 (**2013**) 2132-2140.
[32] A.H. Glenn, *Porcelain enamels: past, present and future*, Analyst, 11 (**1955**) 85-87.
[33] D. Buckton, J. Osborne, *The enamel of Doge Ordelaffo Falier on the Pala d'Oro in Venice*, Gesta, 39 (**2000**) 43-49.
[34] B. De Chancel, B. Drake Boehm, B. Barrièr, E. Taburet, I. Biron, J. Bequet, M.M. Gauthier, M.T. Wypyski, M. Pastoreau, P. Dandrige, *Enamels of Limoges 1110-1350*, The Metropolitan Museum of Art, New York, US, **1996**.
[35] R. Smith, J.H. Carlson, R.M. Newman, *An investigation into the deterioration of painted Limoges enamel plaques c. 1470–530*, Studies in Conservation, 32 (**1987**) 102-113.

[36] T. Drayman-Weisser, *The early painted enamels of Limoges in the Walters Art Museum: historical context and observations on past treatments*, Journal of the American Institute for Conservation, 42 (**2003**) 279-312.
[37] V.K. Ostoia, *A late mediaeval plique-à-jour enamel*, The Metropolitan Museum of Art Bulletin, 4 (**1945**) 78-80.
[38] C. Machado, A. Machado, T. Palomar, M. Vilarigues, *Grisaille in historical written sources*, Journal of Glass Studies, 61 (**2019**) 71-86.
[39] H. Ditrich, *SEM-EDS micro-analytical data from enamel samples of Cellini's salt cellar "Saliera"*, Practical Metallography, 47 (**2010**) 259-261.
[40] E.S. Dawes, *Some early experiences in enameling cast iron*, Journal of the American Ceramic Society, 6 (**1923**) 234-237.
[41] A.I. Andrews, S. Pagliuca, *Porcelain vitreous enamels and industrial enamelling processes*, third ed., International Enamellers Institute and Porcelain Enamel Institute, Mantova, Italy, **2011**.
[42] C.A.W. Vollrath, *Early history of enamelling in the Vollrath company*, Journal of the American Ceramic Society, 6 (**1923**) 237-240.
[43] H.L. Cook, *Observations upon the effect of various electrolytes when added to enamel suspensions made with and without clay*, Journal of the American Ceramic Society, 10 (**1927**) 344-346.
[44] H.F. Staley, *Developments in enameling technology during the past twenty-five years*, Journal of the American Ceramic Society, 6 (**1923**) 240-244.
[45] B.W. King Jr., A.I. Andrews, *Reactions taking place during smelting of superopaque antimony enamels*, Journal of the American Ceramic Society, 23 (**1940**) 225-228.
[46] K. Kopplin, *Evolution of cookstove designs and manufacturing techniques*, in: W.D. Faust (Ed.) *Proceedings of the 62nd Porcelain Enamel Institute Technical Forum: Ceramic Engineering and Science Proceedings***2000**.
[47] R.D. Landrum, L. Frost, *Titanium enamels*, Journal of the American Ceramic Society, 3 (**1920**) 316-321.
[48] R.J. Jesseman, D.L. Bowley, *Effect of steel thickness on direct-on cover coat enamel adherence rating*, in: W.J. Smothers (Ed.) *Proceedings of the 48th Porcelain Enamel Technical Forum: Ceramic Engineering and Science Proceedings*, John Wiley & Sons**1987**.
[49] R.J. Jesseman, D.L. Bowley, *Effect of different steels on adherence of porcelain enamel applied electrostatically*, in: W.J. Smothers (Ed.) *Proceedings of the 48th Porcelain Enamel Technical Forum: Ceramic Engineering and Science Proceedings*, John Wiley & Sons**1987**.
[50] W. Buckley, M. Horton, *Plant experiences with porcelain enamel powder - a panel presentation*, in: J.B. Wachtman Jr. (Ed.) *Proceedings of the 48th Porcelain Enamel Technical Forum: Ceramic Engineering and Science Proceedings*, John Wiley & Sons**1988**.
[51] J.F. Zeiss, *New concepts in powder systems*, in: W.D. Smothers (Ed.) *Proceedings of the 41th Porcelain Enamel Technical Forum: Ceramic Engineering and Science Proceedings*, John Wiley & Sons**1980**.
[52] J.F. Wright, J. White, *Pickle-free production experiences worldwide*, in: W.J. Smothers (Ed.) *Proceedings of the 47th Porcelain Enamel Technical Forum: Ceramic Engineering and Science Proceedings*, John Wiley & Sons**1986**.

[53] N.M. Sedalia, F.J. Williams, D.H. Luehrs, *Production experiences with pickle-free systems for wet process operations - a panel discussion*, in: W.J. Smothers (Ed.) *Proceedings of the 48th Porcelain Enamel Technical Forum: Ceramic Engineering and Science Proceedings*, John Wiley & Sons**1987**.
[54] J.P. Hingsbergen, *Influences of steel on pickle-free systems*, in: J.B. Wachtman Jr. (Ed.) *Proceedings of the 48th Porcelain Enamel Technical Forum: Ceramic Engineering and Science Proceedings*, John Wiley & Sons**1988**.
[55] S. Rossi, E. Scrinzi, A.M. Compagnoni, A. Gallucci, Y. Gjata, *Enamel and design. The potential of enamelled materials*, Fausto Lupetti Editore, Bologna, Italy, **2011**.
[56] J. Jozefowski, *Frit making*, in: J.B. Watchman (Ed.) *Proceedings of the 49th Porcelain Enamel Technical Forum: Ceramic Engineering and Science Proceedings*, John Wiley & Sons**1988**.
[57] F.N. Francioli, *The raw materials outlook*, in: W.J. Smothers (Ed.) *Proceedings of the 46th Porcelain Enamel Technical Forum: Ceramic Engineering and Science Proceedings*, John Wiley & Sons**1985**.
[58] S. Rossi, C. Zanella, R. Sommerhuber, *Influence of mill additives on vitreous enamel properties*, Materials & Design, 55 (**2014**) 880-887.
[59] L.R. Hall, *Availability of frit raw materials*, in: W.J. Smothers (Ed.) *Proceedings of the 41th Porcelain Enamel Technical Forum: Ceramic Engineering and Science Proceedings*, John Wiley & Sons**1980**.
[60] L.R. Kirk, *Function and action of opacifiers*, Journal of the American Ceramic Society, 15 (**1932**) 226-226.
[61] C. Jacobs, W.J. Baldwin, *Effects of zirconium-type opacifiers on properties of glazes*, Journal of the American Ceramic Society, 37 (**1954**) 258-266.
[62] A.I. Andrews, R.W. Gates, *Solubility of a zirconium oxide opacifier in enamel glass*, Journal of the American Ceramic Society, 23 (**1940**) 288-290.
[63] W.A. Joseph, *Matte surfaces - uses, problems, solutions*, in: W.J. Smothers (Ed.) *Proceedings of the 45th Porcelain Enamel Technical Forum: Ceramic Engineering and Science Proceedings*, John Wiley & Sons**1984**.
[64] D. Balmer, *Pigments and the environment*, in: W.J. Smothers (Ed.) *Proceedings of the 50th Porcelain Enamel Technical Forum: Ceramic Engineering and Science Proceedings*, John Wiley & Sons**1989**.
[65] C.H. Zwermann, A.I. Andrews, *Relation of particle size and charcateristics of light reflected from porcelain enamel surfaces*, Journal of the American Ceramic Society, 23 (**1940**) 93-102.
[66] R.A. Eppler, *Inverse spinel pigments*, Journal of the American Ceramic Society, 66 (**1983**) 794-801.
[67] A.J. Eroles, A.L. Friedberg, *Color and structural character of CdS-CdSe pigments*, Journal of the American Ceramic Society, 48 (**1965**) 223-227.
[68] A.I. Andrews, C.H. Zwermann, *Fundamentals of color in porcelain enamels*, Journal of the American Ceramic Society, 22 (**1939**) 65-72.
[69] D. Balmer, *Focus on porcelain enamel pigments: are they hazardous?*, in: W.J. Smothers (Ed.) *Proceedings of the 45th Porcelain Enamel Technical Forum: Ceramic Engineering and Science Proceedings*, John Wiley & Sons**1984**.
[70] A.M. Lynch, *Role of cobalt oxide in porcelain enamel*, in: J.B. Wachtman Jr. (Ed.) *Proceedings of the 54th Porcelain Enamel Technical Forum: Ceramic Engineering and Science Proceedings*, John Wiley & Sons**1993**.

[71] E.E. Marbaker, H.S. Saunders, L.N. Baumer, *Effects of some electrolytes on color value of enamels made from a standard titania-opacified frit*, Journal of the American Ceramic Society, 32 (**1949**) 297-304.
[72] O. Kazmina, V. Borovoy, V. Semenova, *White vitreous enamel for ferrous metals with preliminary thermal activation of frit*, Ceramics International, 47 (**2021**) 28471-28478.
[73] E.E. Howe, R.L. Fellows, *Effect of manganese, nickel, and cobalt oxide upon the adherence and reboiling properties of a groud-coat enamel*, Journal of the American Ceramic Society, 20 (**1937**) 319-324.
[74] K. Kautz, *Observations on the function of adherence-promoting oxides in ground-coat enamels*, Journal of the American Ceramic Society, 22 (**1939**) 250-255.
[75] D.H. Luehrs, *Pickle-free ground coat production experience*, in: W.D. Smothers (Ed.) *Proceedings of the 43rd Porcelain Enamel Technical Forum: Ceramic Engineering and Science Proceedings*, John Wiley & Sons**1982**.
[76] A.L. Friedberg, F.A. Petersen, *Systematic study of simple titania-bearing porcelain enamels*, Journal of the American Ceramic Society, 33 (**1950**) 17-24.
[77] R.F. Patrick, *Some factors affecting the opacity, color, and color stability of titania-opacified enamels*, Journal of the American Ceramic Society, 34 (**1951**) 96-102.
[78] C.J. Kinzie, J.A. Plunkett, *Titanium compounds and application thereof in vitreous enamels*, Journal of the American Ceramic Society, 18 (**1935**) 117-122.
[79] A.L. Friedberg, R.B. Fischer, F.A. Petersenr, *Effect of size and shape of titanium oxide crystals on spectrophotometric properties of titanium-bearing porcelain* Journal of the American Ceramic Society, 31 (**1948**) 246-253.
[80] L.N. Biller, *Porcelain enamel powders for pyrolitic oven and acid -resistant applications*, in: W.J. Smothers (Ed.) *Proceedings of the 47th Porcelain Enamel Technical Forum: Ceramic Engineering and Science Proceedings*, John Wiley & Sons**1986**.
[81] A.E. Farr, *Developments in chemical resistant/pyrolitic pickle-free systems*, in: W.J. Smothers (Ed.) *Proceedings of the 47th Porcelain Enamel Technical Forum: Ceramic Engineering and Science Proceedings*, John Wiley & Sons**1986**.
[82] S. Rossi, L. Bergamo, M. Calovi, V. Fontanari, *Effect of enamel coatings on the mechanical properties of aluminium foams*, Mechanics of Advanced Materials and Structures, 26 (**2019**) 1130-1139.
[83] S. Rossi, L. Bergamo, V. Fontanari, *Fire resistance and mechanical properties of enamelled aluminium foam*, Materials & Design, 132 (**2017**) 129-137.
[84] P.R. Lee, *Latest in aluminium enamels*, in: J.B. Watchman (Ed.) *Proceedings of the 50th Porcelain Enamel Technical Forum: Ceramic Engineering and Science Proceedings*, John Wiley & Sons**1989**.
[85] A. Compagnoni, *Reduction or elimination of vanadium in enamel for aluminium*, *Proceedings of the XXI International Enamellers Congress***2008**, pp. 18-22.
[86] M.E. Manson, *Sodium silicate, a new enamel raw material*, Journal of the American Ceramic Society, 14 (**1931**) 490-494.
[87] A. Umbertazzi, N. Wojciechowski, *Smalto porcellanato - la forma della materia*, Hoepli, Milano, Italy, **2002**.
[88] B.W. King Jr., A.I. Andrews, *Identity and amounts of fluoride crystals present in enamels*, Journal of the American Ceramic Society, 22 (**1939**) 123-133.

[89] A.I. Andrews, E.E. Howe, *The effect of fluorides on the properties of white sheet-iron enamels*, Journal of the American Ceramic Society, 17 (**1934**) 288-291.
[90] D.L. Voges, *Porcelain enamel: properties and applications*, in: J.B. Watchman (Ed.) *Proceedings of the 58th Porcelain Enamel Technical Forum: Ceramic Engineering and Science ProceedingsS*, John Wiley & Sons**1996**.
[91] R.L. Fellows, J.L. McLaughlin, *Study of milling and its effect on properties of porcelain enamel slips*, Journal of the American Ceramic Society, 22 (**1939**) 260-264.
[92] W.O. Fuller, *Milling practices and parameters*, in: J.B. Watchman (Ed.) *Proceedings of the 52nd Porcelain Enamel Technical Forum: Ceramic Engineering and Science Proceedings*, John Wiley & Sons**1991**.
[93] F.R. Porter, H.H. Holscher, *The use of finely milled enamels*, Journal of the American Ceramic Society, 18 (**1935**) 39-42.
[94] E.E. Marbaker, H.S. Saunders, L.N. Baumer, *Effects of various clays used in mill additions on properties of a titania-opacified enamel*, Journal of the American Ceramic Society, 31 (**1948**) 260-267.
[95] M.E. Manson, *The use of bentonite for suspending enamels*, Journal of the American Ceramic Society, 6 (**1923**) 790-793.
[96] C.J. Harbert, J.W. Iliff, *Uverite - a mill addition opacifier for porcelain enamel*, Journal of the American Ceramic Society, 29 (**1946**) 93-98.
[97] M.K. Blanchard, A.I. Andrews, *Fundamental properties of soluble salts in enamel mill liquors*, Journal of the American Ceramic Society, 27 (**1944**) 17-24.
[98] M. Dignatici, A. Chavez-Valdez, F. Andreola, C. Siligardi, A.R. Boccaccini, *Effect of additives on the dispersion and electrophoretic deposition of highly diluted enamel suspensions*, International Ceramic Review, 64 (**2015**) 45-48.
[99] W.N. Harrison, *Vitreous enamel slips and their control*, Journal of the American Ceramic Society, 10 (**1927**) 970-994.
[100] G.F. Elliott, *Current practices in enamelling cast iron by the wet-process method*, in: W.D. Smothers (Ed.) *Proceedings of the 44th Porcelain Enamel Technical Forum: Ceramic Engineering and Science Proceedings*, John Wiley & Sons**1983**.
[101] *EN 10209 "Cold rolled low carbon steel flat products for vitreous enamelling - technical delivery conditions"*, European Committee for Standardization, Bruxelles, Belgium, **2013**.
[102] D.A. Todd, *Properties and enamelling characteristics of sheet steels for porcelain enamelling*, in: W.D. Smothers (Ed.) *Proceedings of the 42nd Porcelain Enamel Technical Forum: Ceramic Engineering and Science Proceedings*, John Wiley & Sons**1981**.
[103] X. Huang, Z. Zhang, X. Liu, Y. Zhao, X. Li, *Variations of microstructure and resistance to fish-scaling of a hot rolled enamel steel before and after enamel firing*, Journal of Materials Research and Technology, 11 (**2021**) 466-473.
[104] Y.T. Lin, L.J. Chiang, Y.C. Lin, H.W. Yen, *New approaches in understanding the effects of hydrogen trapping and the fishscaling resistance of enameled steels*, Surface and Coatings Technology, 399 (**2020**) 126135.
[105] L.L. Steele, *Enamelability of cold-rolled aluminium-killed steels*, in: W.D. Smothers (Ed.) *Proceedings of the 43rd Porcelain Enamel Technical Forum: Ceramic Engineering and Science Proceedings*, John Wiley & Sons**1982**.

[106] S. Rossi, F. Russo, N. Gasparre, V. Fontanari, *Influence of graphene addition on the mechanical and surface properties of vitreous enamel coatings*, Surface & Coatings Technology, 398 (**2020**) 126071.
[107] M. Bukovec, K. Xhanari, M. Finšgar, *Development and analysis of frits for enamelling AA2024, AA6082 and AA7075 aluminium alloys*, Materials and Corrosion, 72 (**2021**) 660-671.
[108] M. Chen, M. Shen, X. Wang, S. Zhu, F. Wang, *Interfacial reaction between $SiO_2$–$Al_2O_3$–ZnO–CaO based glass coatings and K38G superalloy substrates*, Surface and Coatings Technology, 216 (**2013**) 145-151.
[109] M. Wu, M. Chen, S. Zhu, F. Wang, *Protection mechanism of enamel–alumina composite coatings on a Cr-rich nickel-based superalloy against high-temperature oxidation*, Surface and Coatings Technology, 285 (**2016**) 57-67.
[110] J.D. Bennet, *Cold cleaning prior to porcelain enamelling*, in: W.D. Smothers (Ed.) *Proceedings of the 41st Porcelain Enamel Technical Forum: Ceramic Engineering and Science Proceedings*, John Wiley & Sons**1980**.
[111] D. Song, R. Tang, F. Yang, Y. Qiao, J. Sun, J. Jiang, A. Ma, *Development of high-performance enamel coating on grey iron by low-temperature sintering*, Materials, 11 (**2018**) 2183.
[112] A.A. Zaitsev, V.S. Mogil'chenko, *Improving the enamelling properties and quality of cast iron equipment*, Glass and Ceramics, 25 (**1968**) 93-96.
[113] E.P. Poste, *The blistering of cast iron enamel*, Journal of the American Ceramic Society, 16 (**1933**) 277-292.
[114] R.R. Danielson, *The cleaning of sheet steel and iron for enamelling purposes*, Journal of the American Ceramic Society, 2 (**1919**) 883-894.
[115] W. McClure, *Cost-effectiveness of detergent concentrates for metal preparation*, in: W.D. Smothers (Ed.) *Proceedings of the 44th Porcelain Enamel Technical Forum: Ceramic Engineering and Science Proceedings*, John Wiley & Sons**1983**.
[116] G.D. Kent, *Basics of cleaning*, in: W.D. Smothers (Ed.) *Proceedings of the 48th Porcelain Enamel Technical Forum: Ceramic Engineering and Science Proceedings*, John Wiley & Sons**1983**.
[117] D.R. Sauder, *Use of a no-nickel, no-pickle system for application of porcelain-enamel powder*, in: W.D. Smothers (Ed.) *Proceedings of the 43rd Porcelain Enamel Technical Forum: Ceramic Engineering and Science Proceedings*, John Wiley & Sons**1982**.
[118] R.R. Fusselbaugh, B.T. Sweely, *A method of control of enamel for dipping flat ware*, Journal of the American Ceramic Society, 8 (**1925**) 303-306.
[119] R.J. Whitesell, *Effect of some electrolytes on the consistency of a dipping enamel*, Journal of the American Ceramic Society, 22 (**1939**) 265-270.
[120] J.E. Sams, W. McGohan, J.J. Canfield, *Factors affecting sagging tests on enameling iron*, Journal of the American Ceramic Society, 24 (**1941**) 137-140.
[121] H.-J. Thiele, *Boiler/water heater inside coating with wet enamel*, in: W.D. Faust (Ed.) *Proceedings of the 66th Porcelain Enamel Institute Technical Forum: Ceramic Engineering and Science Proceedings***2004**, pp. 79-91.
[122] C.J. Labant, C.L. Hackler, *Differences and comparisons of wet and powder porcelain enamel covercoats*, in: J.B. Watchman (Ed.) *Proceedings of the 50th Porcelain Enamel Technical Forum: Ceramic Engineering and Science Proceedings*, John Wiley & Sons**1989**.

[123] R. Fleischmann, W. Schaper, R. Schünemann, *Some aspects of the electrophoretic enamel deposition*, Electrochimica Acta, 29 (**1984**) 77-80.
[124] H.W. Hoffmann, T.L. Stalter, *Electrodeposition: status and outlook*, in: W.D. Smothers (Ed.) *Proceedings of the 41st Porcelain Enamel Technical Forum: Ceramic Engineering and Science Proceedings*, John Wiley & Sons**1980**.
[125] J.A. Olenick, W. Joseph, *Electrophoretic enamelling – an area of steady advancement*, in: W.D. Smothers (Ed.) *Proceedings of the 43rd Porcelain Enamel Technical Forum: Ceramic Engineering and Science Proceedings*, John Wiley & Sons**1982**.
[126] S. Rossi, E. Scrinzi, *Evaluation of the abrasion resistance of enamel coatings*, Chemical Engineering and Processing-Process Intensification, 68 (**2013**) 74-80.
[127] R.P. Corbett, B. Makin, *Electrostatic application of vitreous enamel in dry powder form*, Transactions of the IMF, 51 (**1973**) 160-164.
[128] J.B. Willis, *Electrostatic spraying of porcelain enamels*, Journal of the American Ceramic Society, 28 (**1945**) 121-133.
[129] R.G. Rion, *Alternatives for handling porcelain enamel solid wastes*, in: W.D. Smothers (Ed.) *Proceedings of the 41st Porcelain Enamel Technical Forum: Ceramic Engineering and Science Proceedings*, John Wiley & Sons**1980**.
[130] L. Fan, F. Tang, G. Chen, S.T. Reis, M.L. Koenigstein, *Corrosion resistances of steel pipe coated with two types of enamel by two coating processes*, Journal of Materials Engineering and Performance, 27 (**2018**) 5341-5349.
[131] W. Joseph, *Two-coat/one-fire alternatives*, in: W.D. Smothers (Ed.) *Proceedings of the 42nd Porcelain Enamel Technical Forum: Ceramic Engineering and Science Proceedings*, John Wiley & Sons**1981**.
[132] M.A. Martinez, J. Abenojar, M. Bahrami, F. Velasco, *One-step enameling and sintering of low-carbon steels*, Metals, 11 (**2021**).
[133] F. Cillero, *Industrial achievements of powder enamelling*, in: W.D. Smothers (Ed.) *Proceedings of the 41st Porcelain Enamel Technical Forum: Ceramic Engineering and Science Proceedings*, John Wiley & Sons**1980**.
[134] D.R. Rogers, *Emerging trends in the use of porcelain enamel powders*, in: W.D. Smothers (Ed.) *Proceedings of the 44th Porcelain Enamel Technical Forum: Ceramic Engineering and Science Proceedings*, John Wiley & Sons**1983**.
[135] L.C. Kolar, *Energy efficient furnace systems*, in: W.D. Smothers (Ed.) *Proceedings of the 42nd Porcelain Enamel Technical Forum: Ceramic Engineering and Science Proceedings*, John Wiley & Sons**1981**.
[136] W.C. Bennight, L.S. Smith, C.C. Vicary, E.M. Thoben, *Energy savings with improved furnaces and other plant modifications*, in: W.D. Smothers (Ed.) *Proceedings of the 53rd Porcelain Enamel Technical Forum: Ceramic Engineering and Science Proceedings*, John Wiley & Sons**1982**.
[137] J.D. Sullivan, *Glass metal reactions and physical properties of enamels*, in: W.D. Smothers (Ed.) *Proceedings of the 42nd Porcelain Enamel Technical Forum: Ceramic Engineering and Science Proceedings*, John Wiley & Sons**1981**.
[138] B.W. King, H.P. Tripp, W.H. Duckworth, *Nature of adherence of porcelain enamels to metals*, Journal of the American Ceramic Society, 42 (**1959**) 504-525.
[139] A. Bachara, A. Mabrouka, D.D.S. Menesesa, E. Verona, Y. Sadallahd, P. Echeguta, F. Bentisse, *Effect of thermal treatment on the property of enamel coating on steel substrate*, Journal of Materials and Environmental Sciences, 8 (**2017**) 3884-3891.

[140] W.A. Joseph, *Structure of enamel coatings*, in: W.D. Smothers (Ed.) *Proceedings of the 48th Porcelain Enamel Technical Forum: Ceramic Engineering and Science Proceedings*, John Wiley & Sons**1987**.
[141] R.E. Ott, *Effect of furnace moisture on ground-coat surface quality*, in: W.D. Smothers (Ed.) *Proceedings of the 44th Porcelain Enamel Technical Forum: Ceramic Engineering and Science Proceedings*, John Wiley & Sons**1983**.
[142] H. Qian, S. Chen, T. Wang, G. Cheng, X. Chen, Z. Xu, Q. Zeng, Y. Liu, D. Yan, *Silicon nitride modified enamel coatings enable high thermal shock and corrosion resistances for steel protection*, Surface and Coatings Technology, 421 (**2021**) 127474.
[143] J.W. Goodwin, K.E. Whitelock, *The importance of colour and its stability in vitreous enamels*, Materials & Design, 6 (**1985**) 172-176.
[144] E. Voß, *Chemically resistant enamel*, Ceramic Transactions, 215 (**2010**) 169-175.
[145] S. Rossi, N. Parziani, C. Zanella, *Abrasion resistance of vitreous enamel coatings in function of frit composition and particles presence*, Wear, 332-333 (**2015**) 702-709.
[146] S. Rossi, M. Fedel, F. Deflorian, N. Parziani, *Abrasion and chemical resistance of composite vitreous enamel coatings with hard particles*, Surface and Interface Analysis, 48 (**2016**) 834-844.
[147] C.J. Vernon, *The changing nature of laundry detergents*, in: W.D. Smothers (Ed.) *Proceedings of the 50th Porcelain Enamel Technical Forum: Ceramic Engineering and Science Proceedings*, John Wiley & Sons**1989**.
[148] A.M. Lynch, *Effect of composition of today's laundry detergents*, in: J.B. Watchman (Ed.) *Proceedings of the 55th Porcelain Enamel Technical Forum: Ceramic Engineering and Science Proceedings*, John Wiley & Sons**1989**.
[149] A. Conde, J. de Damborenea, *Monitoring of vitreous enamel degradation by electrochemical noise*, Surface and Coatings Technology, 150 (**2002**) 212-217.
[150] A. Conde, J.J. de Damborenea, *Electrochemical impedance spectroscopy for studying the degradation of enamel coatings*, Corrosion Science, 44 (**2002**) 1555-1567.
[151] X. Ronghai, S. Xin, Q. Ni, H. Zeng, M. Li, *Initial corrosion characteristics of enamel coated carbon steel in hot tap water*, Russian Journal of Electrochemistry, 57 (**2021**) 636-643.
[152] F. Tang, G. Chen, J.S. Volz, R.K. Brow, M. Koenigstein, *Microstructure and corrosion resistance of enamel coatings applied to smooth reinforcing steel*, Construction and Building Materials, 35 (**2012**) 376-384.
[153] R. Pérez, A. Querejeta, M.Á. Corres, J. Muñoz, H.J. Grande, P. Honnerová, *Thermal behaviour of vitreous ceramic coatings obtained by electrophoretic deposition for furnace components*, Ceramics International, 46 (**2020**) 20695-20706.
[154] M. Bukovec, K. Xhanari, T. Lešer, B. Petovar, M. Finšgar, *Analysis of the enameled AISI 316LVM stainless steel*, Journal of Materials Engineering and Performance, 27 (**2018**) 1122-1129.
[155] C.X. Li, X.Y. Yang, X.W. Qu, W.S. Li, Y.J. Sun, J.T. Zhao, *Effects of quartz and feldspar on microstructure and friction and wear properties of enamel coating*, Surface Technology, 50 (**2021**) 221-229.

[156] S. Rossi, M. Calovi, D. Velez, J. Munoz, *Influence of addition of hard particles on the mechanical and chemical behavior of vitreous enamel*, Surface & Coatings Technology, 357 (**2019**) 69-77.
[157] S. Rossi, M. Calovi, D. Velez, I. Rodriguez, M. del Rincon, J.M. Munoz, H.J. Grande, *Microstructural analysis and surface modification of a vitreous enamel modified with corundum particles*, Advanced Engineering Materials, 21 (**2019**) 1900231.
[158] N. Çöpoğlu, B. Çiçek, *Abrasion resistant glass-ceramic coatings reinforced with WC-nanoparticles*, Surface and Coatings Technology, 419 (**2021**) 127275.
[159] N. Çöpoğlu, O. Karaahmet, T. Cengiz, H. Gökdemir, B. Çiçek, *$TiB_2$ embedded borosilicate coatings with improved wear resistance*, Surface Engineering, 37 (**2021**) 1449-1456.
[160] B.J. Connerm, *Consumer attitudes on ranges*, in: W.D. Smothers (Ed.) *Proceedings of the 41st Porcelain Enamel Technical Forum*, John Wiley & Sons**1980**, pp. 2.
[161] R.W. Knopik, *The porcelain enamel product in the appliance marketplace*, in: W.D. Smothers (Ed.) *Proceedings of the 46th Porcelain Enamel Technical Forum: Ceramic Engineering and Science Proceedings*, John Wiley & Sons**1985**, pp. 2.
[162] A.M. Lynch, *Charcaterization of pickle-free, wet pyrolitic enamels*, in: W.D. Smothers (Ed.) *Proceedings of the 48th Porcelain Enamel Technical Forum: Ceramic Engineering and Science Proceedings*, John Wiley & Sons**1987**.
[163] C.L. Hackler, K.O. Helm, *Latest porcelain enamel application technology for appliance components*, in: J.B. Wachtman Jr. (Ed.) *Proceedings of the 49th Porcelain Enamel Technical Forum: Ceramic Engineering and Science Proceedings*, John Wiley & Sons**1988**.
[164] W.D. Faust, *Overview: pyrolitic enamels*, in: J.B. Wachtman Jr. (Ed.) *Proceedings of the 51st Porcelain Enamel Technical Forum: Ceramic Engineering and Science Proceedings*, John Wiley & Sons**1990**.
[165] D.E. McCloskey, *Porcelain enamel vs competitive materials – a comparison*, in: W.D. Smothers (Ed.) *Proceedings of the 47th Porcelain Enamel Technical Forum: Ceramic Engineering and Science Proceedings*, John Wiley & Sons**1990**.
[166] W.H. Scarlet, *Architectural applications – a resurging market*, in: W.D. Smothers (Ed.) *Proceedings of the 45th Porcelain Enamel Technical Forum: Ceramic Engineering and Science Proceedings*, John Wiley & Sons**1984**.
[167] C. Ferrari, C. Mugoni, M. Montorsi, C. Siligardi, *On a solar reflective ceramic based glaze for asphalt shingle*, Ceramics International, 43 (**2017**) 14710-14717.
[168] A.V. Ryabova, A.Y. Fanda, E.A. Yatsenko, M.G. Lee, *Development of compositions of new enamel coatings with various operational and decorative properties to protect steel architectural and construction panels*, **2021**, pp. 684-692.
[169] C.G. Strobach, *Glasslining hot water tanks with cobalt-free materials*, in: W.D. Smothers (Ed.) *Proceedings of the 41st Porcelain Enamel Technical Forum*, John Wiley & Sons**1980**.
[170] C. Williams, *Production on water heaters tanks using porcelain enamel powder*, in: J.B. Wachtman Jr. (Ed.) *Proceedings of the 49th Porcelain Enamel Technical Forum: Ceramic Engineering and Science Proceedings*, John Wiley & Sons**1988**.
[171] W.D. Faust, *Glass-ceramic enamels for high-temperature application*, in: W.D. Smothers (Ed.) *Proceedings of the 47th Porcelain Enamel Technical Forum: Ceramic Engineering and Science Proceedings*, John Wiley & Sons**1986**.

[172] E.K. Jensen, *Interior coatings for flues of domestic water heaters*, in: W.D. Smothers (Ed.) *Proceedings of the 44th Porcelain Enamel Technical Forum: Ceramic Engineering and Science Proceedings*, John Wiley & Sons**1983**.
[173] *UNI EN ISO 9000 "Sistemi di gestione per la qualita' - fondamenti e vocabolario"*, Ente Nazionale Italiano di Certificazione, Milano, Italy, **2015**.
[174] S.T. Reis, M. Koenigstein, L. Fan, G. Chen, L. Pavić, A. Moguš-Milanković, *The Effects of Silica on the Properties of Vitreous Enamels*, 12 (**2019**) 248.
[175] L.V. Klimova, Ryabova, A. V., & Kerimova, V. V. , *Chemically Resistant Glass-Enamel Coating for the Protection of Steel Pipelines*, Materials Science Forum, 992 (**2020**) 598-604.
[176] R. Pérez, A. Querejeta, M.Á. Corres, J. Muñoz, H.-J. Grande, P. Honnerová, *Thermal behaviour of vitreous ceramic coatings obtained by electrophoretic deposition for furnace components*, Ceramics International, 46 (**2020**) 20695-20706.
[177] G. Yan, W. Yu, S. Shen, *High-temperature nanoindentation for temperature-dependent mechanical behavior of enamel coating*, Surface and Coatings Technology, 374 (**2019**) 541-548.
[178] S. Rossi, F. Deflorian, E. Scrinzi, *Comparison of different abrasion mechanisms on aesthetic properties of organic coatings*, Wear, 267 (**2009**) 1574-1580.
[179] D.M. Kennedy, M.S.J. Hashmi, *Methods of wear testing for advanced surface coatings and bulk materials*, Journal of Materials Processing Technology, 77 (**1998**) 246-253.
[180] D. Culliton, A. Betts, S. Carvalho, D. Kennedy, *Improving Tribological Properties of Cast Al-Si Alloys through Application of Wear-Resistant Thermal Spray Coatings*, Journal of Thermal Spray Technology, 22 (**2013**) 491-501.
[181] J. Sun, H. Mukamal, Z. Liu, W. Shen, *Analysis of the Taber Test in Characterization of Automotive Side Windows*, Tribology Letters, 13 (**2002**) 49-54.
[182] C.-X. Li, X.-Y. Yang, X.W. Qu, W.-S. Li, Y.-J. Sun, J.-T. Zhao, *Effects of quartz and feldspar on microstructure and friction and wear properties of enamel coating*, Surface Technology, 50 (**2021**) 221-229.
[183] S. Rossi, E. Scrinzi, *Evaluation of the abrasion resistance of enamel coatings*, Chemical Engineering and Processing: Process Intensification, 68 (**2013**) 74-80.
[184] S. Rossi, F. Russo, M. Calovi, M. Del Rincon, D. Velez, *The influence of the size of corundum particles on the properties of chemically resistant porcelain enamels*, Ceramics International, 47 (**2021**) 11618-11627.
[185] Y. Liao, B. Zhang, M. Chen, M. Feng, J. Wang, S. Zhu, F. Wang, *Self-healing metal-enamel composite coating and its protection for TiAl alloy against oxidation under thermal shock in NaCl solution*, Corrosion Science, 167 (**2020**) 108526.
[186] T. Isobe, K. Daimon, T. Sato, T. Matsubara, Y. Hikichi, T. Ota, *Spark plasma sintering technique for reaction sintering of Al2O3/Ni nanocomposite and its mechanical properties*, Ceramics International, 34 (**2008**) 213-217.
[187] W.-H. Tuan, Y.-P. Pai, *Mechanical Properties of Al2O3-NiAl Composites*, 82 (**1999**) 1624-1626.
[188] V. Imbeni, I.M. Hutchings, M.J.W. Breslin, *Abrasive wear behaviour of an Al2O3–Al co-continuous composite*, 233 (**1999**) 462-467.
[189] Y. Waku, M. Suzuki, Y. Oda, Y. Kohtoku, *Improving the fracture toughness of MgO–Al2O3–SiO2 glass/molybdenum composites by the microdispersion of flaky molybdenum particles*, Journal of Materials Science, 32 (**1997**) 4549-4557.

[190] Y.-e. Qi, Y.-S. Zhang, L.-T. Hu, *High-temperature self-lubricated properties of Al2O3/Mo laminated composites*, Wear, 280-281 (**2012**) 1-4.
[191] E. Apel, J. Deubener, A. Bernard, M. Höland, R. Müller, H. Kappert, V. Rheinberger, W. Höland, *Phenomena and mechanisms of crack propagation in glass-ceramics*, Journal of the Mechanical Behavior of Biomedical Materials, 1 (**2008**) 313-325.
[192] S. Padmanapan, V. Selvarajan, S.V. Joshi, G. Sundararajan, *Experimental design and performance analysis of alumina coatings deposited by a detonation spray process*, Journal of Physics D: Applied Physics, 34 (**2000**) 131.
[193] M. Chen, S. Zhu, M. Shen, F. Wang, Y. Niu, *Effect of NiCrAlY platelets inclusion on the mechanical and thermal shock properties of glass matrix composites*, Materials Science and Engineering: A, 528 (**2011**) 1360-1366.
[194] W. Zhai, L. Bai, R. Zhou, X. Fan, G. Kang, Y. Liu, K. Zhou, *Recent progress on wear-resistant materials: designs, properties, and applications*, Advanced Science, 8 (**2021**) 2003739.
[195] L. Gong, I.A. Kinloch, R.J. Young, I. Riaz, R. Jalil, K.S.J.A.M. Novoselov, *Interfacial stress transfer in a graphene monolayer nanocomposite*, 22 (**2010**) 2694-2697.
[196] R.J. Young, I.A. Kinloch, L. Gong, K.S.J.C.S. Novoselov, Technology, *The mechanics of graphene nanocomposites: a review*, 72 (**2012**) 1459-1476.
[197] S.C. Tjong, K.C. Lau, *Abrasion resistance of stainless-steel composites reinforced with hard TiB2 particles*, Composites Science and Technology, 60 (**2000**) 1141-1146.
[198] C. García-Cordovilla, J. Narciso, E. Louis, *Abrasive wear resistance of aluminium alloy/ceramic particulate composites*, Wear, 192 (**1996**) 170-177.
[199] B. Lauke, S.-Y. Fu, *Aspects of fracture toughness modelling of particle filled polymer composites*, Composites Part B: Engineering, 45 (**2013**) 1569-1574.
[200] T. Rouxel, B. Baron, P. Verdier, T. Sakuma, *SiC particle reinforced oxynitride glass: stress relaxation, creep and strain-rate imposed experiments*, Acta Materialia, 46 (**1998**) 6115-6130.
[201] J.A. Yeomans, *Ductile particle ceramic matrix composites— scientific curiosities or engineering materials?*, Journal of the European Ceramic Society, 28 (**2008**) 1543-1550.
[202] F.A. Bruera, G.R. Kramer, M.L. Vera, A.E. Ares, *Evaluation of surface pretreatment stages of Al 1050 to obtain nanostructured anodic films*, Superlattices and Microstructures, 130 (**2019**) 103-116.
[203] *UNI EN ISO 4288 "Specifiche geometriche dei prodotti (GPS) - Stato della superficie: Metodo del profilo - Regole e procedure per il rilevamento dello stato della superficie"*, Ente Italiano di Normazione, Milano, Italy, **2000**.
[204] G. Bierwagen, D. Tallman, J. Li, L. He, C.J.P.i.o.c. Jeffcoate, *EIS studies of coated metals in accelerated exposure*, 46 (**2003**) 149-158.
[205] F.J. Tang, G.D. Chen, J.S. Volz, R.K. Brow, M. Koenigstein, *Corrosion behavior of enamel coated steel rebar by EIS*, Advanced Materials Research, Trans Tech Publ, **2012**, pp. 445-453.
[206] E. Scrinzi, S. Rossi, F. Deflorian, *Effect of slurry mechanical damage on the properties of an organic coating system*, Surface and Coatings Technology, 203 (**2009**) 2974-2981.

[207] T. Yamamoto, M. Olsson, S. Hogmark, *Three-body abrasive wear of ceramic materials*, Wear, 174 (**1994**) 21-31.
[208] I. Hutchings, P. Shipway, *Wear by hard particles*, in: I. Hutchings, P. Shipway (Eds.) *Tribology*, Butterworth-Heinemann**2017**, pp. 165-236.
[209] *ISO 10545 "Ceramic tiles — Part 7: Determination of resistance to surface abrasion for glazed tiles"*, International Organization for Standardization, Geneva, Switzerland, **1996**.
[210] V. Bellido-González, N. Stefanopoulos, F. Deguilhen, *Friction monitored scratch adhesion testing*, Surface and Coatings Technology, 74-75 (**1995**) 884-889.
[211] P.J. Burnett, D.S. Rickerby, *The relationship between hardness and scratch adhession*, Thin Solid Films, 154 (**1987**) 403-416.
[212] F.-b. Wu, J.-g. Duh, *Scratch behavior and in situ acoustic emission analysis of PVD chromium nitride coatings on mild steel with electroless nickel interlayers*, Surface and Coatings Technology, 162 (**2003**) 106-112.
[213] A. Tucci, L. Esposito, L. Malmusi, A. Piccinini, *Surface deterioration and scratch resistance of polished porcelain stoneware tiles.* , Key Engineering materials,, 264-268 (**2004**) 1519-1522.
[214] S. Zhang, D. Sun, Y. Fu, H. Du, *Toughness measurement of thin films: a critical review*, Surface and Coatings Technology, 198 (**2005**) 74-84.
[215] G. Jaeger, I. Endler, M. Heilmaier, K. Bartsch, A. Leonhardt, *A new method of determining strength and fracture toughness of thin hard coatings*, Thin Solid Films, 377-378 (**2000**) 382-388.
[216] G. Gille, K. Wetzig, *Investigations on mechanical behaviour of brittle wear-resistant coatings I. Experimental results*, Thin Solid Films, 110 (**1983**) 37-54.
[217] U. Wiklund, M. Bromark, M. Larsson, P. Hedenqvist, S. Hogmark, *Cracking resistance of thin hard coatings estimated by four-point bending*, Surface and Coatings Technology, 91 (**1997**) 57-63.
[218] S. Rossi, M. Fedel, L. Da Col, F. Deflorian, S. Petrolli, *Coatings to increase the corrosion behaviour of aluminium foam*, Surface Engineering, 33 (**2017**) 405-409.
[219] K. Xhanari, M. Finšgar, *Organic corrosion inhibitors for aluminum and its alloys in chloride and alkaline solutions: A review*, Arabian Journal of Chemistry, 12 (**2019**) 4646-4663.
[220] J. Zhang, M. Klasky, B.C. Letellier, *The aluminum chemistry and corrosion in alkaline solutions*, Journal of Nuclear Materials, 384 (**2009**) 175-189.
[221] H. Zhu, *Graphene: fabrication, characterizations, properties and applications*, (**2017**).
[222] R.R. Nair, P. Blake, A.N. Grigorenko, K.S. Novoselov, T.J. Booth, T. Stauber, N.M.R. Peres, A.K. Geim, *Fine Structure Constant Defines Visual Transparency of Graphene*, 320 (**2008**) 1308-1308.
[223] R. Sanjinés, M.D. Abad, C. Vâju, R. Smajda, M. Mionić, A. Magrez, *Electrical properties and applications of carbon based nanocomposite materials: An overview*, Surface and Coatings Technology, 206 (**2011**) 727-733.
[224] K.M.F. Shahil, A.A. Balandin, *Thermal properties of graphene and multilayer graphene: Applications in thermal interface materials*, Solid State Communications, 152 (**2012**) 1331-1340.
[225] D.G. Papageorgiou, I.A. Kinloch, R.J. Young, *Mechanical properties of graphene and graphene-based nanocomposites*, Progress in Materials Science, 90 (**2017**) 75-127.

[226] C. Lee, X. Wei, J.W. Kysar, J.J.s. Hone, *Measurement of the elastic properties and intrinsic strength of monolayer graphene*, 321 (**2008**) 385-388.
[227] D. Berman, A. Erdemir, A.V. Sumant, *Graphene: a new emerging lubricant*, Materials Today, 17 (**2014**) 31-42.
[228] M. Tabandeh-Khorshid, E. Omrani, P.L. Menezes, P.K. Rohatgi, *Tribological performance of self-lubricating aluminum matrix nanocomposites: Role of graphene nanoplatelets*, Engineering Science and Technology, an International Journal, 19 (**2016**) 463-469.
[229] V.B. Mohan, K.-t. Lau, D. Hui, D. Bhattacharyya, *Graphene-based materials and their composites: A review on production, applications and product limitations*, Composites Part B: Engineering, 142 (**2018**) 200-220.
[230] J. Du, H.-M. Cheng, *The Fabrication, Properties, and Uses of Graphene/Polymer Composites*, 213 (**2012**) 1060-1077.
[231] P. Miranzo, M. Belmonte, M.I. Osendi, *From bulk to cellular structures: A review on ceramic/graphene filler composites*, Journal of the European Ceramic Society, 37 (**2017**) 3649-3672.
[232] O. Bayrak, M. Ionita, E. Demirci, V.V.J.A.P.L. Silberschmidt, *Optical properties of graphene-based materials in transparent polymer matrices*, 109 (**2016**) 081905.
[233] L.-C. Tang, Y.-J. Wan, D. Yan, Y.-B. Pei, L. Zhao, Y.-B. Li, L.-B. Wu, J.-X. Jiang, G.-Q.J.C. Lai, *The effect of graphene dispersion on the mechanical properties of graphene/epoxy composites*, 60 (**2013**) 16-27.
[234] J. Liang, Y. Huang, L. Zhang, Y. Wang, Y. Ma, T. Guo, Y.J.A.F.M. Chen, *Molecular-level dispersion of graphene into poly (vinyl alcohol) and effective reinforcement of their nanocomposites*, 19 (**2009**) 2297-2302.
[235] R.K. Layek, S. Samanta, D.P. Chatterjee, A.K.J.P. Nandi, *Physical and mechanical properties of poly (methyl methacrylate)-functionalized graphene/poly (vinylidine fluoride) nanocomposites: Piezoelectric β polymorph formation*, 51 (**2010**) 5846-5856.
[236] P. Song, Z. Cao, Y. Cai, L. Zhao, Z. Fang, S.J.P. Fu, *Fabrication of exfoliated graphene-based polypropylene nanocomposites with enhanced mechanical and thermal properties*, 52 (**2011**) 4001-4010.
[237] F. Chen, J. Ying, Y. Wang, S. Du, Z. Liu, Q.J.C. Huang, *Effects of graphene content on the microstructure and properties of copper matrix composites*, 96 (**2016**) 836-842.
[238] O. Tapasztó, L. Tapasztó, H. Lemmel, V. Puchy, J. Dusza, C. Balázsi, K.J.C.I. Balázsi, *High orientation degree of graphene nanoplatelets in silicon nitride composites prepared by spark plasma sintering*, 42 (**2016**) 1002-1006.
[239] J. Dusza, J. Morgiel, A. Duszová, L. Kvetková, M. Nosko, P. Kun, C. Balázsi, *Microstructure and fracture toughness of Si3N4+graphene platelet composites*, Journal of the European Ceramic Society, 32 (**2012**) 3389-3397.
[240] Y. Fan, L. Wang, J. Li, J. Li, S. Sun, F. Chen, L. Chen, W. Jiang, *Preparation and electrical properties of graphene nanosheet/Al2O3 composites*, Carbon, 48 (**2010**) 1743-1749.
[241] K. Wang, Y. Wang, Z. Fan, J. Yan, T. Wei, *Preparation of graphene nanosheet/alumina composites by spark plasma sintering*, Materials Research Bulletin, 46 (**2011**) 315-318.

[242] P. Kun, O. Tapasztó, F. Wéber, C. Balázsi, *Determination of structural and mechanical properties of multilayer graphene added silicon nitride-based composites*, Ceramics International, 38 (**2012**) 211-216.
[243] L. Zhang, W. Liu, C. Yue, T. Zhang, P. Li, Z. Xing, Y. Chen, *A tough graphene nanosheet/hydroxyapatite composite with improved in vitro biocompatibility*, Carbon, 61 (**2013**) 105-115.
[244] X. Liu, J. Li, X. Yu, H. Fan, Q. Wang, S. Yan, L. Wang, W. Jiang, *Graphene nanosheet/titanium carbide composites of a fine-grained structure and improved mechanical properties*, Ceramics International, 42 (**2016**) 165-172.
[245] G.B. Yadhukulakrishnan, S. Karumuri, A. Rahman, R.P. Singh, A. Kaan Kalkan, S.P. Harimkar, *Spark plasma sintering of graphene reinforced zirconium diboride ultra-high temperature ceramic composites*, Ceramics International, 39 (**2013**) 6637-6646.
[246] F. Chen, D. Jin, K. Tyeb, B. Wang, Y.-H. Han, S. Kim, J.M. Schoenung, Q. Shen, L. Zhang, *Field assisted sintering of graphene reinforced zirconia ceramics*, Ceramics International, 41 (**2015**) 6113-6116.
[247] M. Belmonte, A. Nistal, P. Boutbien, B. Román-Manso, M.I. Osendi, P. Miranzo, *Toughened and strengthened silicon carbide ceramics by adding graphene-based fillers*, Scripta Materialia, 113 (**2016**) 127-130.
[248] Y.-W. MAI, B.R. LAWN, *Crack-Interface Grain Bridging as a Fracture Resistance Mechanism in Ceramics: II, Theoretical Fracture Mechanics Model*, 70 (**1987**) 289-294.
[249] X. Wang, W. Xing, L. Song, H. Yang, Y. Hu, G.H.J.S. Yeoh, C. Technology, *Fabrication and characterization of graphene-reinforced waterborne polyurethane nanocomposite coatings by the sol–gel method*, 206 (**2012**) 4778-4784.
[250] B. Pan, G. Xu, B. Zhang, X. Ma, H. Li, Y.J.P.-p.t. Zhang, engineering, *Preparation and tribological properties of polyamide 11/graphene coatings*, 51 (**2012**) 1163-1166.
[251] D. Berman, A. Erdemir, A.V.J.C. Sumant, *Few layer graphene to reduce wear and friction on sliding steel surfaces*, 54 (**2013**) 454-459.
[252] H. Li, Y. Xie, K. Li, L. Huang, S. Huang, B. Zhao, X. Zheng, *Microstructure and wear behavior of graphene nanosheets-reinforced zirconia coating*, Ceramics International, 40 (**2014**) 12821-12829.
[253] H. Porwal, P. Tatarko, R. Saggar, S. Grasso, M. Kumar Mani, I. Dlouhý, J. Dusza, M.J. Reece, *Tribological properties of silica–graphene nano-platelet composites*, Ceramics International, 40 (**2014**) 12067-12074.
[254] J. Balko, P. Hvizdoš, J. Dusza, C. Balázsi, J. Gamcová, *Wear damage of Si3N4-graphene nanocomposites at room and elevated temperatures*, Journal of the European Ceramic Society, 34 (**2014**) 3309-3317.
[255] P. Hvizdoš, J. Dusza, C. Balázsi, *Tribological properties of Si3N4–graphene nanocomposites*, Journal of the European Ceramic Society, 33 (**2013**) 2359-2364.
[256] H.J. Kim, S.-M. Lee, Y.-S. Oh, Y.-H. Yang, Y.S. Lim, D.H. Yoon, C. Lee, J.-Y. Kim, R.S. Ruoff, *Unoxidized Graphene/Alumina Nanocomposite: Fracture- and Wear-Resistance Effects of Graphene on Alumina Matrix*, Scientific Reports, 4 (**2014**) 5176.
[257] M. Belmonte, C. Ramírez, J. González-Julián, J. Schneider, P. Miranzo, M.I. Osendi, *The beneficial effect of graphene nanofillers on the tribological performance of ceramics*, Carbon, 61 (**2013**) 431-435.

[258] M. Calovi, S. Dirè, R. Ceccato, F. Deflorian, S. Rossi, *Corrosion protection properties of functionalised graphene–acrylate coatings produced via cataphoretic deposition*, Progress in Organic Coatings, 136 (**2019**) 105261.
[259] M.C. M. Fen, Z. Yu, Z. Chen, J. Chen, S. Zhu, F. Wang, *Crystallization and wear behavior of SiO2-Al2O3-ZrO2-Ba(Sr,Ca)O glass-ceramics added with Cr2O3 by different methods*, Ceramics International, 45 (**2019**) 22617.22624.
[260] S.Y. Choi, J.M. Ahn, *Viscous Sintering and Mechanical Properties of 3Y-TZP-Reinforced LAS Glass-Ceramic Composites*, 80 (**1997**) 2982-2986.
[261] M. Montazerian, P. Alizadeh, B. Eftekhari Yekta, *Processing and properties of a mica–apatite glass–ceramic reinforced with Y-PSZ particles*, Journal of the European Ceramic Society, 28 (**2008**) 2693-2699.
[262] X. Wang, M. Shen, M. Chen, S. Zhu, F. Wang, *Microstructure stabilization of a novel glass/YSZ composite coating material by adding alumina particles*, Ceramics International, 41 (**2015**) 9753-9762.
[263] S. Chakraborty, D. Debnath, A.R. Mallick, P.K. Das, *Mechanical and thermal properties of hot pressed ZrB2 system with TiB2*, International Journal of Refractory Metals and Hard Materials, 46 (**2014**) 35-42.
[264] M. Chen, S. Zhu, M. Shen, F. Wang, Y. Niu, *Thermophysical Properties of Alumina Particle Reinforced Glass Matrix Composites*, 10 (**2013**) 224-233.
[265] M. Chen, M. Shen, S. Zhu, F. Wang, *Comparative study of interfacial reaction between superalloy substrate and glass coating with and without alumina particles incorporation*, Applied Surface Science, 271 (**2013**) 228-233.
[266] M. Chen, S. Zhu, F. Wang, *Strengthening mechanisms and fracture surface characteristics of silicate glass matrix composites with inclusion of alumina particles of different particle sizes*, Physica B: Condensed Matter, 413 (**2013**) 15-20.
[267] A. Faeghiniaa, A. Zamanian, *Wear Resistance of Nano Alumina Containing SiO 2 -B 2 O 3 -Na 2 O Glass-Ceramic on Steel Substrate*, Tribology in Industry, 402 (**2016**) 402-411.
[268] F.F. LANGE, *Fracture Energy and Strength Behavior of a Sodium Borosilicate Glass-Al2O3 Composite System*, 54 (**1971**) 614-620.
[269] G. Bolelli, V. Cannillo, L. Lusvarghi, T. Manfredini, *Glass-alumina composite coatings by plasma spraying. Part I: Microstructural and mechanical characterization*, Surface and Coatings Technology, 201 (**2006**) 458-473.
[270] D. Zheng, S. Zhu, F. Wang, *Oxidation and hot corrosion behavior of a novel enamel-Al2O3 composite coating on K38G superalloy*, Surface and Coatings Technology, 200 (**2006**) 5931-5936.
[271] J.-M. Tian, Y.-L. Zhang, S.-X. Zhang, X.-P. Luo, *Mechanical Properties and Microstructure of Alumina-Glass Composites*, 82 (**1999**) 1592-1594.
[272] E. Bernardo, G. Scarinci, *Sintering behaviour and mechanical properties of Al2O3 platelet-reinforced glass matrix composites obtained by powder technology*, Ceramics International, 30 (**2004**) 785-791.
[273] A.R. Boccaccini, V. Winkler, *Fracture surface roughness and toughness of Al2O3-platelet reinforced glass matrix composites*, Composites Part A: Applied Science and Manufacturing, 33 (**2002**) 125-131.
[274] E. Bernardo, F. Andreola, L. Barbieri, I. Lancellotti, *Sintered Glass–Ceramics and Glass–Ceramic Matrix Composites from CRT Panel Glass*, 88 (**2005**) 1886-1891.

[275] E. Bernardo, G. Scarinci, S. Hreglich, *Development and mechanical characterization of Al2O3 platelet-reinforced glass matrix composites obtained from glasses coming from dismantled cathode ray tubes*, Journal of the European Ceramic Society, 25 (**2005**) 1541-1550.
[276] E. Bernardo, R. Castellan, S. Hreglich, *Al2O3-platelet reinforced glass matrix composites from a mixture of wastes*, Journal of Materials Science, 42 (**2007**) 2706-2711.
[277] N.P. Padture, *Advanced structural ceramics in aerospace propulsion*, Nature Materials, 15 (**2016**) 804-809.
[278] J.S. Pelz, N. Ku, M.A. Meyers, L.R. Vargas-Gonzalez, *Additive manufacturing of structural ceramics: a historical perspective*, Journal of Materials Research and Technology, 15 (**2021**) 670-695.
[279] J. Rödel, A.B.N. Kounga, M. Weissenberger-Eibl, D. Koch, A. Bierwisch, W. Rossner, M.J. Hoffmann, R. Danzer, G. Schneider, *Development of a roadmap for advanced ceramics: 2010–2025*, Journal of the European Ceramic Society, 29 (**2009**) 1549-1560.
[280] A.J. Ruys, *3 - Fracture mechanics and design principles for metal-reinforced ceramics*, in: A.J. Ruys (Ed.) *Metal-Reinforced Ceramics*, Woodhead Publishing**2021**, pp. 45-67.
[281] G.H. Staab, *Introduction to composite materials*, in: G.H. Staab (Ed.) *Laminar Composites*, Butterworth-Heinemann, Woburn, **1999**, pp. 1-16.
[282] D.J. Green, R.H. Hannink, M.V. Swain, *Transformation toughening of ceramics*, CRC press**2018**.
[283] D.J. Green, *Compressive surface strengthening of brittle materials*, Journal of Materials Science, 19 (**1984**) 2165-2171.
[284] V. Krstic, P.S. Nicholson, *Toughening of glasses by metallic particles*, Journal of the American Ceramic Society, 65 (**1981**) 499-504.
[285] R.O. Ritchie, *Toughening materials: enhancing resistance to fracture*, 379 (**2021**) 20200437.
[286] A.J. Ruys, *1 - Introduction to metal-reinforced ceramics*, in: A.J. Ruys (Ed.) *Metal-Reinforced Ceramics*, Woodhead Publishing**2021**, pp. 1-20.
[287] M. Chmielewski, K. Pietrzak, *Processing, microstructure and mechanical properties of Al2O3–Cr nanocomposites*, Journal of the European Ceramic Society, 27 (**2007**) 1273-1279.
[288] G. de Portu, S. Guicciardi, C. Melandri, F. Monteverde, *Wear behaviour of Al2O3–Mo and Al2O3–Nb composites*, Wear, 262 (**2007**) 1346-1352.
[289] Y. Ji, J.A.J.J.o.M.S. Yeomans, *Microstructure and mechanical properties of chromium and chromium/nickel particulate reinforced alumina ceramics*, 37 (**2002**) 5229-5236.
[290] E. Bernardo, G. Scarinci, A. Maddalena, S. Hreglich, *Development and mechanical properties of metal–particulate glass matrix composites from recycled glasses*, Composites Part A: Applied Science and Manufacturing, 35 (**2004**) 17-22.
[291] R. Kerans, T. Parthasarathy, *Crack deflection in ceramic composites and fiber coating design criteria*, Composites Part A: Applied Science and Manufacturing, 30 (**1999**) 521-524.
[292] I. Dlouhy, A.R. Boccaccini, *Preparation, microstructure and mechanical properties of metal-particulate/glass-matrix composites*, Composites Science and Technology, 56 (**1996**) 1415-1424.

[293] G. Banuprakash, V. Katyal, V.S.R. Murthy, G.S. Murty, *Mechanical behaviour of borosilicate glass-copper composites*, Composites Part A: Applied Science and Manufacturing, 28 (**1997**) 861-867.
[294] Q. Chang, D.L. Chen, H.Q. Ru, X.Y. Yue, L. Yu, C.P. Zhang, *Toughening mechanisms in iron-containing hydroxyapatite/titanium composites*, Biomaterials, 31 (**2010**) 1493-1501.
[295] F. Pernot, R. Rogier, *Mechanical properties of phosphate glass-ceramic-316 L stainless steel composites*, Journal of Materials Science, 28 (**1993**) 6676-6682.
[296] D. Bucevac, *Heat treatment for strengthening silicon carbide ceramic matrix composites*, in: I.M. Low (Ed.) *Advances in ceramic matrix composites*, Woodhead Publishing**2014**, pp. 141-163.
[297] A.J. Ruys, *2 - A review of metal-reinforced ceramics*, in: A.J. Ruys (Ed.) *Metal-Reinforced Ceramics*, Woodhead Publishing**2021**, pp. 21-43.
[298] J.G. ZWISSLER, M.E. FINE, G.W. GROVES, *Strength and Toughness of a Ceramic Reinforced with Metal Wires*, 60 (**1977**) 390-396.
[299] F. Wang, Y. Liu, *Mechanical and tribological properties of ceramic-matrix friction materials with steel fiber and mullite fiber*, Materials & Design, 57 (**2014**) 449-455.
[300] D.E. Alman, J.A. Hawk, *Abrasive wear behavior of a brittle matrix ($MoSi_2$) composite reinforced with a ductile phase (Nb)*, Wear, 251 (**2001**) 890-900.
[301] Y. Liao, M. Chen, M. Feng, Q. Wang, J. Wang, S. Zhu, F. Wang, *Thermal shock and self-healing behavior of the enamel composite coatings with addition of various nanoparticles at temperatures of 700 and 800 °C*, Corrosion Science, 191 (**2021**) 109747.
[302] M. Zawischa, S. Makowski, M. Kuczyk, V. Weihnacht, *Comparison of fracture properties of different amorphous carbon coatings using the scratch test and indentation failure method*, Surface and Coatings Technology, 435 (**2022**) 128247.
[303] S. Gholizadeh, *A review of non-destructive testing methods of composite materials*, Procedia Structural Integrity, 1 (**2016**) 50-57.
[304] D.G. Eitzen, H.N.G. Wadley, *Acoustic emission: etsablishing the fundamentals*, JOURNAL OF RESEARCH of the National Bureau of Standards, 89 (**1984**) 75-100.
[305] C.R. Ríos-Soberanis, *Acoustic Emission Technique, an Overview as a Characterization Tool in Materials Science*, Journal of Applied Research and Technology, 9 (**2011**) 367-379.
[306] M. Saeedifar, D. Zarouchas, *Damage characterization of laminated composites using acoustic emission: A review*, Composites Part B: Engineering, 195 (**2020**) 108039.
[307] K. Hamdi, G. Moreau, Z. Aboura, *Digital image correlation, acoustic emission and in-situ microscopy in order to understand composite compression damage behavior*, Composite Structures, 258 (**2021**) 113424.
[308] A. Bendaoued, A. Zahrouni, M. Messaoud, O. Harzallah, S. Bistac, R. Salhi, *Understanding the effect of nanoparticles TiO2, Al2O3 and SiO2 on damage mechanisms of a polymer composite*, Ceramics International, 49 (**2023**) 4160-4167.
[309] W. Li, G. Palardy, *Damage monitoring methods for fiber-reinforced polymer joints: A review*, Composite Structures, 299 (**2022**) 116043.
[310] G.N. Morscher, Z. Han, *Damage Determination in Ceramic Composites Subject to Tensile Fatigue Using Acoustic Emission. LID - 10.3390/ma11122477 [doi] LID - 2477*.

[311] F. Wang, X. Teng, Y. Jiang, X. Hu, M. Lu, X. Guo, X. Liu, X. Liu, D. Yu, *Damage analysis of a SiCf/SiC ceramic matrix composite under stepwise fatigue loading with acoustic emission*, Journal of the European Ceramic Society, 42 (**2022**) 4086-4097.
[312] E. Maillet, A. Singhal, A. Hilmas, Y. Gao, Y. Zhou, G. Henson, G. Wilson, *Combining in-situ synchrotron X-ray microtomography and acoustic emission to characterize damage evolution in ceramic matrix composites*, Journal of the European Ceramic Society, 39 (**2019**) 3546-3556.
[313] J.P. McCrory, A. Vinogradov, M.R. Pearson, R. Pullin, K.M.J.S.T.i.C.E. Holford, *Acoustic Emission Monitoring of Metals*, (**2021**).
[314] A. Shanyavskiy, M. Banov, *Acoustic emission methods for lifetime estimations in aircraft structures*, Theoretical and Applied Fracture Mechanics, 109 (**2020**) 102719.
[315] D.V. Chernov, V.M. Matyunin, V.A. Barat, A.Y. Marchenkov, S.V. Elizarov, *Investigation of Acoustic Emission in Low-Carbon Steels during Development of Fatigue Cracks*, Russian Journal of Nondestructive Testing, 54 (**2018**) 638-647.
[316] J.M. Miguel, J.M. Guilemany, B.G. Mellor, Y.M. Xu, *Acoustic emission study on WC–Co thermal sprayed coatings*, Materials Science and Engineering: A, 352 (**2003**) 55-63.
[317] S.S. Golru, M.M. Attar, B. Ramezanzadeh, *Effects of different surface cleaning procedures on the superficial morphology and the adhesive strength of epoxy coating on aluminium alloy 1050*, Progress in Organic Coatings, 87 (**2015**) 52-60.
[318] Z.H. Jin, H.H. Ge, W.W. Lin, Y.W. Zong, S.J. Liu, J.M. Shi, *Corrosion behaviour of 316L stainless steel and anti-corrosion materials in a high acidified chloride solution*, Applied Surface Science, 322 (**2014**) 47-56.
[319] E. Rocha-Rangel, *Fracture Toughness Determinations by Means of Indentation Fracture.* , in: J. Cuppoletti (Ed.) *Nanocomposites with Unique Properties and Applications in Medicine and Industry*, Intech Open, London, **2011**.
[320] A.G. EVANS, E.A. CHARLES, *Fracture Toughness Determinations by Indentation*, 59 (**1976**) 371-372.
[321] K. Niihara, R. Morena, D.P.H. Hasselman, *Evaluation ofKIc of brittle solids by the indentation method with low crack-to-indent ratios*, Journal of Materials Science Letters, 1 (**1982**) 13-16.
[322] H. Miyazaki, Y. Yoshizawa, *A reinvestigation of the validity of the indentation fracture (IF) method as applied to ceramics*, Journal of the European Ceramic Society, 37 (**2017**) 4437-4441.
[323] T. Rouxel, S. Yoshida, *The fracture toughness of inorganic glasses*, 100 (**2017**) 4374-4396.
[324] S. Yoshida, *Indentation deformation and cracking in oxide glass –toward understanding of crack nucleation*, Journal of Non-Crystalline Solids: X, 1 (**2019**) 100009.
[325] Y. Kato, H. Yamazaki, S. Yoshida, J. Matsuoka, *Effect of densification on crack initiation under Vickers indentation test*, Journal of Non-Crystalline Solids, 356 (**2010**) 1768-1773.
[326] R. Limbach, A. Winterstein-Beckmann, J. Dellith, D. Möncke, L. Wondraczek, *Plasticity, crack initiation and defect resistance in alkali-borosilicate glasses: From normal to anomalous behavior*, Journal of Non-Crystalline Solids, 417-418 (**2015**) 15-27.

[327] R.D. maschio, A. Maddalena, I. Calliari, *Radial crack initiation in glass by Vickers indentation*, Materials Chemistry and Physics, 11 (**1984**) 443-451.
[328] M. Biesuz, M. Bortolotti, F. Tessarolo, R. Canteri, P. Giopato, G. Nollo, A. Chiappini, M. Vilémová, V.M. Sglavo, G.D. Sorarù, *Solid-state field-assisted ion exchange of Ag in lithium aluminum silicate glass-ceramics: A superfast processing route toward stronger materials with antimicrobial properties*, Journal of the European Ceramic Society, 42 (**2022**) 1750-1761.
[329] P.M. Ramsey, H.W. Chandler, T.F. Page, *Bending tests to estimate the through-thickness strength and interfacial shear strength in coated systems*, Thin Solid Films, 201 (**1991**) 81-89.
[330] J.O. Carneiro, J.P. Alpuim, V. Teixeira, *Experimental bending tests and numerical approach to determine the fracture mechanical properties of thin ceramic coatings deposited by magnetron sputtering*, Surface and Coatings Technology, 200 (**2006**) 2744-2752.
[331] J.L. Amorós, A. Blasco, J.V. Carceller, V. Sanz, *Acuerdo esmalte-soporte (I): causas y factores de los que depende*, Tecnica Ceramica, 178 (**1997**) 582-592.
[332] J.H. Healy, L.K. Breeze, *Effect of heat treatment on porperties of enamel-steel composites*, Journal of the American Ceramic Society, 41 (**1958**) 381-386.
[333] J.L. Amorós, A. Blasco, J.V. Carceller, V. Sanz, *Acuerdo esmalte-soporte (II) expansion termica de soportes y esmaltes ceramicos*, Tecnica Ceramica, 179 (**1997**) 644-657.
[334] F.G. Franceschini, O.R. Klegues Montedo, S. Arcaro, C.P. Bergmann, *Aluminum borophosphate glaze-coated aluminum alloy substrate: Coating properties and coating/substrate coupling*, Ceramics International, 47 (**2021**) 2050-2057.
[335] M. Paganelli, D. Sighinolfi, *The optical fleximeter to study deformations on ceramics*, Industrial Ceramics, 29 (**2009**) 43-48.
[336] Y.-K. Son, C.-J. Lee, J.-M. Lee, B.-M. Kim, *Deformation prediction of porcelain-enameled steels with strain history by press forming and high-temperature behavior of coating layer*, Transactions of Nonferrous Metals Society of China, 22 (**2012**) s838-s844.
[337] R.G. Budynas, J.K. Nisbett, *Shigley's Mechanical Engineering Design*, McGraw-Hill Companies, New York, **2011**.
[338] M. Gallo, F. Magaletti, C.M. Casciola, *Heterogeneous bubble nucleation dynamics*, Journal of Fluid Mechanics, 906 (**2021**) A20.
[339] F.J. Maile, G. Pfaff, P. Reynders, *Effect pigments—past, present and future*, Progress in Organic Coatings, 54 (**2005**) 150-163.
[340] G.S. Frankel, J.D. Vienna, J. Lian, J.R. Scully, S. Gin, J.V. Ryan, J. Wang, S.H. Kim, W. Windl, J. Du, *A comparative review of the aqueous corrosion of glasses, crystalline ceramics, and metals*, Materials Degradation, 2 (**2018**) 15.
[341] S. Gin, J.-M. Delaye, F. Angeli, S. Schuller, *Aqueous alteration of silicate glass: state of knowledge and perspectives*, npj Materials Degradation, 5 (**2021**) 42.
[342] V. Marimuthu, I. Dulac, K. Kannoorpatti, *Significance of Pourbaix Diagrams to Study the Corrosion Behaviour of Hardfacing Alloys Based on Chromium Carbides at 298 K (25 °C)*, Journal of Bio- and Tribo-Corrosion, 2 (**2016**) 17.
[343] B.F. Chen, J. Hwang, G.P. Yu, J.H. Huang, *In situ observation of the cracking behavior of TiN coating on 304 stainless steel subjected to tensile strain*, Thin Solid Films, 352 (**1999**) 173-178.

[344] U. Wiklund, P. Hedenqvist, S. Hogmark, *Multilayer cracking resistance in bending*, Surface and Coatings Technology, 97 (**1997**) 773-778.
[345] A. Koutsomichalis, M. Vardavoulias, N. Vaxevanidis, *HVOF sprayed WC-CoCr coatings on aluminum: tensile and tribological properties*, IOP Conference Series: Materials Science and Engineering, 174 (**2017**) 012062.
[346] A. Tucci, J.B. Guion, L. Esposito, *Microstructure and Scratch Resistance of Ceramic Surfaces*, **2009**.
[347] V. Cannillo, L. Esposito, E. Rambaldi, A. Sola, A. Tucci, *Microstructural and mechanical changes by chemical ageing of glazed ceramic surfaces*, Journal of the European Ceramic Society, 29 (**2009**) 1561-1569.
[348] H.H. Nguyen, S. Wan, K.A. Tieu, S.T. Pham, H. Zhu, *Tribological behaviour of enamel coatings*, Wear, 426-427 (**2019**) 319-329.
[349] A. International, *ASTM C1624 "Standard Test Method for Adhesion Strength and Mechanical Failure Modes of Ceramic Coatings by Quantitative Single Point Scratch Testing"*, ASTM International, West Conshohocken, PA, US, **2022**.
[350] S.J. Bull, *Failure modes in scratch adhesion testing*, Surface and Coatings Technology, 50 (**1991**) 25-32.
[351] X. Li, B. Bhushan, *Micro/nanomechanical characterization of ceramic films for microdevices*, Thin Solid Films, 340 (**1999**) 210-217.
[352] M. Bourchak, I.R. Farrow, I.P. Bond, C.W. Rowland, F. Menan, *Acoustic emission energy as a fatigue damage parameter for CFRP composites*, International Journal of Fatigue, 29 (**2007**) 457-470.
[353] F. Mohamad, T.S. Cevat, A. Mehdi, P. Farzad, *Fracture Characteristics of AISI D2 Tool Steel at Different Tempering Temperatures Using Acoustic Emission and Fuzzy C-Means Clustering*, Arabian Journal for Science and Engineering, 38 (**2013**) 2205-2217.
[354] J. Voyer, F. Gitzhofer, M.I. Boulos, *Study of the performance of TBC under thermal cycling conditions using an acoustic emission rig*, Journal of Thermal Spray Technology, 7 (**1998**) 181-190.
[355] D. Dalmas, S. Benmedhakène, H. Kébir, C. Richard, A. Laksimi, J.M. Roleandt, *Investigation of failure mechanisms in WC–Co coated materials*, Surface and Coatings Technology, 173 (**2003**) 130-143.
[356] M. Surgeon, E. Vanswijgenhoven, M. Wevers, O. Van Der Biest, *Acoustic emission during tensile testing of SiC-fibre-reinforced BMAS glass-ceramic composites*, Composites Part A: Applied Science and Manufacturing, 28 (**1997**) 473-480.